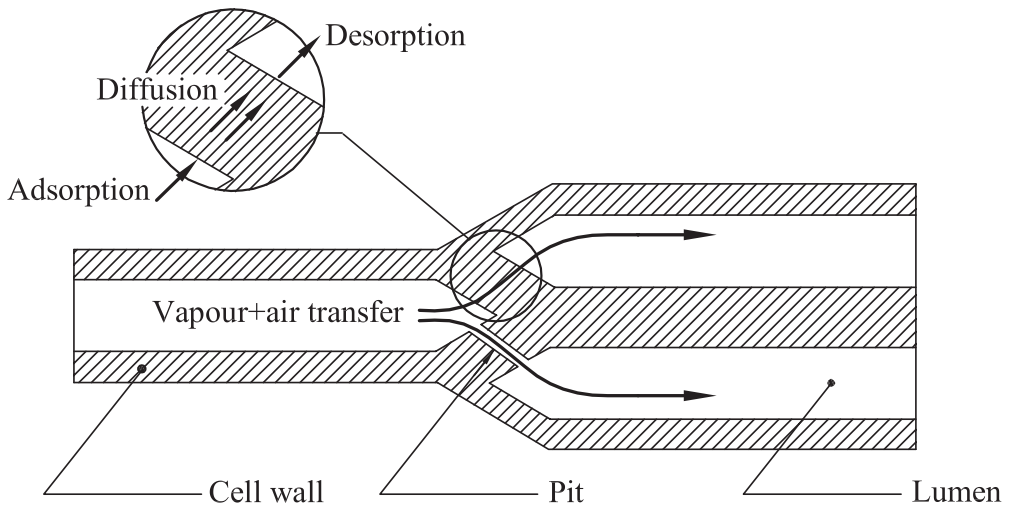


Kristian Krabbenhøft

Moisture Transport in Wood

A Study of Physical--Mathematical Models and their Numerical Implementation



Moisture Transport in Wood

A Study of Physical–Mathematical Models and their Numerical Implementation

Kristian Krabbenhøft

Ph.D. Thesis

Department of Civil Engineering
Technical University of Denmark

2003

Moisture Transport in Wood

A Study of Physical–Mathematical Models and their Numerical Implementation

Copyright (c), Kristian Krabbenhøft, 2003

Printed by Eurographic A/S, Copenhagen

Department of Civil Engineering

Technical University of Denmark

ISBN number: 87-7877-225-7

Byg Rapport R-153

Preface

This thesis is submitted as a partial fulfilment of the requirements for the Danish Ph.d. degree. The study has taken place at the Department of Civil Engineering in the period August 2000 to September 2003, with Professor Lars Damkilde as principal supervisor and Reader Preben Hoffmeyer as co-supervisor.

The thesis is organized in seven chapters, where the first three contain general and introductory remarks, and the last four are summaries, with some extensions, of previously published articles. These are

- K. Krabbenhøft and L. Damkilde. A model for non-Fickian moisture transfer in wood, *Materials and Structures*, 16 pages (2003). Accepted for publication.
- K. Krabbenhøft and L. Damkilde. On the prospects of applying double porosity models to the problem of infiltration of water in wood, *Materials and Structures*, 21 pages (2003). Submitted.
- K. Krabbenhøft, C. Bechgaard, L. Damkilde and P. Hoffmeyer. Finite element analysis of boron diffusion in wooden poles, *Wood and Fiber Science*, 15 pages (2003). Submitted. Based on a revised version of a paper presented at the 34th Annual Meeting of the International Research Group on Wood Preservation, May 2003, Brisbane, Australia.
- K. Krabbenhøft and L. Damkilde. A mixed enthalpy-temperature finite element method for generalized phase-change problems, *Numerical Heat Transfer*, 22 pages (2003). Submitted. Based on a revised version of a paper to be presented at the Ninth International Conference on Civil and Structural Computing, September 2003, Egmond-aan-Zee, The Netherlands.

Acknowledgements

The project would not have been possible without the aid of a number of people. First and foremost, I would like to thank Lars Damkilde for his support and competent guidance through the world of mechanics, starting with my mid-term project in 1998 and extending to the present date. In particular, I would like to acknowledge the not insignificant amounts of time invested in me by Lars, for example in form of his ‘Saturday School’, which besides providing an excellent discussion forum also fostered a relaxed and friendly atmosphere.

I would also like to thank my family for their support and encouragement throughout my time at DTU.

Finally, the study has been funded by the Danish Research Agency under Project No. 9901363: ‘Modeling the Effects of Moisture and Load History on the Mechanical Properties of Wood’. The financial support is gratefully acknowledged.

Lyngby, August 2003

Kristian Krabbenhøft

Abstract

The ability to predict the moisture variations in wood is important in a number of cases. The applications are extremely wide, ranging from the conditions in the living tree to moisture induced deformations in timber structures. In between, in the course of transformation from living tree to structural timber, a number of processes such as drying and preservative treatment involve the transport and heat and mass.

In this report three particular scenarios are dealt with, and in addition, some general numerical procedures for the solution of the transport models have been developed. The main contributions of the thesis are summarized in Chapters 4 to 7.

In Chapter 2 the structure and basic features of wood as related to moisture transport are briefly discussed. Both hardwoods and softwoods are treated with particular emphasis on the different liquid and gas pathways resulting from the microscopic structure of the woods.

In Chapter 3 the general theory of moisture transport in porous media is reviewed. The relevant conservation equations are stated and the constitutive relations governing the transport of the different water phases are discussed. The application of this theory to wood is then considered and a number of apparent discrepancies pointed out. These relate particularly to the common assumption of thermodynamic equilibrium as well as to the transport of vapour and air within the wooden cellular structure. Further, the mechanisms governing the transport of free water at moisture contents slightly above the fiber saturation point are discussed, and it is demonstrated that some care must be taken when applying the conventional generalized Darcy's law.

In Chapter 4 the problem of moisture transport below the fiber saturation point is treated. Here the conventional models often fail to describe the transport of moisture, both qualitatively as well as quantitatively, and one often speaks of the behaviour being 'non-Fickian'. A new model capable of describing this behaviour is presented. As in previous attempts of modeling the transfer of water below the fiber saturation point, the transport of bound water and water vapour are described separately from one another such that a state of non-equilibrium exists. The gradual approach to equilibrium is accounted for by linking the water phases via a mass transfer term whose principal functional variation is discussed in some detail. It is found that in order to accommodate the experimental facts a measure of the proximity to equilibrium has to be introduced such that the rate of conversion of water vapour to bound water and vice versa depends on two parameters: the absolute

bound water moisture content and the proximity to equilibrium. With the model a set of sorption experiments is fitted and on the basis of this, the principle variation of the material parameters discussed. Furthermore, some of the consequences of the assumed state of non-equilibrium are illustrated by computing apparent diffusivities from a number of simulated experiments. As has also been reported in the literature this results in sample length dependent diffusion coefficients.

In Chapter 5 some of the problems associated with free water flow above the fiber saturation point are described. Here it is important to distinguish between the removal of free water and the infiltration of free water into wood. Especially for the problem of infiltration have a number of discrepancies been reported. Indeed, it seems that whereas the conventional models predict time scales in the order of seconds or minutes, the time scales observed in experiments are in the order of days or weeks. Moreover, in a number of recent experimental studies have the moisture distributions proven to be very far from what would be expected in the basis of the conventional models.

In Chapter 6 the problem of wood preservation is treated. The type of preservative treatment dealt with consists of placing the preservative in solid form in the wood, after which it is then carried throughout the wood by a combination of convection and diffusion. In a concrete application the treatment of wooden poles with a boron compound was considered.

In Chapter 7 the numerical methods for the solution of the models developed are dealt with. The similarity between the equation governing the flow of water in partially saturated porous media and the conduction of heat in solids with simultaneous change of phase is pointed out. Using this similarity, a iterative method recently proposed for the latter problem is applied to the former problem. The method proves to be most efficient and is shown to in fact be a reformulation of the so-called variable switching technique. Further topics dealt with are spatial weighting procedures and analytical derivation of some of the tangent matrices commonly encountered in coupled heat and mass transfer computations. Finally, some of the features of drying are discussed and a three dimensional wood drying example presented.

Table of Contents

1	Introduction	1
1.1	Scope	2
2	Wood – structure and basic features	3
2.1	Structure on the macroscopic level	3
2.2	Softwood – the microscopic level	4
2.2.1	Earlywood and latewood	5
2.2.2	Pit aspiration	5
2.3	Hardwood – the microscopic level	6
2.4	Ultra- and molecular structure	9
3	General mathematical modeling of moisture transport	11
3.1	What is ‘moisture’?	11
3.2	Total moisture diffusion models	12
3.3	Phase separation models	13
3.4	Constitutive relations	16
3.4.1	Bound water	16
3.4.2	Gas – water vapour and air	16
3.4.3	Free water	19
	Partially saturated conditions	19
	Fully saturated conditions	24
3.5	The enthalpy equation	25
3.5.1	Conventional formulation	25
3.5.2	Alternative formulation	28
3.5.3	Summary of governing equations	28
4	Moisture transport below the fiber saturation point	31
4.1	Conventional model	31
4.2	Mechanisms of moisture transport	32
4.3	Experimental results	33

4.4	The new model	34
4.4.1	The sorption term	35
4.5	Results	35
4.5.1	Apparent diffusivities	35
4.5.2	Two-dimensional transfer	37
4.6	Conclusions and future work	38
5	Moisture transport above the fiber saturation point	41
5.1	Reported anomalies	41
5.2	Double porosity and permeability models	43
5.3	Length scale effects	44
5.3.1	Example	44
5.4	Conclusions and future work	47
6	Towards modeling preservation processes	49
6.1	Governing equations	50
6.2	Simplified transport model	50
6.3	Material parameters	51
6.4	Results	52
6.5	Conclusions and future work	52
7	Numerical solution procedures	55
7.1	Classification of diffusion-type equations	56
7.1.1	ϕ -form	57
7.1.2	θ -form	58
7.1.3	Mixed form	59
7.2	Solution of nonlinear discrete formulations	59
7.3	Advantages and disadvantages of the different forms	60
7.4	Variable switching techniques	61
7.5	A new mixed-variable iterative procedure	62
7.5.1	Application to the Richards equation	64
7.5.2	Examples	65
	Example 1	66
	Example 2	68
	Example 3	68
7.5.3	Equivalence between variable switching and new method	70
7.6	Application of mixed-variable procedure to wood	72
7.6.1	Variable smoothing	74
7.6.2	Example	74

7.7	Implementation issues	79
7.7.1	Integration of conductivity matrices	80
	Example	82
7.7.2	Jacobian construction	85
	Implementation	86
	Special cases	87
	Generalization to multiple variable problems	88
	Numerical differentiation	88
7.8	Conclusions and future work	89
8	Conclusions	91
	Bibliography	93
	List of Symbols	99
	List of Figures	101
	List of Tables	105
	Article I A model for non-Fickian moisture transfer in wood	
	Article II On the prospects of applying double porosity models to the problem of infiltration of water in wood	
	Article III Finite element analysis of boron diffusion in wooden poles	
	Article IV A mixed enthalpy-temperature finite element method for generalized phase-change problems	

Chapter 1

Introduction

In virtually all regards, wood and water are two inseparable quantities. To biologists the flow and content of water and water borne chemicals in the living tree are important indicators of the health status [40, 57]. Next, after felling, the wood must be dried before use as structural timber. Since green wood may contain water in excess of 800 kg/m^3 , there are significant costs associated with this process. Furthermore, since wood may deform as a result of the water being removed in a non-uniform manner, the quality of the end product depends to a large extent on the drying process. Finally, when in service, for example as structural timber, the moisture content and its temporal variations may give rise to a number of undesirable effects, including further moisture induced mechanical deformations as well as rot, fungal growth and other types of biological degradation, all of which are highly sensitive to the moisture content. To prevent these last processes from taking place wood is often treated by preservatives in the form of aqueous solutions. Here the transport of water, and in addition one or more chemicals contained in the water, are responsible for the overall process.

Thus, the transport of water plays a key role in a large number of scenarios. The models applied for the description of this transport are, however, often inadequate in the sense that only for a limited range of conditions, or perhaps not at all, do they compare well with experiments. Often this is attributed to a lack of accurate material parameters entering into the models, which is again attributed to the variability of wood, whereas the validity of the models themselves is only rarely questioned. Although the lack of accurate material parameters is probably in many cases responsible for the poor correlation between experiment and theory, there are a number of other cases where the observed behaviour deviates so fundamentally from what should be expected, that the validity of the classical models must naturally come under very close scrutiny.

In recent years there has been a growing awareness that the classical models may need revision, first of all in order to describe the most basic situations, but moreover, also in order to be able to extend these models to new scenarios. An example of this is models describing the transport of preservatives. Although very closely related to the problem of water transport, the classical models are not obviously extended to deal with this problem.

1.1 Scope

The scope of this thesis is to contribute to the development of models which accurately describe the transport of primarily water in wood. Furthermore, since a key ingredient, both in the development and application of these models is the availability of efficient numerical solution procedures, some work has also been devoted to this issue.

The major contributions of the thesis are summarized in Chapters 4–7. In Chapter 2 the basic features of wood as related to the transport of moisture are briefly reviewed. In Chapter 3 the general theoretical approach to transport of water in wood is described. Chapter 4 is concerned with a new model for transport of moisture below the fiber saturation point. The model is compared with a number of sorption experiments and excellent agreement is found. In Chapter 5 some of the problems associated with transport of free water above the fiber saturation point are described and some possible models discussed. Furthermore, a set of experimental data is fitted to within a reasonable accuracy. In Chapter 6 the problem of wood preservation is treated. Finally, in Chapter 7 numerical methods are dealt with. The general approach is described, and a new and very efficient method for solving the highly nonlinear equations encountered in the description of free water flow above the fiber saturation point is presented.

Chapter 2

Wood – structure and basic features

In this chapter a summary of the structure and basic features of wood is given. Particular attention is paid to the properties which govern the transport of fluids within the wooden cellular structure. A knowledge of the structure of wood is useful primarily as a means of understanding experimentally observed phenomena. Moreover, it serves as a physical justification of some of the models presented in later chapters.

Wood can be divided into two broad classes, commonly referred to as softwood and hardwood. Although these names can be somewhat misleading since some softwoods are harder than some hardwoods, they are nevertheless useful in that they cover two rather distinct types of cellular arrangements. In the following the structure of both softwood and hardwood, as related to transport phenomena, are discussed.

We will deal with four levels with which four different length scales are associated. First, the macroscopic level on which hardwood and softwood to a certain degree can be treated together. Secondly, the microscopic level where the differences between hardwoods and softwoods manifest themselves most clearly. And finally, the ultra-structural and molecular levels on which the structural and chemical composition of the cell wall is dealt with.

2.1 Structure on the macroscopic level

Before the cellular structure of softwood and hardwood are described, some features common to all woods will be summarized. The trunk of any tree has three physical functions: it must support the crown, it must conduct minerals upwards from the roots to the crown, and it must store manufactured food until needed.

Whereas the entire trunk contributes to the support of the crown, it is only in the outer circumference that conduction and storage take place. The wood located in this portion of the tree is termed sapwood, whereas the remaining part is referred to as heartwood. The width of the sapwood zone is usually much smaller than the width of the heartwood zone, and only rarely exceeds one third of the total width [16].

As the tree grows, former sapwood cells will gradually be transformed to heartwood cells. In this transformation a number of chemical changes takes place which gives the heartwood a distinctly darker color than the sapwood, see Figure 2.1.

With respect to the overall flow properties of the two types of wood, sapwood is usually significantly more permeable than heartwood, which is not surprising since the two types of wood have different functions in the living tree. Also, the sapwood porosity is slightly higher than that of the heartwood. These factors affect the ability of each type of wood to conduct water. However, as will be discussed later, in the drying of wood several geometrical changes take place on the microscopic level such that the permeability of green wood is usually very much different from that of dried wood.

Further visual inspection of a typical cross section as that depicted in Figure 2.1 also reveals the existence of a set of concentric rings with origin in the center (pith) of the tree. These growth rings originate as a result of the progress in growing within each season, and give rise to the three principal axes of wood.

2.2 Softwood – the microscopic level

The structure of a typical softwood is shown in Figure 2.2. As shown, the cellular arrangement is one of long interconnected cells with approximately square cross sections. These cells are aligned such that three principal directions can easily be identified. In softwoods the cells do not extend through the whole trunk to form an unbroken pathway, but have tapered ends such that the cells do in fact form independent and relatively closed units, see Figure 2.3. The conduction in the longitudinal direction thus takes place through pits located on the cell walls, primarily in radial sections. The resistance offered by these pits make up a significant portion of the total resistance to longitudinal flow.

In the two other directions flow also takes place via the interconnecting pits, and in the radial direction furthermore through ray cells as shown in the figure. This generally results in the permeability being slightly higher in the radial direction than in the tangential direction, although most pits are located on the radial surfaces and thus facilitate tangential flow.

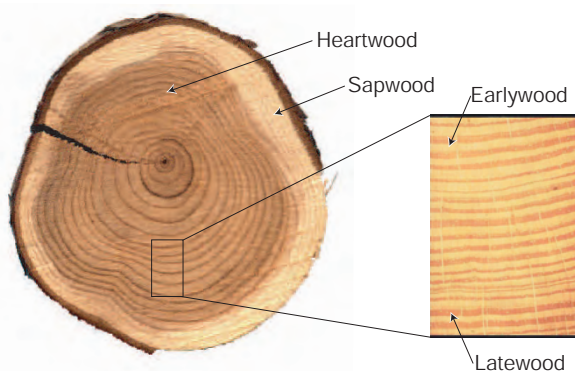


Figure 2.1 Cross section of a softwood trunk.

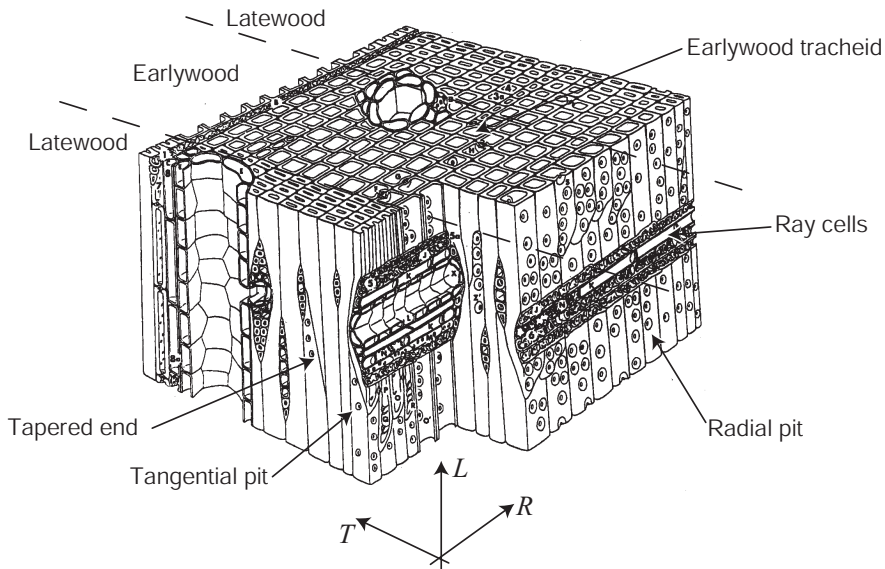


Figure 2.2 Structure of softwood, southern pine [55].

2.2.1 Earlywood and latewood

The growth rings clearly visible in Figure 2.1 are a result of the presence of cells with different dimensions. In the beginning of the growing season the tree will form cells whose primary function is that of conduction. Such cells are thin-walled and have a high degree of connectivity, i.e. a large number of pits on the cell walls. This wood, named earlywood, will appear as being rather light in colour.

In contrast, the darker part of a year ring, the latewood, consists of cells with the opposite features. Now the primary purpose is that of support rather than conduction and the shape of the cells reflects this by being much denser and having fewer interconnecting pits.

2.2.2 Pit aspiration

As already touched upon, there is usually a marked difference in the flow properties of green and dried wood. In the light of the preceding, it would be reasonable to assume that the permeability of earlywood is much higher than that of latewood. This because the porosity is higher and further, due to a much larger number of interconnecting pits. This is also the case, but however, only in the green state. The reason for this must be found in the pit aspiration phenomenon. The pits connecting the cells have a structure as shown in Figure 2.4. In the green state the pit torus will be suspended from the margo strands and positioned in the middle of the pit chamber such that flow is not seriously

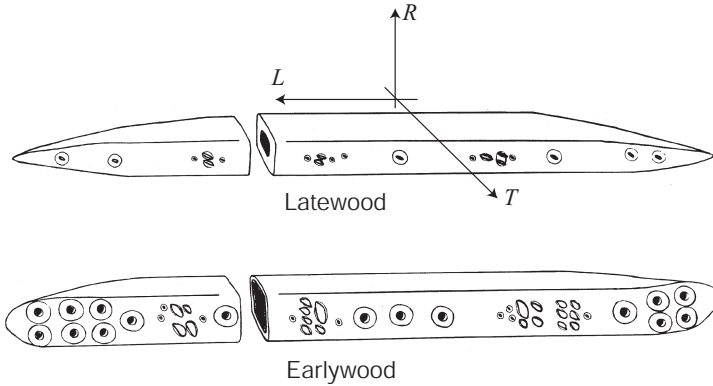


Figure 2.3 *Earlywood and latewood cells* [55].

hindered. As water is removed, however, tension stresses will develop as a result of water menisci in the chamber and these stresses will displace the torus to such a degree that the pit is effectively closed. Subsequently the torus is kept in the deflected position by strong hydrogen bonds between the torus and the cell wall. Pit aspiration is mainly irreversible, such that rewetting with water will only cause partial reduction in the number of aspirated pits.

As for the difference between earlywood and latewood pit aspiration, it has been observed that much less aspiration takes place in the latewood, which is attributed to a greater stiffness of latewood margo strands. Thus, it can be observed that dried latewood is generally more permeable than dried earlywood [55], contrary to what should be expected and contrary to what is the case in the green state. This effect is most pronounced for sapwood, since in the heartwood there is a tendency to deposition of encrusting materials over the torus and margo strands, such that there is a high probability that pits which are not already aspirated will, nevertheless, be blocked.

2.3 Hardwood – the microscopic level

The structure of hardwood is very different from that of softwood. Moreover, there is a much greater variability from species to species. In general, two types of hardwood can be identified, referred to as ring porous and diffuse porous respectively.

In figure 2.6 the microscopic structure of a diffuse porous hardwood is shown. For these types of hardwood the cell sizes do not change very much throughout the growing season and the result is an even distribution of the large vessels, which are surrounded by cells with a much smaller diameter. As in softwoods ray cells provide radial flow paths. In the longitudinal direction the flow takes place via the larger vessels, whose ends, in contrast to what is the case in softwoods, are not closed. This makes hardwoods much more permeable in the longitudinal direction than softwoods. Tangential flow is again by way

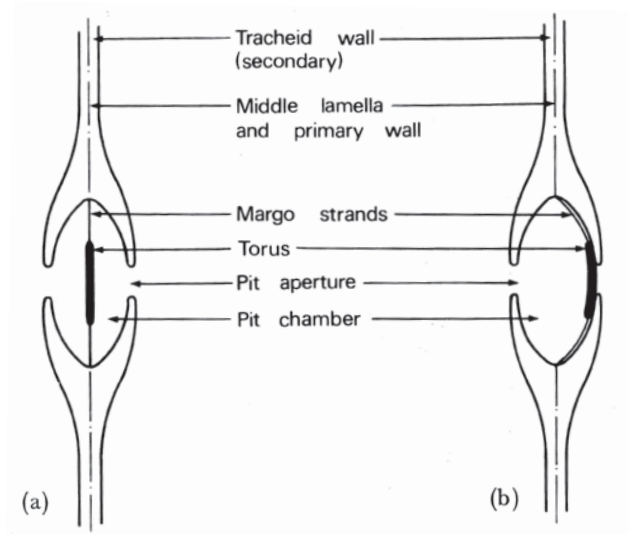


Figure 2.4 Cross section of bordered pit [16].

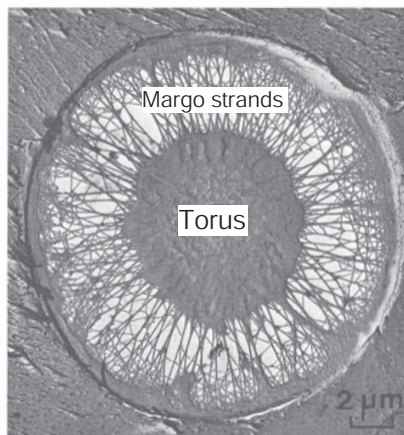


Figure 2.5 Unspirated bordered pit [55].

of interconnecting pits, but in comparison to softwoods, these are generally much smaller, and from the beginning rather impermeable. These features result in a much smaller difference between the permeability of green and dried wood.

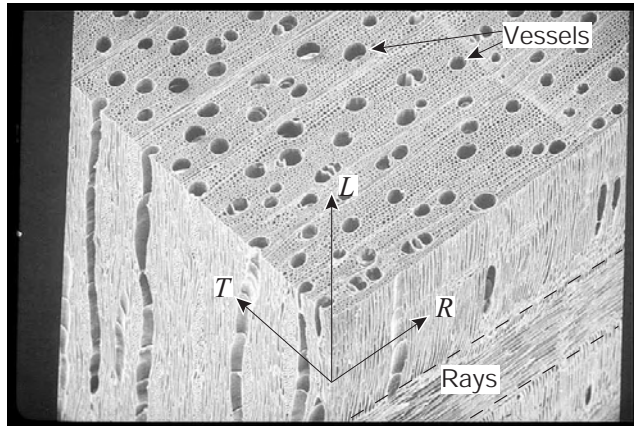


Figure 2.6 *Microscopic structure of a diffuse porous hardwood, sugar maple [60].*

The ring porous hardwoods have similar properties, but the growth rings can now be clearly identified, see Figure 2.7.
For both types of hardwood the sapwood is more permeable than the heartwood, and the earlywood more permeable than the latewood.

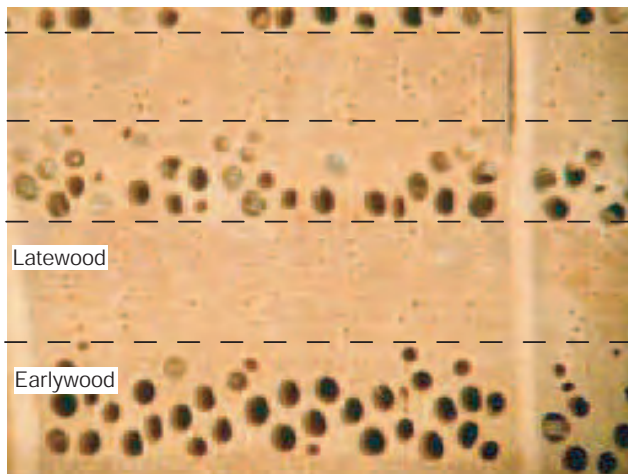


Figure 2.7 *Microscopic structure of a ring porous hardwood, red oak [60].*

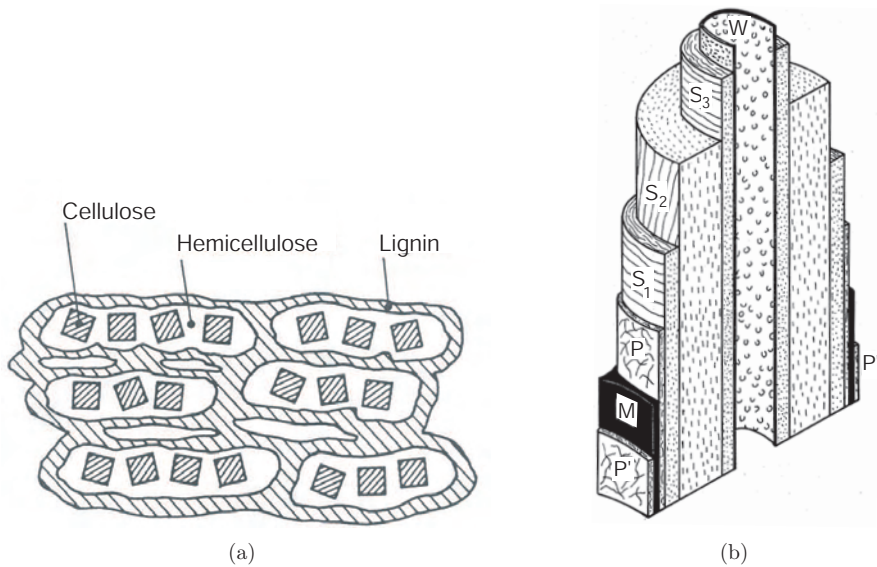


Figure 2.8 Cross section of a microfibril [66] (a) and structure of the cell wall [55] (b).

2.4 Ultra- and molecular structure

Wood consists for the most part of three polymers: cellulose, hemicellulose, and lignin. The relative amounts of these three polymers vary from species to species, but usually cellulose accounts for 40–50% whereas approximately equal amounts of hemicellulose and lignin make up the rest, [66, 16, 55]. These polymers are the constituents of the composite structure of the so-called microfibrils, Figure 2.8 (a). These resemble long threads with a typical length of some 5000 nm and a width of 10–20 nm.

The cell wall is composed of microfibrils packed in a number of distinct layers as shown in Figure 2.8 (b). In the primary wall (P,P') the microfibrils are randomly oriented whereas the layers S₁–S₃ are each composed of microfibrils in a more regular arrangement. In spruce the relative thickness of the different layers is $P : S_1 : S_2 : S_3 = 5 : 9 : 85 : 1$, whereas the innermost layer, the so-called warty layer, is much thinner than the S₃ layer.

Finally, the individual cells are bonded together by the middle lamella (M) to form the overall microscopic structure.

Since the different polymers comprising wood each have different properties, e.g. different sorption isotherms, wood is in fact a composite material where the overall behaviour is a result of the features of the individual components and their arrangement in the cell wall.

Chapter 3

General mathematical modeling of moisture transport

In this chapter the general mathematical framework used throughout the thesis is presented. Two common models are presented and compared to each other. Furthermore, common constitutive relations are discussed and certain problems with these when applied to wood are pointed out. Finally, different forms of the enthalpy equation are discussed with particular reference to its numerical implementation.

3.1 What is ‘moisture’?

So far the terms ‘moisture’ and ‘moisture content’ have been used rather loosely and without any clear definition of what these terms in fact cover. Of course, most people intuitively take ‘moisture’ as being synonymous with ‘water’ and thus, the use of these terms is not really an obstacle in making meaningful statements about the qualitative nature of the problem. However, when it comes to the actual modeling of moisture transport it is very useful, if not absolutely necessary, to consider in more detail the different phases of water involved in the given process.

Water in wood may exist in three different forms, either as free water, as bound water or as water vapour. Each of these forms of water have widely different characteristics, some of which are summarized below.

- **Free water.** This is also referred to as liquid water or capillary water. Free water is transported through the lumens and pits of the wood.
- **Bound water.** This is the water which is chemically bound to the wood substance. When speaking of bound water transfer we mean the transfer of water within the cell walls and **not** the transfer of ‘moisture’ below the fiber saturation point which includes a simultaneous transfer of bound water and water vapour.
- **Water vapour.** This is the third kind of water generally found in wood. The transfer of vapour is rather complicated and involves probably both diffusion through

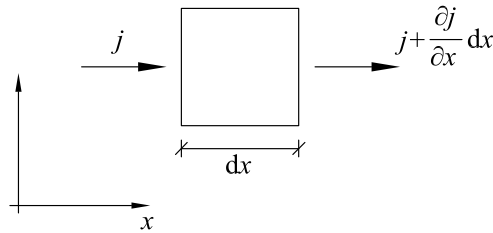


Figure 3.1 One dimensional infinitesimal element.

lumens and pits as well as an adsorption–diffusion–desorption mechanism through the cell walls.

Below the fiber saturation point only bound water and water vapour exists. Although the bound water usually comprises by far the larger part of the total weight of water, it is important to consider the transfer of each of the two components separately as will be shown in Chapter 4.

Since the fibers have only a limited capacity to hold moisture, above some point any additional water will appear as free water within the wood. In green wood there are usually appreciable amounts of free water present and thus, the problem of describing the transfer of this free water is an important one to which considerable effort has been devoted. However, as will be shown in this chapter and further in Chapter 5, several issues remain unresolved and may in fact require an entirely different approach to the one traditionally taken.

3.2 Total moisture diffusion models

In comparison to other physical phenomena it is rather easy to formulate a conceptual model describing the transport of moisture, i.e. water, in porous materials. The basic requirement is that the total mass is conserved. Considering the case of one dimensional transport a relevant conservation equation would be

$$\frac{\partial C}{\partial t} = -\frac{\partial j}{\partial x} \quad (3.1)$$

where $\partial j/\partial x$ is the net mass flux out of an infinitesimal element as shown in Figure 3.1 and C is the mass of water per unit volume of porous material.

Next, an expression for the flux in relation to the moisture content C is needed. As a first approximation it seems natural to take this as being proportional to the gradient in moisture content by some proportionality factor \mathcal{D} , i.e.

$$j = -\mathcal{D} \frac{dC}{dx} \quad (3.2)$$

Inserting this into (3.1) one obtains the classical diffusion equation

$$\frac{\partial C}{\partial t} = \frac{\partial}{\partial x} \left(\mathcal{D} \frac{\partial C}{\partial x} \right) \quad (3.3)$$

This equation has numerous analogies throughout the physical sciences, e.g. in describing heat conduction, lubrication, consolidation, etc. With respect to moisture transport in wood the earliest application of (3.3) appears to be that of Tuttle in 1925 [64], where the diffusion coefficient was taken to be constant. Usually, a variation with moisture content is assumed and in many cases the physical behaviour can then be simulated quite well, especially below the fiber saturation point and especially during drying, see e.g. [29].

Although the total moisture diffusion model is very crude and the deeper physics of the problem not really accounted for, it is quite attractive since only one material parameter is required. Moreover, as will be shown later, it is in fact, at least under isothermal conditions, equivalent to other more advanced models.

However, a number of discrepancies have also been reported. These relate particularly to the case of adsorption, where it has been shown that the total diffusion model is not adequate. Rather than considering the total moisture content, it seems that it is necessary to separate the phases, i.e. under the fiber saturation point, bound water and water vapor. The transport of the these phases can then be described separately from each other. In addition, some mechanism responsible for the interchange between bound water and vapour must considered. Such models are discussed below.

3.3 Phase separation models

As described in the above, water comes in three different phases. For each of these phases a conservation equation can be considered. For general non-hygroscopic porous media Whitaker [67, 69] has derived such a set of conservation equations. This was done by first considering the conservation equations of each of the phases present in point form, that is without any explicit reference to the porous nature of the medium. An averaging procedure was then applied and a set of averaged conservation equations resulted. These can be written as

$$\begin{aligned} \text{Free water:} \quad & \frac{\partial}{\partial t} (\varepsilon_w \langle \rho_w \rangle^w) + \nabla \cdot (\langle \rho_w \rangle^w \langle \mathbf{v}_w \rangle) = -\langle \dot{m}_{wv} \rangle - \langle \dot{m}_{wb} \rangle \\ \text{Bound water:} \quad & \frac{\partial}{\partial t} (\varepsilon_s \langle \rho_b \rangle^s) + \nabla \cdot (\langle \rho_b \rangle^s \langle \mathbf{v}_b \rangle) = -\langle \dot{m}_{bv} \rangle + \langle \dot{m}_{wb} \rangle \\ \text{Water vapour:} \quad & \frac{\partial}{\partial t} (\varepsilon_g \langle \rho_v \rangle^g) + \nabla \cdot (\langle \rho_v \rangle^g \langle \mathbf{v}_v \rangle) = \langle \dot{m}_{wv} \rangle + \langle \dot{m}_{bv} \rangle \\ \text{Dry air:} \quad & \frac{\partial}{\partial t} (\varepsilon_g \langle \rho_a \rangle^g) + \nabla \cdot (\langle \rho_a \rangle^g \langle \mathbf{v}_a \rangle) = 0 \end{aligned} \quad (3.4)$$

where ρ_α are the densities, or concentrations, of the different components, i.e. solid skeleton (s), free water (w), gas (g), bound water (b) and air (a), where the gas phase

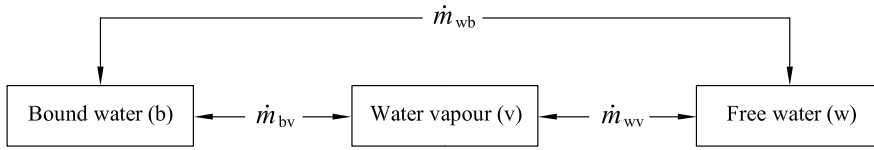


Figure 3.2 Phase transitions.

refers to the mixture of vapour of air. The corresponding velocities are given by \mathbf{v}_α . The conservation equations of Whitaker for non-hygroscopic porous media have been supplemented with one describing the transfer of bound water. Furthermore, as can be seen, an equation considering the conservation of dry atmospheric air is also included. This enables a correct description of the significant pressure gradients which may develop during high temperature drying. In addition to these equations, also an energy balance equation must be included. This equation will be discussed in some detail later on.

In (3.4) two different averaging measures are used, namely the intrinsic phase average

$$\langle \psi \rangle^\alpha = \frac{1}{V_\alpha} \int_V \psi \, dV \quad (3.5)$$

and the superficial average

$$\langle \psi \rangle = \frac{1}{V} \int_V \psi \, dV \quad (3.6)$$

where V is the total volume and V_α the volume of the α -phase. The phase volume fractions ε_α are given by

$$\varepsilon_\alpha = \frac{V_\alpha}{V}, \quad \alpha = s, w, g \quad (3.7)$$

and thus, the four equations must be supplemented with the geometric constraint

$$\varepsilon_s + \varepsilon_w + \varepsilon_g = 1 \quad (3.8)$$

The right hand side $\langle \dot{m}_{\alpha\beta} \rangle$ terms describe the exchange of mass between the different phases, i.e. $\langle \dot{m}_{vw} \rangle$ describes the conversion of vapour to free water and vice versa, see Figure 3.2.

Compared to the total moisture diffusion model there are two principal differences. First of all, the phases have been separated such that it is possible to ascribe different constitutive relations to the different phases. For example, as will be discussed later on, the driving force behind the motion of the free water could be assumed to be capillary pressure, whereas the vapour velocity could be assumed diffusive with the vapour concentration as driving force. Secondly, the right hand side phase conversion terms permit a state of non-equilibrium between the different phases, and in our opinion this is in fact the most significant difference between the two models.

The averaging procedure developed and applied by Whitaker is capable of producing many

interesting theoretical results. For example, starting from the Navier–Stokes equations, the generalized Darcy’s law for porous media can be derived mathematically [68]. However, the concept of considering moisture transport in porous media from some kind of average point of view is of course quite classical – in the laboratory material parameters are determined from samples with dimensions which, it is hoped, will be representative of the dimensions to which the model is ultimately applied. Thus, we emphasize that there is nothing fundamentally new in the way the equations (3.4) are formulated, the different averaging measures are only included for reasons of mathematical consistency.

As discussed in the above, the presence of phase conversion terms in principle permit a state on non–equilibrium. However, in almost all applications of (3.4), to wood as well to other porous materials, it is assumed that a state of equilibrium exists at all times. Thus, the three separate equations can be added to yield one equation, describing the transfer of total water. This is given by

$$\begin{aligned} \frac{\partial}{\partial t} (\varepsilon_w \langle \rho_w \rangle^w + \varepsilon_g \langle \rho_v \rangle^g + \varepsilon_s \langle \rho_b \rangle^s) + \\ \nabla \cdot (\langle \rho_w \rangle \langle \mathbf{v}_w \rangle^w + \langle \rho_v \rangle \langle \mathbf{v}_v \rangle^g + \langle \rho_b \rangle^s \langle \mathbf{v}_b \rangle) = 0 \end{aligned} \quad (3.9)$$

Now, since the total volumetric water content is given by

$$C = \varepsilon_w \langle \rho_w \rangle^w + \varepsilon_g \langle \rho_v \rangle^g + \varepsilon_s \langle \rho_b \rangle^s \quad (3.10)$$

and we may define a total water flux \mathbf{j} by

$$\mathbf{j} = \langle \rho_w \rangle \langle \mathbf{v}_w \rangle^w + \langle \rho_v \rangle \langle \mathbf{v}_v \rangle^g + \langle \rho_b \rangle^s \langle \mathbf{v}_b \rangle \quad (3.11)$$

the total water transfer equation (3.9) is seen to be but a more elaborate version of (3.1). Thus, the real difference between the two approaches lies in the separation of the phases as a means of obtaining a type of composite constitutive relation comprising the contributions from the different phases. Whereas this is arguably more satisfying from a physical point of view and furthermore, may provide insights which are not otherwise picked up, it could be feared that the total experimental uncertainty in the case where three or more separate experiments have to be conducted would exceed the uncertainty in the single experiment required if the phases are not separated.

It should be emphasized that whereas the phase–equilibrium assumption is usually made, we could also have maintained the original state of non–equilibrium and then postulated expressions for $\langle \dot{m}_{\alpha\beta} \rangle$ with the property that as time passes the system tends towards an equilibrium state. For example, for non–hygroscopic porous media we could use an expression similar to the one governing the evaporation from a wet surface, i.e.

$$\dot{m}_{wv} = \mu k_p (p_{vs} - p_v) \quad (3.12)$$

where p_v is the vapor pressure and p_{vs} is the saturated vapour pressure which for non–hygroscopic materials often to a good approximation can be assumed to be equal to the equilibrium vapour pressure. Since \dot{m}_{wv} accounts for the exchange per unit volume the

surface mass transfer coefficient k_p must be multiplied by the ratio of internal surface area to total volume μ .

Thus, although the phase–equilibrium assumption is almost always made, the equations (3.4) still form the basis of other models where a state of non–equilibrium is assumed to exist. Such models will be presented in Chapters 4 and 5

3.4 Constitutive relations

In this section the different constitutive relations required in the phase separation model are summarized and several unresolved problems as related to these are pointed out. In the following we will occasionally simplify the notation such that all densities (concentrations) refer to intrinsic averages if nothing else is stated, i.e.

$$\rho_w \equiv \langle \rho_w \rangle^w, \quad \rho_b \equiv \langle \rho_b \rangle^s, \quad \rho_v \equiv \langle \rho_v \rangle^g, \quad \rho_a \equiv \langle \rho_a \rangle^g \quad (3.13)$$

Similarly, if nothing else is stated, the velocities refer to superficial averages, i.e.

$$\mathbf{v}_w \equiv \langle \mathbf{v}_w \rangle, \quad \mathbf{v}_b \equiv \langle \mathbf{v}_b \rangle, \quad \mathbf{v}_v \equiv \langle \mathbf{v}_v \rangle, \quad \mathbf{v}_a \equiv \langle \mathbf{v}_a \rangle \quad (3.14)$$

3.4.1 Bound water

The bound water constitutive relation is probably the least controversial, and under normal conditions the bound water flux is the smallest contributor to the total transport. It is generally accepted that the motion of bound water within the cell wall can be described via a gradient law of the type

$$\langle \rho_b \rangle^s \langle \mathbf{v}_b \rangle = -\langle \rho_s \rangle \mathbf{D}_b \nabla (\langle \rho_b \rangle / \langle \rho_s \rangle) \quad (3.15)$$

or in a more conventional notation

$$\mathbf{j}_b = -\rho_0 \mathbf{D}_b \nabla W_b \quad (3.16)$$

where $\rho_0 \equiv \langle \rho_s \rangle$ (kg/m³) is the density of gross wood, W_b (kg/kg) the dry base moisture content, and \mathbf{D}_b (m²/s) the 3 × 3 diffusivity tensor. For Sitka spruce this has been determined experimentally by Stamm [59, 55] who found a variation in the longitudinal direction as shown in Figure 3.3. As expected the diffusivity increases with increasing moisture content and temperature, which can be attributed to the bonding forces decreasing as moisture content and temperature increase.

3.4.2 Gas – water vapour and air

The transfer of water vapour and air is described by a combination of the laws of Darcy and Fick. Traditionally, no distinction is made between wood and other porous materials such as soils and concrete when describing the transfer of water vapour and dry. [45, 49, 43, 48, 44]. The equations following from this approach are summarized next, after which some of the implications and apparent discrepancies arising from neglecting the fundamental differences between the structure of wood and other porous materials are

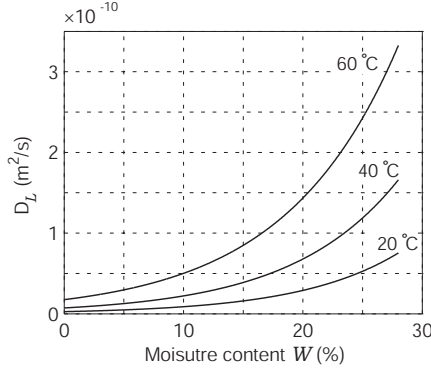


Figure 3.3 Diffusivity of bound water in the longitudinal direction.

pointed out.

When describing the transport of gases such as water vapour and dry atmospheric air it is necessary to consider both convective and diffusive modes of transfer. Thus, the velocities \mathbf{v}_v and \mathbf{v}_a appearing in the conservation equations (3.4) are decomposed into two contributions

$$\mathbf{v}_v = \mathbf{v}_g + \mathbf{u}_v \quad \text{and} \quad \mathbf{v}_a = \mathbf{v}_g + \mathbf{u}_a \quad (3.17)$$

where \mathbf{v}_g is the total gas mass average velocity and \mathbf{u}_v and \mathbf{u}_a are the diffusive mass average velocities. Inserting this into the conservation equations yields

$$\underbrace{\frac{\partial}{\partial t}(\varepsilon_g \rho_\alpha)}_{\text{accumulation}} + \underbrace{\nabla \cdot (\rho_\alpha \mathbf{v}_g)}_{\text{convection}} + \underbrace{\nabla \cdot (\rho_\alpha \mathbf{u}_\alpha)}_{\text{diffusion}} = 0, \quad \alpha = v, a \quad (3.18)$$

For the convective transfer Darcy's law is used, i.e. the mass average velocity is given by

$$\mathbf{v}_g = \frac{\mathbf{K}_g \mathbf{K}_{rg}}{\mu_g} \nabla p_g \quad (3.19)$$

For the diffusive part of the transfer Fick's law is used

$$\rho_v \mathbf{u}_v = -\rho_g \mathbf{D}_{\text{eff}}^{va} \nabla (\rho_v / \rho_g) \quad (3.20)$$

and

$$\rho_a \mathbf{u}_a = -\rho_g \mathbf{D}_{\text{eff}}^{av} \nabla (\rho_a / \rho_g) \quad (3.21)$$

From the definition of the mass average velocity

$$\mathbf{v}_g = \frac{\rho_v \mathbf{v}_v + \rho_a \mathbf{v}_a}{\rho_g} \quad (3.22)$$

it follows that

$$\begin{aligned}\rho_g \mathbf{V}_g &= \rho_v \mathbf{V}_v + \rho_a \mathbf{V}_a = \rho_g \mathbf{V}_g + \rho_v \mathbf{u}_v + \rho_a \mathbf{u}_a \\ \Rightarrow \rho_v \mathbf{u}_v + \rho_a \mathbf{u}_a &= 0\end{aligned}\tag{3.23}$$

and since

$$\nabla(\rho_v/\rho_g) = -\nabla(\rho_a/\rho_g)\tag{3.24}$$

it can be seen that the diffusion coefficients must necessarily be related by

$$\mathbf{D}_{\text{eff}}^{\text{va}} = \mathbf{D}_{\text{eff}}^{\text{av}} = \mathbf{D}_{\text{eff}}\tag{3.25}$$

This implies that the diffusion of vapour into air is accompanied by a opposite directed diffusion of air into vapour

$$\rho_g \mathbf{D}_{\text{eff}} \nabla(\rho_v/\rho_g) = -\rho_g \mathbf{D}_{\text{eff}} \nabla(\rho_a/\rho_g)\tag{3.26}$$

Thus, when describing the transfer of water vapour and dry air in this way no distinction is made as to the pathways along which these two components are transported. This may, however, be quite erroneous in the case of wood. Thus, it seems reasonable to assume that the transfer of air, and other gases which do not react with the wood substance, takes place exclusively through the voids of the cells and through the pits connecting the cells. But whether the major part of the vapour transfer is also along this pathway is, however, another question. In fact, several observations indicate that this may not be the case. Rather, these observations indicate that the bulk of the vapour transfer takes place through the cell walls of the wood. That is, on one side of the cell wall an adsorption takes place followed by diffusion through the cell wall and finally a desorption on the opposite side of the cell wall as shown in Figure 3.4.

If flow through the pits did indeed provide the principal pathway for vapour transfer, then it is hard to explain the significant moisture dependence of the apparent diffusivities as measured in cup experiments, see e.g. [66]. Of course, in cup experiments the total transfer constitutes both vapour and bound water transfer where the bound water diffusivity as discussed earlier is a strong function of the moisture content. However, the variation of the apparent diffusivity is usually much greater than would be expected taking this into consideration. Further evidence of the cell wall pathway as the dominating mechanism has been provided by Siau [55] who in a geometric model of the cellular structure of a typical softwood, neglecting pits, computed effective vapour diffusivities which are in good agreement with experimental findings.

The hypothesis of the cell wall adsorption–diffusion–desorption mechanism being the dominant for vapour transfer has some major implications on the general theoretical framework discussed in the above. Since in this case the vapour–air and air–vapour diffusivities are no longer identical, (3.26) no longer holds. Neither, does it make sense to talk about a convective total gas transfer since in the convective flow only a part of the vapour is transported. It seems then that there is only really experimental justification for applying a Fickian type gradient law for the transfer of vapour, i.e.

$$\rho_v \mathbf{v}_v = \mathbf{D}_{\text{eff}} \nabla \rho_v\tag{3.27}$$

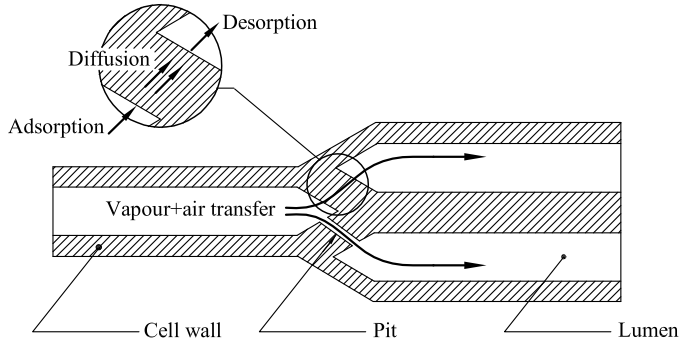


Figure 3.4 Water vapour and air transfer.

where the potential ρ_v is somewhat arbitrarily chosen and only under isothermal conditions is equivalent to other relevant potentials. Here it should be pointed out that under moderate temperatures, e.g. less than 50 °C or so, convective transfer is usually negligible and since $\rho_v/\rho_g \ll 1$ Fick's law as given by (3.20) does in fact reduce to something quite close to (3.27) [67].

At higher temperatures, however, convection can be expected to play some role, and the question then remains as to just how the air pressure gradients should be included in the air–vapour constitutive relations.

3.4.3 Free water

The free water constitutive relation is usually assumed to follow the generalized Darcy's law by which the mass average velocity of the free water is given by

$$\mathbf{v}_w = -\frac{\mathbf{K}_w \mathbf{K}_{rw}}{\mu_w} \nabla(p_w + \rho g z) \quad (3.28)$$

or in terms of mass flux

$$\mathbf{j}_w = \rho_w \mathbf{v}_w = -\rho_w \frac{\mathbf{K}_w \mathbf{K}_{rw}}{\mu_w} \nabla(p_w + \rho g z) \quad (3.29)$$

where z is the upward directed coordinate opposite to which gravity acts, \mathbf{K}_w is the absolute permeability, \mathbf{K}_{rw} the relative permeability and μ_w the dynamic viscosity of water. The water pressure p_w has two different interpretations depending on whether the medium is partially or fully saturated. This is discussed below.

Partially saturated conditions

Under partially saturated conditions the water pressure is equal to the sum of the capillary pressure and the gas pressure

$$p_w = p_c + p_v + p_a \quad (3.30)$$

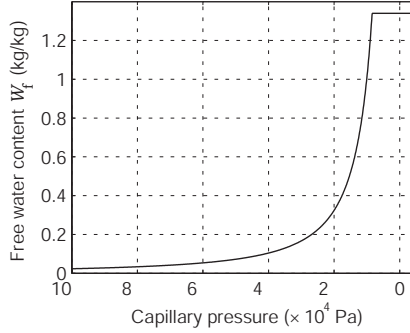


Figure 3.5 *Capillary pressure as function of free water content for softwood at 20°C, according to [48].*

where the capillary p_c pressure is a function of the degree of saturation and temperature. This is often taken as varying principally as

$$p_c = \sigma(T)p(W_f) \quad (3.31)$$

where $\sigma(T)$ is the surface tension of water which depends only on the temperature and $p(W_f)$ is a function which depends only on the degree of saturation, or alternatively, on the free water content W_f given by

$$W_f = \frac{\rho_w}{\rho_0} \varphi S \quad (3.32)$$

where φ is the porosity and S the degree of saturation.

In this way, the capillary pressure–saturation curve needs only determination at one temperature whereas the general temperature dependence is correlated via temperature dependence of the surface tension of water which is a well–described quantity.

If gas pressures and gravity are temporarily ignored, (3.29) can be expanded in terms of W_f as

$$\begin{aligned} \mathbf{j}_w &= -\rho_w \frac{\mathbf{K}_w \mathbf{K}_{rw}}{\mu_w} \nabla \left[\sigma(T) \left(\frac{\partial p}{\partial W_f} \right) \nabla W_f + p(W_f) \left(\frac{\partial \sigma}{\partial T} \right) \nabla T \right] \\ &= \mathbf{K}_W \nabla W_f + \mathbf{K}_T \nabla T \end{aligned} \quad (3.33)$$

Thus, a general non–isothermal constitutive relation is obtained through only one experimentally determined curve, a typical example of which is shown in Figure 3.5. In comparison, the total moisture diffusion model would require separate determination of the coefficients \mathbf{K}_W and \mathbf{K}_T at different moisture contents and temperatures, which, needless to say, is a formidable task.

As for the relative permeabilities \mathbf{K}_{rw} , these should equal unity for fully saturated conditions and then decrease as the saturation decreases. This decrease expresses the gradual

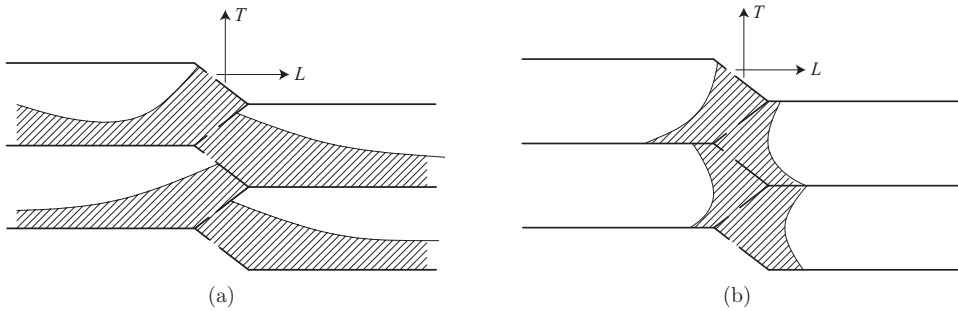


Figure 3.6 Free water distribution in wood at high (a) and at low (b) degrees of saturation.

loss of continuity of the water phase as the saturation decreases. The orthotropy of wood plays an important part in this regard. Looking in more detail at the mechanism of water transfer in softwood this can be expected to take place via the pits located primarily at the ends of the tapered section of the cells, see Figures 3.6 (a)–(b). As the resistance to flow is generally much smaller in the longitudinal direction than in the transverse direction it can be expected that the effective conductivity is also much larger in the longitudinal direction. However, because of the particular structure of wood this is only the case at relatively high degrees of saturation. This situation is depicted in Figure 3.6 (a). The water phase still has a high degree of continuity and longitudinal transfer will be dominant. At lower degrees of saturation the water collects at the tapered ends and the degree of continuity of the free water phase decreases. This means that longitudinal transfer is severely hindered while the transverse transfer is much less affected. Thus, in [48] the relative permeabilities in the three principal directions of a non-specified softwood were taken as

$$K_{rw}^L = S^8, \quad K_{rw}^T = K_{rw}^R = S^3 \quad (3.34)$$

whereas the absolute permeabilities were reported to be

$$K_w^L = 10^{-12} \text{ m}^2, \quad K_w^T = \frac{1}{2} K_w^R = 10^{-16} \text{ m}^2 \quad (3.35)$$

The ratio between the longitudinal and tangential effective permeabilities are thus

$$\frac{K_w^L K_{rw}^L}{K_w^T K_{rw}^T} = \frac{K^L}{K^T} = 10^4 S^5 \quad (3.36)$$

which means that below $S \simeq 0.15$ the transfer of free water is faster in the tangential direction than in the longitudinal direction. Indeed, as the saturation decreases below some value, the longitudinal free water flow becomes so small that it is practically zero. This flow of free water at low degrees of saturation in wood and other porous materials has recently been the subject of some controversy. In some fields, e.g. those dealing with the flow of water in soils, the so-called irreducible saturation point is an integral part of almost all constitutive relations, e.g. the very commonly applied parameterization of van Genuchten [65]. That is, below some degree of saturation S_{irr} the flow of free water is

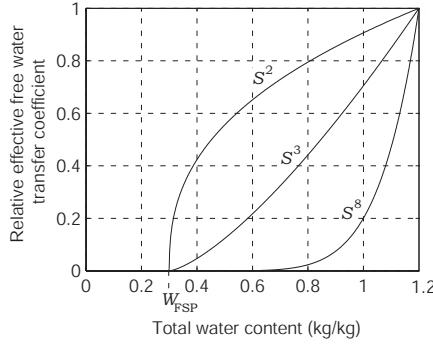


Figure 3.7 Relative effective free water transfer coefficients as function water content.

assumed not to take place at all. For wood the irreducible saturation concept has also been used, with S_{irr} typically being taken as $S_{irr} \simeq 0.1$ [58, 44]. Whereas the irreducible saturation concept may provide a good approximation to the conditions in soil, it has some rather undesirable consequences when it comes to hygroscopic materials such as wood. Thus, all experimental evidence, see e.g. [62], points to a rather smooth transition between the hygroscopic and partially saturated states and the effective transfer coefficient should thus be equally smooth. On the other hand, if the irreducible saturation concept is adopted, there exists a range above the fiber saturation point and below the irreducible saturation point where all water transfer takes place solely as vapour diffusion/convection. Since in this range the equilibrium vapour pressure is very close to the saturated vapour pressure, no significant gradients in vapour pressure exist and the transfer by this mode is not nearly enough to account for the smooth transition between the hygroscopic and partially saturated states observed experimentally.

Whereas the relative permeabilities (3.34) do not make explicit reference to an irreducible saturation point, the variation of the relative permeabilities with saturation is so extreme, that a de facto irreducible saturation point is created. This can be seen by the effective transfer coefficients

$$\mathbf{K}_{eff} = \rho_w \frac{\mathbf{K}_r \mathbf{K}_{rw}}{\mu_w} \left(\frac{\partial p_c}{\partial W} \right) \quad (3.37)$$

which have been plotted in Figure 3.7 for different expressions of the relative permeability (each curve has been normalized with respect to the value at $W = 1.2$). As can be seen the effective transfer coefficient in the case where $K_r = S^8$ practically disappears around $W = 0.6$, whereas the limit at which the transfer becomes negligible gradually decreases as the polynomial exponent in the expression for the relative permeability decreases. Thus, a de facto irreducible saturation point is created, e.g. for $K_r = S^8$ around $W = 0.6$. This fact, which has also been pointed out by Couture et al. [12], is reflected in the corresponding simulations, e.g. those concerning drying, in a way which is regarded unrealistic. Examples of this are shown in Figures 3.8–3.10 where the relative permeabilities

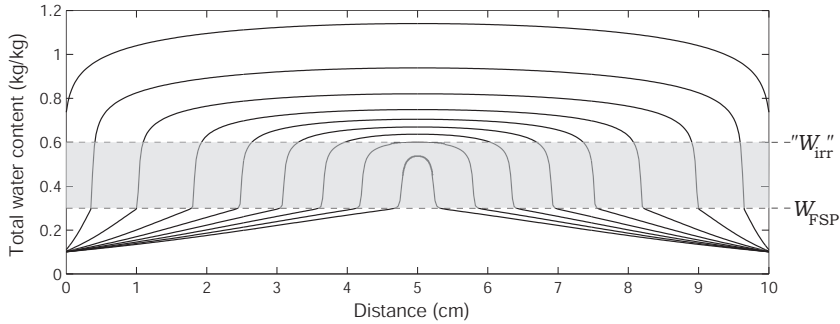


Figure 3.8 Simulated one dimensional drying profiles with $K_{rw} = S^8$ corresponding to longitudinal transfer.

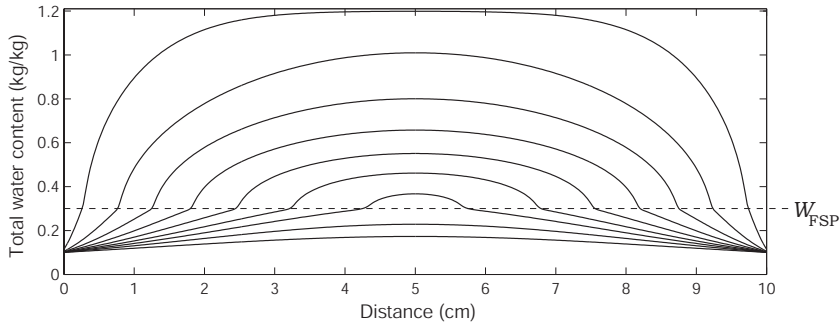


Figure 3.9 Simulated one dimensional drying profiles with $K_{rw} = S^3$ corresponding to tangential transfer.

corresponding to the effective transfer coefficients shown in Figure 3.7 have been used in a one-dimensional drying simulation.

The figures show the drying profiles at different times and as can be seen the results for $K_r = S^8$ display a characteristic jump extending from the fiber saturation point and to around $W = 0.6$. For $K_r = S^3$ the profiles look more realistic, whereas quite a smooth transition is achieved for $K_r = S^2$. For the last two simulations also the bound water and vapour diffusivities play a role in achieving this smooth transition, whereas the principal character of the profiles for K_r cannot be altered unless grossly unrealistic values of the bound water and water vapour diffusivities are assumed.

To account in more detail for the mechanisms of water transfer at low degrees of saturation Goyeneche et al. [24, 25] have recently proposed a film-flow model for free water below a certain saturation. With this model they were able to compute the corresponding relative permeabilities such that the usual model could be applied directly. Furthermore, experiments on ideal capillaries seems to verify the model.

Thus, it seems that there is physical justification for assuming transport of free water in

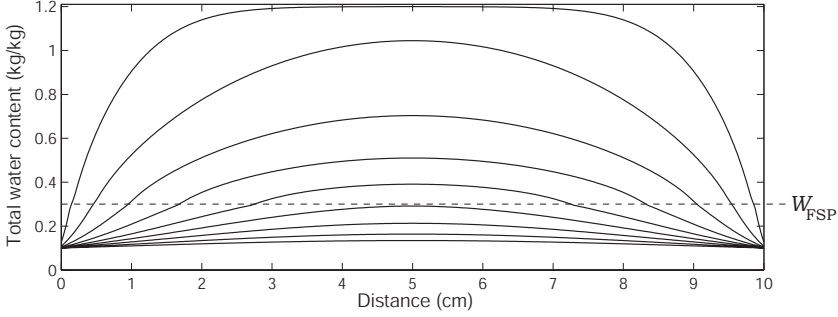


Figure 3.10 Simulated one dimensional drying profiles with $K_{rw} = S^2$.

the entire range of the partially saturated conditions. As a minimum the relative permeabilities should reflect this, and thus, the simple functional relationship $K_r = S^\alpha$ seems to be inappropriate for large values of α .

Fully saturated conditions

Under fully saturated conditions the water pressure is a variable in its own right. In order to properly include the effects of this pressure, the water and porous medium compressibility should be considered. The general free water conservation equation without any sinks or sources can be written as

$$\frac{\partial}{\partial t}(\varphi \rho_w S) + \nabla \cdot (\rho_w \mathbf{v}_w) = 0 \quad (3.38)$$

where φ is the porosity and S the degree of saturation. Under partially saturated conditions the porosity and the density of water are usually assumed constant. However, compressibility can be included by the following linear relations [18]

$$\rho_w = \rho_w^\circ (1 + c_w(p_w - p_w^\circ)) \quad (3.39)$$

$$\varphi = \varphi^\circ (1 + c_m(p_w - p_w^\circ)) \quad (3.40)$$

where c_w is the water compressibility, c_m the porous medium compressibility, and ρ_w° and φ° reference values at the pressure p_w° . The accumulation term can now be expanded as

$$\frac{\partial}{\partial t}(\varphi \rho_w S) = A \frac{\partial S}{\partial t} + B \frac{\partial p_w}{\partial t} \quad (3.41)$$

where

$$A = \varphi^\circ \rho_w^\circ [1 + c_m c_w (p_w - p_w^\circ)^2 + c_m (p_w - p_w^\circ) + c_w (p_w - p_w^\circ)] \quad (3.42)$$

$$B = \varphi^\circ \rho_w^\circ S [c_m + c_w + 2c_m c_w (p_w - p_w^\circ)] \quad (3.43)$$

Now, since $c_m(p_w - p_w^\circ) \ll 1$ and $c_w(p_w - p_w^\circ) \ll 1$, an approximate governing equation taking compressibility effects into account can be written as

$$\varphi^\circ \rho_w^\circ \frac{\partial S}{\partial t} + \varphi^\circ \rho_w^\circ S (c_m + c_w) \frac{\partial p_w}{\partial t} + \nabla \cdot (\rho_w \mathbf{v}_w) = 0 \quad (3.44)$$

where the term $\nabla \cdot (\rho_w \mathbf{v}_w)$ can be simplified in a similar way.

In the case of wood it is hard to find applications where compressibility effects play any significant role. However, the presence of a pressure accumulation term usually makes the numerical solution procedures more stable. Furthermore, it can be shown that (3.44) supplemented with prescribed flux boundary conditions is non-unique unless some compressibility is assumed [30].

3.5 The enthalpy equation

The equations (3.4) describing the conservation of mass should be supplemented with an equation describing the conservation of enthalpy. This equation takes three phenomena into account. Firstly, the usual conduction of heat described by Fourier's law. Secondly, the changes in enthalpy resulting from change of phase, i.e. sorption, evaporation and condensation. And finally, the convective transfer of heat, i.e. the effect that heat is carried in the mass flux.

In the following we will compare two different formulations of the enthalpy equation, the conventional and an alternative formulation. Although equivalent, they each have advantages as well as disadvantages. Whereas the conventional formulation is quite instructive it is inconvenient when it comes to numerical implementation. On the other hand, the alternative formulation is less instructive, but much more convenient from a numerical implementation point of view.

3.5.1 Conventional formulation

The finite element formulation of enthalpy conservation, see e.g. [20, 22, 53, 21], typically begins by stating the governing equation [67, 69]

$$\underbrace{\rho C_p \frac{\partial T}{\partial t}}_{\text{accumulation}} + \underbrace{\Delta h_{\text{vap}} \dot{m}_{\text{wv}} + \Delta h_{\text{sorp}} \dot{m}_{\text{bv}}}_{\text{heat of evaporation and sorption}} + \underbrace{(c_{\text{pw}} \rho_w \mathbf{v}_w + c_{\text{pb}} \rho_b \mathbf{v}_b + c_{\text{pv}} \rho_v \mathbf{v}_v + c_{\text{pa}} \rho_a \mathbf{v}_a) \cdot \nabla T}_{\text{convection}} = \underbrace{\nabla \cdot (\mathbf{k}_T \nabla T)}_{\text{conduction}} \quad (3.45)$$

where

$$\rho C_p = \varepsilon_s \rho_s c_{\text{ps}} + \varepsilon_w \rho_w c_{\text{pw}} + \varepsilon_g \rho_v c_{\text{pv}} + \varepsilon_g \rho_a c_{\text{pa}} \quad (3.46)$$

Again we have supplemented the equation given in [67, 69] with the appropriate terms accounting for the bound water phase. The equation (3.45) is intuitively clear. From usual linear heat conduction we immediately recognize the accumulation term, now comprised

of the densities and capacities of the different phases, and the conduction term on the right hand side. Also, latent heat effects and convective transfer enter into the heat balance in a natural way which is well known from standard heat conduction.

Let's now take a look at how the conservation equation is derived. The general multi-phase enthalpy conservation equation is given by

$$\begin{aligned} \frac{\partial}{\partial t}(\varepsilon_s \rho_s h_s + \varepsilon_w \rho_w h_w + \varepsilon_w \rho_w h_w + \varepsilon_g \rho_v h_v + \varepsilon_g \rho_a h_a) + \\ \nabla \cdot (\rho_w h_w \mathbf{v}_w + \rho_b h_b \mathbf{v}_b + \rho_v h_v \mathbf{v}_v + \rho_a h_a \mathbf{v}_a) = \nabla \cdot (\mathbf{k}_T \nabla T) \end{aligned} \quad (3.47)$$

where we have already used Fourier's law for the diffusive heat flux. Expansion of the accumulation and convection terms yields

$$\begin{aligned} \varepsilon_s \rho_s \frac{\partial h_s}{\partial t} + \\ h_w \frac{\partial}{\partial t}(\varepsilon_w \rho_w) + \varepsilon_w \rho_w \frac{\partial h_w}{\partial t} + h_w \nabla \cdot (\rho_w \mathbf{v}_w) + \rho_w \mathbf{v}_w \cdot \nabla h_w + \\ h_b \frac{\partial}{\partial t}(\varepsilon_s \rho_b) + \varepsilon_s \rho_b \frac{\partial h_b}{\partial t} + h_b \nabla \cdot (\rho_b \mathbf{v}_b) + \rho_b \mathbf{v}_b \cdot \nabla h_b + \\ h_v \frac{\partial}{\partial t}(\varepsilon_g \rho_v) + \varepsilon_g \rho_v \frac{\partial h_v}{\partial t} + h_v \nabla \cdot (\rho_v \mathbf{v}_v) + \rho_v \mathbf{v}_v \cdot \nabla h_v + \\ h_a \frac{\partial}{\partial t}(\varepsilon_g \rho_a) + \varepsilon_g \rho_a \frac{\partial h_a}{\partial t} + h_a \nabla \cdot (\rho_a \mathbf{v}_a) + \rho_a \mathbf{v}_a \cdot \nabla h_a = \nabla \cdot (\mathbf{k}_T \nabla T) \end{aligned} \quad (3.48)$$

This equation can now be simplified by substituting the right hand sides of the mass conservation equations (3.4) into (3.48). This gives

$$\begin{aligned} \varepsilon_s \rho_s \frac{\partial h_s}{\partial t} + \varepsilon_w \rho_w \frac{\partial h_w}{\partial t} + \varepsilon_s \rho_b \frac{\partial h_b}{\partial t} + \varepsilon_g \rho_v \frac{\partial h_v}{\partial t} + \varepsilon_g \rho_a \frac{\partial h_a}{\partial t} + \\ \dot{m}_{wv}(h_v - h_w) + \dot{m}_{bv}(h_v - h_b) + \dot{m}_{wb}(h_b - h_w) + \\ \rho_w \mathbf{v}_w \cdot \nabla h_w + \rho_v \mathbf{v}_v \cdot \nabla h_v + \rho_a \mathbf{v}_a \cdot \nabla h_a = \nabla \cdot (\mathbf{k}_T \nabla T) \end{aligned} \quad (3.49)$$

We now assume a *linear* relationship between enthalpy and temperature¹ given by

$$h_\alpha = h_\alpha^\circ + c_{p\alpha}(T - T^\circ), \quad \alpha = s, w, b, v, a \quad (3.50)$$

and furthermore, assume local thermal equilibrium, i.e.

$$T_\alpha = T, \quad \alpha = s, w, b, v, a \quad (3.51)$$

¹This assumption (R4, p. 130 in [67]) which is a cornerstone in arriving at the final result (3.45) may be circumvented as shown in Section 3.5.2.

The heat of vaporization is defined as

$$\Delta h_{\text{vap}} = h_v - h_w = h_v^\circ - h_w^\circ + (c_{\text{pw}} - c_{\text{pv}})(T - T^\circ) \quad (3.52)$$

where $^\circ$ refers to some reference state, e.g. $T^\circ = 298 \text{ K}$ at which $h_w^\circ = -1,588 \text{ kJ/kg}$ and $h_v^\circ = -1,343 \text{ kJ/kg}$. The heat of sorption is defined as

$$\Delta h_{\text{sorp}} = h_v - h_b = h_v^\circ - h_b^\circ + (c_{\text{pb}} - c_{\text{pv}})(T - T^\circ) \quad (3.53)$$

As for the remaining term describing the transition of bound water to free water and vice versa, we will assume

$$\dot{m}_{\text{wb}}(h_b - h_w) = 0 \quad (3.54)$$

This assumption is quite reasonable, since if any such transition of bound water to free water or vice versa takes place, then it will take place in the vicinity of the fiber saturation point where, by definition, $h_b = h_w$.

With these definitions of enthalpy and heat of evaporation and sorption, we arrive at the final form of the governing equation (3.45). Although (3.45) is very instructive it leads to a rather complicated finite element implementation. This is primarily due to the convective term. The matrix-vector form of this term will be of the type

$$(c_{\text{pw}}\rho_w\mathbf{v}_w + \dots) \cdot \nabla T \sim \mathbf{K}_c \mathbf{T} \quad (3.55)$$

where \mathbf{K}_c will look something like

$$\mathbf{K}_c = \int_{\Omega} \mathbf{N}^T (\rho_w h_w \mathbf{v}_w + \rho_b h_b \mathbf{v}_b + \rho_v h_v \mathbf{v}_v + \rho_a h_a \mathbf{v}_a) \nabla \mathbf{N} \, d\Omega \quad (3.56)$$

where the velocities are to be determined on the basis of the gradients of the driving forces. Thus, (3.56) can be written principally as

$$\mathbf{K}_c = \int_{\Omega} \mathbf{N}^T [(\mathbf{k}_w \nabla \mathbf{N} \mathbf{p}_w)^T + (\mathbf{k}_b \nabla \mathbf{N} \mathbf{W}_b)^T + (\mathbf{k}_v \nabla \mathbf{N} \mathbf{p}_v)^T + (\mathbf{k}_a \nabla \mathbf{N} \mathbf{p}_a)^T] \nabla \mathbf{N} \, d\Omega \quad (3.57)$$

This form is most inconvenient, first of all because it is unsymmetric and secondly, because there are significant difficulties involved with determining the derivatives

$$\frac{\partial}{\partial \mathbf{T}} (\mathbf{K}_c(P_w, W_b, P_v, P_a, T, \dots) \mathbf{T}) \quad (3.58)$$

needed in an iterative solution scheme. Moreover, in reality the bound water enthalpy is not only a function of temperature, but also of bound water content. Also the appearance of the source terms $\dot{m}_{\alpha\beta}$ in the equation is inconvenient, i.e. if the total water transfer assumption is made, these have to be substituted for the appropriate mass conservation equations.

These difficulties motivate the alternative form of the governing equation discussed in the following.

3.5.2 Alternative formulation

The starting point is again the general conservation equation

$$\begin{aligned} \frac{\partial}{\partial t}(\varepsilon_s \rho_s h_s + \varepsilon_w \rho_w h_w + \varepsilon_b \rho_b h_b + \varepsilon_g \rho_v h_v + \varepsilon_g \rho_a h_a) + \\ \nabla \cdot (\rho_w h_w \mathbf{v}_w + \rho_b h_b \mathbf{v}_b + \rho_v h_v \mathbf{v}_v + \rho_a h_a \mathbf{v}_a) = \nabla \cdot (\mathbf{k}_T \nabla T) \end{aligned} \quad (3.59)$$

We now simply define the enthalpies as being functions of an arbitrary number of state variables

$$h_\alpha = h_\alpha(W_f, W_b, T, \dots), \quad \alpha = s, w, b, v, a \quad (3.60)$$

Next, we define a new variable

$$H = \varepsilon_s \rho_s h_s + \varepsilon_w \rho_w h_w + \varepsilon_b \rho_b h_b + \varepsilon_g \rho_v h_v + \varepsilon_g \rho_a h_a \quad (3.61)$$

such that the governing equation can be written principally as

$$\frac{\partial H}{\partial t} + \nabla \cdot (\mathbf{k}_w \nabla p_w + \mathbf{k}_b \nabla W_b + \mathbf{k}_v \nabla p_v + \mathbf{k}_a \nabla p_a) = \nabla \cdot (\mathbf{k}_T \nabla T) \quad (3.62)$$

Thus, we are left with the well-known symmetric conductive terms which can be easily handled.

The alternative governing equation is of a so-called mixed type in that the accumulation term must be related to the other state variables such as temperature through the enthalpy-temperature relation. However, rather than expanding the continuous form of the governing equation in a number of chosen state variables, the link between the different variables is not made until the discrete form of (3.62) has been set up. The solution of such equations is discussed in detail in Chapter 7.

3.5.3 Summary of governing equations

Below the final form of the governing equations are given.

Total water:

$$\frac{\partial C_w}{\partial t} = \nabla \cdot [\mathbf{K}_{tw} \nabla (p_w + \rho_w g z) + \mathbf{K}_{tb} \nabla W_b + \mathbf{K}_{tv} \nabla p_v + \mathbf{K}_{ta} \nabla p_a] \quad (3.63)$$

$$C_w = \rho_0 (W_f + W_b) + \varphi \left(1 - \frac{\rho_0 W_f}{\rho_w \varphi} \right) \frac{p_v M_v}{RT} \simeq \rho_0 (W_f + W_b)$$

$$\mathbf{K}_{tw} = \rho_w \frac{\mathbf{K}_w \mathbf{K}_{rw}}{\mu_w}$$

$$\mathbf{K}_{tb} = \rho_0 \mathbf{D}_b \quad (3.64)$$

$$\mathbf{K}_{tv} = \frac{p_v M_v}{RT} \frac{\mathbf{K}_g \mathbf{K}_{rg}}{\mu_g} + \frac{M_v M_a p_a}{RT (M_v p_v + M_a p_a)} \mathbf{D}_{\text{eff}}$$

$$\mathbf{K}_{ta} = \frac{p_v M_v}{RT} \frac{\mathbf{K}_g \mathbf{K}_{rg}}{\mu_g} - \frac{M_v M_a p_v}{RT (M_v p_v + M_a p_a)} \mathbf{D}_{\text{eff}}$$

Dry air:

$$\frac{\partial C_a}{\partial t} = \nabla \cdot [\mathbf{K}_{aa} \nabla p_a + \mathbf{K}_{av} \nabla p_v] \quad (3.65)$$

$$\begin{aligned} C_a &= \varphi \left(1 - \frac{\rho_0 W_f}{\rho_w \varphi} \right) \frac{p_a M_a}{RT} \\ \mathbf{K}_{aa} &= \frac{p_a M_a}{RT} \frac{\mathbf{K}_g \mathbf{K}_{rg}}{\mu_g} + \frac{M_v M_a p_v}{RT(M_v p_v + M_a p_a)} \mathbf{D}_{\text{eff}} \\ \mathbf{K}_{av} &= \frac{p_a M_a}{RT} \frac{\mathbf{K}_g \mathbf{K}_{rg}}{\mu_g} - \frac{M_v M_a p_a}{RT(M_v p_v + M_a p_a)} \mathbf{D}_{\text{eff}} \end{aligned} \quad (3.66)$$

Enthalpy:

$$\frac{\partial H}{\partial t} = \nabla \cdot (K_{hw} \nabla p_w + \mathbf{K}_{hb} \nabla W_b + \mathbf{K}_{hv} \nabla p_v + \mathbf{K}_{ha} \nabla p_a + \mathbf{K}_{hh} \nabla T) \quad (3.67)$$

$$H = \rho_0 h_s + W_f h_w + W_b h_b + \varphi \left(1 - \frac{\rho_0 W_f}{\rho_w \varphi} \right) \frac{p_v M_v}{RT} h_v + \varphi \left(1 - \frac{\rho_0 W_f}{\rho_w \varphi} \right) \frac{p_a M_a}{RT} h_a$$

$$\mathbf{K}_{hw} = h_w \mathbf{K}_{tw}$$

$$\mathbf{K}_{hb} = h_b \mathbf{K}_{tb}$$

$$\mathbf{K}_{hv} = h_v (\mathbf{K}_{tv} + \mathbf{K}_{av})$$

$$\mathbf{K}_{ha} = h_a (\mathbf{K}_{aa} + \mathbf{K}_{ta})$$

$$\mathbf{K}_{hh} = \mathbf{k}_T$$

(3.68)

Chapter 4

Moisture transport below the fiber saturation point

From a structural engineering point of view the transport of moisture below the fiber saturation point is perhaps the most interesting: under normal service conditions the moisture content of wooden structures will only rarely exceed the fiber saturation point and furthermore, it is below the fiber saturation point that virtually all moisture induced mechanical deformations take place. For these reasons the subproblem of moisture transport below the fiber saturation point has traditionally received far more attention than the general problem which includes also the free water transport. However, whereas the commonly applied models in many cases compare well with experiments, several severe discrepancies have also been observed. In the following some of these are described and a model is presented which to certain degree is capable of capturing the experimentally observed behaviour in adsorption. The model is described in detail in [36]

4.1 Conventional model

Traditionally the total diffusion model discussed in the previous chapter has been applied to the problem of moisture transport below the fiber saturation point. That is, the total water content is considered and the transport described by the classical diffusion equation

$$\frac{\partial C}{\partial t} = \frac{\partial}{\partial x} \left(\mathcal{D} \frac{\partial C}{\partial x} \right) \quad (4.1)$$

where C is the mass of water per unit volume and \mathcal{D} the diffusivity. Often this equation is formulated in terms of the dry base moisture content W (kg/kg) as

$$\rho_0 \frac{\partial W}{\partial t} = \frac{\partial}{\partial x} \left(\rho_0 \mathcal{D} \frac{\partial W}{\partial x} \right) \quad (4.2)$$

or in terms the equilibrium relative humidity H as

$$\rho_0 \left(\frac{dW}{dH} \right) \frac{\partial H}{\partial t} = \frac{\partial}{\partial x} \left[\rho_0 \left(\frac{dW}{dH} \right) \mathcal{D} \frac{\partial H}{\partial x} \right] \quad (4.3)$$

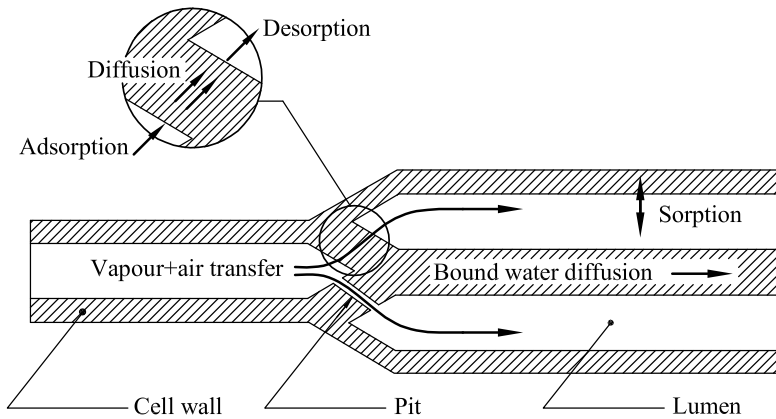


Figure 4.1 Mechanisms of moisture transport below the fiber saturation point.

where dW/dH is the slope of the sorption isotherm.

As discussed in the previous chapter this model makes use of the assumption that the different water phases, i.e. in this case water vapour and bound water, are in equilibrium and can be treated as one entity.

4.2 Mechanisms of moisture transport

The overall mechanism of moisture transport in wood below the fiber saturation point can be divided into three parts as sketched in Figure 4.1. First of all, within the solid skeleton which forms a coherent network, a transport of bound water is possible. The transport of this has been quantified by Stamm [59] in terms of diffusion with bound water content as driving force. Secondly, a transport of water within the cellular structure is possible. As described in the previous chapter, there is some uncertainty as to the pathways of this vapour transport. Nevertheless, that water vapour is transported is an indisputable fact, and as a good approximation, at least under moderated temperatures and isothermal conditions, it can be assumed that this transport is also of a diffusive nature. The last contribution to the overall behaviour is the sorption mechanism linking the bound water and the water vapour. It can easily be imagined that the vapour pressure in the lumens is not necessarily in equilibrium with the bound water content of the wood substance. However, as the sorption isotherm dictates the conditions will progress towards an equilibrium state, and the water which must then necessarily be exchanged between the cell wall and the lumen is accounted for by the sorption mechanism.

The applicability of the conventional model then rests upon the time scale associated with the sorption mechanism. If sorption takes place at a much faster rate than any of the other processes, such that a state of non-equilibrium is immediately compensated for, then the exact nature of the sorption mechanism is of no importance for the overall problem. In

this case it is rather the diffusion of bound water and water vapour which governs the process. If, on the other hand, sorption is extremely slow, then the importance of water vapour transport diminishes in the sense that as long as the vapour transfer is of rate such that in adsorption vapour is always available at the sorption sites, and in desorption, is transported away immediately, then the sorption will govern the overall behaviour.

What makes the problem of moisture transport in wood below the fiber saturation point interesting is that the overall behaviour lies somewhere in between these two extremes.

4.3 Experimental results

In the late fifties and early sixties Christensen and Kelsey [5, 8, 7, 6] carried out a number of adsorption experiments, which displayed some extreme anomalies that could not be explained in terms of diffusion or any other known mechanisms. The experiments were conducted on single cell walls and other very thin slices of wood in an environment of pure vapour, i.e. before the experiments were initiated atmospheric air was evacuated from the sorption chamber. Under these experimental conditions several factors which would be assumed to affect the behaviour of gross wood can be eliminated. First of all, the diffusion of water vapour within the wooden cellular structure is irrelevant, and since the experiments were conducted in an environment of pure vapour, the boundary layer usually present between the wood and surrounding atmosphere was non-existent. Thus, the experiments can be regarded as being most ideal in terms of quantifying the sorption behaviour of the wood substance itself. For this subproblem the diffusion equation could again be assumed valid. However, the experimental results immediately ruled this out since the time scale of the experiments were largely independent of the length of the samples, and since a number of phenomena not in any way compatible with diffusion were observed.

The most noticeable of these was that when a sample in equilibrium with a given relative humidity was subjected to an abrupt increase in relative humidity, then the approach to equilibrium seemed to depend on magnitude of the relative humidity change, and this in a way that the smaller the step was, the slower was the approach to equilibrium, see [36] for a detailed discussion.

More recently, Wadsö [66] has shown that also for larger samples does the cell wall sorption influence the behaviour in a way such that a model, which somehow accounts for the sorption on the cell wall level is necessary.

The different responses not describable in terms of the total moisture diffusion model (4.1) are often labeled non-Fickian or anomalous. This includes sorption curves which display abrupt changes not usually seen in diffusion experiments, apparently sample length dependent diffusion coefficients, and results which display a significant dependence upon the magnitude of the step change in relative humidity.

A simple and rigorous test of the applicability of diffusion models such as (4.1) consists of performing the same one-dimensional sorption experiment on samples of different length, see Figure 4.2. When the fractional weight increase is plotted as function of the square root of time divided by the respective sample lengths, the resulting curves should be superimposed on one another [13], even if the diffusivity is a function of the moisture

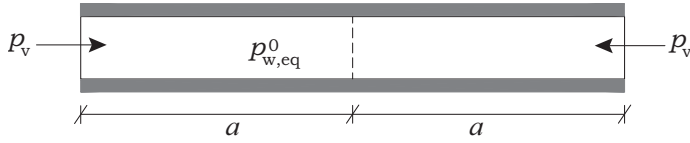


Figure 4.2 One dimensional sorption experiment.

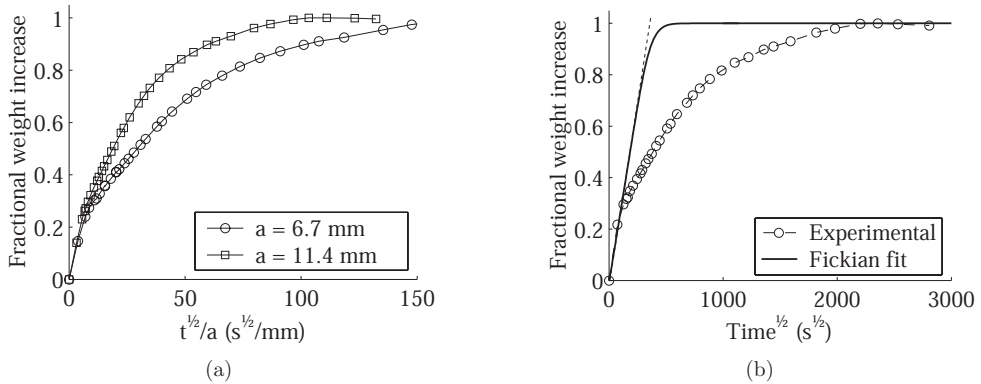


Figure 4.3 Failure of Fickian models.

content¹. Examples of such a curves are shown in Figure 4.3 (a). Two samples with half-lengths of $a = 6.7$ mm and $a = 11.4$ mm are initially in equilibrium with 75% RH after which they are subjected to a step increase to 84% RH. As can be seen, the resulting curves are far from superimposed. Moreover, the shape of the fractional weight increase curves are very uncharacteristic of diffusion. Here one would expect an initially linear curve, with the slope gradually decreasing from around $E = 0.7$, with E being the fractional weight increase. In Figure 4.3 (b) the difficulties in quantifying the non-Fickian behaviour in terms of a diffusion model are illustrated. If the initial slope is used as a basis for determining the diffusion coefficient, the solid curve results. As can be seen, the experimental results are fitted very poorly and the abrupt change in slope which occurs around $E = 0.25$ is not captured at all.

4.4 The new model

The new model developed for moisture transport below the fiber saturation point begins by separating the bound water and water vapour and then describing the transport of

¹This follows from the well-known Boltzmann transformation by which the concentration as function of position and time is expressed in terms of one variable $\xi = xt^{-\frac{1}{2}}$.

these by two coupled equations, in the one dimensional case given by

$$\begin{aligned}\frac{\partial C_w}{\partial t} &= \frac{\partial}{\partial x} \left(\mathcal{D}_w \frac{\partial C_w}{\partial x} \right) + \dot{m} \\ \frac{\partial C_v}{\partial t} &= \frac{\partial}{\partial x} \left(\mathcal{D}_v \frac{\partial C_v}{\partial x} \right) - \dot{m}\end{aligned}\tag{4.4}$$

where C_w is the bound water content, C_v the vapour content, and \mathcal{D}_w and \mathcal{D}_v the bound water and water vapour diffusivities respectively. The coupling term, i.e. the sorption term, is given by \dot{m} .

4.4.1 The sorption term

Whereas the necessity of separating the phases has previously been recognized by a number of authors, see e.g. [1, 14, 52], less attention has been paid to the sorption term. This is usually taken as something to the effect of

$$\dot{m} = \frac{dm}{dt} = h(p_v - p_{w,eq})\tag{4.5}$$

where $p_{w,eq}$ is the equilibrium vapour pressure corresponding to the current bound water content, p_v the lumen vapour pressure, and h a sorption constant. However, as is shown in [36], with the use of a constant h it is not possible to reproduce some of the basic experimental facts, such as the influence of the magnitude of the sorption step. Rather, it is shown that h should depend on at least two parameters: the absolute moisture content and some measure of the proximity to equilibrium. This latter quantity was chosen as the ratio of the equilibrium vapour pressure $p_{w,eq}$ to the actual vapour pressure p_v such that

$$h = h(C_w, p_{w,eq}/p_v)\tag{4.6}$$

A full discussion as to how h should vary with these two parameters is given in [36].

4.5 Results

In [36] the model was calibrated to fit a set of eight sorption experiments previously published by Wadsö [66]. These experiments displayed various degrees of anomalous sorption behaviour and were all fitted very well using reasonable and consistent assumptions about the sorption term and water vapour and bound water diffusivities. In the following a few other examples of its application are given.

4.5.1 Apparent diffusivities

A one dimensional adsorption experiment can be used to determine the diffusion coefficient of the total moisture diffusion model (4.1). The experiment proceeds by subjecting a one dimensional sample in equilibrium with some vapour pressure to a higher vapour pressure at the ends of the sample, see Figure (4.2). Using the moisture content per unit volume

of gross wood as potential the diffusion coefficient may be computed using the formula, see [13],

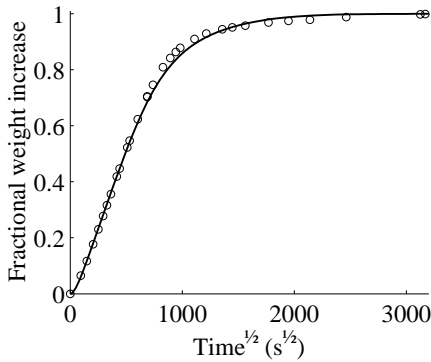
$$D = \frac{\pi a^2}{4} \left(\frac{dE}{d\sqrt{t}} \right)^2 \quad (4.7)$$

where a is the half-length of the sample, E is the fractional weight increase, and $dE/d\sqrt{t}$ is taken as the initial slope of the sorption curve. In the following the influence on the sample length is examined by computing apparent diffusion coefficients. This is done for two steps in relative humidity: 54% to 75% and 75% to 84% for the longitudinal and tangential directions. Since for small samples the slope of the sorption curve may vary quite considerably within the first few percent of relative moisture uptake, the time to half sorption has been used to define the slope in (4.7), i.e. the diffusion coefficient is computed as

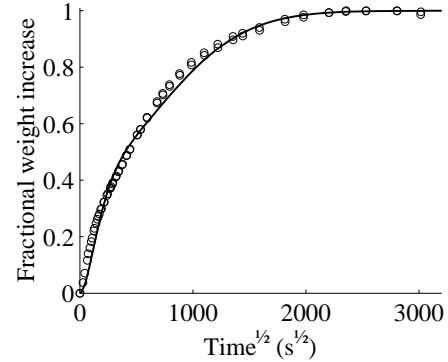
$$D = \frac{\pi a^2}{16 t_{0.5}} \quad (4.8)$$

where $t_{0.5}$ is the time at which $E = 0.5$. Typical examples of fractional weight increase versus square root of time curves are shown in Figure 4.4.

The overall sorption behaviour is governed by a combination of water vapour diffusion and cell wall sorption. Whereas the time scale associated with the vapour diffusion is sample length dependent as predicted by the diffusion equation, the sorption is independent of length. Therefore, when computing apparent diffusivities as described above, these can be expected to display a variation with sample length which is not compatible with diffusion. Examples of this is shown in Figure 4.5. It should be emphasized that for small samples the apparent diffusion coefficients are non-physical quantities incapable of describing the moisture transfer. Thus, the variation of the apparent diffusion coefficients with sample length should only be seen as an approximate measure of the relative importance of



(a) $a = 8.1$ mm, flow in tangential direction, RH = 54% \rightarrow 75%.



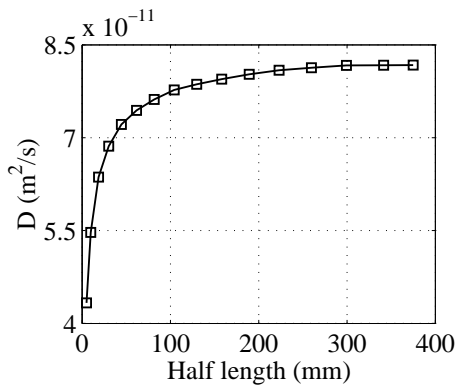
(b) $a = 11.4$ mm, flow in tangential direction, RH = 75% \rightarrow 84%.

Figure 4.4 Computed (—) and experimental [66] sorption curves (o).

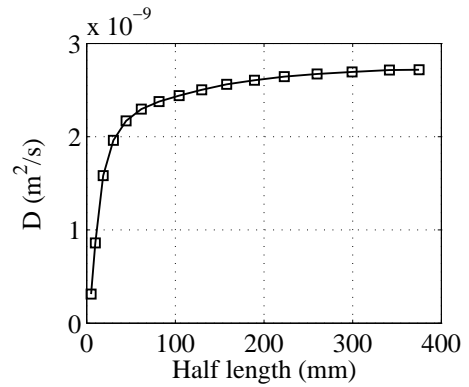
gaseous vapour transfer compared to cell wall sorption. As seen from the figure the sample length effect is more pronounced at higher humidities where the resistance to cell wall sorption is relatively greater than at lower humidities. Furthermore, for both steps the apparent diffusion coefficients attain constant values more rapidly in the case of tangential moisture transfer, since the relatively low vapour diffusion coefficients in this direction tend to govern the overall sorption behaviour.

4.5.2 Two-dimensional transfer

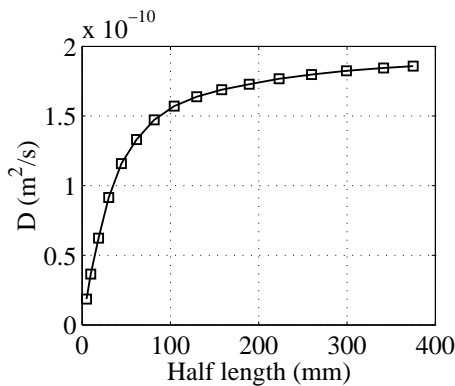
The model presented in the preceding is easily extended to two and three spatial dimensions. In the following sorption experiment on a two dimensional orthotropic sample is considered. The sample, see Figure 4.6, has a length/width ratio of 2 and combined tan-



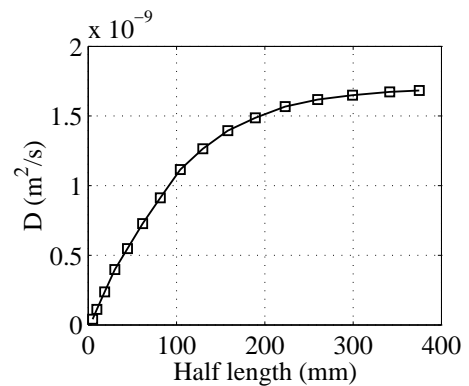
(a) RH = 54% → 75%. Tangential.



(b) RH = 54% → 75%. Longitudinal.



(c) RH = 75% → 84%. Tangential.



(d) RH = 75% → 84%. Longitudinal.

Figure 4.5 Computed apparent diffusion coefficients

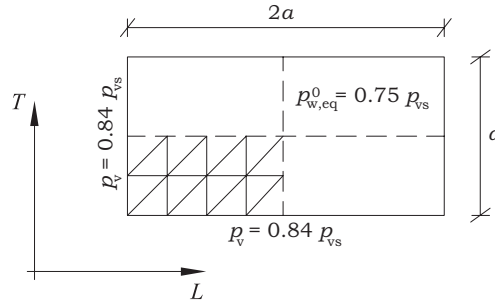


Figure 4.6 Two-dimensional wooden slab.

gential and longitudinal transfer is considered. The sample is initially in equilibrium with a vapour pressure corresponding to 75% RH. At time $t = 0$ the vapour pressure at the external surfaces is raised to 84% RH. The temperature throughout the computation is 23° C. The symmetry is exploited such that only one quarter of the slab is modeled with linear triangular elements.

In Figure 4.7 the fractional weight increase as a function of the square root of time is shown for different values of the width a . As expected the response appears Fickian with an approximately linear slope up to around $E = 0.6$ – 0.7 for large sample dimensions. However, as the dimensions decrease the characteristic "anomalous" responses observed in one-dimensional sorption experiments are recovered. This involves abrupt changes in the slope of the curves below $E = 0.5$ and subsequently, a rather slow approach to equilibrium. Also, we observe the expected characteristic that the moisture uptake becomes almost independent of sample dimensions as these become small. Thus, it is primarily for small dimensions that the non-Fickian effects are of importance, whereas for structural timber with dimensions of e.g. 5×10 cm the moisture uptake can probably in most cases be described adequately by a global diffusion equation assuming instantaneous equilibrium between vapour pressure and bound water.

4.6 Conclusions and future work

Several issues concerning the model developed still remain largely unsolved. First of all, experimental verification is needed. Here the focus should be on cell wall sorption rather than bound water and water vapour diffusion. That is, the aim of the experiments should be the determination of the sorption constant h . Ideally, this should be determined over a large range of absolute moisture contents, equilibrium proximity measures, and temperatures, air velocities etc.

Secondly, at present no satisfactory physical explanation has been given to the variation of h . In [36] it is speculated that the swelling stresses which develop as a result of sorption could be responsible for the behaviour. Although no definite conclusions can be drawn

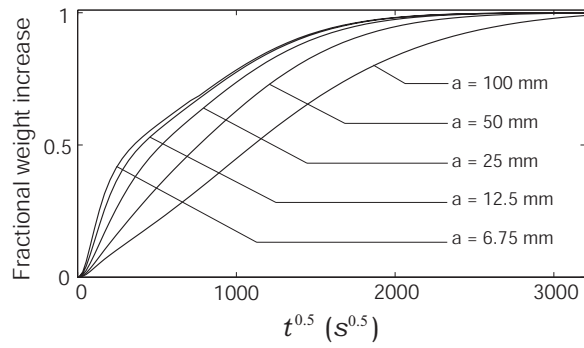


Figure 4.7 Moisture uptake for two-dimensional samples.

as to the influence of swelling stresses, it seems nevertheless, to hold some promise in producing an explanation.

Chapter 5

Moisture transport above the fiber saturation point

The flow of water in wood above the fiber saturation point is an important part of the two common industrial processes of drying and treatment with artificial preservatives. Traditionally, far more attention has been given to the former of these problems, although it is in fact the latter which presents the greater challenges.

Drying can be seen as being comprised to two different mechanisms, namely surface evaporation and internal transfer. At the exchange surface there is an evaporation of water, the rate of which depends on the surface moisture content, temperature, etc. In turn, this evaporation induces a transport of water from the internal of the wood to the exchange surface. In many practical wood drying applications, the evaporation at the surface is the dominant and rate determining mechanism. This means that the rate of drying in many cases is quite insensitive to the exact nature of the internal transfer properties, and since evaporation is much easier to quantify than internal transfer, it is not surprising that a good agreement between theory and experiment is often found.

The reverse process of infiltration is more complicated. Here the uptake of water is governed solely by the internal transfer properties, and any misrepresentation of these will be reflected directly in the computed results.

5.1 Reported anomalies

The difficulties with describing free water transport as related to infiltration are well known, see e.g. [16, 55, 2]. However, only very little effort at quantifying the behaviour seems to have been made, both experimentally as well as theoretically.

Two notable characteristics, however, have been qualitatively well described. The first of these is that in a normal sample of gross wood, water is transported more rapidly in some parts than in others [55, 2]. And secondly, the apparent permeability seems to be sample length dependent such that it decreases with increasing sample length [16, 2].

The first of these anomalies have been studied in a recent experimental study [47]. In Figure 5.1 (a) the moisture content profiles resulting from infiltration into a sample of

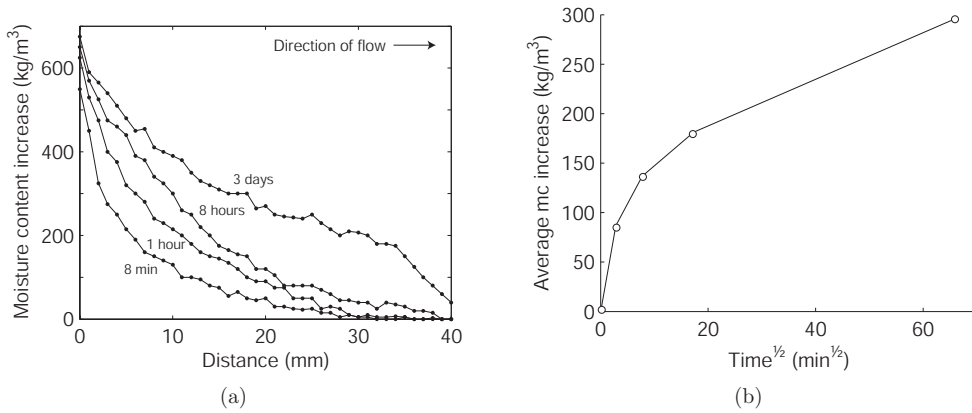


Figure 5.1 Infiltration in beech [47].

beech are shown. As can be seen the moisture content increases rapidly near the wet end whereas the following infiltration is very slow. This is clearly seen from the fractional weight increase curve, Figure 5.1 (b), which seems to display the characteristics of the water being sorbed in several different stages with the rate decreasing as the water content increases. The explanation given in [47] for this behaviour is that a portion of the water is carried very rapidly in the vessels with a simultaneous, but much slower, infiltration into the denser material surrounding the vessel. Another example of an anomalous infiltration in wood is shown in Figure 5.2 where the material is fir sapwood. These moisture content

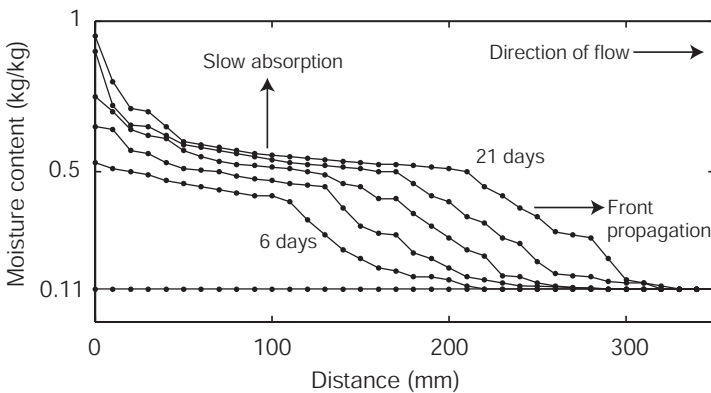


Figure 5.2 Infiltration in fir sapwood [28].

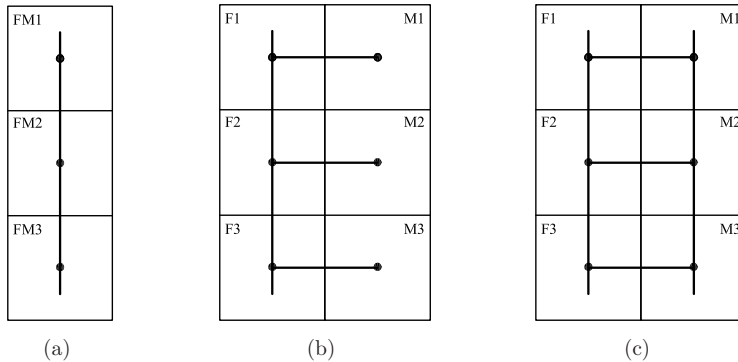


Figure 5.3 *Transport models: single continuum model (a), double-porosity model (b), and double-permeability model (c).*

profiles are particularly interesting in that they clearly reveal both the propagation of a front as well as a simultaneous slow absorption.

The characteristic that water may be carried rapidly in some parts of the wood while in other part the infiltration is much slower also manifests itself in the fact that the latewood of softwoods is more easily treated with preservatives than the earlywood [55]. This fact, which may be somewhat contradictory to what should be expected based on the structure and number of pits in earlywood and latewood cells of typical softwoods, is attributed to the fact that pit aspiration in latewood cells is much more rare than in earlywood cells. Nevertheless, regardless of the causes of the phenomenon, there seems to be two or more different levels of permeability such that water may be transported very easily through some parts of the wood and with more difficulty through other parts. In hardwoods the situation is the same. Referring to Figures 2.6 and 2.7 it is not difficult to imagine that water may be transported very rapidly through the larger vessels than through the dense material surrounding these vessels.

5.2 Double porosity and permeability models

Such considerations lead naturally to what is known as double porosity and double permeability models. These models, which are commonly applied to fractured soils, consider two zones with two different sets of flow properties. The models are illustrated in Figure 5.3 where the two zones are denoted F and M. For these two zones, two independent conservation equations are considered, such that the flow through the larger pores is described independently of the flow through the smaller pores. However, since some equilibration can be expected to take place with time, the two equations are coupled by a term accounting for the mass transfer between the two zones. In [37] the possibilities of applying such models to wood are discussed, and it is found that both for hardwoods as well as for softwoods should the models be applicable.

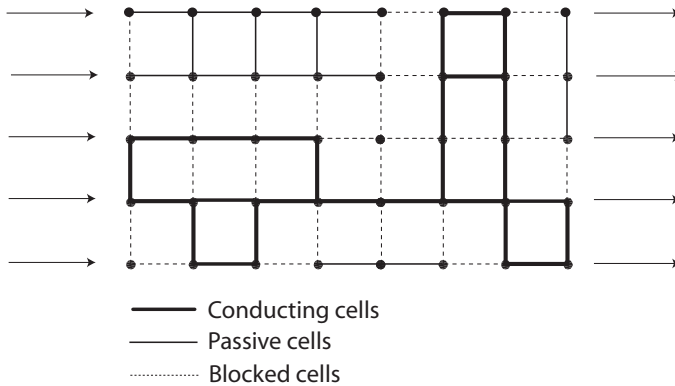


Figure 5.4 Two dimensional network model.

5.3 Length scale effects

Concerning the dependence of the apparent permeability upon the dimensions of the sample, this can be explained by the fact that in softwoods the flow of water takes place through the pits connecting the individual cells. Since during drying, an appreciable number of these pits become aspirated, it is reasonable to assume that the probability of encountering an unbroken flow path decreases with the length of this flow path. Moreover, it is entirely possible that a typical sample of wood does not constitute a coherent network, but contain internal parts with no, or very little, connection to the surface.

The proper treatment of these phenomena must necessarily be by way of statistical models accounting for the internal connectivity. A simple mechanistic model of the connectivity of softwoods is illustrated in Figure 5.4. Each branch is thought to represent a cell, and these may either have full or zero conductivity. Depending on the conductivity probability and the size of the model, i.e. the number of branches, a network which is more or less coherent is formed. As illustrated in the figure, cells with full conductivity may be cut off from the principal network such that water transport to and from these cells is impossible or very slow. This could possibly emulate the so-called wet spots often experienced in drying. Such statistical models have previously been presented in [46].

5.3.1 Example

In the following a few examples of the application of the above described model are given. In order to illustrate the length scale effect the number of cells in the transverse is kept constant and equal to $N_T = 50$ whereas the number of cells in the longitudinal direction is varied. This corresponds to considering one-dimensional samples of different lengths, but with identical cross sectional areas perpendicular to the principal direction of flow. In the following a longitudinal conductivity probability of $P_L = 0.8$ is assumed whereas the tangential is conductivity probability $P_T = 0.2$.

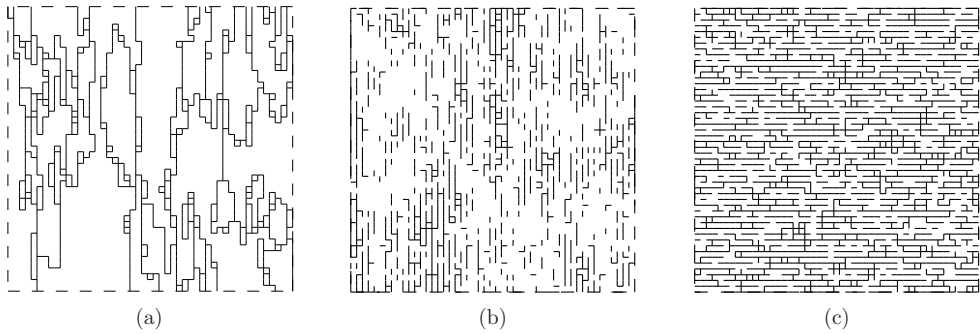


Figure 5.5 Network model with $N_L/N_T = 1.0$. Conducting cells (a), passive cells (b), blocked cells (c).

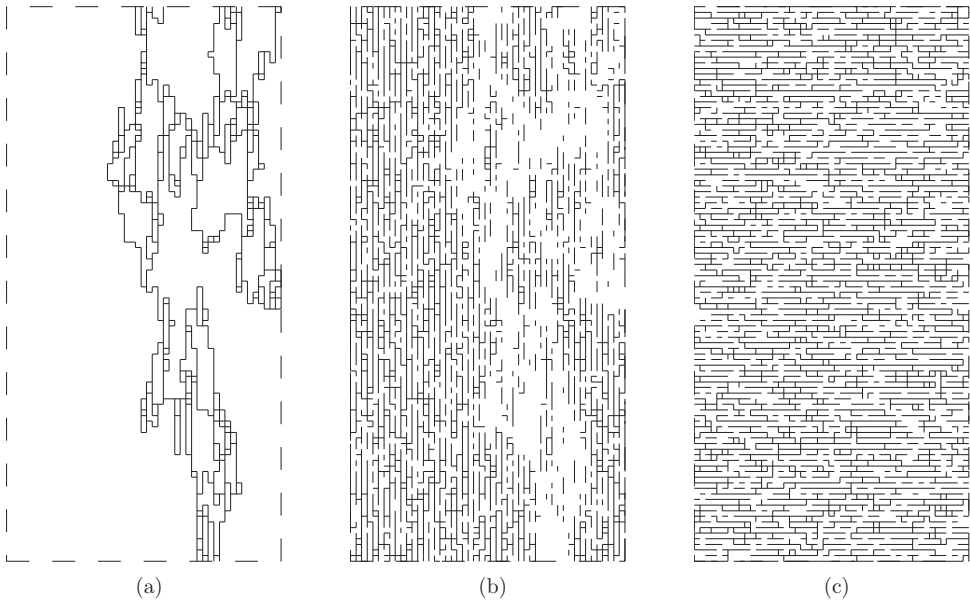


Figure 5.6 Network model with $N_L/N_T = 2.0$. Conducting cells (a), passive cells (b), blocked cells (c).

Representative examples of the simulations with different ratios of longitudinal to tangential number of cells are shown in Figures 5.5–5.7. As can be seen, the overall connectivity gradually decreases as the number of longitudinal cells increases. Also, it should be noticed that although there is a large number of cells with full longitudinal conductivity, most of these are cut off from the principal network. One of the most significant differences between the network model and the usual macroscopic model is that the transverse flow

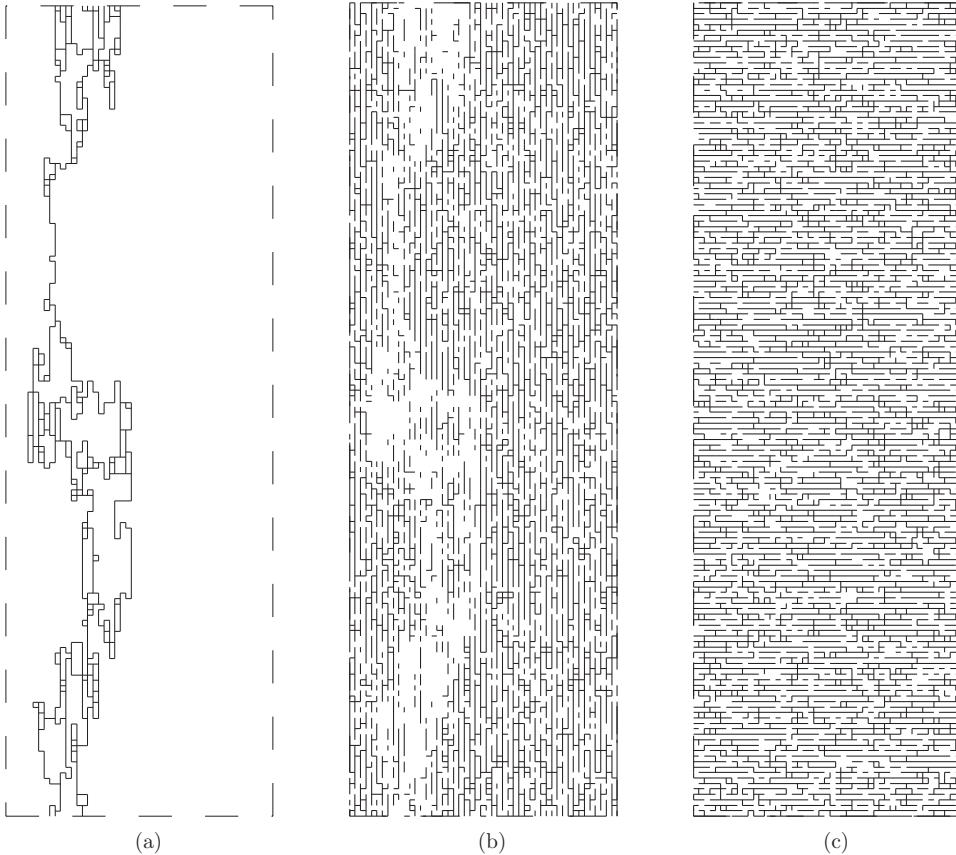


Figure 5.7 Network model with $N_L/N_T = 3.0$. Conducting cells (a), passive cells (b), blocked cells (c).

properties influence the flow in the longitudinal direction. The effect of coupling between transverse and longitudinal conductivities is illustrated in Figure 5.8 where the mean longitudinal conductivity for $N_L/N_T = 1.0$ has been plotted as function of the intrinsic longitudinal and transverse connectivity probabilities. Naturally, when $P_T = 1.0$ the intrinsic longitudinal connectivity determines the overall flow properties and conversely, when $P_T = 0.0$ the only way of transporting water is via unbroken longitudinal pathways, the probability of which are each $P_L^{N_L}$.

As can be seen, the mean longitudinal conductivity varies quite significantly for large values of P_L and small values of P_T . Thus, network models such as the one discussed in the above could perhaps be used to explain not only the flow properties of wood, but also the observed, and generally very large, variability of these.

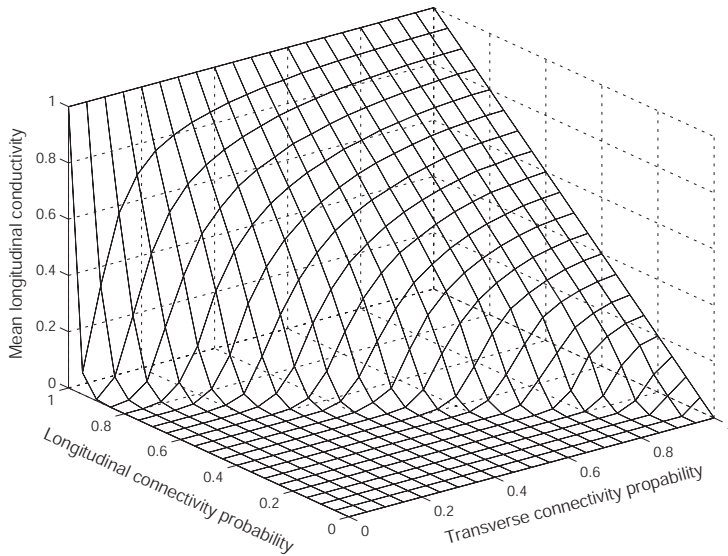


Figure 5.8 Mean longitudinal conductivity for $N_L/N_T = 1.0$.

5.4 Conclusions and future work

It appears that of the various transport problems associated with wood, it is the free water transport which is by far the most difficult to account for. And this is particularly the case in infiltration since overall process is here determined solely by the internal transfer properties, as opposed to the case of drying where the overall rate to a large extent is determined by the rate of evaporation at the exchange surfaces. In the above two different phenomena have been described and possible models have been presented. The first phenomena, namely that of the water moving along different pathways with widely different flow properties can be accounted for by double porosity and permeability models. Although these models significantly increase the overall complexity since more than twice the number of material parameters are required, there is in principle hope that these could be determined experimentally. As for the length scale effect there appears to be some difficulty at arriving at a similar general macroscopic model. Thus, as discussed, it may be necessary to incorporate statistical models in order to describe the internal transfer properties. This, however, means that the deterministic way of thinking when applying conventional models must be abandoned. Thus, in practice a computation would begin by generating a representative fluid network similar to those shown in Figures 5.5–5.7, and a simulation could then be run using a single continuum or possibly double porosity or permeability model. And this procedure would then be repeated a number of times, e.g. a hundred or a thousand times.

There are, however, two problems involved with this. First of all, the procedure is of

course much more demanding than the any of the conventional procedures in terms of time required. Secondly, the question of exactly how the generation of representative fluid should take place, i.e. what kind of input should be used, is not easy to answer, and is in fact a significant problem in itself. Therefore, a more practical approach would be to simply incorporate a length scale dependence into Darcy's law. This was done by Bramhall [3] who used a modified Darcy's law on the form

$$q = Ke^{-bL} \frac{dp}{dx} \quad (5.1)$$

where q is the flow rate, p the fluid pressure, K the permeability, b a positive constants, and L the length of a one-dimensional sample. This of course gives a correlation between sample length and overall conductivity, but it does not account for the fact that effective conductivity gradually decreases from the wet end and in towards the center of the sample. Therefore, a more appropriate relation would be

$$q = Kg(x) \frac{dp}{dx} \quad (5.2)$$

where $g(x)$ is a function which gradually decreases as x increases, e.g.

$$g(x) = e^{-bx} \quad (5.3)$$

where the constant b should then be determined experimentally. With such a relation phenomena similar to those captured by the generation of fluid networks should be possible to simulate.

Chapter 6

Towards modeling preservation processes

Usually, heat and mass transfer computations are applied to wood either in order to describe the process of drying or in order to simulate the effects of general environmental conditions such as changing temperatures and moisture content. As a natural extension of such computations the transfer of an additional species representing a wood preservative has been considered.

In the concrete case described in [34] the preservative was boron and the application was remedial treatment of wooden utility poles. That is, whereas most utility poles have usually received a primary treatment, they may later on require some additional treatment. This can be administered by drilling one or more holes into the pole from some point just above the ground surface and extending below ground towards the center of the pole, see Figure 6.1. These holes are then filled with boron in solid form which reacts easily with the water contained in the wood and is then transported throughout the pole.

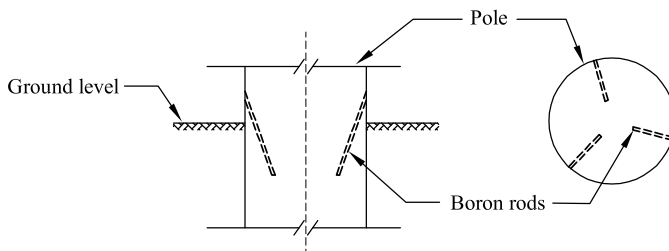


Figure 6.1 *Boron treatment of wooden poles.*

6.1 Governing equations

The major question to be answered is as to how the transport of dissolved boron takes place. We initially considered the general conservation equation

$$\frac{\partial}{\partial t}(\varphi SC) + \nabla \cdot (C\mathbf{v}_w) = -\nabla \cdot \mathbf{j} \quad (6.1)$$

where φ is the porosity, S is the water saturation, C the concentration of boron in the water, \mathbf{v}_w the free water mass average velocity, and \mathbf{j} the mass flux of boron. For diffusive boron transfer in pure water we would expect this to follow a Fickian relation given by

$$\mathbf{j} = -\mathbf{D}_0 \nabla C \quad (6.2)$$

In an isotropic porous medium we would have to reduce this by at least a factor of φS such that the effective diffusive boron flux

$$\mathbf{j} = -\varphi S \mathbf{D}_0 \nabla C \quad (6.3)$$

However, the liquid pathways in wood taken into consideration, this estimate is probably much too high, at least in the radial and tangential directions. Therefore, we use an effective boron diffusion coefficient such that the flux becomes

$$\mathbf{j} = -\varphi S \mathbf{D}_B \nabla C \quad (6.4)$$

where \mathbf{D}_B , in contrast to \mathbf{D}_0 , is not constant but varies with moisture content. In the above equation the intrinsic boron concentration C is used, i.e. the concentration of boron in the free water within the wood. If the superficial concentration $\langle C \rangle$, i.e. the mass of boron per unit volume of wood, is used then the flux is given by

$$\mathbf{j} = \mathbf{D}_B \nabla \langle C \rangle = \varphi S \mathbf{D}_B \nabla C \quad (6.5)$$

and since superficial concentration is related to the intrinsic concentration by

$$\langle C \rangle = \varphi SC \quad (6.6)$$

the governing equation can then be written either as

$$\frac{\partial}{\partial t}(\varphi SC) + \nabla \cdot (C\mathbf{v}_w) = \nabla \cdot (\varphi S \mathbf{D}_B \nabla C) \quad (6.7)$$

or as

$$\frac{\partial \langle C \rangle}{\partial t} + \nabla \cdot \left(\frac{\langle C \rangle}{\varphi S} \mathbf{v}_w \right) = \nabla \cdot (\mathbf{D}_B \nabla \langle C \rangle) \quad (6.8)$$

6.2 Simplified transport model

The description of boron transport in wooden poles is a rather complicated problem involving numerous parameters which are largely unknown, or at least very poorly described in the literature. Furthermore, there are a number of environmental parameters which

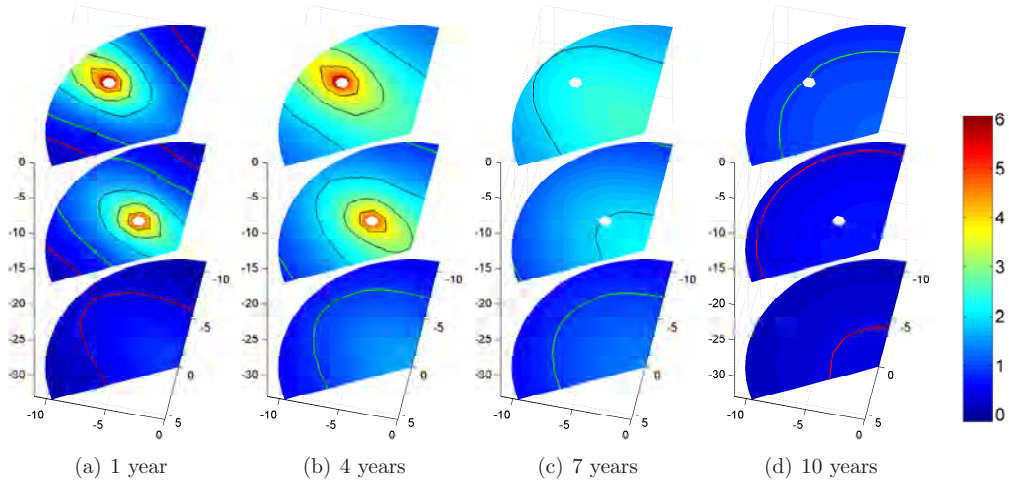


Figure 6.2 *Boron distributions. Three rods, pole diameter of 22 cm. Red line indicates 0.5 kg/m^3 limit and green line 1.0 kg/m^3 limit*

could affect the transport of boron. These include varying temperature and humidity, rainfall and the conditions in the soil. However, since the primary purpose of the work was to demonstrate that practical problems such as the one treated are within reach of solution, a number of simplifications were made. These are all described in detail in [34]. Here we shall only mention the two most important ones. The first of these is that of negligible convective transfer. This assumption is very convenient since it reduces the governing equation to a simple diffusion equation given by

$$\frac{\partial \langle C \rangle}{\partial t} = \nabla \cdot (\mathbf{D}_B \nabla \langle C \rangle) \quad (6.9)$$

The second assumption is that of steady state conditions throughout the simulations which had a time scope of some 10–12 years.

These assumptions are both questionable, but in the light of the difficulties involved with obtaining even the most basic material parameters, not altogether unacceptable.

6.3 Material parameters

Whereas wood preservation processes are qualitatively well described and much is known about the chemistry and biology of the problem, see e.g. [23], very little effort has been directed at the application of models such as the one described in the above. This of course means that experimentally determined material parameters required for such models are very scarce.

In [34] the diffusion coefficients were taken from the measurements of Ra [51] to which a large uncertainty must be ascribed, as is described in detail in [34].

The other major factor influencing the results is leaching, i.e. the transport of boron out

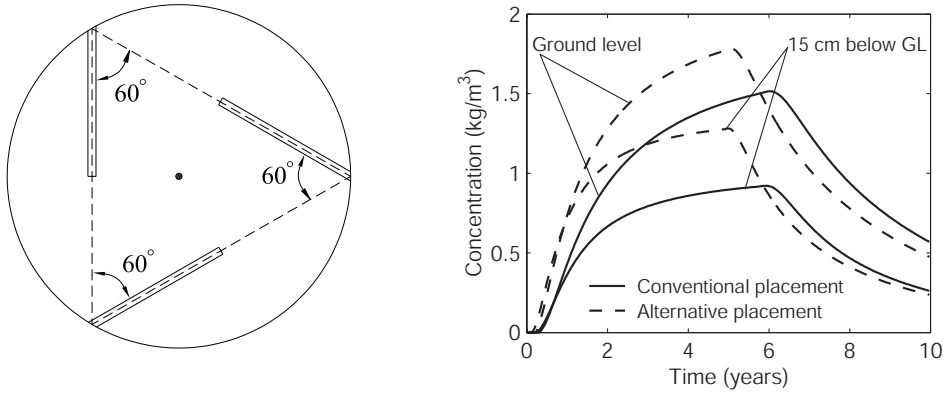


Figure 6.3 Alternative placement of rods (a) and some effects (b). Three rods, pole diameter of 20 cm.

of the surface of the pole and into the ground. For this subproblem a type of convection boundary condition was proposed and the required material parameter estimated on the basis of an analogy between heat and boron transfer.

6.4 Results

In spite of the difficulties involved with both material parameters and boundary conditions, reasonable results were produced, and, it must be emphasized, not at the expense of using unreasonable material parameters. However, at this stage, the computations should be seen primarily as a means of extracting qualitative rather than quantitative information. As an example of this, different types of rod placements in the pole were considered, and it was found that an alternative placement to what is usually preferred could improve the quality of the overall treatment considerably. In Figures 6.2(a)-(d) the concentrations in a pole with a conventional placement of the rods are shown. An alternative placement as shown in Figure 6.3(a) was then considered. Here the rods have been placed in a spiral arrangement rather than pointing towards the center of the pole as illustrated in Figure 6.1. In Figure 6.3 the effects of the alternative placement are shown by the minimum concentrations at different levels compared to what one achieves with the conventional placement.

6.5 Conclusions and future work

Whereas the results obtained in [34] were in general quite encouraging, the long term goal of simulating the complete treatment process from when the rods are inserted and until all boron has been washed out, is still not within immediate reach. Apart from the uncertainties regarding the transport of water, which as demonstrated in the previous chapters are significant, the most pressing issue concerns boron diffusion coefficients.

In an experimental study undertaking the determination of these it would be very desirable to first determine the diffusion coefficient of boron compound in pure water and then express the boron coefficients in wood as a fraction of this. Not only would that give a direct measure of the resistance offered by wood, but would also give an idea of the continuity of the water phase at low degrees of saturation. Ultimately, it could be hoped that a correlation between boron diffusion coefficients and free water transfer coefficients could be established.

Also, it would be of interest to examine the influence of convective transfer, which would not involve any additional practical difficulties – in the first type of experiment the samples are equilibrated to some moisture content and then sealed, whereas the second type of experiment involves also a transfer of water.

Finally, it is necessary to formulate appropriate boundary conditions and then determine the associated material parameters. As for the first part of this task, the general convection type boundary condition which is well-established in the transfer of both heat and moisture, seems promising. Secondly, different physical conditions at the boundary, ranging from pure water to moist soil, should be considered. At the time of writing, a first step in this regard has been taken in an experimental study at the University of Toronto, where the leaching in samples submerged in fresh water is being sought quantified [11].

Chapter 7

Numerical solution procedures

In wood science and in fact, materials science in general, efficient numerical methods are important for at least three reasons.

Firstly, in the development of new models such as those presented in this thesis one is always faced with the problem of supplying material parameters which make the model fit the experimental results as well as possible. In the present this has been done by simple trial and error, and of course with a good feeling for the neighbourhood in which the optimal parameters are to be found. When this is done it is desirable to have an efficient and robust numerical procedure.

The second reason is along the same lines. Because, instead of determining the parameters as sketched in the above, an alternative would be to use some kind of inverse modeling. Exactly how this should be carried out is uncertain, but will inevitably involve solving the same equations thousands or tens of thousands of times. Thus, a factor of 50 may mean the difference between a week and a year.

Lastly, it must be expected that in the not so far future, inclusion of the statistical variation of the model parameters will become an integral part of any computation involving wood. Such computations will again require thousands of runs, each with slightly different parameters, and thus, a factor of 10–100 may mean the difference between making such computations practically feasible or not.

The models presented in previous chapters are all formulated in terms of a set of partial differential equations. In only a few cases can these be solved analytically, or otherwise, by hand calculation methods. Thus, in general some kind of numerical procedure must be applied. For the types of equations dealt with in this thesis, i.e. diffusion type equations, finite difference methods or the more modern equivalents such as the control volume method, are often used, see e.g. [48, 44, 43, 49, 63].

In this work, however, we have exclusively applied the finite element method. Thus, it would not be appropriate to go into a deeper discussion of the relative merits of each method. We will, however, remark that for the type of problems dealt with here, there are no inherent problems with the finite element method, provided that certain trivial provision are taken. These include the use of low order elements, regular grids, and lumped mass matrices. Indeed, if these criteria are met, the two methods are in many cases equivalent. Detailed discussions of the two methods are given in [9, 26, 10].

In recent years, coupled heat and mass transfer problems have become quite common, and the primary focus has often been on the numerical solution method rather than on the physics of the problem. Applications include wood drying [49, 48, 63], non-isothermal consolidation of soils [20, 22] and concrete exposed to high temperatures as during fire [21]. However, in our opinion, the numerical methods applied are often far from optimal. In [20, 22] for example, both eight and nine node plane elements are used, although these are known to cause possibly very severe non-physical oscillations in the computed results. Moreover, it seems that consistent mass matrices are used, and no particular mention is made of the convergence of the Newton iterations. Finally, the choice of primary state variables is inappropriate and is known to result in non-conservative solutions.

Concurrent with the development in the solution of coupled heat and mass transfer problems, there has been a significant effort, primarily within the soil sciences, to develop efficient numerical methods for the solution of the simpler problem of isothermal single-phase free water flow, see e.g. [19, 18, 38, 61, 15, 31, 32, 30, 50, 71, 33, 17, 56].

In most coupled heat and mass transfer problems it is the equation governing the flow of water which is by far the most nonlinear and, thus causes the most problems. In the following, therefore, rather than solving equations whose validity is questionable by methods whose efficiency is even more questionable, we will concentrate on developing an efficient method for the problem of isothermal flow of water.

The method presented has already been applied successfully to the related problem of heat conduction with phase change [35]. In the following we will demonstrate its applicability, first to the problem of free water flow in soils governed by the so-called Richards equation, and then to the problem of water transport in wood where, in addition to free water, also bound water and water vapour is included.

Secondly, some of the more practical problems are discussed. These relate particularly to the appropriate weighting of diffusive and convective terms. Thus, it is well-known that in highly nonlinear diffusion-type problems there is the possibility of encountering solutions with spurious non-physical oscillations. These can, however, be countered by appropriate weighting of the material parameters over each element.

Finally, the issue of computing the tangent matrices required in Newton's method is treated. Most often these matrices are determined numerically. However, we present a general set of formulas enabling exact analytical determination of the matrices. The use of these will generally be more cost efficient and further, it will reduce or eliminate the possibility of round-off and other numerical errors often encountered when computing tangent matrices numerically.

7.1 Classification of diffusion-type equations

In many cases diffusion-type equations describing the transport of some conservative substance, e.g. heat or mass, are naturally formulated as

$$\frac{\partial \theta}{\partial t} = \nabla \cdot (\lambda \nabla \phi) \quad (7.1)$$

where the left-hand side accounts for the accumulation of the conserved substance per unit volume per unit time. Thus, the variable θ could be enthalpy per unit volume or water

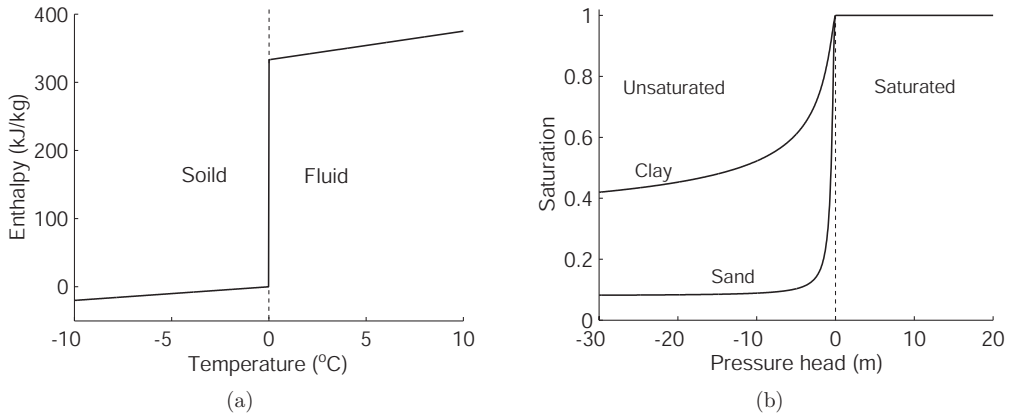


Figure 7.1 *Enthalpy–temperature curve for water (a) and pressure–saturation curves for sand and clay (b).*

per unit volume. The right hand side describes the diffusive transfer of the substance by proportionality to a gradient in some driving force ϕ and with the proportionality factor(s) being described through λ . Thus, for the heat conduction problem ϕ would be temperature, and for the problem of unsaturated flow in porous media, capillary pressure. Depending on the particular problem in question additional terms may also be included, e.g. those describing sources and sinks, gravity, etc. The most important point is, however, the appearance of two variables in the governing equation. Thus, in order to solve the equation, a relation between θ and ϕ must be established. And this is where the primary source of numerical difficulties originates. Because in many cases, the θ – ϕ relation is extremely nonlinear. Two examples of this are shown in Figure 7.1. Figure 7.1 (a) shows the enthalpy (θ) of water as function of temperature (ϕ), and in 7.1 (b) the saturation (θ) of two porous materials are shown as function of the pressure head (ϕ). In the porous media flow problem also the conductivity λ is a strong function of the saturation, but as will be shown, the most critical issue concerns the θ – ϕ relation.

The governing equation (7.1) supplemented with the appropriate θ – ϕ relation gives rise to the possibility of three different formulations, which are equivalent in the continuous versions, but which possess very different properties when it comes to their numerical implementation.

7.1.1 ϕ –form

The ϕ form of the governing equation can be written as

$$C \frac{\partial \phi}{\partial t} = \nabla \cdot (\lambda \nabla \phi) \quad (7.2)$$

where the ‘capacitance’ is given by

$$C = \frac{\partial \theta}{\partial \phi} \quad (7.3)$$

The discrete finite element formulation with the backward Euler scheme applied to the time derivative of ϕ then reads

$$\mathbf{C}_{n+1} \frac{\boldsymbol{\phi}_{n+1} - \boldsymbol{\phi}_n}{\Delta t} + \mathbf{K}_{n+1} \boldsymbol{\phi}_{n+1} + \mathbf{f}_{n+1} = \mathbf{0} \quad (7.4)$$

where the capacitance and conductivity matrices are given by

$$\mathbf{C} = \int_{\Omega} \mathbf{N}^T \mathbf{C} \mathbf{N} \, d\Omega, \quad \mathbf{K} = \int_{\Omega} \mathbf{B}^T \boldsymbol{\lambda} \mathbf{B} \, d\Omega \quad (7.5)$$

and \mathbf{f} defines the boundary conditions which will be dealt with in detail later on. Of the three possible formulations the ϕ -form is perhaps the most inefficient. This is due to the representation of the capacitance. Thus, if the θ - ϕ relation is highly nonlinear as shown e.g. in 7.1 (a) the most important part of it, i.e. the part with the highest slope, may be missed altogether. Thus, the discrete ϕ -form is generally non-conservative although, of course, in the limit of infinitely small time steps, the method is conservative. In the literature concerned with phase-change problems, i.e. with an enthalpy-temperature relation as shown in Figure 7.1 (a), the ϕ -form has traditionally been rather popular. In addition to using very small time steps, some approximation to the capacitance is usually applied. Thus, Del Guidice et al. [27] suggest replacing C by a spatially smoothed equivalent given by

$$C \approx \frac{\nabla \theta \cdot \nabla \phi}{\nabla \phi \cdot \nabla \phi} \quad (7.6)$$

whereas Morgan et al. [41] use a temporal average given by

$$C_{n+1} \approx \frac{\theta_n - \theta_{n-1}}{\phi_n - \phi_{n-1}} \quad (7.7)$$

where $n + 1$ refers to the new state, n to the current and $n - 1$ to the previous state. Other averaging schemes are described in [39]. Although these schemes do improve the enthalpy balance, the time step is still severely restricted and furthermore, non-physical temperature oscillations may occur.

In the case of porous media flow, the ϕ -form has also been rather widely applied, see e.g. [38] for a survey of commonly applied methods. Here, similar approximations to C as those used in the phase change problem are often applied. This again improves mass balance, but again the magnitude of the time step is rather restricted. However, for porous media flow problems, the ϕ -form has the distinct advantage that ϕ , i.e. the water pressure or pressure head, is a unique variable for both partially and fully saturated conditions, such that in this case there seems to be some justification to using the ϕ -form, at least over the θ -form, which will be discussed subsequently.

7.1.2 θ -form

The θ -form of the governing equation is given by

$$\frac{\partial \theta}{\partial t} = \nabla \cdot (\mathbf{D} \nabla \theta) \quad (7.8)$$

where

$$\mathbf{D} = C^{-1}\boldsymbol{\lambda} \quad (7.9)$$

The discrete form can be written as

$$\mathbf{M} \frac{\boldsymbol{\theta}_{n+1} - \boldsymbol{\theta}_n}{\Delta t} + \mathbf{K}_{n+1} \boldsymbol{\theta}_{n+1} + \mathbf{f}_{n+1} = \mathbf{0} \quad (7.10)$$

where

$$\mathbf{M} = \int_{\Omega} \mathbf{N}^T \mathbf{N} \, d\Omega, \quad \mathbf{K} = \int_{\Omega} \mathbf{B}^T \mathbf{D} \mathbf{B} \, d\Omega \quad (7.11)$$

This form is generally quite efficient and furthermore, is perfectly conservative. It is, however, not applied nearly as often as the ϕ -form; in heat conduction, probably because the concept of enthalpy as variable is somewhat queer, and in porous media flow because the moisture content is only a unique variable in the partially saturated range – note that slope of the curve depicted in 7.1 (b) is zero for pressures greater than zero such that $C = 0$ and (7.8) breaks down.

7.1.3 Mixed form

The mixed form retains the original continuous formulation (7.1) and then proceeds to approximate both θ and ϕ in terms of finite element functions, i.e.

$$\theta(\mathbf{x}, t) \approx \mathbf{N}(\mathbf{x})\boldsymbol{\theta}(t), \quad \phi(\mathbf{x}, t) \approx \mathbf{N}(\mathbf{x})\boldsymbol{\phi}(t) \quad (7.12)$$

This gives rise to a set of discrete equations given by

$$\mathbf{M} \frac{\boldsymbol{\theta}_{n+1} - \boldsymbol{\theta}_n}{\Delta t} + \mathbf{K}_{n+1} \boldsymbol{\phi}_{n+1} + \mathbf{f}_{n+1} = \mathbf{0} \quad (7.13)$$

where

$$\mathbf{M} = \int_{\Omega} \mathbf{N}^T \mathbf{N} \, d\Omega, \quad \mathbf{K} = \int_{\Omega} \mathbf{B}^T \boldsymbol{\lambda} \mathbf{B} \, d\Omega \quad (7.14)$$

These equations are then solved and in the course of this the appropriate θ - ϕ relation is applied to each node of the mesh. For porous media flow the mixed form seems to have been applied first by Celia et al. [4], whereas it has only recently been applied to the phase change problem [35]. The mixed form is the most general of the three different forms and is, as the θ -form, conservative.

7.2 Solution of nonlinear discrete formulations

The three different discrete formulations of the governing equation (7.1) all result in a set of highly nonlinear equations. These must then be solved and here yet a number of possibilities exist. The simplest possible, and not at all uncommon, method is to step forward in time in a semi-explicit scheme, for the ϕ -form given by

$$\boldsymbol{\phi}_{n+1} = -(\mathbf{C}_n + \Delta t \mathbf{K}_n)^{-1} (\mathbf{C}_n \boldsymbol{\phi}_n + \Delta t \mathbf{f}_n) \quad (7.15)$$

where \mathbf{C} may or may not be approximated by one of the expressions (7.6) or (7.7). The θ -form can be solved in a similar way. Often these types of solution procedures do not include any rules for selecting an appropriate time step – a reasonably small time step is simply selected to begin with and then kept constant throughout. Recently, however, Kavetski et al. [33] have developed a method for automatic time step selection and error control for the solution of the ϕ -form, in this case pressure form, of the governing equation arising from flow through porous media.

The alternative to these semi-explicit methods are the fully iterative methods. Such methods are widely used in the simulation of flow through porous media, in particular through soils. Since the ϕ -form in this case suffers from poor mass balance properties and since the θ -form breaks down under fully saturated conditions, the method of choice is often the mixed form. For the iterative solution of this equation the residual is first stated as

$$\mathbf{r}_{n+1} = \mathbf{M} \frac{\boldsymbol{\theta}_{n+1} - \boldsymbol{\theta}_n}{\Delta t} + \mathbf{K}_{n+1} \boldsymbol{\phi}_{n+1} + \mathbf{f}_{n+1} = \mathbf{0} \quad (7.16)$$

Since this set of m equations contains $2m$ variables, a choice as to which variables are the primary ones, must be made. Since only the $\boldsymbol{\phi}$ -variables are unique, these are often chosen as the primary, whereas the secondary variables $\boldsymbol{\theta}$ are then determined on the basis of $\boldsymbol{\phi}$. The iterative Newton–Raphson scheme can then be written as

$$\begin{aligned} \boldsymbol{\phi}_{n+1}^0 &= \boldsymbol{\phi}_n, \quad \boldsymbol{\theta}_{n+1}^0 = \boldsymbol{\theta}_n \\ \Delta \boldsymbol{\phi}_{n+1}^j &= -(\mathbf{J}_{n+1}^j)^{-1} \mathbf{r}_{n+1}^j \\ \boldsymbol{\phi}_{n+1}^{j+1} &= \boldsymbol{\phi}_{n+1}^j + \Delta \boldsymbol{\phi}_{n+1}^j \\ \boldsymbol{\theta}_{n+1}^{j+1} &= \theta(\boldsymbol{\phi}_{n+1}^{j+1}) \end{aligned} \quad (7.17)$$

where j refers to the iteration number and n to the time step. The Jacobian is given by

$$\mathbf{J} = \left(\frac{\partial \mathbf{r}}{\partial \boldsymbol{\phi}} \right)^\top \quad (7.18)$$

and is usually unsymmetric. For this and other reasons some approximation to the exact Jacobian is often used, e.g.

$$\mathbf{J}_{\text{approx}} = \mathbf{M} \left[\frac{\partial \boldsymbol{\theta}}{\partial \boldsymbol{\phi}} \right] + \Delta t \mathbf{K} \quad (7.19)$$

whereby the iterative scheme is referred to as the Picard or modified Newton–Raphson procedure.

7.3 Advantages and disadvantages of the different forms

With respect to the efficiency of the different formulations when solved iteratively, it has been observed that the θ -form usually performs much better than the ϕ -form. Similarly, when the mixed form is applied this method is usually much more efficient and robust

when θ are used as primary variables than if, as in the scheme sketched above, ϕ are taken as the primary variables. However, the θ -form as well as the mixed form with θ as primary variables both break down under fully saturated conditions. Thus, the properties of the different formulations can be summarized as in Table 7.1 where Mixed- ϕ refers to the mixed form with ϕ as primary variables, and Mixed- θ to the mixed form with θ as primary variables. Here the labels PASS and especially FAIL should only be taken literally regarding the generality/uniqueness and mass balance tests. That is, either the formulation allows for both partially and fully saturated conditions to be treated or it does not and likewise, either the formulation is mass conservative or it is not. The efficiency/robustness test is somewhat more subjective since the properties of the ϕ -forms of course approach those of the θ -forms as the time step decreases.

From Table (7.1) it would appear that the appropriate choice of method in a given situation would depend on the particular circumstances in question. For example, if one is sure that only partially saturated conditions will exist in a given problem, then the mixed- θ method would appear to be a good choice. On the other hand, if fully saturated conditions do occur then one has no choice but to apply the mixed- ϕ form if also mass conservation is required. Unfortunately, in many cases one cannot predict beforehand whether or not fully saturated conditions will occur at some point in the simulation. In general porous media flow, the effect of gravity may induce such conditions, and in drying simulations the effects of pressure and temperature gradients often lead to fully saturated conditions in part of the medium. Thus, whereas it is essential to be able to deal with fully saturated conditions, the far larger part of the computations are usually concerned with the partially saturated state. That is, during the drying of wood for example, it is only in the very beginning of the process that the ends of a typical board may be fully saturated. Once the drying has progressed for some time only partially saturated conditions will have to be dealt with.

7.4 Variable switching techniques

This reality has motivated the development of methods which seek to exploit the best features of the different formulations. That is, the general conservative nature of the mixed forms, and the uniqueness of the mixed- ϕ form together with the efficiency of the

Form	Eff./robust.	Gen./unique.	Mass balance
ϕ -form	FAIL	PASS	FAIL
θ -form	PASS	FAIL	PASS
Mixed- ϕ	FAIL	PASS	PASS
Mixed- θ	PASS	FAIL	PASS

Table 7.1 Results of efficiency/robustness, generality/unique-ness, and mass balance tests for different numerical formulations.

mixed- θ form. Such considerations inevitably lead to the so-called variable switching technique, where depending on the state of a given node, either θ or ψ is taken as primary variable. These methods have been applied successfully by Forsyth [19] and Diersch and Perrochet [15] to single phase flow through porous media and by Yu and Forsyth [70] also to multi-phase flow.

As an example of the variable switching technique, consider a three node element with in which the two nodes 1 and 2 are fully saturated and node 3 is partially saturated. The primary variable vector would then be

$$\mathbf{X} = [\phi_1, \phi_2, \theta_3]^T \tag{7.20}$$

whereas the Jacobian associated with this primary variable vector is given by

$$\mathbf{J}_X = \left(\frac{\partial \mathbf{r}}{\partial \mathbf{X}} \right)^T = \begin{bmatrix} \partial r_1 / \partial \phi_1 & \partial r_1 / \partial \phi_2 & \partial r_1 / \partial \theta_3 \\ \partial r_2 / \partial \phi_1 & \partial r_2 / \partial \phi_2 & \partial r_2 / \partial \theta_3 \\ \partial r_3 / \partial \phi_1 & \partial r_3 / \partial \phi_2 & \partial r_3 / \partial \theta_3 \end{bmatrix} \tag{7.21}$$

where the residual is still given by (7.16). Thus, regardless of the choice of primary variables, the same set of equations is solved.

As for the choice of primary variables [19, 15] recommend that a switch is made from saturation to pressure once the saturation reaches 0.99. The state of the primary variables are monitored in each Newton iteration, and the possible switch performed immediately after the switching criteria are fulfilled. This procedure gives rise to a possible inconsistency. Thus, if a node is at a degree of saturation of, say, $S = 0.98$ and then in the next iteration the predicted saturation in that node exceeds unity, e.g. $S = 1.02$, there is a problem. In [19, 15] procedures for handling this situation are not described, but we would assume that the saturation is set equal to unity and the pressure then determined on the basis of this value, after which, in the next iteration the pressure is used as primary variable.

7.5 A new mixed–variable iterative procedure

In the following we will describe a new and very efficient and robust method for solving the mixed form of the governing equation. It turns out that the method is in fact equivalent to the variable switching technique, but much easier to implement and furthermore, without any of the problems associated with the transition from partially to fully saturated conditions described in the above. Before the algorithm is derived, however, it would be appropriate to look into the reasons for the inefficiency of the mixed- ϕ method.

This is illustrated in Figure 7.2. In Figure 7.2 (a) the steps taken in the mixed- ϕ method are shown. We start at a point (ϕ_0, θ_0) and then compute an increment $\Delta\phi$. The θ -variable is then updated as $\theta = \theta(\phi_0 + \Delta\phi)$. The new state is, however, extremely sensitive to the magnitude of the increment $\Delta\phi$. Indeed, if this increment is given a small perturbation $\delta\phi$ the consequences with respect to θ are quite severe in that we then arrive at the point $\theta = \theta(\phi_0 + \Delta\phi + \delta\phi)$ which is ‘far’ from $\theta = \theta(\phi_0 + \Delta\phi)$. Thus, even small differences in $\Delta\phi$ may result in huge differences in the new value of θ . Under such circumstances

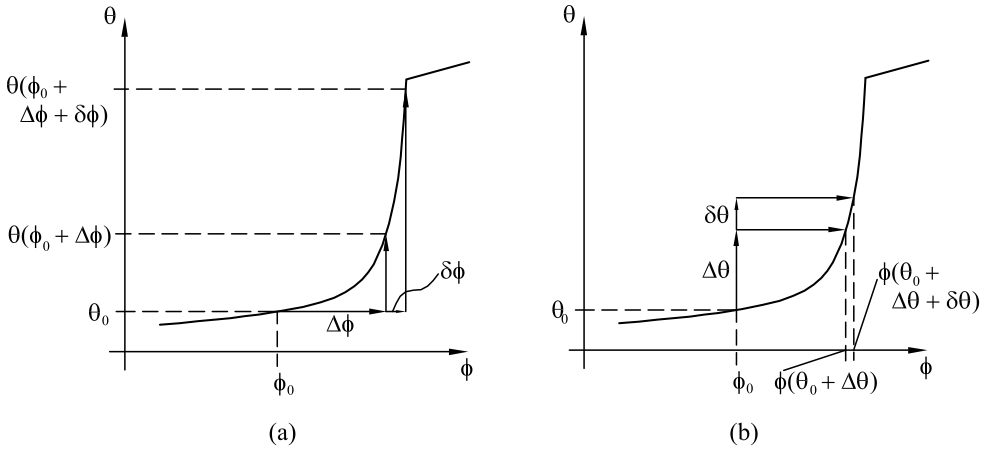


Figure 7.2 Mixed- ϕ (a) and mixed- θ (b) methods.

Newton's method is bound to fail.

In Figure 7.2 (b) the mixed- θ -method is illustrated. Here a small perturbation in $\Delta\theta$ results in an even smaller change in ϕ , and thus, this algorithm is much more unlikely to experience divergence of the iterations.

It is important to realize that whereas the often extreme variation of the conductivity with the state variables of course does not improve the chance of convergence, it is the nonlinearity of the θ - ϕ curve which is primarily responsible for failure of the iterations.

The new iterative procedure attempts at paying due attention to this fact. Also the fact that in general ϕ is the only unique variable must be taken into consideration. Therefore, in each iteration an increment $\Delta\phi_{n+1}^j$ is computed in the usual way as with the mixed- ϕ method. Next, instead of updating the θ -variables as $\theta_{n+1}^{j+1} = \theta(\phi_{n+1}^j + \Delta\phi_{n+1}^j)$ as is done in the conventional method, an increment $\Delta\tilde{\theta}_{n+1}^j$ is computed as

$$\Delta\tilde{\theta}_{n+1}^j = \left[\frac{\partial\theta}{\partial\phi} \right]_{n+1}^j \Delta\phi_{n+1}^j \quad (7.22)$$

An intermediate point $\tilde{\theta}_{n+1}^{j+1}$ is then computed as

$$\tilde{\theta}_{n+1}^{j+1} = \theta_{n+1}^j + \Delta\tilde{\theta}_{n+1}^j \quad (7.23)$$

Each node in the mesh is now checked and if the value of $\tilde{\theta}_{n+1}^{j+1}$ fulfills certain criteria, then we set

$$\theta_{n+1}^{j+1} = \tilde{\theta}_{n+1}^{j+1} \quad (7.24)$$

for that node and then compute the corresponding nodal value of ϕ_{n+1}^{j+1} as

$$\phi_{n+1}^{j+1} = \phi(\theta_{n+1}^{j+1}) \quad (7.25)$$

If the value of $\tilde{\theta}_{n+1}^{j+1}$ does not meet the criteria then we proceed as in the conventional mixed- ϕ method by updating ϕ and then determining the corresponding value of θ on the basis of this.

The update criterion depends on the particular problem in question. If θ denotes saturation and $\tilde{\theta} > 1$ then clearly the conventional update must be used, and if not, the alternative update can be used. In the next section the new iterative procedure is applied to the so-called Richards equation and full details on its implementation given.

7.5.1 Application to the Richards equation

In the soil sciences the equation describing the flow of water in soils is often referred to as the Richards equation. In the one dimensional case this may be written as [32]

$$\frac{\partial \theta}{\partial t} + c_0 \theta \frac{\partial \phi}{\partial t} = \frac{\partial}{\partial z} \left[k(\psi) \frac{\partial}{\partial z} (\psi + z) \right] \quad (7.26)$$

In this equation θ is the volumetric water content, ψ the pressure head, $K(\psi)$ hydraulic conductivity and z the upwards directed coordinate opposite to which gravity acts. Furthermore, water and porous medium compressibility are included via and so-called storativity c_0 , see Section 3.4.3. For the θ - ψ relation and the variation of the hydraulic conductivity, the so-called van Genuchten parameterization [65] is often used. This is given by

$$\theta(\psi) = \begin{cases} \frac{\theta_s - \theta_r}{[1 + (\alpha|\psi|^n)]} + \theta_r, & \psi < 0 \\ \theta_s, & \psi \geq 0 \end{cases} \quad (7.27)$$

$$K(\psi) = \begin{cases} k_s \frac{\{1 - (\alpha|\psi|)^{n-1} [1 + (\alpha|\psi|^n)]^{-m}\}^2}{[1 + (\alpha|\psi|^n)]^{\frac{1}{2}m}}, & \psi < 0 \\ k_s, & \psi \geq 0 \end{cases} \quad (7.28)$$

where θ_r is the residual water content, θ_s the maximum water content and n , m , α and k_s parameters describing the properties of the soil. Typical ψ - θ and ψ - $K(\psi)$ curves are shown in Figure 7.3. If we neglect compressibility effects the finite element-backward Euler formulation of (7.26) reads

$$\mathbf{r}_{n+1} = \mathbf{M}(\boldsymbol{\theta}_{n+1} - \boldsymbol{\theta}_n) + \Delta t \mathbf{K}_{n+1} \boldsymbol{\psi}_{n+1} + \Delta t \mathbf{f}_{n+1} + \Delta t \mathbf{q}_{n+1} = \mathbf{0} \quad (7.29)$$

where

$$\mathbf{M} = \int_{\Omega} \mathbf{N}^T \mathbf{N} \, d\Omega, \quad \mathbf{K} = \bar{k}_s \int_{\Omega} \mathbf{B}^T \mathbf{B} \, d\Omega \quad (7.30)$$

$$\mathbf{f} = \bar{k}_s \int_{\Omega} \mathbf{B}^T \, d\Omega, \quad \mathbf{q} = \int_{\Gamma} \mathbf{N}^T q_n \, d\Gamma \quad (7.31)$$

where \bar{k}_s is the mean hydraulic conductivity over an element, i.e. for a two-node element $\bar{k}_s = \frac{1}{2}[k_s(\psi_1) + k_s(\psi_2)]$. It should be noted here that other types of conductivity weighting

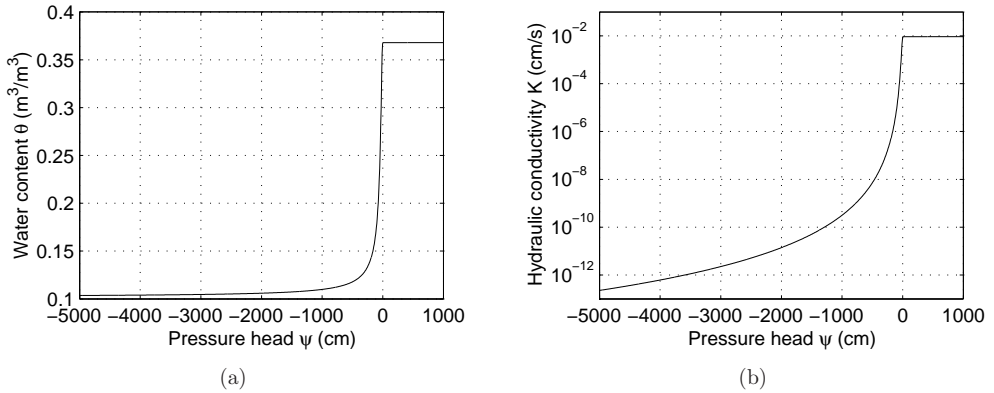


Figure 7.3 Pressure head–water content curve (a) and hydraulic conductivity (b) for a coarse grained soil [4].

may be applied, and in some cases may even be necessary, see [18]. For the case dealt with here, however, the above central weighting scheme produces satisfactory results.

The iterative procedure now begins with computing an increment $\Delta\psi_{n+1}^j$. On the basis of this increment we compute

$$\Delta\tilde{\theta}_{n+1}^j = \left[\frac{\partial\theta}{\partial\psi} \right] \Delta\psi_{n+1}^j \quad (7.32)$$

Each node is now checked and if $\theta_{n+1}^j + \Delta\tilde{\theta}_{n+1}^j < \theta_{\text{TOL}}$ then $\theta_{n+1}^{j+1} = \theta_{n+1}^j + \Delta\tilde{\theta}_{n+1}^j$ for that node and the corresponding pressure is then computed as $\psi_{n+1}^{j+1} = \psi(\theta_{n+1}^{j+1})$. If, on the other hand, $\theta_{n+1}^j + \Delta\tilde{\theta}_{n+1}^j \geq \theta_{\text{TOL}}$ then the pressure is updated in the usual way as $\psi_{n+1}^{j+1} = \psi_{n+1}^j + \Delta\psi_{n+1}^j$ and the water content computed as $\theta_{n+1}^{j+1} = \theta(\psi_{n+1}^{j+1})$. The full iterative procedure is given in Table 7.2 and illustrated in Figure 7.4.

7.5.2 Examples

In this section the performance of the new iterative procedure is compared to the conventional mixed- ψ procedure. The example involves the infiltration of water into a one dimensional 60 cm column of soil with van Genuchten parameters $k_s = 0.00922$ cm/s, $\theta_r = 0.102$, $\theta_s = 0.368$, $\alpha = 0.0355$ cm⁻¹, $n = 2.0$ and $m = 1 - 1/n = 0.5$. These parameters, which correspond to what is shown in Figure 7.3, have been used by numerous authors in evaluating the performance of numerical procedures, see e.g. [4, 38, 31]. In all cases the full Newton method is applied, i.e. the exact Jacobian is used, and in all tests the time step is taken to vary as

$$\Delta t_{n+1} = 2\sqrt{t_n \Delta t_0} + \Delta t_0 \quad (7.33)$$

such that the entire time step selection procedure is controlled by the initial time step Δt_0 . This time step selection results in the front propagating at approximately the same

Initial point: $\boldsymbol{\theta}_{n+1}^0 = \boldsymbol{\theta}_n$, $\boldsymbol{\psi}_{n+1}^0 = \boldsymbol{\psi}_n^0$

Iterations: $j = 0, \dots, j_{\max}$

Residual and Jacobian: $\mathbf{r}_{n+1}^j, \mathbf{J}_{n+1}^j$

Increment: $\Delta\boldsymbol{\psi}_{n+1}^j = -(\mathbf{J}_{n+1}^j)^{-1}\mathbf{r}_{n+1}^j$

Prediction: $\tilde{\boldsymbol{\theta}}_{n+1}^{j+1} = \boldsymbol{\theta}_{n+1}^j + \left[\frac{\partial \boldsymbol{\theta}}{\partial \boldsymbol{\psi}} \right] \Delta\boldsymbol{\psi}_{n+1}^j$

Variable check: $k = 1, \dots$, number of nodes

if $(\tilde{\boldsymbol{\theta}}_{n+1}^{j+1})_k < \theta_{\text{TOL}}$

$(\theta_{n+1}^{j+1})_k = (\tilde{\boldsymbol{\theta}}_{n+1}^{j+1})_k$

$(\psi_{n+1}^{j+1})_k = \psi((\tilde{\boldsymbol{\theta}}_{n+1}^{j+1})_k)$

else

$(\psi_{n+1}^{j+1})_k = (\psi_{n+1}^j)_k + (\Delta\psi_{n+1}^j)_k$

$(\theta_{n+1}^{j+1})_k = \theta((\psi_{n+1}^{j+1})_k)$

end variable check

end iteration

Table 7.2 Iterative procedure for the Richards equation

discrete speed throughout the time stepping, i.e. for arbitrary times t_n and t_{n+1} , and corresponding front positions z_{n+1} and z_n , the discrete velocity of the front is given by

$$V_f = \frac{\Delta z_{n+1}}{\Delta t_{n+1}} = \frac{z_{n+1} - z_n}{t_{n+1} - t_n} \simeq \text{const.}, \quad n = 0, \dots, n_{\max} \quad (7.34)$$

where V_f depends only on Δt_0 .

In all the examples the switch between the two methods of update is made when the predicted effective saturation reaches a value close to unity, i.e. when

$$\tilde{S}^e = \frac{\tilde{\theta} - \theta_r}{\theta_s - \theta_r} > S_{\text{TOL}}^e \quad (7.35)$$

where a value of $S_{\text{TOL}}^e = 0.9995$ has been used in all examples. Furthermore, in all examples we have assumed vanishing compressibility, i.e. $c_0 = 0$.

Example 1

In the first example constant pressure head boundary conditions are imposed as $\psi_{\text{top}} = -75$ cm and $\psi_{\text{bottom}} = -1000$ cm and the initial pressure head is $\psi_{\text{init}} = -1000$ cm through-

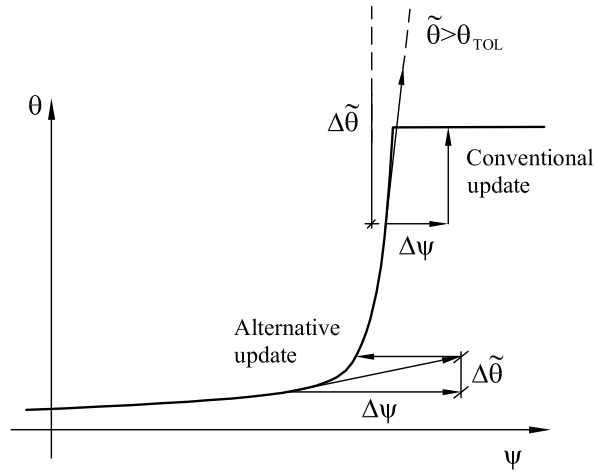


Figure 7.4 Iterative procedure for the Richards equation

out the domain as in [4, 38, 31]. The efficiency of the method under these conditions is shown in Table 7.3, and the moisture content and pressure head profiles illustrated in Figure 7.5. As can be seen the new method clearly outperforms the conventional mixed- ψ method. Not only are the iteration counts lower, but whereas the mixed- ψ method fails at large values of Δt_0 the new method seems to handle this without any significant problems.

Δt_0 (s)	No. Step	Mixed- ψ		New method	
		No. Iter	Iter/Step	No. Iter	Iter/Step
0.1	1000	2979	2.99	2010	2.01
1.0	317	1264	3.99	947	2.99
10.0	100	698	6.98	404	4.04
50.0	45	1463	32.5	199	4.42
100.0	32	941	29.4	165	5.12
500.0	15	†	†	97	6.47
1000.0	10	†	†	70	7.00

Table 7.3 Comparison of conventional mixed- ψ scheme and new iterative procedure. Example 1, $\psi_{\text{init}} = -1000$ cm, $\psi_{\text{top}} = -75$ cm and $\psi_{\text{bottom}} = -1000$ cm. † Convergence not achieved after 200 iterations.

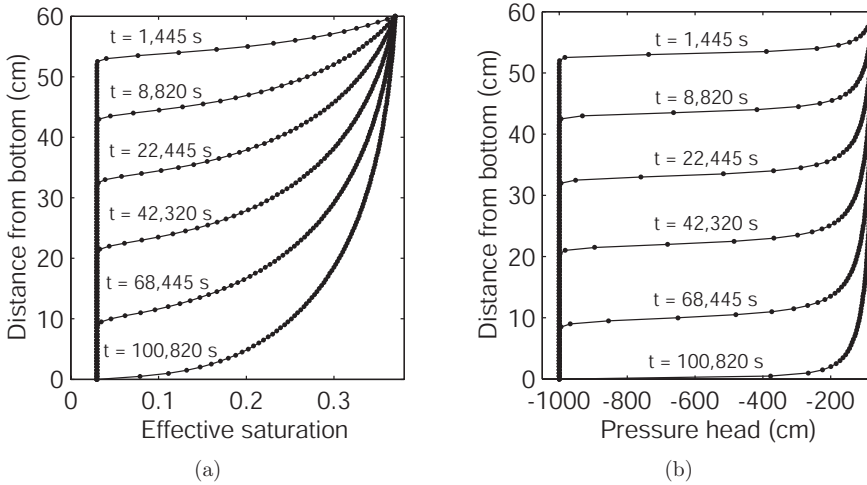


Figure 7.5 Moisture content (a) and pressure head (b) profiles. Example 1, $\psi_{top} = -75$ cm and $\psi_{bottom} = -1000$ cm, $\Delta t_0 = 5.0$ s.

Example 2

Next a somewhat more challenging example is considered. The material and geometry is identical to that of the previous example, but the bottom is now a no-flow boundary, $q_{bottom} = 0$ and at the top a pressure of $\psi_{top} = +100$ cm, i.e. the infiltration is carried out with a constant free water level of 100 cm at the top of the column.

The solution statistics are given in Table 7.4. Compared to the previous example, somewhat higher iteration counts are seen. In Figure 7.6 the reason for this is shown: because of the high pressure at the top, the front are much sharper and furthermore, the variations in saturation within the column is much greater. Again the mixed- ψ method has problems with convergence for large time steps, although quite surprisingly, it does converge for the two largest values of Δt_0 . On the other hand, the new method converges regardless of the time step, and although the number of iterations per time step increases as the time step increases, the total number of iterations decreases.

Example 3

As a final example we now consider the case where the soil is initially very dry corresponding to $\psi_{init} = -10,000$ cm, and otherwise all other parameters are as in the previous example. Such conditions are known to cause severe problems with the convergence of the mixed- ψ method [19]. The results shown in Table 7.5 confirm this. The new method, however, is largely unaffected as compared to the previous example.

Together, these three examples clearly demonstrated the superiority of the new method over the conventional mixed- ψ method. The comparisons made are perhaps not entirely fair in that an automatic adjustment of the time step could surely bring the mixed- ψ

Δt_0 (s)	No. Step	Mixed- ψ		New method	
		No. Iter	Iter/Step	No. Iter	Iter/Step
0.0005	775	3207	4.14	2877	3.66
0.001	548	2630	4.80	2192	4.00
0.01	174	†	†	929	5.34
0.1	55	†	†	447	8.12
1.0	18	321	17.8	219	12.2
10.0	6	180	30.0	140	23.3

Table 7.4 Comparison of conventional mixed- ψ scheme and new iterative procedure. Example 2, $\psi_{init} = -1000$ cm, $\psi_{top} = 100$ cm and $q_{bottom} = 0$. †Convergence not achieved after 200 iterations.

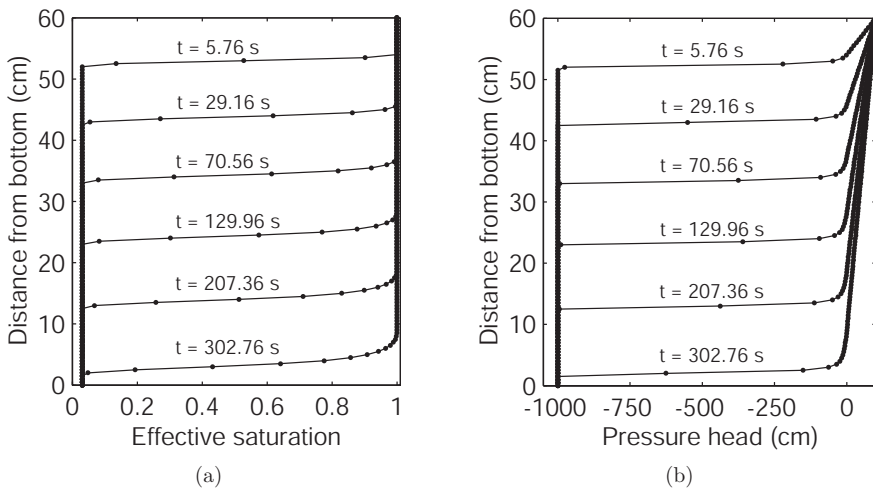


Figure 7.6 Moisture content (a) and pressure head (b) profiles. Example 2, $\psi_{top} = 100$ cm and $q_{bottom} = 0$, $\Delta t_0 = 0.01$ s.

method to converge. Moreover, for very small time steps the difference between the two methods is not too great, and thus, if the goal is to produce very accurate solutions the mixed- ψ method should be adequate. Thus, the main virtue of the new method lies in its ability to perform very well for large time steps. Moreover, the method should also be ideally suited to produce steady state solutions, where the initial guess is usually quite critical for the chances of convergence.

Finally, it should be emphasized that the new method can be coded by some quite insignificant modifications to existing mixed- ψ codes. Furthermore, the additional cost involved with the new method as compared to the conventional one is also insignificant since the

Δt_0 (s)	No. Step	Mixed- ψ		New method	
		No. Iter	Iter/Step	No. Iter	Iter/Step
0.0001	1733	6547	3.78	5495	3.17
0.0002	1225	4964	4.05	4076	3.33
0.0005	775	†	†	2837	3.66
0.001	548	†	†	2195	4.01
0.01	174	†	†	959	5.52
0.1	55	†	†	483	8.78
1.0	18	†	†	254	14.1
10.0	6	†	†	174	29.0

Table 7.5 Comparison of conventional mixed- ψ scheme and new iterative procedure. Example 3, $\psi_{init} = -10,000$ cm, $\psi_{top} = 100$ cm and $q_{bottom} = 0$. †Convergence not achieved after 200 iterations.

bulk of the computations will be concerned with the computation of the pressure head increments, for which the two methods require the solution of the same set of equations.

7.5.3 Equivalence between variable switching and new method

Whereas the variable switching technique in a given node makes use of either water content or pressure head depending on the state in the node, the new method employs two types of update. However, as shall be shown in the following, the two methods are in fact equivalent, with the slight exception that the new method in some cases handles the transition from partially to fully saturated conditions in a more logical and consistent way.

If the medium is fully saturated it is obvious that the variable switching method and the new method are identical because in this case they both take the form of the conventional mixed- ψ form. Under partially saturated conditions, however, it is not so obvious. Here the variable switching method uses the moisture content as primary variable whereas the new method uses the alternative update.

If moisture content is used as primary variable the new iterative state $(\theta_{n+1}^{j+1}, \psi_{n+1}^{j+1})$ is computed through the following steps¹

$$\begin{aligned}
 \Delta \theta &= -\mathbf{J}_\theta^{-1} \mathbf{r} \\
 \theta_{new} &= \theta + \Delta \theta \\
 \psi_{new} &= \psi(\theta_{new})
 \end{aligned}
 \tag{7.36}$$

¹In order to avoid clouding the major point with indices, in the following matrices and vectors refer to the iterative point $(\)_{n+1}^j$ if nothing else is indicated, whereas $(\)_{new}$ refers to the new iterative point $(\)_{n+1}^{j+1}$

where the moisture Jacobian is given by

$$\mathbf{J}_\theta = \frac{\partial \mathbf{r}}{\partial \boldsymbol{\theta}} = \frac{\partial \mathbf{r}}{\partial \boldsymbol{\psi}} \frac{\partial \boldsymbol{\psi}}{\partial \boldsymbol{\theta}} = \mathbf{J}_\psi \mathbf{C} \quad (7.37)$$

where

$$\mathbf{C} = \frac{\partial \boldsymbol{\psi}}{\partial \boldsymbol{\theta}} \quad (7.38)$$

The steps taken in (7.36) to compute the new state may be written in more compact form as

$$\boldsymbol{\psi}_{\text{new}} = \psi(\boldsymbol{\theta} - \mathbf{J}_\theta^{-1} \mathbf{r}) \quad (7.39)$$

If the pressure head is taken as primary variable and the alternative update is used the new state is computed as

$$\begin{aligned} \Delta \boldsymbol{\psi} &= -\mathbf{J}_\psi^{-1} \mathbf{r} \\ \Delta \boldsymbol{\theta} &= \mathbf{C}^{-1} \Delta \boldsymbol{\psi} \\ \boldsymbol{\theta}_{\text{new}} &= \boldsymbol{\theta} + \Delta \boldsymbol{\theta} \\ \boldsymbol{\psi}_{\text{new}} &= \psi(\boldsymbol{\theta}_{\text{new}}) \end{aligned} \quad (7.40)$$

or in compact form

$$\boldsymbol{\psi}_{\text{new}} = \psi(\boldsymbol{\theta} - \mathbf{C}^{-1} \mathbf{J}_\psi^{-1} \mathbf{r}) \quad (7.41)$$

Now, using (7.37) and the fact that for general non-singular matrices \mathbf{A} and \mathbf{B} , the inverse of the product is related to the product of the inverse by the relation

$$(\mathbf{AB})^{-1} = \mathbf{B}^{-1} \mathbf{A}^{-1} \quad (7.42)$$

it can be seen that

$$\mathbf{J}_\theta^{-1} = (\mathbf{J}_\psi \mathbf{C})^{-1} = \mathbf{C}^{-1} \mathbf{J}_\psi^{-1} \quad (7.43)$$

which means that (7.39) and (7.41) are identical, i.e.

$$\psi(\boldsymbol{\theta} - \mathbf{J}_\theta^{-1} \mathbf{r}) = \psi(\boldsymbol{\theta} - \mathbf{C}^{-1} \mathbf{J}_\psi^{-1} \mathbf{r}) \quad (7.44)$$

Thus, it has been shown that the alternative update in fact corresponds to using the moisture content as primary variable as in the variable switching technique. As already discussed, the use of pressure head as primary variable is equivalent to the conventional update, and the new method is then seen to be reformulation of the variable switching method. However, whereas the variable switching technique chooses primary variables solely on the basis of the current nodal values, the new method chooses the method of update based on a new predicted state, and is in this way more consistent in that no provisions have to be made in order to ensure that the saturation does not attain values greater than unity. In other words, if the predicted saturation is greater than unity, the conventional update is used and if not, the alternative update is applied as shown in Figure 7.2. With the primary variable switching technique, however, one can easily encounter situations where in the beginning of the iterations, the saturation is below unity and then at some point, when the transition to the fully saturated state is made, exceeds unity.

7.6 Application of mixed-variable procedure to wood

Due to the presence of bound water, hygroscopic materials such as wood are considerably more complicated than non-hygroscopic materials such as soil. Whereas typical problems of water transport in soils only involve a rather limited part of the capillary pressure-saturation curve, the solution of water transfer problems typically involve a much larger part of the curve. This is both the case for drying as well as for infiltration into wood initially below the fiber saturation point.

For hygroscopic media the transition between the partially saturated and hygroscopic ranges may cause some problems, since at the fiber saturation point there is an abrupt change in the status of the different variables. First of all, the capillary pressure is no longer defined, and secondly, the total moisture content has to be separated into bound and free water parts. In the following the problems associated with the transition between the partially saturated and hygroscopic ranges are addressed. The resulting algorithm bears some similarities with that presented for the Richards equation in that, depending on a predicted state, different types of update may be applied.

We consider the total water conservation equation

$$\rho_0 \frac{\partial W}{\partial t} = \nabla \cdot [\mathbf{K}_w \nabla (p_w + \rho_w g z)] + \nabla \cdot (\mathbf{K}_v \nabla p_v) + \nabla \cdot (\mathbf{K}_b \nabla W_b) \quad (7.45)$$

where W is the dry base total moisture content (kg/kg), p_w the water pressure, W_b the bound water content (kg/kg), and the effective transport coefficients \mathbf{K}_w , \mathbf{K}_v , and \mathbf{K}_b are given in (3.64).

The discrete form of the governing equation can be written as

$$\begin{aligned} \mathbf{r}_{n+1} &= \mathbf{M}(\mathbf{W}_{n+1} - \mathbf{W}_n) + \\ \Delta t (\mathbf{K}_{w,n+1} \mathbf{p}_{w,n+1} + \mathbf{K}_{v,n+1} \mathbf{p}_{v,n+1} + \mathbf{K}_{b,n+1} \mathbf{W}_{b,n+1} + \mathbf{f}_{n+1} + \mathbf{q}_{n+1}) &= \mathbf{0} \end{aligned} \quad (7.46)$$

where n again refers to the current, known state, and $n + 1$ to the new state.

Since in the following, the particular problem of handling the transition between the partially saturated and hygroscopic ranges is not considered, we will solve the discrete equations with the total moisture content as primary variable. Of course, the water pressure \mathbf{p}_w is the only variable which is unique under all conditions, including full saturation. However, since the material parameters are defined in terms of moisture content rather than total water pressure, the implementation with \mathbf{p}_w as primary variable is somewhat awkward. Furthermore, the occurrence of fully saturated conditions also leads to other considerations, such as how to treat the gas pressures. Since a full treatment of these problems is outside of the scope of the present work, we will assume partially saturated conditions throughout, and in this case, the choice of moisture content as primary variable is quite natural. However, as was shown with the Richards equation, the choice of primary variable and the method of update are two sides of the same coin. Therefore, even though in following the method will be explained with \mathbf{W} as primary variable, the equivalent algorithm with \mathbf{p}_w as primary variable appears simply reversing the type of

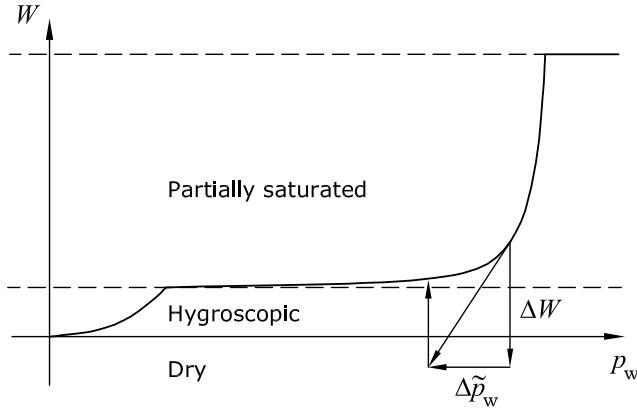


Figure 7.7 Alternative update in case of negative moisture content.

update and relating the Jacobians as

$$\mathbf{J}_W \left[\frac{\partial \mathbf{W}}{\partial \mathbf{p}_w} \right] = \mathbf{J}_{p_w} \quad (7.47)$$

where

$$\mathbf{J}_W = \frac{\partial \mathbf{r}}{\partial \mathbf{W}}, \quad \mathbf{J}_{p_w} = \frac{\partial \mathbf{r}}{\partial \mathbf{p}_w} \quad (7.48)$$

As with the Richards equation the iterative procedure begins by computing an increment, in this case a moisture increment,

$$\mathbf{J}_{n+1}^j \Delta \mathbf{W}_{w,n+1}^j = -\mathbf{r}_{n+1}^j \quad (7.49)$$

after which the new iterative state is computed by a simple update

$$\mathbf{W}_{n+1}^{j+1} = \mathbf{W}_{n+1}^j + \Delta \mathbf{W}_{n+1}^{j+1} \quad (7.50)$$

and all other variables computed with \mathbf{W}_{n+1}^{j+1} as argument.

As was shown, this procedure has good chances of converging and is generally very robust. However, for hygroscopic materials a problem may occur in that the computed moisture contents in the course of the iterations may become negative. This situation is sketched in Figure 7.7. Since the hygroscopic range is relatively narrow and since the governing equation contains three different driving forces, this situation is quite common. The cure for this problem is to compute a water pressure $\tilde{\mathbf{p}}_w$ by

$$\tilde{\mathbf{p}}_w = \mathbf{p}_w + \left[\frac{\partial \mathbf{p}_w}{\partial \mathbf{W}} \right] \Delta \mathbf{W} \quad (7.51)$$

and then update the moisture content as

$$\mathbf{W} = W(\tilde{\mathbf{p}}_w) \quad (7.52)$$

after which the other variables may be computed on the basis of this moisture content. This method is seen to be very similar to the one used for the Richards equation and as such, further details on its implementation will not be given here.

7.6.1 Variable smoothing

To further aid the transition from partially saturated to hygroscopic conditions, it may be beneficial to smooth some of the variables. As already discussed, the free water content must be separated from the bound water content. That is, the total water content is given by

$$W = W_b + W_f \quad (7.53)$$

where

$$W_b = \min(W_{\text{FSP}}, W), \quad W_f = \max(0, W - W_{\text{FSP}}) \quad (7.54)$$

These functions can be smoothed as follows

$$W_b \simeq 2 \frac{W_b^* - W_{\text{FSP}}}{1 + \exp\left(2 \frac{W - W_b^*}{W_{\text{FSP}} - W_b^*}\right)} + W_{\text{FSP}} \quad (7.55)$$

$$W_f \simeq -2 \frac{W_f^* - W_{\text{FSP}}}{1 + \exp\left(-2 \frac{W - W_f^*}{W_{\text{FSP}} - W_f^*}\right)} + 2(W_f^* - W_{\text{FSP}})$$

where W_b^* is slightly smaller than W_{FSP} and W_f^* slightly larger. An example is shown in Figure 7.8 where $W_b^* = 0.1$, $W_f^* = 0.5$, and $W_{\text{FSP}} = 0.30$. These parameters are, however, quite extreme – in actual computations we would use e.g. $W_b^* = 0.29$ and $W_f^* = 0.31$ and the smoothed water contents are then hardly distinguishable from the exact water contents indicated by dashed curves in the figure. It should be mentioned that the total moisture content is never computed from (7.53); only when the bound or free water contents are needed are these computed on the basis of the total water content by (7.55). The total moisture content \mathbf{W} is updated iteratively as described in the above. Thus, the variable smoothing is in fact equivalent to smoothing the effective transport coefficients.

7.6.2 Example

In the following an example of wood drying is presented. The internal transfer parameters used can be found in [48]. As boundary condition we use the common convection condition with the equilibrium vapour pressure as driving force, i.e. the outward directed flux at exchange surfaces is given by

$$j_n = \beta(p_{v,\text{eq}}^{\text{es}} - p_v^\infty) \quad (7.56)$$

where in the following $\beta = 70 \times 10^{-9} \text{ Pa}^{-1} \text{ kg m}^{-2} \text{ s}^{-1}$ and $p_v^\infty/p_{v,s} = 0.1$.

A board with a $5 \times 10 \text{ cm}$ cross section and a length of a is considered. By symmetry considerations this board can be reduced to one eighth such that the mesh shown in Figure (7.9) is used. On the surfaces visible in the figure the convection boundary condition

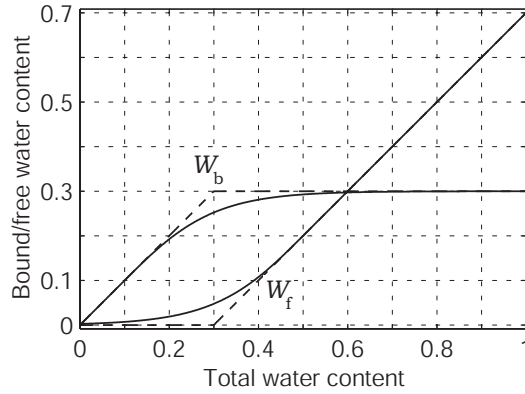
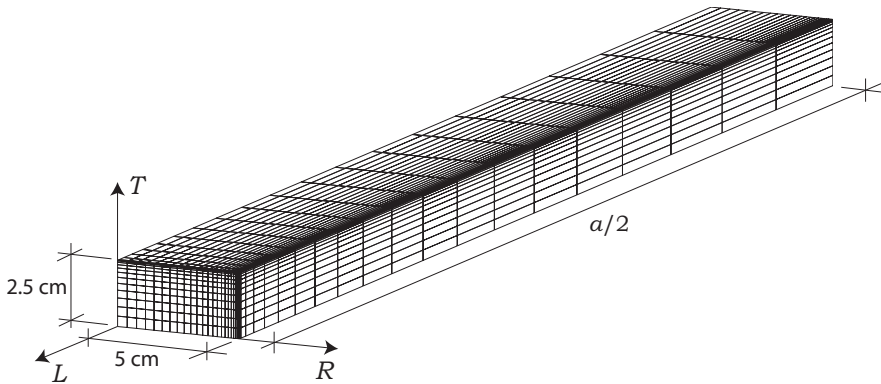


Figure 7.8 Variable smoothing.

Figure 7.9 Mesh ($N_T \times N_R \times N_L = 12 \times 24 \times 20$) used for wood drying simulations. Note refinement around exchange surfaces.

(7.56) is applied and on all other surfaces the flux is equal to zero. In all examples the temperature is 60°C .

All implementation was done in MATLAB with the biconjugate gradients stabilized method (`bicgstab`) used for the solution of the Jacobian system of equations (7.49). For the largest example run, this method turned out to be approximately 100 faster than the most efficient direct method that MATLAB has to offer. Although this number is not universal, it does illustrate the potential gain from using iterative methods for the solution of the non-symmetric type of equation systems dealt with in nonlinear heat and mass transfer computations.

In Figures (7.10) and (7.11) moisture distributions at selected times in a board with $a = 100$ cm are shown. As can be seen the transfer is largely two-dimensional such that

very little variation is observed along the longitudinal axis. Thus, the two-dimensional R/T model often used to model the drying of boards with much greater length than width seems completely justified. In Figure (7.12) the average moisture contents as function of time is shown. Also shown is the curve corresponding to a constant rate of evaporation through the exchange surfaces, i.e. with the average moisture content given by

$$\rho_0 V \frac{dW_{av}}{dt} = A_{es} \beta (p_{vs} - p_{v\infty}) \quad (7.57)$$

where we have used the fact that above the fiber saturation point the equilibrium vapour pressure is very close to the saturation pressure. As can be seen the drying

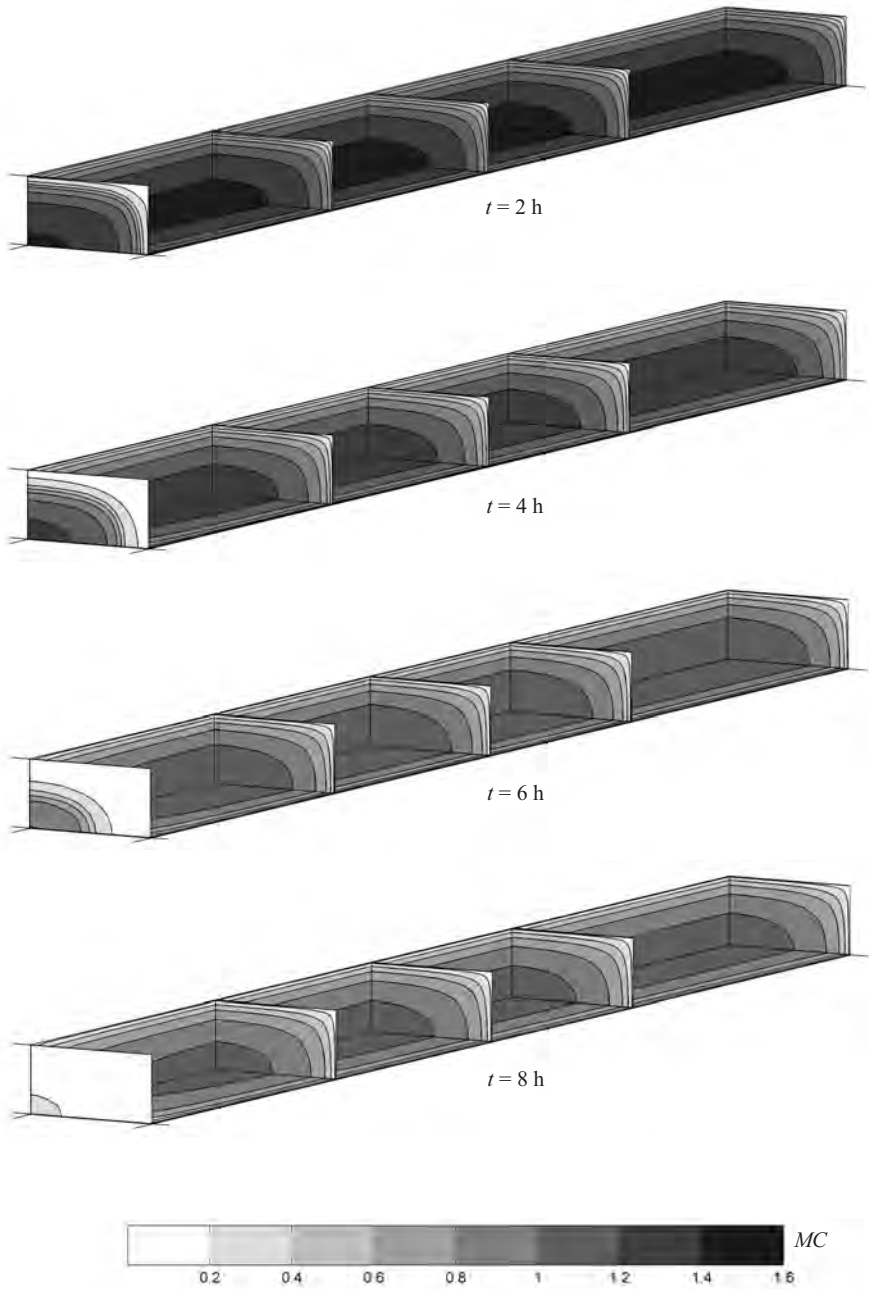


Figure 7.10 Evolution of the drying process, $a/2 = 50$ cm,
 $T = 60^\circ\text{C}$, $W_0 = 1.5$ kg/kg.

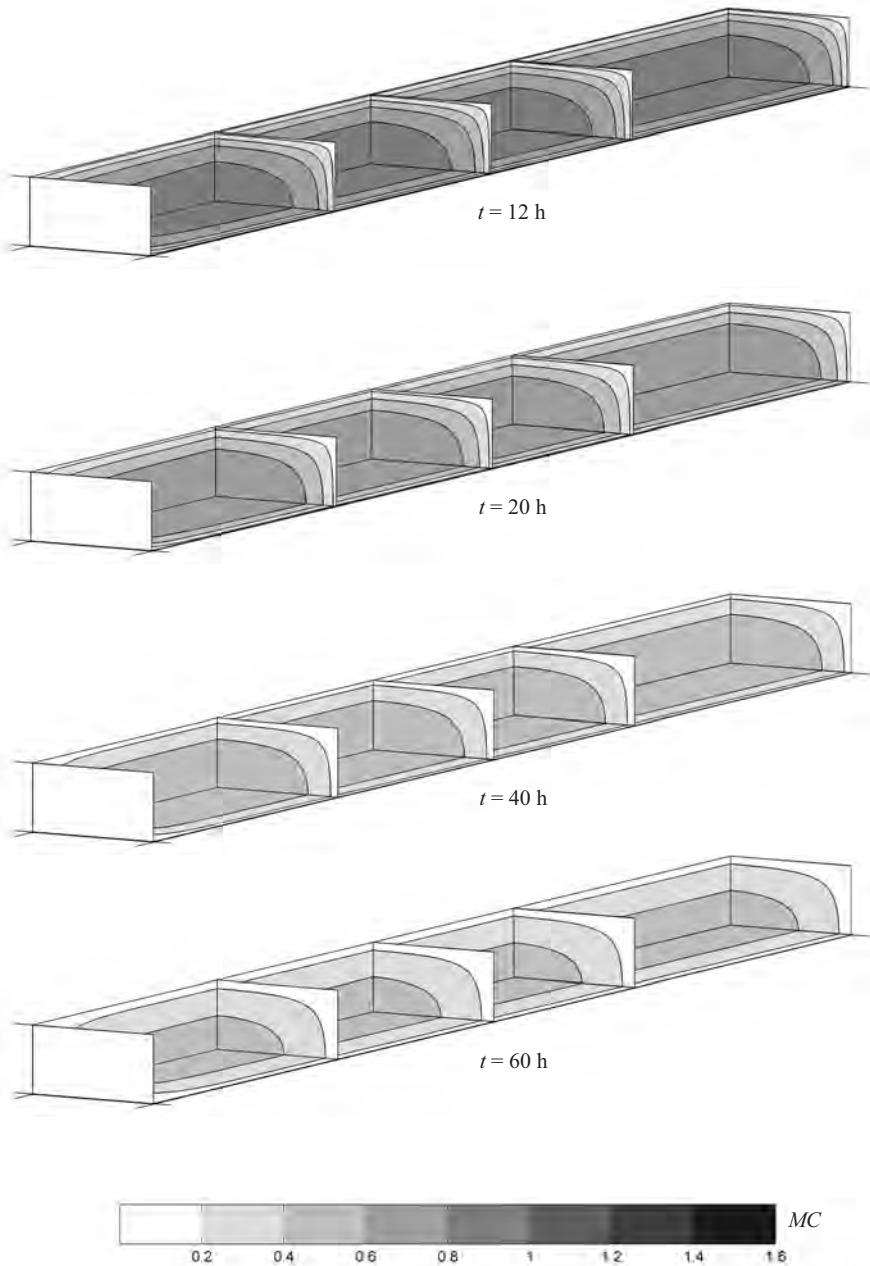


Figure 7.11 Evolution of the drying process, $a/2 = 50$ cm,
 $T = 60^\circ\text{C}$, $W_0 = 1.5$ kg/kg.

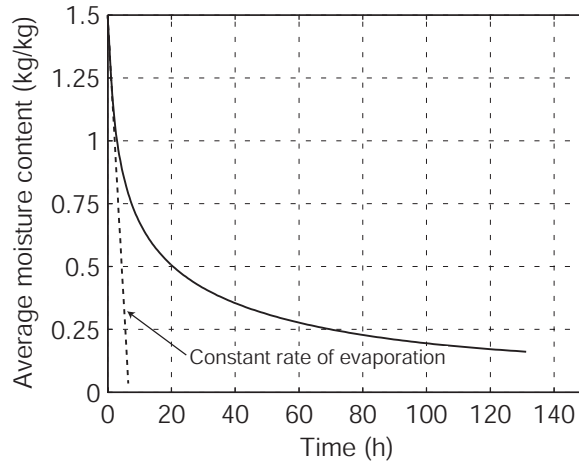


Figure 7.12 Average moisture content as function of time,
 $a/2 = 50 \text{ cm}$, $T = 60^\circ \text{C}$, $W_0 = 1.5 \text{ kg/kg}$.

curve follows (7.57) very closely down to around $W = 1.0 \text{ kg/kg}$. Thus, above this moisture content evaporation is rate determining, whereas below the internal transfer becomes increasingly dominant as the internal transfer coefficients decrease with decreasing moisture content.

In order to examine the influence of the length in comparison to the dimensions of the cross section, the example was rerun for boards with identical cross sections, but with different lengths. The results of these analyses are shown in Figure 7.13 in terms of the average moisture content as function of time, and as can be seen the length of the board means only very little in this regard.

As for the efficiency of the iterative procedure we generally require slightly more iterations than was the case with the Richards equation. The above examples were all run using 220 time steps and the total number of iterations was approximately 1400 corresponding to ~ 6.5 iterations per time step.

7.7 Implementation issues

In the following some of the issues necessary for an efficient implementation are discussed. First a number of different weighting schemes are presented. In this context an example is which demonstrates the need for upstream weighting is given. Secondly, the analytical derivation of tangent matrices is discussed. Formulas which should be directly applicable in implementations are given. Furthermore, a number of special cases are discussed and finally the formulas are extended to general multi-variable problems such as those encountered in coupled heat and mass transfer.

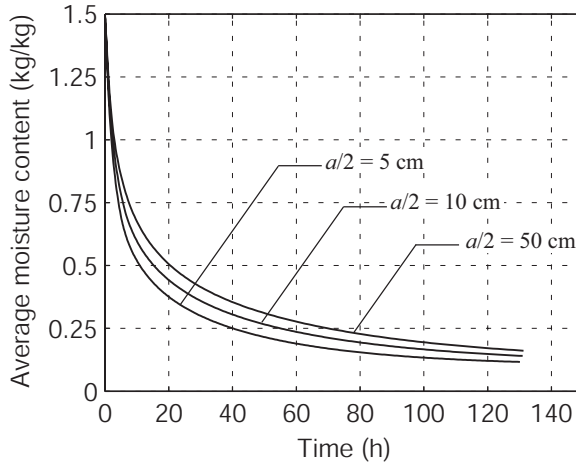


Figure 7.13 Average moisture content as function of time for boards of different length, $T = 60^\circ\text{C}$, $W_0 = 1.5\text{ kg/kg}$.

7.7.1 Integration of conductivity matrices

For highly nonlinear conductivity problems such as the ones treated in the above, the appropriate integration of the conductivity matrices is an important issue. Use of the standard Galerkin finite element method leads to conductivity matrices of the type

$$\mathbf{K}(\mathbf{u}) = \int_{\Omega} \mathbf{B}^T \mathbf{D}(\mathbf{N}\mathbf{u}) \mathbf{B} \, d\Omega \quad (7.58)$$

Since \mathbf{D} is usually highly nonlinear, numerical integration techniques must almost always be used in evaluating such matrices.

As an alternative to the ‘consistent’ integration (7.58), some representative average value of \mathbf{D} could be used, for example

$$\bar{\mathbf{D}} = \eta \mathbf{D}(u_i) + (1 - \eta) \mathbf{D}(u_j) \quad (7.59)$$

where i and j refer to element node numbers. This would then lead to

$$\mathbf{K}(\mathbf{u}) = \bar{\mathbf{D}} \int_{\Omega} \mathbf{B}^T \mathbf{B} \, d\Omega \quad (7.60)$$

Of course, this may be seen as a special case of (7.58), namely

$$\begin{aligned} \mathbf{K}(\mathbf{u}) &= \eta \int_{\Omega} \mathbf{B}^T \mathbf{D}(\mathbf{N}(x_i, y_i, z_i) \mathbf{u}) \mathbf{B} \, d\Omega \\ &+ (1 - \eta) \int_{\Omega} \mathbf{B}^T \mathbf{D}(\mathbf{N}(x_j, y_j, z_j) \mathbf{u}) \mathbf{B} \, d\Omega \end{aligned} \quad (7.61)$$

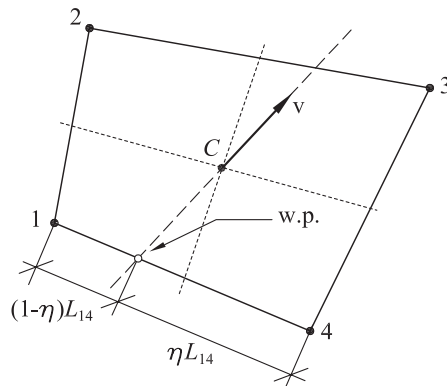


Figure 7.14 Upstream weighting for four-node element.

In numerical fluid dynamics it is well known that upstream weighting can improve the computed results significantly. In fact, in order to avoid non-physical oscillations in the state variables it is in many cases necessary. For nonlinear diffusion problems the situation is similar. Although pure diffusion problems are usually much easier to handle than those involving convective transport, the presence of highly nonlinear constitutive relations can lead to a front-like behaviour such as is typically seen in problems involving convective transport. In mathematical terms non-physical oscillations are possible when the diagonal entries in the tangent matrix become negative or when the off-diagonal entries become positive. These facts have been used in a very comprehensive analysis by Forsyth [18] who concluded that only full upstream weighting is unconditionally stable and hence should be used routinely. A practical procedure, applicable to arbitrary elements, has been presented by Diersch and Perrochet [15], who suggested evaluating the average conductivity on the basis of direction of the current flux. The procedure is sketched in Figure 7.14 for a four-node element. In each time step, before entering into the iterations, an appropriate weighting point (w.p.) is selected. This is taken as the intersection between the flux direction as given in the center of the element and the element boundary, as shown in the Figure. The average conductivity is then computed as indicated in (7.59), where we would have $i = 1$ and $j = 4$. This procedure is of course straight forward to generalize to three dimensions.

It should be emphasized that forward weighting generally deteriorates the accuracy of the solution compared to what can be achieved with a central weighting, where $\bar{\mathbf{D}}$ is taken as the average of all the nodal values. However, the possibility of non-physical oscillations is often viewed as so undesirable that a solution which on an average basis is less accurate, but which still complies with the fundamental physical principles, is preferred.

Example

We will illustrate the effects of different weighting strategies on the classical convection–diffusion equation

$$\rho c \left(\frac{\partial T}{\partial t} + \mathbf{v} \cdot \nabla T \right) = \nabla \cdot (\lambda \nabla T) \quad (7.62)$$

This equation describes e.g. the transfer of heat in a fluid moving at velocity a \mathbf{v} . The density of the fluid is ρ , the heat capacitance c , and the conductivity λ . This equation is often used as a model problem in the development of efficient solution strategies for the Navier–Stokes equations, see e.g. [39].

In the one dimensional case, using linear two–node elements, an element Peclet number can be defined as

$$\text{Pe} = \frac{u \delta x}{\lambda} \quad (7.63)$$

where δx is the element size and u the fluid velocity. It is well–known that for $\text{Pe} > 2$ the standard Galerkin scheme produces solutions with non–physical temperature oscillations. To remedy this, a number of upwinding strategies have been developed. These usually involve the use of weighting functions different from those used to interpolate the temperature.

Here, however, we will take a different course and formulate the original equation in terms of a nonlinear diffusion problem, which, however, is in effect linear and can be solved in one iteration. The origin of the original equation (7.62) is a general statement of conservation of enthalpy which may be written as

$$\frac{\partial}{\partial t}(\rho h) + \nabla \cdot (\rho h \mathbf{v}) = \nabla \cdot (\lambda \nabla T) \quad (7.64)$$

In addition, the mass balance of the fluid can be expressed as

$$\frac{\partial \rho}{\partial t} + \nabla \cdot (\rho \mathbf{v}) = 0 \quad (7.65)$$

Equation (7.64) can be expanded as

$$\rho \frac{\partial h}{\partial t} + h \frac{\partial \rho}{\partial t} + h \nabla \cdot (\rho \mathbf{v}) + \rho \mathbf{v} \cdot \nabla h = \nabla \cdot (\lambda \nabla T) \quad (7.66)$$

Now, using (7.65) the above can be simplified to

$$\rho \frac{\partial h}{\partial t} + \rho \mathbf{v} \cdot \nabla h = \nabla \cdot (\lambda \nabla T) \quad (7.67)$$

and, finally, using $h = cT$, with c assumed constant, we arrive at the convection–diffusion equation (7.62). In the following, however, we not make this simplification beforehand, but instead make use of the ‘natural’ conservation equations (7.64)–(7.65). Without loss of generality we can assume the velocity given in terms of a gradient-type law as

$$\mathbf{v} = -\nabla P \quad (7.68)$$

where P can be thought of as a ‘driving pressure’ [m^2/s] in analogy with e.g. Darcy’s law. Inserting this into (7.64)–(7.65), two coupled equations appear as

$$\rho c \frac{\partial T}{\partial t} = \nabla \cdot (\lambda \nabla T) + \nabla \cdot (\rho c T \nabla P) \quad (7.69)$$

$$\nabla \cdot (\rho \nabla P) = 0 \quad (7.70)$$

where we have assumed that ρ is constant. These equations are clearly of the standard diffusive type, with a nonlinear diffusivity $\rho c T$ appearing in the last term of (7.69). Thus, the finite element formulation is straight forward to derive, the result being written principally as

$$\begin{bmatrix} \mathbf{C} & \mathbf{0} \\ \mathbf{0} & \mathbf{0} \end{bmatrix} \begin{bmatrix} \dot{\mathbf{T}} \\ \dot{\mathbf{P}} \end{bmatrix} + \begin{bmatrix} \mathbf{K}_{TT} & \mathbf{K}_{TP} \\ \mathbf{0} & \mathbf{K}_{PP} \end{bmatrix} \begin{bmatrix} \mathbf{T} \\ \mathbf{P} \end{bmatrix} + \begin{bmatrix} \mathbf{f}_T \\ \mathbf{f}_P \end{bmatrix} = \begin{bmatrix} \mathbf{0} \\ \mathbf{0} \end{bmatrix} \quad (7.71)$$

However, the integration of the term

$$\mathbf{K}_{TP} = \int_{\Omega} \mathbf{B}^T \rho c T \mathbf{B} \, d\Omega \quad (7.72)$$

should be considered in some detail. If the standard Galerkin procedure is applied we simply perform the integration in a consistent manner, e.g. for a two–node element as

$$\mathbf{K}_{TP} = \rho c \frac{1}{2} (T_0 + T_1) \frac{1}{l} \begin{bmatrix} 1 & -1 \\ -1 & 1 \end{bmatrix} \quad (7.73)$$

The upstream weighting procedure described in the above, however, suggests representing the integral as

$$\mathbf{K}_{TP} = \rho c T_0 \frac{1}{l} \begin{bmatrix} 1 & -1 \\ -1 & 1 \end{bmatrix} \quad (7.74)$$

where it is assumed that the motion of the fluid takes place from left to right, i.e. from node 0 to node 1.

A very simple numerical example is now considered. It involves a one dimensional slab of length 1.0. At $x = 0.0$ we have $T = 1.0$ and at $x = 1.0$ the temperature is $T = 0.0$. The conductivity is $\lambda = 0.1$, the velocity $u = 3$, and $\rho c = 1.0$. The exact steady state solution is given by

$$T(x) = 1 - \frac{\exp(\rho c u x / \lambda) - 1}{\exp(\rho c u / \lambda) - 1} \quad (7.75)$$

First a mesh of eight equally spaced elements is used, giving an element Peclet number of $Pe = 3.75$. The steady–state temperature distribution is shown in Figure 7.15. In Figure 7.15 (a) the results obtained with a central weighting, i.e. corresponding to (7.73) are shown, and as seen the temperature distribution oscillates about the exact solution in a non–physical manner. In contrast the upstream weighting produces a stable, although not very accurate, solution – the front is said to be smeared due to fake or artificial diffusion. Next, the number of elements is increased to 24 corresponding to $Pe = 1.25$. The results are shown in Figure 7.16. Since the Peclet number is now less than 2, the central weighting, Figure 7.16 (a), produces a non–oscillatory solution which, furthermore, is somewhat more accurate than what is obtained with the upstream weighting, Figure 7.16 (b). Thus,

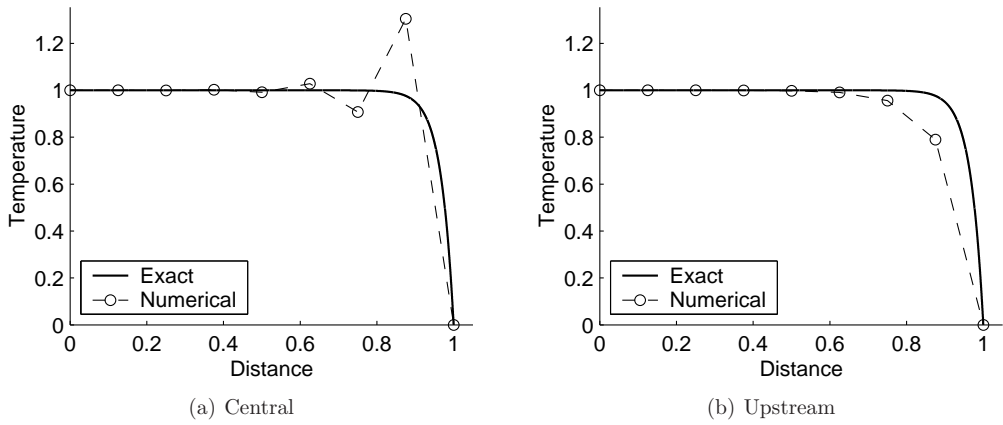


Figure 7.15 Steady state solution of convection–diffusion equation with $Pe = 3.75$.

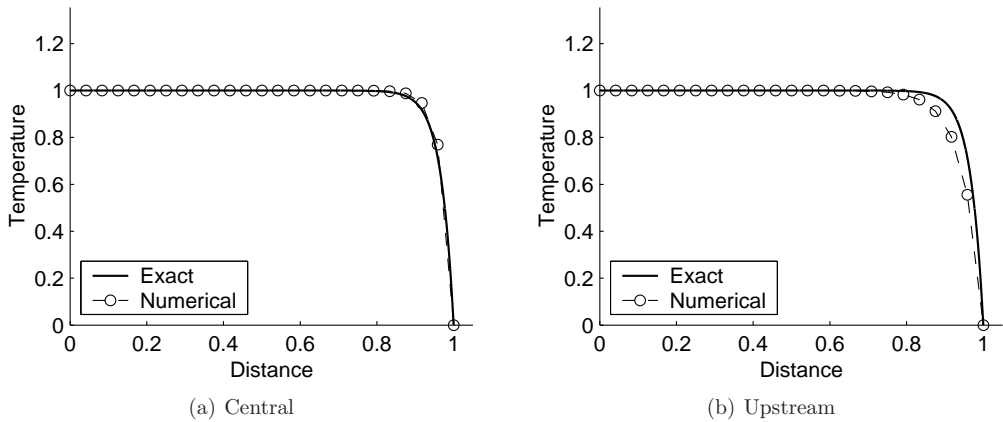


Figure 7.16 Steady state solution of convection–diffusion equation with $Pe = 1.25$.

in general there seems to be a trade-off between accuracy and stability. The weighting may of course be adjusted to the particular circumstances, and for one dimensional problems such procedures have been devised [39]. However, for general multi-dimensional problems, possibly involving a variety of material nonlinearities, there does not appear to be a scheme which ensures both optimal accuracy as well as stability.

It is worth noting that although in this case the discrete equations (7.71) represent the problem of convective heat transfer, the form of the equations correspond to a common coupled diffusion type system. Thus, it can be expected that forward weighting is nec-

essary for wide variety of problems where, in contrast to what is the case with the one dimensional convection–diffusion problem, non–physical oscillations may be difficult to predict beforehand.

Finally, it should be mentioned that whereas the equation system (7.71) is in principle nonlinear through \mathbf{K}_{TP} , this nonlinearity may be removed by considering P known. If this is done \mathbf{K}_{TP} becomes linear in T and the equations can be solved in one iteration.

7.7.2 Jacobian construction

In the preceding the Jacobians used in Newton’s method have all been assumed known. In the following some of the more common Jacobians encountered in heat and mass transfer computations are given in a matrix–vector format which should resemble the format used in actual implementations quite closely.

In the following some formulas for the tangent matrices involving conductivity matrices are given. Consider two conductivity matrices given by

$$\mathbf{K}(\mathbf{u}) = \int_{\Omega} \mathbf{B}^T \mathbf{D}(\mathbf{A}\mathbf{u}) \mathbf{B} \, d\Omega, \quad \mathbf{K}(\mathbf{v}) = \int_{\Omega} \mathbf{B}^T \mathbf{D}(\mathbf{A}\mathbf{v}) \mathbf{B} \, d\Omega \quad (7.76)$$

where in the following \mathbf{A} is assumed constant. We then have

$$\frac{\partial^T}{\partial \mathbf{u}} (\mathbf{K}(\mathbf{u})\mathbf{u}) = \mathbf{K} + \mathbf{K}_G^{uu} \quad (7.77a)$$

$$\frac{\partial^T}{\partial \mathbf{u}} (\mathbf{K}(\mathbf{u})\mathbf{v}) = \mathbf{K}\mathbf{C}_{vu} + \mathbf{K}_G^{uv} \quad (7.77b)$$

$$\frac{\partial^T}{\partial \mathbf{u}} (\mathbf{K}(\mathbf{v})\mathbf{u}) = \mathbf{K} + \mathbf{K}_G^{vu}\mathbf{C}_{vu} \quad (7.77c)$$

where \mathbf{C}_{vu} is a diagonal matrix containing the derivative $\partial v/\partial u$ evaluated at each node

$$\mathbf{C}_{vu} = \frac{\partial \mathbf{v}}{\partial \mathbf{u}} = \begin{bmatrix} (\partial v/\partial u)_1 & & \\ & \ddots & \\ & & (\partial v/\partial u)_{n_{\text{dof}}} \end{bmatrix} \quad (7.78)$$

In the special case where u and v are independent state variables, e.g. pressure and temperature, we have $\mathbf{C}_{vu} = \mathbf{0}$. The matrices \mathbf{K}_G^{rs} are given by

$$\mathbf{K}_G^{rs} = \int_{\Omega} \mathbf{B}^T \mathbf{G}(\mathbf{A}\mathbf{r}) \mathbf{B} \mathbf{s} \mathbf{A} \, d\Omega \quad (7.79)$$

where

$$\mathbf{G}(r) = \begin{bmatrix} \frac{\partial \mathbf{D}_{11}}{\partial r} & \frac{\partial \mathbf{D}_{12}}{\partial r} & \frac{\partial \mathbf{D}_{13}}{\partial r} \\ & \frac{\partial \mathbf{D}_{22}}{\partial r} & \frac{\partial \mathbf{D}_{23}}{\partial r} \\ \text{symm.} & & \frac{\partial \mathbf{D}_{33}}{\partial r} \end{bmatrix} \quad (7.80)$$

The gradient conductivity matrices \mathbf{K}_G are unsymmetric which is a disadvantage over using simply the current conductivity matrix as the tangent matrix, also referred to as Picard iterations. Therefore, only if the benefits are significant in terms of convergence should the exact tangent matrix be used. For coupled systems, however, the global system matrix is inherently unsymmetric and using unsymmetric tangent submatrices should not present any additional complications.

In the case of wood the material parameters are usually defined with respect to the intrinsic directions, i.e. the radial, tangential and longitudinal directions. In this coordinate system $\mathbf{D}(r)$ is a diagonal matrix $\mathbf{D}_d(r)$. To permit use in a usual Cartesian coordinate system this diagonal matrix is transformed as

$$\mathbf{D}(r) = \mathbf{\Lambda}^T \mathbf{D}_d(r) \mathbf{\Lambda} \quad (7.81)$$

where $\mathbf{\Lambda}$ contains the direction cosines. Furthermore, it is easily shown that in this case the gradient matrix \mathbf{G} is given by

$$\mathbf{G}(r) = \mathbf{\Lambda}^T \mathbf{G}_d(r) \mathbf{\Lambda} \quad (7.82)$$

where $\mathbf{G}_d(r)$ contains the derivatives of the three independent material coefficients with respect to r .

Implementation

We now consider the implementation of the various formulas. As an example, consider 7.77b. The easiest way to proceed is then to compute matrices

$$\mathbf{K}(\mathbf{u}) = \int_{\Omega} \mathbf{B}^T \mathbf{D}(\mathbf{A}\mathbf{u}) \mathbf{B} \, d\Omega \quad (7.83)$$

and

$$\tilde{\mathbf{K}}_G^{uv} = \int_{\Omega} \mathbf{B}^T \mathbf{G}(\mathbf{A}\mathbf{u}) \mathbf{B} \, d\Omega \quad (7.84)$$

The tangent matrix can then be computed as

$$\mathbf{K}_t = \mathbf{K} \mathbf{C}_{uv} + \tilde{\mathbf{K}}_G^{uv} \mathbf{v} \mathbf{A} \quad (7.85)$$

If the conductivities are to be weighted for example as

$$\bar{\mathbf{D}} = \eta \mathbf{D}(u_i) + (1 - \eta) \mathbf{D}(u_j) \quad (7.86)$$

where i and j refer to node numbers, then it is necessary to first compute the matrices \mathbf{K} and \mathbf{K}_G in node i using $\mathbf{A}_i = \mathbf{N}(x_i, y_i, z_i)$ and then in node j with $\mathbf{A}_j = \mathbf{N}(x_j, y_j, z_j)$. Finally, the total matrices are computed as

$$\mathbf{K} = \eta \mathbf{K}_i + (1 - \eta) \mathbf{K}_j \quad (7.87)$$

and

$$\mathbf{K}_t = \eta \mathbf{K}_{t,i} + (1 - \eta) \mathbf{K}_{t,j} \quad (7.88)$$

Special cases

The above formulas and directions for implementation are completely general. However, in the important special case where the variable part of the conductivity matrix is a scalar function the formulas may be simplified. This case occurs in soils where the absolute permeability may be defined by intrinsic directions as in wood whereas the relative permeability is a scalar function, i.e.

$$\mathbf{D} = \mathbf{I}D_{\text{rel}}(u) + \mathbf{D}_{\text{abs}} \quad (7.89)$$

where \mathbf{I} is the identity matrix. In this case we define

$$\mathbf{A} = [\eta; \quad 1 - \eta] \quad (7.90)$$

and then proceed by computing a matrix

$$\tilde{\mathbf{K}} = \int_{\Omega} \mathbf{B}^T \mathbf{D}_{\text{abs}} \mathbf{B} \, d\Omega \quad (7.91)$$

The conductivity matrix is given by

$$\mathbf{K} = \mathbf{A} \mathbf{D}_{\text{rel}}(\mathbf{u}) \tilde{\mathbf{K}} \quad (7.92)$$

where $\mathbf{D}(\mathbf{u})$ contains the nodal relative permeabilities

$$\mathbf{D}_{\text{rel}}(\mathbf{u}) = [D_{\text{rel}}(u_1), \dots, D_{\text{rel}}(u_{n_{\text{dof}}})]^T \quad (7.93)$$

The tangent matrix can be computed as

$$\mathbf{K}_t = \mathbf{K} + \tilde{\mathbf{K}} \mathbf{v} \mathbf{A} \text{diag}(\mathbf{D}'_{\text{rel}}(\mathbf{u})) \quad (7.94)$$

where $\mathbf{D}'(\mathbf{u})$ contains the derivative of the nodal relative permeabilities

$$\mathbf{D}'_{\text{rel}}(\mathbf{u}) = [\partial D_{\text{rel}}/\partial u(u_1), \dots, \partial D_{\text{rel}}/\partial u(u_{n_{\text{dof}}})]^T \quad (7.95)$$

Another special case appears in the case where \mathbf{D} is a diagonal matrix, possibly with the elements being variable and different from each other, i.e.

$$\mathbf{D}(r) = \begin{bmatrix} D_x(r) & & \\ & D_y(r) & \\ & & D_z(r) \end{bmatrix} \quad (7.96)$$

In this case the conductivity matrix is given by

$$\mathbf{K} = \int_{\Omega} \left[\frac{\partial^T \mathbf{N}}{\partial x} D_x \frac{\partial \mathbf{N}}{\partial x} + \frac{\partial^T \mathbf{N}}{\partial y} D_y \frac{\partial \mathbf{N}}{\partial y} + \frac{\partial^T \mathbf{N}}{\partial z} D_z \frac{\partial \mathbf{N}}{\partial z} \right] d\Omega \quad (7.97)$$

and the above procedure then applies directly for each of the submatrices comprising the total conductivity matrix.

Generalization to multiple variable problems

Consider now the case where the conductivity is a function of two or more variables which may be mutually dependent, i.e.

$$\mathbf{K} = \mathbf{K}(\mathbf{u}, \mathbf{v}, \mathbf{w}, \dots) \quad (7.98)$$

and we want to determine

$$\mathbf{K}_t = \frac{\partial^\top}{\partial \mathbf{u}}(\mathbf{K}(\mathbf{u}, \mathbf{v}, \mathbf{w}, \dots)\mathbf{u}) \quad (7.99)$$

Such situations commonly occur in coupled heat and mass transfer computations where \mathbf{u} could be air pressure, \mathbf{v} temperature and \mathbf{w} saturation. In this case the tangent matrix can be computed by means of the differentiation rule

$$\begin{aligned} \frac{\partial^\top}{\partial \mathbf{u}}(\mathbf{K}(\mathbf{u}, \mathbf{v}, \mathbf{w}, \dots)\mathbf{u}) &= \frac{\partial^\top}{\partial \mathbf{u}}(\mathbf{K}(\mathbf{u}, \mathbf{v}_0, \mathbf{w}_0, \dots)\mathbf{u}) + \frac{\partial^\top}{\partial \mathbf{u}}(\mathbf{K}(\mathbf{u}_0, \mathbf{v}, \mathbf{w}_0, \dots)\mathbf{u}_0) \\ &+ \frac{\partial^\top}{\partial \mathbf{u}}(\mathbf{K}(\mathbf{u}_0, \mathbf{v}_0, \mathbf{w}, \dots)\mathbf{u}_0) + \dots \end{aligned} \quad (7.100)$$

where subscript 0 indicates that the variable is considered constant when the tangent matrix formulas (7.77) are applied. Furthermore, the two last terms in the above expression may be expanded as

$$\frac{\partial^\top}{\partial \mathbf{u}}(\mathbf{K}(\mathbf{u}_0, \mathbf{v}, \mathbf{w}_0, \dots)\mathbf{u}_0) = \frac{\partial^\top}{\partial \mathbf{v}}(\mathbf{K}(\mathbf{u}_0, \mathbf{v}, \mathbf{w}_0, \dots)\mathbf{u}_0) \left(\frac{\partial \mathbf{v}}{\partial \mathbf{u}} \right) \quad (7.101)$$

$$\frac{\partial^\top}{\partial \mathbf{u}}(\mathbf{K}(\mathbf{u}_0, \mathbf{v}_0, \mathbf{w}, \dots)\mathbf{u}_0) = \frac{\partial^\top}{\partial \mathbf{w}}(\mathbf{K}(\mathbf{u}_0, \mathbf{v}_0, \mathbf{w}, \dots)\mathbf{u}_0) \left(\frac{\partial \mathbf{w}}{\partial \mathbf{u}} \right) \quad (7.102)$$

and the formulas (7.77) can now be directly applied.

In the case of three mutually dependent variables u , v , and w the above tangent matrix would be

$$\mathbf{K}_t = \frac{\partial^\top}{\partial \mathbf{u}}(\mathbf{K}(\mathbf{u}, \mathbf{v}, \mathbf{w})\mathbf{u}) = \mathbf{K} + \mathbf{K}_G^{uu} + \mathbf{K}_G^{vu} \mathbf{C}_{vu} + \mathbf{K}_G^{wu} \mathbf{C}_{wu} \quad (7.103)$$

where the fact that $\mathbf{C}_{u_0v} = \mathbf{C}_{u_0w} = \mathbf{0}$ has been utilized. If u is independent of both v and w , we have $\mathbf{C}_{vu} = \mathbf{C}_{wu} = \mathbf{0}$ and the above formula reduces to (7.77a).

Numerical differentiation

As an alternative to the above formulas, the Jacobian may determined numerically. In this case the Jacobian can be computed column by column as

$$\mathbf{J}(:, i) = \frac{\mathbf{r}(u_1, \dots, u_i + \delta, \dots, u_n) - \mathbf{r}(u_1, \dots, u_i, \dots, u_n)}{\delta} \quad (7.104)$$

where δ must be chosen as being small enough to accurately approximate the exact result and large enough to avoid numerical errors. Often a value of $\delta = 10^{-7}$ is used although,

strictly speaking, it should be chosen on the basis of the magnitude of the variables involved, see e.g. [42].

Although numerical determination of the Jacobian is more expensive and more prone to errors than the analytical procedure, it is nevertheless attractive in that the part of the code concerned with the determination of the Jacobian can be implemented as being independent of the nature of the problem in question. Thus, if the aim is to produce a very general code capable of dealing with arbitrary couplings the numerical method could be preferred, whereas for specialized codes with limited scopes of application the analytical method should be the most efficient.

Finally, the possibility of combining the two approaches should be mentioned. If some of the material parameters involved display discontinuities in the first derivatives then it may be useful to approximate the gradient around these discontinuities numerically. The approximate gradient can then be used in the analytical tangent matrix formulas. In the examples concerned with the Richards equation this method was used in order to handle the abrupt change in the derivative of the hydraulic conductivity when going from partially to fully saturated conditions.

7.8 Conclusions and future work

In the above several important issues have been touched upon, including the iterative procedure, choice of state variables, weighting schemes and exact tangent matrices. A very important issue, which has not been dealt with, however, is that of automatic time step selection. For single phase problems it is not too hard to implement some kind automatic time step selection, based for example, on the progress of the iterations or the relative change of the solution from one time step to another. Recently, however, more rigorous methods have been implemented for different forms of the Richards equation [31, 32, 33]. Here the time step was selected on the basis of a prescribed error tolerance, such that the temporal error of the final solution could in fact be determined beforehand. Moreover, it was shown that it was possible to formulate non-iterative semi-explicit schemes which were competitive with their iterative fully implicit counterparts. Also, the methods were all implemented using the current conductivity matrices, and not the exact tangent matrices. Thus, a number of the issues that one usually has to deal with were lumped into the one problem of selecting an appropriate time step. If this time step selection procedure can be formulated in a sufficiently general way, and this was claimed to have been achieved in the above references, then the implementation of a particular nonlinear transport problem boils down to setting up the element matrices, and this is of course offers a tremendous reduction in complexity over the usual procedure. Although the above cited works all deal with single phase flow there should not be any significant obstacles in formulating similar schemes for general multi-phase flow problems, and in our opinion this may well be the way to proceed in the development of a general coupled heat and mass transfer code. However, since in ‘non-iterative’ schemes one iteration has to be carried out per time step, the choice of state variable, or alternatively, the type of update used will still have the potential of improving the performance significantly, at least above some specified error tolerance.

Whereas temporal discretization errors may be controlled and reduced at little additional cost, the issue of improving the spatial discretization is a more involved problem. Besides simply refining the mesh, only two other options really exist. The first of these is to use higher order element. Although this should in principle improve the solution, it introduces a number of other complications. These are primarily related to the possibility of non-physical solutions which are known to be possible even in one dimensional steady state situations. Furthermore, for higher order elements there is no obvious way of lumping mass matrices, and in addition, the consistent mass matrices may contain negative elements. Therefore, only linear elements which do not violate the fundamental principles of physics should be used. In one dimension the only choice is thus the two-node element, and in two and three dimensions three and four and four and eight node elements, which furthermore are subject to certain geometric constraints [54].

The second possibility of improving the quality of the solution without refining the mesh consists of adjusting the conductivity weighting scheme according to the nature of the problem. This was demonstrated by central and upstream weightings for the convection-diffusion problem. Whereas upstream weighting results in stable solutions, this is achieved at the expense of accuracy. Thus, a relevant question to pose is to just how far upstream the weighting point should be placed. For the one dimensional steady state convection-diffusion problem it is possible to determine an optimal point, as function of the Peclet number, which ensures stability and at the same time maximizes the accuracy [39]. However, for general multi-dimensional transient and coupled problems such a point is not easy to determine, and one often resorts to procedures such as the one of Diersch and Perrochet [15] discussed in the above. Thus, the formulation of stable yet accurate weighting schemes for multi-dimensional problems seems to offer the possibility of improved accuracy at no or very little additional cost.

Chapter 8

Conclusions

This focus of this thesis has been the flow of water in wood. In addition, also the transport of additional components, e.g. representing preservative chemicals, has been considered. We have focused particularly on phenomena for which current models fail or produce very inaccurate results. For these phenomena alternative models, which to a higher degree are able to capture the physics of the problems, have been formulated.

For the problem of moisture transport below the fiber saturation point a new model has been formulated, and as demonstrated it shows quite some promise in terms of capturing phenomena which so far have been difficult or impossible to quantify. The corner stone of the model is the separation of water vapour and bound water. However, it is shown that whereas this separation is absolutely necessary, it is not in itself sufficient to describe the fundamental non-Fickian characteristics such as the dependence upon the magnitude of the sorption step. Thus, any further research should concentrate first and foremost on the cell wall sorption rather than on the diffusion of water vapour and bound water.

Next, the problem of free water transport, particularly as related to infiltration, has been considered. Here, double porosity and permeability models, which are commonly used in connection with fractured soils, have been applied. The validity of these models when applied to wood is discussed and it is concluded that especially in the case of hardwoods should the models be applicable. This is further demonstrated by examination of experimental results and the fit of some of these by the double permeability model.

The general mathematical framework used allows for a straight forward inclusion of additional species. This has been utilized to study the problem of wood preservation by artificial preservatives. A concrete example of the treatment of wooden poles partially embedded in soil by boric acid was presented. Although the overall problem contains many unknowns, not least when it comes to material parameters, it is demonstrated that the possibility of applying mathematical and numerical models to practical problems is a very real one. With a better knowledge of the material parameters involved these models could well prove valuable in the prediction of the effects of a given type of treatment.

Finally, numerical solution procedures are dealt with. For the transport of free water a new iterative procedure has been formulated. This method has previously proved its worth in the mathematically similar problem of heat conduction with change of phase. It is shown that the method is equivalent to the so-called variable switching procedure. It is, however, much simpler to implement and furthermore, permits a more natural transition

Conclusions

between partially and fully saturated conditions. Further issues dealt with are the integration of conductivity matrices and analytical construction of tangent matrices. Both these issues are crucial in ensuring an efficient and robust numerical implementation.

Bibliography

- [1] I. ABSETZ AND S. KOPONEN. Fundamental diffusion behaviour of wood. In P. HOFFMEYER, editor, “International Conference on Wood-Water Relations”, pages 89–106, Copenhagen, Denmark (1996). COST Action E8. Mechanical Performance of Wood and Wood Products.
- [2] W. B. BANKS. Addressing the problem of non-steady state liquid flow in wood. *Wood Science and Technology* **15**, 171–177 (1981).
- [3] G. BRAMHALL. The validity of Darcy’s Law in the axial penetration of wood. *Wood Science and Technology* **5**, 121–134 (1971).
- [4] M. A. CELIA, S. ZISMAN, AND P. BINNING. A general mass-conservative numerical solution for the unsaturated flow equation. *Water Resources Research* **26**(7), 1483–1496 (1990).
- [5] G. N. CHRISTENSEN. The rate of sorption by wood and pulp. *Appita* **13**, 112–123 (1959).
- [6] G. N. CHRISTENSEN. The rate of sorption by thin materials. In A. WEXLER AND P. A. WINN, editors, “Humidity and Moisture”, volume 4, pages 279–293, Reinhold Pub. Corp., N.Y. (1965).
- [7] G. N. CHRISTENSEN AND K. E. KELSEY. Die Geschwindigkeit der Wasserdampfsorption durch Holz. *Holz als Roh- und Werkstoff* **17**(5), 189–203 (1959).
- [8] G. N. CHRISTENSEN AND K. E. KELSEY. Die Sorption von Wasserdampf durch die chemischen Bestandteile des Holzes. *Holz als Roh- und Werkstoff* **17**(5), 178–188 (1959).
- [9] G. COMINI AND S. DEL GUIDICE. A physical interpretation of conventional finite-element formulations of conduction-type problems. *International Journal for Numerical Methods in Engineering* **32**(3), 559–570 (1991).
- [10] G. COMINI, S. DEL GUIDICE, AND C. NONINO. Energy balances in CVFEM and GFEM formulations of convection-type problems. *International Journal for Numerical Methods in Engineering* **39**(13), 2249–2263 (1996).
- [11] P. COOPER. University of Toronto. Personal Communication (June 2003).

- [12] F. COUTURE, W. JOMAA, AND J.-R. PUIGGALI. Relative permeability relations: A key factor for a drying model. *Transport in Porous Media* **23**, 303–335 (1996).
- [13] J. CRANK. “The Mathematics of Diffusion”. Oxford University Press (1967).
- [14] M. J. CUNNINGHAM. A model to explain ”anomalous” moisture sorption in wood under step function driving forces. *Wood and Fiber Science* **27**(3), 265–277 (1996).
- [15] H.-J. G. DIERSCH AND P. PERROCHET. On the primary variable switching technique for simulating unsaturated–saturated flows. *Advances in Water Resources* **23**, 271–301 (1999).
- [16] J. M. DINWOODIE. “Timber, its nature and behaviour”. Van Norstrand Reinhold, New York (1981).
- [17] M. W. FARTHING, C. E. KEES, AND C. T. MILLER. Mixed finite element methods and higher order temporal approximations for variably saturated ground water flow. *Advances in Water Resources* **26**, 373–394 (2003).
- [18] P. A. FORSYTH AND M. C. KROPINSKI. Monotonicity considerations for saturated-unsaturated subsurface flow. *SIAM Journal of Scientific Computing* **18**, 1328–1354 (1997).
- [19] P. A. FORSYTH, Y. S. WU, AND K. PRUESS. Robust numerical methods for saturated–unsaturated flow with dry initial conditions in heterogeneous media. *Advances in Water Resources* **18**, 25–38 (1995).
- [20] D. GAWIN, P. BAGGIO, AND B. A. SCHREFLER. Coupled heat, water and gas flow in deformable porous media. *International Journal for Numerical Methods in Fluids* **20**, 969–987 (1995).
- [21] D. GAWIN, F. PESAVENTO, AND B. A. SCHREFLER. Modelling of hygro–thermal behaviour of concrete at high temperature with thermo–chemical and mechanical material degradation. *Computer Methods in Applied Mechanics and Engineering* **192**, 1731–1771 (2003).
- [22] D. GAWIN AND B. A. SCHREFLER. Thermo–hydro–mechanical analysis of partially saturated porous media. *Engineering Computations* **13**, 113–143 (1996).
- [23] B. GOODELL, D. D. NICHOLAS, AND T. P. SCHULTZ (EDS.). “Wood Deterioration and Preservation. Advances in Our Changing World.” American Chemical Society, New York (2003).
- [24] M. GOYENECHÉ, D. LASSEUX, AND D. BRUNEAU. A film–flow model to describe free water transport during drying of a hygroscopic capillary porous medium. *Transport in Porous Media* **48**, 125–158 (2002).
- [25] M. GOYENECHÉ, D. LASSEUX, AND D. BRUNEAU. On a pore-scale film flow approach to describe moisture transfer in a hygroscopic porous medium. *Chemical Engineering Journal* **86**, 165–172 (2002).

- [26] S. DEL GUIDICE AND G. COMINI. A physical interpretation of conservative and nonconservative finite–element formulations of convection–type problems. *International Journal for Numerical Methods in Engineering* **35**(4), 709–727 (1992).
- [27] S. DEL GUIDICE, G. COMINI, AND R. W. LEWIS. Finite element simulation of freezing process in soils. *International Journal for Numerical and Analytical Methods in Geomechanics* **2**, 223–235 (1978).
- [28] K. K. HANSEN AND J. B. JENSEN. Measurements of water movement in pine sapwood using gamma-ray absorption (1995). Unpublished.
- [29] S. K. JENSEN, L. DAMKILDE, AND K. KRABBENHOFT. Non-destructive assesment and FEM simulations of moisture profiles in sitka spruce (*Picea Sitchensis*) during drying. In A. RANTA-MAUNUS, editor, “Advances in the Drying of Wood”. VTT Building and Transport, Espoo, Finland (2001).
- [30] D. KAVETSKI. Temporal integration in numerical models of unsaturated fluid flow. Technical Report 230.11.2002, School of Engineering, University of Newcastle, Newcastle, Australia (2002).
- [31] D. KAVETSKI, P. BINNING, AND S. W. SLOAN. Adaptive time stepping and error control in a mass conservative numerical solution of the mixed Richards equation. *Advances in Water Ressources* **24**, 595–605 (2001).
- [32] D. KAVETSKI, P. BINNING, AND S. W. SLOAN. Adaptive backward Euler time stepping with truncation error control for numerical modelling of unsaturated fluid flow. *International Journal for Numerical Methods in Engineering* **53**(6), 1301–1322 (2002).
- [33] D. KAVETSKI, P. BINNING, AND S. W. SLOAN. Noniterative time stepping schemes with adaptive truncation error control for the solution of richards equation. *Water Resources Research* **31**, 275–292 (2003).
- [34] K. KRABBENHOFT, C. BECHGAARD, L. DAMKILDE, AND P. HOFFMEYER. Finite element analysis of boron diffusion in wooden poles. In J. JARMER, editor, “Proceedings of the 34th Annual Conference of the International Research Group on Wood Preservation”, pages 1–14, Stockholm, Sweden (2003).
- [35] K. KRABBENHOFT AND L. DAMKILDE. A mixed enthalpy–temperature finite element method for generalized phase–change problems. In B. H. V. TOPPING, editor, “Proceedings of the Ninth International Confernce on Civil and Structural Computing”, Edinburgh, UK (2003).
- [36] K. KRABBENHOFT AND L. DAMKILDE. A non–equilibrium model for non–Fickian moisture transfer in wood. *Materials and Structures/Materiaux et Constructions* page 16 (2003). Accepted for publication.

- [37] K. KRABBENHOFT AND L. DAMKILDE. On the prospects of applying dual porosity models to the problem of water uptake in wood. *Materials and Structures/Materiaux et Constructions* (2003). Submitted.
- [38] F. LEHMANN AND PH. ACKERER. Comparison of iterative methods for improved solutions of the fluid flow equation in partially saturated porous media. *Transport in Porous Media* **31**, 275–292 (1998).
- [39] R. W. LEWIS, K. MORGAN, H. R. THOMAS, AND K. N. SEETHARAMU. “The Finite Element Method in Heat Transfer Analysis”. John Wiley & Sons, New York (1996).
- [40] H. K. MOMAHED, S. PATHAK, D. N. ROY, T. C. HUTCHINSON, D. L. McLAUGHLIN, AND J. C. KINCH. Relationship between sugar pine maple decline and corresponding chemical changes in the stem tissue. *Water, Air and Soil Pollution* **96**(4), 321–327 (1997).
- [41] K. MORGAN, R. W. LEWIS, AND O. C. ZIENKIEWICZ. An improved algorithm for heat conduction problems with phase change. *International Journal for Numerical Methods in Engineering* **12**, 1191–1195 (1978).
- [42] S. G. NASH AND A. SOFER. “Linear and nonlinear programming”. McGraw-Hill, New York, N.Y. (1996).
- [43] S. BEN NASRALLAH AND P. PERRE. Detailed study of heat and mass transfer during convective drying of porous media. *International Journal for Heat and Mass Transfer* **31**(5), 957–967 (1988).
- [44] N. OUELHAZI, G. ARNAUD, AND J. P. FOHR. A two-dimensional study of wood plank drying. The effect of gaseous pressure below boiling point. *Transport in Porous Media* **7**(1), 39–61 (1992).
- [45] S. PANG. Relative importance of vapour diffusion and convective flow in modelling of softwood drying. *Drying Technology* **16**, 271–281 (1998).
- [46] P. PERRE. Image analysis, homogenization, numerical simulation and experiment as complementary tools enlighten the relationship between wood anatomy and drying behaviour. *Drying Technology* **15**(9), 2211–2238 (1997).
- [47] P. PERRE. The use of homogenization to simulate heat and mass transfer in wood: towards a double porosity approach. In “Drying ’98 – Proceedings of the International Drying Symposium”, volume A, pages 57–72, Halkidiki, Greece (1998).
- [48] P. PERRÉ AND I. W. TURNER. A 3-D version of TransPore: A comprehensive heat and mass transfer computational model for simulating the drying of porous media. *International Journal of Heat and Mass Transfer* **42**, 4501–4521 (1999).
- [49] P. PERRE AND I. W. TURNER. Transpore: A generic heat and mass transfer computational model for understanding and visualising the drying of porous media. *Drying Technology* **17**(7&8), 1273–1289 (1999).

- [50] I. S. POP. Error estimates for a time discretization method of the Richards' equation. *Computational Geosciences* **6**, 141–160 (2002).
- [51] J. B. RA. “Diffusion of boron in wood”. PhD thesis, Mississippi State University, Mississippi State (May 1999).
- [52] J.-G. SALIN. Mass transfer from wooden surfaces and internal moisture non-equilibrium. *Drying Technology* **14**(10), 2213–2224 (1996).
- [53] B. A. SCHREFLER. Computer modelling in environmental geomechanics. *Computers and Structures* **79**, 229–2223 (2001).
- [54] L. J. SEGERLIND. “Applied Finite Element Analysis”. John Wiley & Sons, Inc., New York, 2. edition (1984).
- [55] J. F. SIAU. “Transport Processes in Wood”. Springer-Verlag, Berlin (1984).
- [56] M. J. SIMPSON AND T. P. CLEMENT. Comparison of finite difference and finite element solutions to the variably saturated flow equation. *Journal of Hydrology* **270**, 49–64 (2003).
- [57] J. S. SPERRY AND J. IKEDA. Xylem cavitation in roots and stems of Douglas–fir and white fir. *Tree Physiology* **17**, 275–280 (1997).
- [58] G. A. SPOLEK AND O. A. PLUMB. Capillary pressure in softwoods. *Wood Science and Technology* **15**, 189–199 (1981).
- [59] A. J. STAMM. Bound–water diffusion into wood in the fiber direction. *Forest Products Journal* **9**, 27–32 (1959).
- [60] SWST. Structure of Wood. Society of Wood Science and Technology, Teaching Unit No. 1, <http://www.swst.org/teach/set2/struct1.html> (June 2003).
- [61] M. D. TOCCI, C. T. KELLEY, C. T. MILLER, AND C. E. KEES. Inexact Newton methods and the method of lines for solving Richards' equation in two space dimensions. *Computational Geosciences* **2**, 291–309 (1998).
- [62] C. TREMBLAY, A. CLOUTIER, AND Y. FORTIN. Determination of the effective water conductivity of red pine sapwood. *Wood Science and Technology* **34**, 109–124 (2000).
- [63] I. W. TURNER AND P. PERRÉ. The use of implicit flux limiting schemes in the simulation of the drying process: A new maximum flow sensor applied to phase mobilities. *Applied Mathematical Modelling* **25**, 513–540 (2001).
- [64] F. TUTTLE. A mathematical theory of the drying of wood. *Journal of the Franklin Institute* **200**, 609–614 (1925).
- [65] M. TH. VAN GENUCHTEN. A closed–form equation for predicting the hydraulic conductivity of unsaturated soils. *Soil Science Society of America Journal* **44**, 892–898 (1980).

Bibliography

- [66] L. WADSÖ. “Studies of Water Vapor Transport and Sorption in Wood”. Doctoral Dissertation, Report TVBM-1013, Lund University, Lund, Sweden (1993).
- [67] S. WHITAKER. Simultaneous heat, mass, and momentum transfer in porous media: A theory of drying. *Advances in Heat Transfer* **13**, 119–203 (1977).
- [68] S. WHITAKER. Flow in porous media I: A theoretical derivation of Darcy’s law. *Transport in Porous Media* **1**, 3–25 (1986).
- [69] S. WHITAKER. Coupled transport in multiphase systems: A theory of drying. *Advances in Heat Transfer* **31**, 1–102 (1998).
- [70] Y. S. WU AND P. A. FORSYTH. On the selection of primary variables in the numerical formulation for modelling multiphase flow in porous media. *Journal of Contaminant Hydrology* **48**, 277–304 (2001).
- [71] X. ZHANG, A. G. BENGOUGH, J. W. CRAWFORD, AND I. M. YOUNG. Efficient methods for solving water flow in variably saturated soils under prescribed flux infiltration. *Journal of Hydrology* **260**, 75–87 (2002).

List of Symbols

Roman symbols

C	Concentration/density [kg m^{-3}]
c	Specific heat [J kg^{-1}]
D, D, \mathcal{D}	Diffusivity [$\text{m}^2 \text{s}^{-1}$]
j, \mathbf{j}	Mass flux [$\text{kg m}^{-2} \text{s}^{-1}$]
\dot{m}	Mass exchange term [$\text{kg m}^{-3} \text{s}^{-1}$]
\mathbf{v}, \mathbf{u}	Velocity [m s^{-1}]
K	Absolute/relative permeability [$-\text{/m}^2$]
k	Heat conductivity [$\text{J m}^{-1} \text{K}^{-1} \text{s}^{-1}$]
M	Molar mass [kg mol^{-1}]
R	Ideal gas constant [$\text{J mol}^{-1} \text{K}^{-1}$]
T	Temperature [K]
V	Volume [m^3]
p	Pressure [Pa]
W	Dry base moisture content
S	Saturation
g	Gravity [m s^{-2}]
h, H	Enthalpy [J kg^{-1} , J m^{-3}]
E	Fractional weight increase

Greek symbols

ε	Volume fraction
μ	Viscosity [$\text{kg m}^{-1} \text{s}^{-1}$]
φ	Porosity
ρ	Concentration/density [kg m^{-3}]
σ	Surface tension [Nm^{-2}]

List of Symbols

Indices

w	Water
f	Free water
v	Water vapour
g	Gas – water vapour + dry air
b	Bound water
c	Capillary
s	Solid skeleton
r	Relative
FSP	Fiber saturation point
surf	External exchange surface

Mathematical symbols

-	Averaging operator
$\nabla \cdot$	Divergence operator
∇	Gradient operator

List of Figures

2.1	Cross section of a softwood trunk.	4
2.2	Structure of softwood, southern pine [55].	5
2.3	Earlywood and latewood cells [55].	6
2.4	Cross section of bordered pit [16].	7
2.5	Unaspirated bordered pit [55].	7
2.6	Microscopic structure of a diffuse porous hardwood, sugar maple [60].	8
2.7	Microscopic structure of a ring porous hardwood, red oak [60].	8
2.8	Cross section of a microfibril [66] (a) and structure of the cell wall [55] (b).	9
3.1	One dimensional infinitesimal element.	12
3.2	Phase transitions.	14
3.3	Diffusivity of bound water in the longitudinal direction.	17
3.4	Water vapour and air transfer.	19
3.5	Capillary pressure as function of free water content for softwood at 20 °C, according to [48].	20
3.6	Free water distribution in wood at high (a) and at low (b) degrees of saturation.	21
3.7	Relative effective free water transfer coefficients as function water content.	22
3.8	Simulated one dimensional drying profiles with $K_{rw} = S^8$ corresponding to longitudinal transfer.	23
3.9	Simulated one dimensional drying profiles with $K_{rw} = S^3$ corresponding to tangential transfer.	23
3.10	Simulated one dimensional drying profiles with $K_{rw} = S^2$	24
4.1	Mechanisms of moisture transport below the fiber saturation point.	32
4.2	One dimensional sorption experiment.	34
4.3	Failure of Fickian models.	34
4.4	Computed (—) and experimental [66] sorption curves (◦).	36
4.5	Computed apparent diffusion coefficients	37
4.6	Two-dimensional wooden slab.	38
4.7	Moisture uptake for two-dimensional samples.	39

5.1	Infiltration in beech [47].	42
5.2	Infiltration in fir sapwood [28].	42
5.3	Transport models: single continuum model (a), double-porosity model (b), and double-permeability model (c).	43
5.4	Two dimensional network model.	44
5.5	Network model with $N_L/N_T = 1.0$. Conducting cells (a), passive cells (b), blocked cells (c).	45
5.6	Network model with $N_L/N_T = 2.0$. Conducting cells (a), passive cells (b), blocked cells (c).	45
5.7	Network model with $N_L/N_T = 3.0$. Conducting cells (a), passive cells (b), blocked cells (c).	46
5.8	Mean longitudinal conductivity for $N_L/N_T = 1.0$	47
6.1	Boron treatment of wooden poles.	49
6.2	Boron distributions. Three rods, pole diameter of 22 cm. Red line indicates 0.5 kg/m ³ limit and green line 1.0 kg/m ³ limit	51
6.3	Alternative placement of rods (a) and some effects (b). Three rods, pole diameter of 20 cm.	52
7.1	Enthalpy-temperature curve for water (a) and pressure-saturation curves for sand and clay (b).	57
7.2	Mixed- ϕ (a) and mixed- θ (b) methods.	63
7.3	Pressure head-water content curve (a) and hydraulic conductivity (b) for a coarse grained soil [4].	65
7.4	Iterative procedure for the Richards equation	67
7.5	Moisture content (a) and pressure head (b) profiles. Example 1, $\psi_{\text{top}} =$ -75 cm and $\psi_{\text{bottom}} = -1000$ cm, $\Delta t_0 = 5.0$ s.	68
7.6	Moisture content (a) and pressure head (b) profiles. Example 2, $\psi_{\text{top}} =$ 100 cm and $q_{\text{bottom}} = 0$, $\Delta t_0 = 0.01$ s.	69
7.7	Alternative update in case of negative moisture content.	73
7.8	Variable smoothing.	75
7.9	Mesh ($N_T \times N_R \times N_L = 12 \times 24 \times 20$) used for wood drying simulations. Note refinement around exchange surfaces.	75
7.10	Evolution of the drying process, $a/2 = 50$ cm, $T = 60$ °C, $W_0 = 1.5$ kg/kg.	77
7.11	Evolution of the drying process, $a/2 = 50$ cm, $T = 60$ °C, $W_0 = 1.5$ kg/kg.	78
7.12	Average moisture content as function of time, $a/2 = 50$ cm, $T = 60$ °C, $W_0 = 1.5$ kg/kg.	79
7.13	Average moisture content as function of time for boards of different length, $T = 60$ °C, $W_0 = 1.5$ kg/kg.	80

7.14 Upstream weighting for four-node element.	81
7.15 Steady state solution of convection-diffusion equation with $Pe = 3.75$	84
7.16 Steady state solution of convection-diffusion equation with $Pe = 1.25$	84

List of Figures

List of Tables

7.1	Results of efficiency/robustness, generality/unique-ness, and mass balance tests for different numerical formulations.	61
7.2	Iterative procedure for the Richards equation	66
7.3	Comparison of conventional mixed- ψ scheme and new iterative procedure. Example 1, $\psi_{\text{init}} = -1000$ cm, $\psi_{\text{top}} = -75$ cm and $\psi_{\text{bottom}} = -1000$ cm. †Convergence not achieved after 200 iterations.	67
7.4	Comparison of conventional mixed- ψ scheme and new iterative procedure. Example 2, $\psi_{\text{init}} = -1000$ cm, $\psi_{\text{top}} = 100$ cm and $q_{\text{bottom}} = 0$. †Convergence not achieved after 200 iterations.	69
7.5	Comparison of conventional mixed- ψ scheme and new iterative procedure. Example 3, $\psi_{\text{init}} = -10,000$ cm, $\psi_{\text{top}} = 100$ cm and $q_{\text{bottom}} = 0$. †Convergence not achieved after 200 iterations.	70

A model for non-Fickian moisture transfer in wood

K. Krabbenhoft¹ and L. Damkilde²

(1) Department of Civil Engineering, Technical University of Denmark, DK-2800 Lyngby, Denmark

Currently at: Department of Civil, Surveying and Environmental Engineering, University of Newcastle, NSW 2300, Australia

(2) Institute of Chemistry and Applied Engineering Science, Aalborg University Esbjerg, DK-6700 Esbjerg, Denmark

ABSTRACT

A model for non-Fickian moisture transfer in wood is presented. The model considers the transfer of water vapour separate from the transfer of bound water. These two components are linked by an equation describing the sorption on the cell wall level. Hereby, a formulation capable of describing known non-Fickian effects, including the effects of step size, absolute moisture content, and sample length, is achieved. The sorption curves predicted by the model are compared with experimental results and good agreement is found.

RÉSUMÉ

Un modèle pour le transfert non-Fickien d'humidité dans le bois est présenté. Le modèle considère le transfert de la vapeur d'eau séparé pour le transfert de l'eau liée. Ces deux composants sont liés par une équation décrivant la sorption au niveau de mur de cellules. Par ceci, une formulation capable de décrire des effets non-Fickien connus, comprenant les effets de la taille d'étape, le contenu d'humidité absolu, et la longueur d'échantillon, est réalisée. Les courbes de sorption prévues par le modèle sont comparées aux résultats expérimentaux et une bonne concordance est trouvée.

1. INTRODUCTION

The mathematical description of the transfer of moisture in wood below the fiber saturation point is often made using two basic assumptions. Firstly, that the moisture flux can be described by a Fickian type gradient law, and secondly that the bound water in the cell walls is at all times in equilibrium with the surrounding mixture of vapour and air as described by the sorption isotherm.

In one dimensional isothermal transfer the moisture flux j is given by

$$j = D_m \frac{dm}{dx} \quad (1)$$

where m is the moisture content and D_m a moisture dependent diffusion coefficient. Using the equilibrium assumption this expression can, alternatively, be formulated with the relative humidity r as potential as

$$j = D_m \frac{dm}{dx} = D_m \left(\frac{dm}{dr} \right) \frac{dr}{dx} = D_r \frac{dr}{dx} \quad (2)$$

where the diffusion coefficient with r as potential is given by

$$D_r = D_m \left(\frac{dm}{dr} \right) \quad (3)$$

By mass conservation considerations unsteady state conditions can then be described by either of the two following partial differential equations

$$\frac{\partial m}{\partial t} = \frac{\partial}{\partial x} \left(D_m \frac{\partial m}{\partial x} \right) \quad \text{or} \quad c \frac{\partial r}{\partial t} = \frac{\partial}{\partial x} \left(D_r \frac{\partial r}{\partial x} \right) \quad (4)$$

where $c = dm/dr$ is the slope of the sorption isotherm.

In the following, the shortcomings of this so-called Fickian model are discussed. An alternative model is then proposed and the capabilities of this model are demonstrated by comparison to experimental results.

2. FAILURE OF FICKIAN MODELS

As already discussed the Fickian models rely upon two basic assumptions, namely that the transfer of moisture is governed by a Fickian type gradient law and that within the wood there exists an equilibrium state such that the moisture content is at all times a unique function of the corresponding relative humidity as given by the sorption isotherm.

The first assumption that the flux of some quantity can be taken as being proportional to the gradient of this quantity by some scalar D is probably reasonable, at least as a first approximation and especially when dealing with a relatively slow transfer under isothermal conditions. However, the second assumption that there is instantaneous equilibrium between the bound water and the water vapour at all times is harder to justify.

Considering in more detail the mechanisms of moisture transfer in the hygroscopic range this must consist of a diffusive, and possibly convective, transfer of water vapour in the cellular structure with simultaneous sorption in the cell walls. In addition, bound water may be transferred within the cell walls by diffusion. Thus, in general the validity of the equilibrium assumption depends on the rate of the diffusive and convective processes in relation to the rate of sorption. If, for example, the resistance to vapour transfer within the wood is very small it is the rate of sorption that will govern the overall process. Conversely, in the case of a high vapour resistance it is the transport of vapour to the sorption sites which will be determining for the overall behaviour.

In many cases the latter scenario is predominant and either of the Fickian models (4) may be applied. There are, however, also cases where the results obtained with the diffusion equation can not be made to fit the experimental data. Such measurements have been made by Wadsö [1]. These experiments, which were conducted on one-dimensional samples with half lengths of 4.8 mm to 11.4 mm, show among others things a dimensional dependence such that if the moisture transfer is to be described by (4) the diffusion coefficient must be made to vary with the length of the sample. This is illustrated in Fig. 1. In Fig. 1 (a) the results of two sorption experiments with samples of different length are shown. The samples were initially in equilibrium with 54% relative humidity and then subjected to a step increase to 75% RH. In the figure the relative weight increase is shown as function of the square root of time divided by the respective sample lengths. If diffusion was the dominant mechanism involved the two experimental curves should be superimposed on each other, *even in the case of a moisture dependent diffusion coefficient*, see e.g. Crank [2]. As is clearly seen this is not the case. If, nevertheless, diffusion is assumed valid this would imply a sample length dependent diffusion coefficient, which is clearly unacceptable from a physical point of view.

In Fig. 1 (b) the results of the same type of experiment is shown, now for a step increase in relative humidity from 75% to 84% and, as can be seen, the situation becomes even more extreme in this case.

Apart from the suggestion that the diffusion coefficient should be moisture dependent, the most commonly mentioned cause of the discrepancies is probably that there could be a finite surface resistance at the ends of the sample. In general this is of course a valid point. However, the air velocity used by Wadsö was 3 m/s, which by Rosen [3] has been shown experimentally to be close to the upper limit at which surface resistance has any effect. Furthermore, in a series of experiments conducted by Christensen [4] the atmospheric air was evacuated from the sorption chamber such that the samples were subjected to an

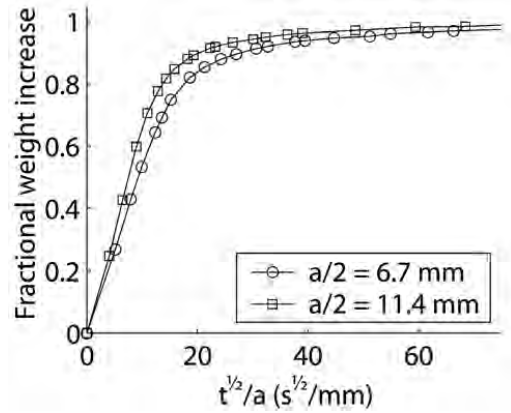


Fig. 1 (a) - Failure by non-Fickian length dependence.

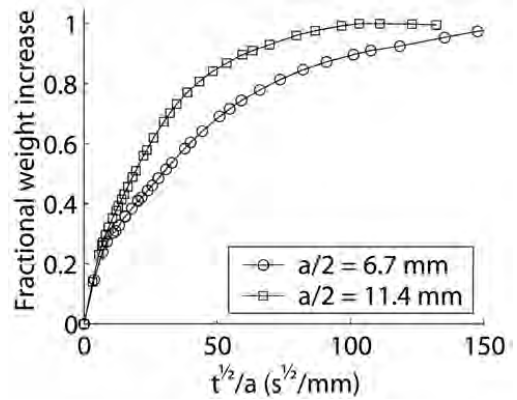


Fig. 1 (b) - Failure by non-Fickian length dependence.

environment of pure vapour. Under these conditions surface resistance can be assumed to be very close to zero, but still the results showed significant deviation from what one would expect on the basis of a diffusion model.

In addition to the obvious discrepancies involved when considering samples of different lengths, another and more fundamental concern is that the sorption curves produced experimentally look very different from what would be expected from Fickian diffusion. This is illustrated in Fig. 2. In Fig. 2 (a) the sorption curve is shown for a sample of half length equal to 11.4 mm. The sample was subjected to a step change in relative humidity from 75% RH to 84% RH. As can be seen the sorption curve displays an abrupt change in slope very early on around a fractional weight increase of $E = 0.2$. This is very uncharacteristic of Fickian process, again, even if the diffusivity varies with moisture content. Such Fickian processes are shown in Fig. 2 (b) where the results of three different simulations with different moisture dependent diffusion coefficients were used. First a constant diffusion coefficient was used after which two simulations with exponentially increasing and decreasing coefficients were performed. In these nonlinear computations the coefficients were varied by a factor of 3 (even though this is much more than can be justified within

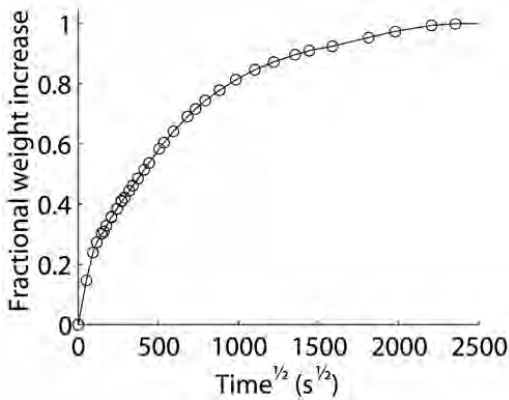


Fig. 2 (a) - Failure of Fickian models. Experimental curve.

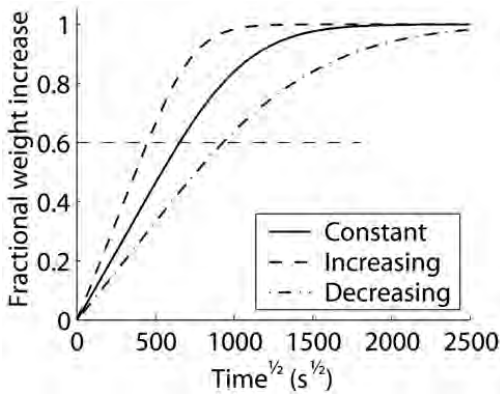


Fig. 2 (b) - Failure of Fickian models. Theoretical curves.

the relatively small sorption step of 75% to 84% RH). As can be seen these curves differ qualitatively only slightly from the results obtained by a constant diffusivity: up to approximately $E = 0.6$ the slope of all three curves are approximately linear, after which the sorption rates decrease in a smooth manner.

Although this demonstration does not constitute a mathematical proof of the impossibility of sorption being a Fickian process, it does illustrate the difficulties involved with fitting experimental results to a Fickian model.

In Wadsö [5] different alternative models for predicting the above mentioned sorption response are reviewed. It is, however, concluded that none of the models are able to capture all of the effects which have been observed experimentally. We believe this in part be due to the fact that the resulting anomalous sorption behaviour is a result of anomalies on different levels. If the bound water-water vapour equilibrium assumption is abandoned it is obvious that the overall behaviour will be influenced by the rate of vapour transfer to the rate of sorption. If vapour transfer is a faster process than sorption then the length of the sample will naturally influence the results in a way which is not predicted by a simple global diffusion equation. However, on the cell wall level a number of other anomalies have been observed.

Christensen [4] performed adsorption measurements on single cell walls and found that large steps in relative humidity gave faster sorption rates than did smaller steps in a way, which was inconsistent with what a diffusion model would predict. Furthermore, the sorption responses for cell walls of different thickness were almost identical indicating that diffusion is not the governing mechanism for cell wall sorption. Similar conclusions were drawn in [6-9].

In the following, both the effects on the cell wall level and the effect of separating the water vapour from the bound water are considered. The result is a non-equilibrium Fickian model, that is, a model where the vapour pressure is not necessarily in equilibrium with the bound water content at all times, but where Fick's law is used throughout to describe diffusive transfer of both bound water within the cell walls and water vapour and air in the lumens.

3. NON-EQUILIBRIUM FICKIAN MODEL

With the considerations of the previous section in mind a model has been formulated where the transfer of water vapour is considered independently from the transfer of bound water in the cell walls, see Fig. 3. The cell wall moisture content is linked to the vapour pressure in the lumens by a term equivalent to that describing the transfer of vapour from a wet surface. Similar models have previously been formulated by Cunningham [10], Salin [11], and Absetz and Koponen [12].

The model presented here refers only to the one-dimensional isothermal case. However, inclusion of additional phases such as free water and dry air is straight forward, as is the extension to two and three spatial dimensions.

3.1 Bound water

The flow of bound water in the cell walls is assumed to be a diffusive process, Siau [13], governed by the following equation

$$\frac{\partial w}{\partial t} = \frac{\partial}{\partial x} \left(D_w \frac{\partial w}{\partial x} \right) + \dot{m} \quad (5)$$

where w is the mass of water per unit volume of gross wood (kg/m^3), D_w is the corresponding diffusion coefficient. The sorption term \dot{m} accounts for the interchange between bound water and water vapour, see Fig. 3. This quantity will be positive in adsorption.

That the transfer of bound water within the cell walls is a diffusive process has been rendered probable by Stamm [11] who measured longitudinal bound water diffusion of

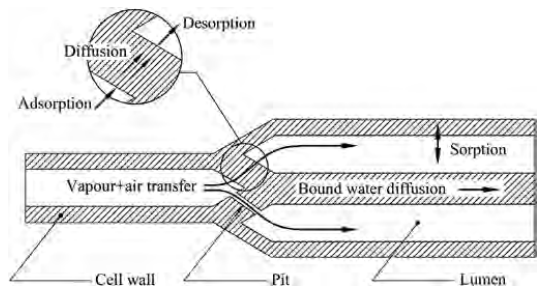


Fig. 3 - Moisture transfer model.

Picea Sitchensis cell wall substance. Although several discrepancies have been reported, such as a difference between steady state and transient measurements, different values in adsorption and desorption and a possible influence of moisture induced stresses, Comstock [12], we shall make the assumption of the bound water transfer being a diffusive process with the diffusion coefficient depending solely on the moisture content and temperature.

3.2 Water vapour

The conservation equation for water vapour is given by

$$\varphi \frac{\partial \rho_v}{\partial t} = -\frac{\partial j}{\partial x} - \dot{m} \quad (6)$$

where ρ_v is the vapour concentration, φ the porosity and j the flux. Since any bound water released from the cell walls will appear as water vapour, the sorption term \dot{m} is again included.

Using Fick's law the flux of vapour is given by

$$j = -\rho_g D_{va}^{eff} \frac{d}{dx} \left(\frac{\rho_v}{\rho_g} \right) \quad (7)$$

where ρ_g is the concentration of total gas, *i.e.* water vapour and dry atmospheric air, and D_{va}^{eff} is the effective vapour diffusivity which can be related to the diffusivity of water vapour in stall air as

$$D_{va}^{eff} = \tau D_{va} \quad (8)$$

where the reduction factor τ accounts for the the resistance within the wood stemming from its porous structure. For D_{va}^{eff} several empirical expressions are available, *e.g.* Schirmer [14],

$$D_{va} = 2.31 \times 10^{-5} \frac{p_a}{p_a + p_v} \left(\frac{T}{273.16} \right)^{1.81} \quad (9)$$

where p_a is the air pressure, in this case the atmospheric pressure, and T the absolute temperature.

If the concentration of vapour is much smaller than the concentration of total gas as is the case under moderate temperatures, Fick's law (7) reduces to the well-known form

$$j = -D_{va}^{eff} \frac{d \rho_v}{dx} \quad (10)$$

By combining (6) and (10) and assuming isothermal conditions the governing equation for vapour transfer can be written in terms of pressure as

$$\varphi \frac{\partial p_v}{\partial t} = \frac{\partial}{\partial x} \left(D_{va}^{eff} \frac{\partial p_v}{\partial x} \right) - \dot{m} \quad (11)$$

3.3 Cell wall sorption

As already mentioned the coupling between the bound water and the water vapour is assumed to follow a type of surface mass transfer relation. From the mass transfer of

vapour from a saturated surface the following relation is known [15]

$$\dot{m} = h(p_v - p_w) \quad (12)$$

where p_w is the vapour pressure at the saturated surface, p_v is the vapour pressure in the surrounding air and h is the mass transfer coefficient. For the case of transfer between the lumens and the cell walls an analogous relation is assumed. In the works of Cunningham [10], Salin [11], and Absetz and Koponen [12], h was assumed constant within the RH-step in question. If the non-Fickian behaviour was solely the result of an internal boundary layer this would probably be reasonable, and these models are then equivalent to the model introduced by Choong and Skaar [16]. The assumption of a constant h , however, has some consequences which are in conflict with the findings of Christensen [4], who listed three major points:

1. For steps of different magnitude but with the same final MC, *e.g.* 5% MC to 10% MC and 8% MC to 10% MC, the sorption rates were lower for the smaller steps.
2. For steps of different magnitude but with the same final MC, *e.g.* 5% MC to 10% MC and 8% MC to 10% MC, the sorption rates were lower for the smaller steps.
3. When starting from a completely dry sample the effect of step size was cancelled, such that a step from 0% MC to 5% gave the same qualitative response as a step from 0% MC to 10% MC.

These statements are also valid if RH is substituted for MC, *i.e.* the shape of the sorption isotherm does not help to explain the anomalies.

The first of the above points can be accommodated by making h depend on the moisture content, and assuming a constant h within steps of relatively small magnitude is thus reasonable.

But the effect that larger steps should result in higher sorption rates than smaller steps cannot be captured by assuming a constant value of h . To see this, consider a sorption process governed by the equation

$$\dot{m} = \frac{dm}{dt} = h_0 (m_\infty - m) \quad (13)$$

where m_∞ is the target moisture content. The solution is given by

$$m = m_\infty - ce^{-h_0 t} \quad (14)$$

where c is a constant of integration determined by the initial moisture content m_0 . The relative moisture uptake is given by

$$E = \frac{m - m_0}{m_\infty - m_0} = 1 - \frac{ce^{-h_0 t}}{m_\infty - m} = 1 - e^{-h_0 t} \quad (15)$$

from which it is clearly seen that the step size effect cannot be modeled using a constant value of h .

A possible interpretation of the step size effect is that close to equilibrium there is an additional 'resistance' to moisture uptake. This is the possibility explored in the following. As a measure of the proximity to equilibrium some function of the ratio of the actual moisture content to

the target moisture content may be used. Thus, one possibility of including the increased resistance close to equilibrium would be

$$\frac{dm}{dt} = h(m_\infty - m) \tag{16}$$

where

$$h = \begin{cases} h_0(1 - m/m_\infty) & \text{in adsorption } (m_\infty > m) \\ h_0(1 - m_\infty/m) & \text{in desorption } (m_\infty < m) \end{cases} \tag{17}$$

and h_0 is a constant.

Considering the case of adsorption the solution to (16) is

$$m = \frac{h_0 t (m_\infty - m) m_\infty + m_0 m_\infty}{h_0 t (m_\infty - m) + m_\infty} \tag{18}$$

or in terms of the fractional moisture uptake

$$E = \frac{(1 - m_0/m_\infty) h_0 t}{1 + (1 - m_0/m_\infty) h_0 t} \tag{19}$$

Clearly, the closer m_0 is to m_∞ the slower the sorption will be. This is illustrated in Fig. 4. More interestingly, however, is that when $m_0 = 0$, i.e. when starting from a completely dry sample, the fractional weight increase reduces to

$$E = \frac{h_0 t}{1 + h_0 t} \tag{20}$$

which is independent of the final moisture content and thereby the step size. This will generally be the case for all relations of the type

$$\frac{dm}{dt} = f(m/m_\infty)(m_\infty - m) \tag{21}$$

and thus, using m/m_∞ as a measure of the proximity to equilibrium has the obvious advantage that the observed behaviour of the canceling of step size effects when starting from completely dry conditions is included directly in the expression for h .

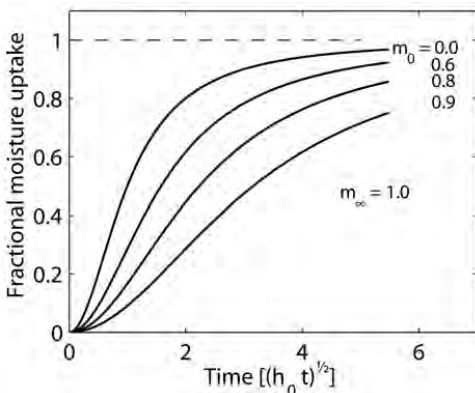


Fig. 4 - Sorption curves for steps of different magnitude.

3.3.1 Relation of adsorption to swelling

In the above, the equilibrium proximity measure was introduced on the grounds of mathematical arguments. There are, however, also indications that this variable has a deeper physical significance. In the works of Christensen, and later also by Skaar *et al.* [17], it was argued that the only plausible explanation for the behaviour was to be found in the swelling which accompanies adsorption. That is, as the wood takes up moisture it swells which, until a stress relaxation has taken place, slows down the sorption of additional water molecules. In analogy with the osmotic pressure equation, Katz [18] originally proposed that the maximum swelling pressure exerted by an elastic gel when the surrounding vapour pressure is raised from some value p_0 to the saturation vapour pressure of the gel p_{sat} would be:

$$\Pi = -\frac{\rho_w RT}{M_w} \ln\left(\frac{p_0}{p_{sat}}\right) \tag{22}$$

where ρ_w is the density of water and M_w the molecular weight. Later Barkas [19] extended this equation to be valid for any pair of vapour pressures p_i and p_f

$$\Pi = -\frac{\rho_w RT}{M_w} \ln\left(\frac{p_i}{p_f}\right) \tag{23}$$

where subscripts i and f indicate the initial and final states respectively. Christensen [4] further explored experimentally the possibility of a relation between sorption and swelling and found that the half-time to sorption was approximately inversely proportional to $\ln(p_i/p_f)$, i.e.

$$\sqrt{t_{0.5}} \approx \frac{a}{-\ln(p_i/p_f)} \tag{24}$$

where a is a constant. This result was interpreted such that the higher potential swelling pressure available the faster the relaxation, and thereby the sorption, will be.

As also admitted by Christensen, the choice of using the half-time to sorption is somewhat arbitrary and not particularly representative of the whole sorption process. However, the results do indicate that the variable $\ln(p_i/p_f)$ could be of vital importance in describing the sorption process.

3.3.2 Application to wood

In the particular case of wood, a similar expression may be used. The equilibrium proximity measure can be taken as the ratio between the equilibrium vapour pressure $p_w(w)$ corresponding to a given moisture content w as defined by the sorption isotherm and the actual vapour pressure p_v . Thus, the term \dot{m} in (5) has the following principal appearance

$$\dot{m} = h\left(\frac{p_w}{p_v}, w, \frac{\partial w}{\partial t}, T, \dots\right)(p_w - p_v) \tag{25}$$

where the influence of the absolute magnitude of the moisture content and temperature have been included. Also, the expressions for h should be different in adsorption and desorption as already discussed. Concerning the expression

for h in adsorption it can be deduced from the results published by Christensen [4] and Wadsö [1] the h should be relatively large in the beginning of the sorption process, *i.e.* when far from equilibrium. This is followed by a rapid decrease as equilibrium is approached, where the point at which h begins to decrease abruptly is determined by the absolute moisture content. An analytical expression able to describe these characteristics is given by

$$h = c_1 \exp \left[-c_2 \left(\frac{p_w}{p_v} \right)^{c_3} \right] + c_4 \quad (26)$$

Whereas this expression contains four parameters which may be adjusted independently we have found that only the parameter c_2 needs to be made dependent on the moisture content in order to fit the experimental results of Wadsö [1] satisfactorily. By varying c_2 a family of curves as shown in Fig. 5 is obtained.

As indicated in the figure the maximum value of h is approximately $h = 2 \times 10^{-6} \text{ kgm}^{-3}\text{s}^{-1}\text{Pa}^{-1}$. This value may be compared to the value of the surface evaporation coefficient k_p which has a typical value of around $k_p = 5 \times 10^{-8} \text{ kgm}^{-2}\text{s}^{-1}\text{Pa}^{-1}$ [15]. The evaporation per unit volume of internal surface should then be at most $\zeta k_p (p_w - p_v)$ where ζ is the internal surface area per unit volume. For typical softwoods this may be taken as approximately $\zeta = 10^5 \text{ m}^{-1}$ giving a maximum value of h of $h_{\text{max}} = 5 \times 10^{-3} \text{ kgm}^{-3}\text{s}^{-1}\text{Pa}^{-1}$. This is well above the maximum value actually used, suggesting that the process of sorption is more complicated and involves other mechanism with much higher times scales than evaporation/condensation.

Since the approach to equilibrium should be slower with higher moisture contents, c_2 has to increase with increasing w . As seen the curves have been constructed such that h is near constant for low values of $p_w = p_v$. Whether this can be experimentally justified is of course an open question. It is, however, an attractive feature to be able to recover the basic surface evaporation equation in the limit of small values of $p_w = p_v$.

In the following the non-Fickian behaviour is described via the sorption term described in the above. Thus, the physical mechanisms responsible for the sorption behaviour are lumped into this one term. This includes also the boundary layer resistance in the lumens. Although this is probably oversimplified, it appears at the current time to be a satisfactory compromise. In a more complete model, however, each of the physical mechanisms contained in the sorption term should be considered separately.

4. RESULTS

In the following a number of sorption simulations are performed and the results compared to those of Wadsö [1].

In all the simulations we use $c_1 = 5 \times 10^{-3} \text{ kgm}^{-3}\text{s}^{-1}\text{Pa}^{-1}$, $c_3 = 50.0$, and $c_4 = 8 \times 10^{-8} \text{ kgm}^{-3}\text{s}^{-1}\text{Pa}^{-1}$. The coefficient c_2 should in principle increase continuously with increasing moisture content in a manner similar to what is shown in Fig. 5 (b). However, at this point there is not sufficient experimental data available to establish such a curve and we have therefore chosen to keep c_2 constant within the two

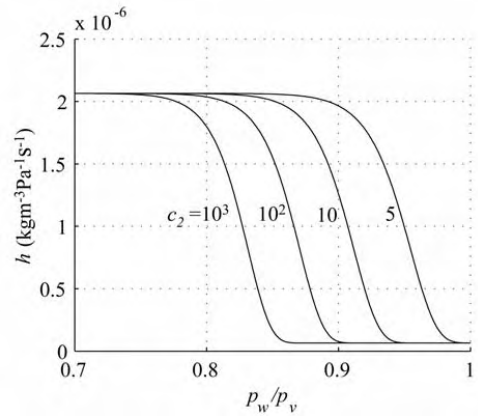


Fig. 5 (a) - Variation of h with c_2 and p_w/p_v .

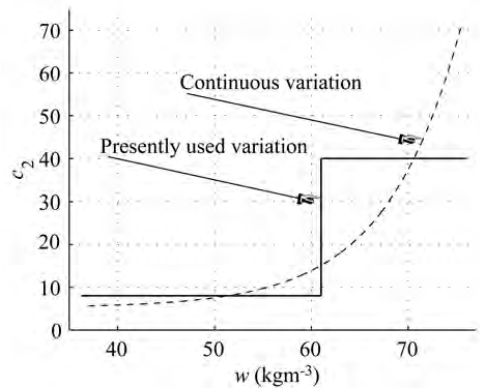


Fig. 5 (b) - Variation of c_2 with absolute moisture content w .

moisture ranges considered. In the first series of experiments the relative humidity is changed from 54% to 75%, whereas in the second series it is varied from 75% to 84%. The corresponding values of c_2 that have been used are $c_2 = 8.0$ and $c_2 = 40.0$ respectively.

Also the water vapour diffusion coefficients are kept constant within each MC-range. In Table 1 the values used in the simulations are compared to values found by Siau [13] on the basis of a geometrical model of the cellular structure of a typical softwood. The latter values have been converted into equivalent diffusion coefficients with vapour pressure as potential. As can be seen, the values used in the simulations are in all cases within the ranges determined by Siau [13].

In the model of Siau the resistance to vapour flow comprises cell lumens as well as cell walls. Thus, strictly speaking, the coefficients can only be regarded as apparent

Table 1 - Values of $\tau = D_{va}^{eff} / D_{va}$ of Siau [13] and values used in the present simulations				
	Trans.	Trans.	Long.	Long.
RH (%)	τ (Siau [13])	τ (Present)	τ (Siau [13])	τ (Present)
54-75	156-56	130	2.8-1.7	1.7
75-84	56-28	30	1.7-1.5	1.7

vapour diffusion coefficients, as in reality vapour is assumed to pass through the cell walls by being sorbed on one side and subsequently released on the other side. This is, however, but one theory of the mechanism of vapour transfer. According to Dinwoodie [20] the principal pathway is through the pits of the cell walls. A diffusion coefficient independent of the moisture content should then be expected. This is not supported by the experimental results presented in the following and we have therefore chosen to adopt the model of Siau.

For the longitudinal bound water diffusion coefficients at a temperature of 23°C we use

$$D_w^L = 3 \times 10^{-11} \text{ m}^2/\text{s} \text{ for } 54\% \leq \text{RH} \leq 75\% \quad (27)$$

and

$$D_w^L = 12 \times 10^{-11} \text{ m}^2/\text{s} \text{ for } 75\% < \text{RH} \leq 75\% \quad (28)$$

The tangential bound water coefficient is related to that in the longitudinal direction by $D_w^t = 3D_w^L$. These values correspond to what is given in [21].

The air velocity reported by Wadsö (3m/s) is assumed to be so high that boundary effects in the layer between the sample and the surrounding air can be ignored. The computed and experimentally determined sorption curves are shown in Figs. 6 and 7. As can be seen from Figs. 6 and 7 all eight sets of sorption experiments are fitted quite well. For all the simulations the qualitative effect of a sudden change in sorption rate is clearly seen and thus, all in all the results suggest that it may be fruitful to consider sorption, or sorption rates, in relation to two variables, namely the moisture content and the proximity to equilibrium, where particularly the last quantity is of importance. Especially, the results for transfer in the tangential direction are satisfactory as the overall response is here governed by a combination of vapour transfer and sorption, whereas for the longitudinal samples the response is governed mainly by sorption.

5. FUTURE EXPERIMENTAL WORK

Clearly, experimental verification of the model presented here is needed. Concerning the sorption terms, the experiments should be conducted on very thin slices of wood such that the diffusion of vapour does not need to be considered. Step increments of varying magnitude in vapour pressure should be applied similarly to what was done by Christensen [4].

As in most mass transfer processes it must be expected that a boundary layer exists on the cell wall surface. To separate this resistance from the non-Fickian effects it would be necessary to conduct the experiments at different air velocities.

In practice the variation of h with w and $p_w = p_v$ should be rather straightforward to determine, namely as

$$h(w, p_w / p_v) = \left(\frac{\partial w}{\partial t} \right) (p_v - p_w)^{-1} \quad (29)$$

or in discrete form as

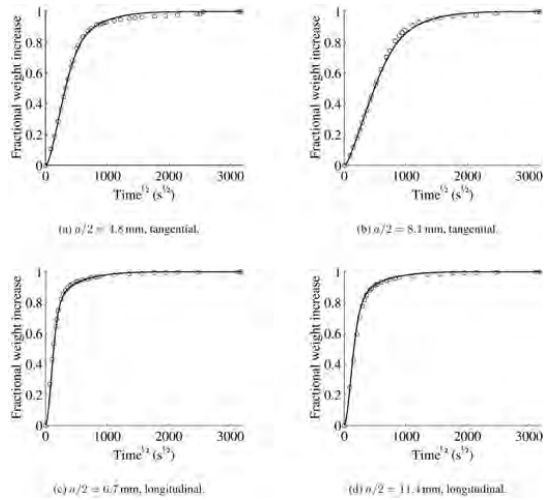


Fig. 6 - Computed and experimental sorption curves for series 1: 54-75% RH.

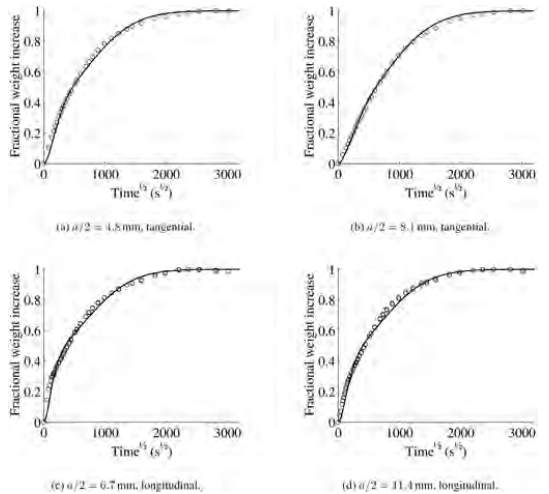


Fig. 7 - Computed and experimental sorption curves for series 2: 75-84% RH.

$$h(w_{n+1}, (p_w / p_v)_{n+1}) = \left(\frac{w_{n+1} - w_n}{t_{n+1} - t_n} \right) (p_{w,n+1} - p_{w,n})^{-1} \quad (30)$$

where n and $n+1$ refer to two consecutive measurement points. A complication, however, is that towards the end of the sorption process both $p_v - p_w$ and $\partial w / \partial t$ (or its discrete approximation) tend to zero, and thus the results may become inaccurate.

An interesting extension of the current application to wood is the application to other biological materials such as plant fibers where similar anomalous effect have recently been observed in an ongoing experimental study conducted at the Technical University of Denmark.

6. CONCLUSIONS

A new model for the transfer of moisture in wood in the hygroscopic range has been formulated. With this model all the common non-Fickian effects reported in the literature can be explained. This is demonstrated by reproducing a set of eight different sorption experiments. The model has been implemented in a general finite element framework where the extension to multiple spatial dimensions is straight forward, see e.g. [22].

Further experimentation is still necessary, both in order to verify the model presented here as well as to study the influences of temperature and the response in desorption in relation to the response in adsorption.

ACKNOWLEDGEMENTS

This work has been funded in part by the Danish Research Agency under Project No. 9901363: 'Modeling the Effects of Moisture and Load History on the Mechanical Properties of Wood'. The financial support is gratefully acknowledged.

NOMENCLATURE

Roman letters

D	Diffusion coefficient
E	Fractional weight increase
h	Sorption constant ($\text{kgm}^{-3}\text{s}^{-1}\text{Pa}^{-1}$)
j	Flux ($\text{kgm}^{-2}\text{s}^{-1}$)
m	Moisture content (kg/kg)
\dot{m}	Sorption term ($\text{kgm}^{-3}\text{s}^{-1}$)
p	Pressure (Pa)
r	Relative humidity (RH)
R	Gas constant ($8.31\text{ Jmol}^{-1}\text{K}^{-1}$)
T	Temperature (K)
w	Moisture content (kgm^{-3})

Greek letters

φ	Porosity
ρ	Density (kgm^{-3})
ζ	Internal area/volume ration (m^{-1})
τ	Vapour diffusivity reduction factor

Sub- and superscripts

a	air
eff	effective
g	gas – vapour+air
L	longitudinal
T	tangential
v	vapour

REFERENCES

- [1] Wadsö, L., 'Unsteady-state water vapour adsorption in wood: An experimental study', *Wood and Fiber Science* **6**(1) (1994) 36-45.
- [2] Crank, J., 'The Mathematics of Diffusion' (Oxford University Press, London, 1967).
- [3] Rosen, H.-N., 'The influence of external resistance on moisture adsorption rates in wood', *Wood and Fiber Science* **10**(3) (1973) 218-228.
- [4] Christensen, G.N., 'The rate of sorption by thin materials', *Humidity and Moisture* **4** (1965) 279-293.
- [5] Wadsö, L., 'Describing non-Fickian water-vapour sorption in wood', *Journal of Materials Science* **29** (1994) 2367-2372.
- [6] Christensen, G.N., 'The rate of sorption by wood and pulp', *Appita* **13** (1959) 112-123.
- [7] Christensen, G.N. and Kelsey, K.E., 'The sorption of water vapour through the chemical components of wood (Die Sorption von Wasserdampf durch die chemischen Bestandteile des Holzes)', *Holz als Roh- und Werkstoff* **17**(5) (1959) 178-188 [in German].
- [8] Christensen, G.N. and Kelsey, K.E., 'The rate of water vapour sorption through wood (Die Geschwindigkeit der Wasserdampfsorption durch Holz)', *Holz als Roh- und Werkstoff* **17**(5) (1959) 189-203 [in German].
- [9] Kelly, M.W. and Hart, C.A., 'Water sorption rates by wood cell walls', *Wood and Fiber Science* **1** (1970) 270-282.
- [10] Cunningham, M.J., 'A model to explain "anomalous" moisture sorption in wood under step function driving forces', *Wood and Fiber Science* **27**(3) (1996) 265-277.
- [11] Salin, J.G., 'Mass transfer from wooden surfaces and internal moisture non-equilibrium', *Drying Technology* **14**(10) (1996) 2213-2224.
- [12] Absetz, I. and Koponen, S., 'Fundamental diffusion behaviour of wood', In Hoffmeyer, P. (editor) 'International Conference on Wood Water Relations', (Copenhagen, 1997).
- [13] Siau, J.F., 'Transport Processes in Wood', (Springer-Verlag, Berlin, 1984).
- [14] Schirmer, R., 'The diffusion coefficient water vapour-air mixtures and the rate of evaporation (Die Diffusionzahl von Wasserdampf-luftgemischem und die Verdampfungsgeschwindigkeit)', *VDI Beihft Verfahrenstechnik* **6** (1938) 170 [in German].
- [15] Wadsö, L., 'Studies of Water-vapor Transport and Sorption in Wood', (Report TVBM-1013, Lund University, Sweden 1993).
- [16] Choong, E.T. and Skaar, C., 'Separating internal and external resistance to moisture removal in wood drying', *Wood Science* **1**(4) (1969) 200-202.
- [17] Skaar, C., Prichananda, C. and Davidson, R.W., 'Some aspects of the dynamic moisture sorption dynamics in wood', *Wood Science* **2**(3) (1970) 179-185.
- [18] Katz, J.R., 'The laws of swelling (Gesetze der Quellung)', *Kollidchemische Beihefte* **9** (1917) 1-182 [in German].
- [19] Barkas, W.W., 'The Swelling of Wood under Stress', (HM Stationary Office, London, 1949).
- [20] Dinwoodie, J.M., 'Timber, its Nature and Behaviour', (Van Nostrand Reinhold, New York, 1981).
- [21] Skaar, C., 'Wood-Water Relations', (Springer-Verlag, Berlin, 1988).
- [22] Zienkiewicz, O.C. and Taylor, R.L., 'The Finite Element Method', (Butterworth-Heinemann, Oxford, 2000).

Paper received: March 19, 2003; Paper accepted: August 27, 2003

Kristian Krabbenhoft · Lars Damkilde

Double porosity models for the description of water infiltration in wood

Received: 10 November 2003 / Published online: 13 November 2004
© Springer-Verlag 2004

Abstract In this paper some of the possibilities of applying double porosity and permeability models to the problem of water infiltration in wood are explored. It is shown that the double porosity model can capture a number of commonly reported anomalies including two-stage infiltration/sorption and apparent sample length dependent transfer parameters. Starting with the double porosity model, several extensions are discussed and the type of principal behaviour possible with the models is elaborated on. Finally, a set of highly anomalous experimental results is fitted to within a reasonable accuracy by a double permeability model.

List of symbols

P	Pressure, Pa
X	Water content (dry porous material basis)
v	Velocity, m s^{-1}
K	Absolute/relative permeability
D, D	Diffusivity, $\text{m}^2 \text{s}^{-1}$ or $\text{kg m}^{-1} \text{s}^{-1} \text{Pa}^{-1}$
M	Molar mass, kg mol^{-1}
R	Ideal gas constant, $\text{J mol}^{-1} \text{K}^{-1}$
T	Temperature, K

Greek symbols

ρ	Concentration/density, kg m^{-3}
μ	Viscosity, $\text{kg m}^{-1} \text{s}^{-1}$
ϕ	Porosity
ε	Volume fraction

K. Krabbenhoft
Department of Civil Engineering, Technical University of Denmark,
Lyngby, Denmark

L. Damkilde
Institute of Chemistry and Applied Engineering Science, Aalborg University Esbjerg,
Esbjerg, Denmark

Present address: K. Krabbenhoft (✉)
Department of Civil, Surveying and Environmental Engineering,
University of Newcastle, NSW, 2300, Australia
E-mail: kristian.krabbenhoft@newcastle.edu.au

Subscripts

w	Water
f	Free water
v	Water vapour
g	Gas—water vapour + dry air
b	Bound water
c	Capillary
s	Solid skeleton
r	Relative
FSP	Fiber saturation point
surf	External exchange surface

Mathematical symbols

-	Averaging operator
$\nabla \cdot$	Divergence operator
∇	Gradient operator

Introduction

The transport of water in wood is an important problem for a number of reasons. Since wood is a material whose mechanical properties are strongly dependent on its moisture content and moisture content history, it is important to be able to assess the influence of the interaction of wooden structures with the surrounding environment. Furthermore, green lumber must be dried before it is used as structural timber, and since this process is both expensive as well as critical for the quality of the end product it is useful to be able to predict the temporal variations of moisture content and temperature during drying. Another problem in which the transport of water is important is in the treatment of wood with artificial preservatives. Traditionally, the bulk of the theoretical and numerical models have been concerned with the problem of drying, i.e. the removal of water, whereas much less work has been done in relation to the reverse problem of infiltration. This problem finds application in preservation processing and in connection with environmental loads such as rain and snow as well as for timber structures partially embedded in soil (Krabbenhoft et al. 2003).

The most complete transport models, such as those treated in Spolek et al. (1985), Ouelhazi et al. (1992), Couture et al. (1996), and Perre and Turner (1999), are based on the classical averaging theorems for porous media flow (see e.g. Whitaker 1977) by which the transport of heat and mass are described by a set of coupled partial differential equations, which make reference to a macroscopic scale rather than the microscopic scale at which the flow through tracheids, pits, and so on, could be considered. This approach is also widely accepted and applied for the transport of heat and mass in a number of other porous materials, most notably soils (see e.g. Lewis and Schrefler 2000). In recent years, however, it has been realized that flow of water in soils is significantly influenced by the presence of heterogeneities such as fractures,

fissures, cracks and macropores (Mortensen 2001; Haria et al. 2003). The flow patterns induced by these heterogeneities cannot be adequately described in the framework of the classical averaging models. On the other hand, although in principle possible, it is not practically feasible to consider the exact nature of the porous medium and include all heterogeneities into the model. Therefore, models have been developed which maintain the overall macroscopic view but which make reference to two or more interacting zones with widely different flow properties. If two zones, commonly referred to as fracture and matrix, are considered the corresponding models are referred to as double porosity or double permeability models depending on whether flow takes place in both zones or only in one (Fig. 1). In Fig. 1a the conventional macroscopic single continuum model is shown. Here no distinction is made between fracture and matrix zones. However, the material parameters may vary throughout the domain as indicated by the three different subdomains FM1–FM3. In the case of wood, a board containing both heartwood and sapwood could possibly be treated by the single continuum model, namely by using two different sets of material parameters for the two different types of wood. In Fig. 1b the double porosity model is shown which considers separately the fracture and matrix zones. As illustrated, flow occurs only in the fracture zone whereas the matrix zone acts as a reservoir which can only store and exchange water with the fracture zone. As a generalization of this model, the double permeability model shown in Fig. 1c considers flow in both the fracture as well as the matrix zone. Thus, the double porosity model appears as a special case of the double permeability model, whereas the single continuum model is contained as a special case in both the double porosity and the double permeability model.

In the drying of wood, good agreement between theory and experiment has generally been found (Spolek et al. 1985; Ouelhazi et al. 1992; Couture et al. 1996; Perre 1987; Pang 1998; Goyeneche et al. 2002); although, several issues, including the description of the flow at low degrees of free water saturation (Couture et al. 1996; Goyeneche et al. 2002), remain somewhat controversial. In infiltration, however, agreement between theory and experiment seems to be much more difficult to attain. Of course, the general set of governing equations

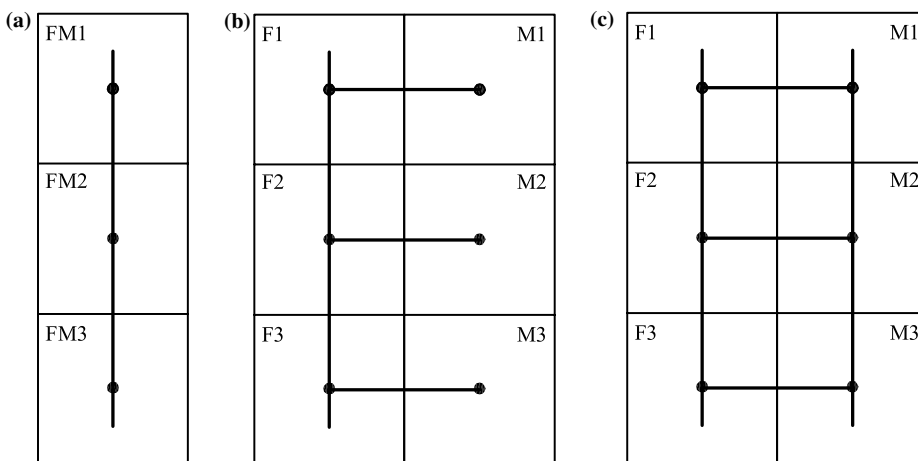


Fig. 1 Transport models: single continuum model (a), double-porosity model (b), and double-permeability model (c). Adapted from Mortensen (2001)

applied in the case of drying are, in principle, also valid in the case of infiltration. However, the rate of drying is often to a large degree governed by the rate of evaporation at the exchange surface, which is relatively easy to quantify, rather than by the internal transfer. In infiltration, on the other hand, the entire process is governed solely by the internal transfer properties, which may be very difficult to quantify in terms of the single continuum model. Indeed, Banks (1981) goes as far as to speculate that [no tag]the precise prediction of liquid penetration rate from steady state permeability data may be illusory'. An example of some of the difficulties encountered is contained in a recent one dimensional infiltration experiment on beech (Perre 1998). Here the theory predicted a time scale in the order of minutes whereas the actual time scale turned out to be in the order of days or weeks. Moreover, the moisture profiles measured seemed to be in very poor agreement with what one would expect on the basis of a single continuum model.

As was suggested in Perre (1998) the observed behaviour is probably due to the structure of the wood. In Fig. 2 the cellular structure of a so-called diffuse porous hardwood, to which category beech belongs, is shown. Looking at this figure it is not hard to conceive that the transport of water of a one dimensional longitudinal sample would be primarily by way of the large vessels with a simultaneous, but much slower infiltration into the denser material surrounding the vessels. This type of transfer corresponds quite closely to what can be represented by the double porosity model illustrated in Fig. 1b. This model thus seems to be a natural extension of the conventional macroscopic model.

This mode of transfer could also be important in other species of wood. In ring porous hardwoods, Fig. 3a, the situation is the same, i.e. large vessels and surrounding dense material. In softwoods, Fig. 3b, it is well-known (see e.g. Siau 1984), that infiltration into dry wood is more rapid in the latewood than in the earlywood, and that the ratio between the transfer rates is greater in the sapwood than in the heartwood. This is perhaps somewhat contrary to what should be expected since in the green state the thinwalled earlywood is much more permeable than the latewood. However, during drying the pits which connect the individual cells, and thus provide the principal pathways for water flow, have a much higher tendency to blocking up in the earlywood than in the latewood.

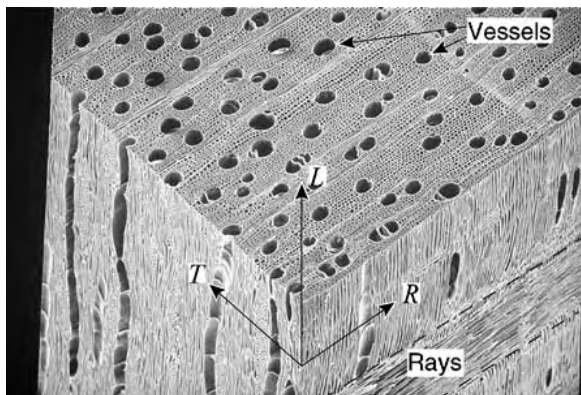


Fig. 2 Microscopic structure of a diffuse porous hardwood (sugar sample) (Structure of Wood 2003)

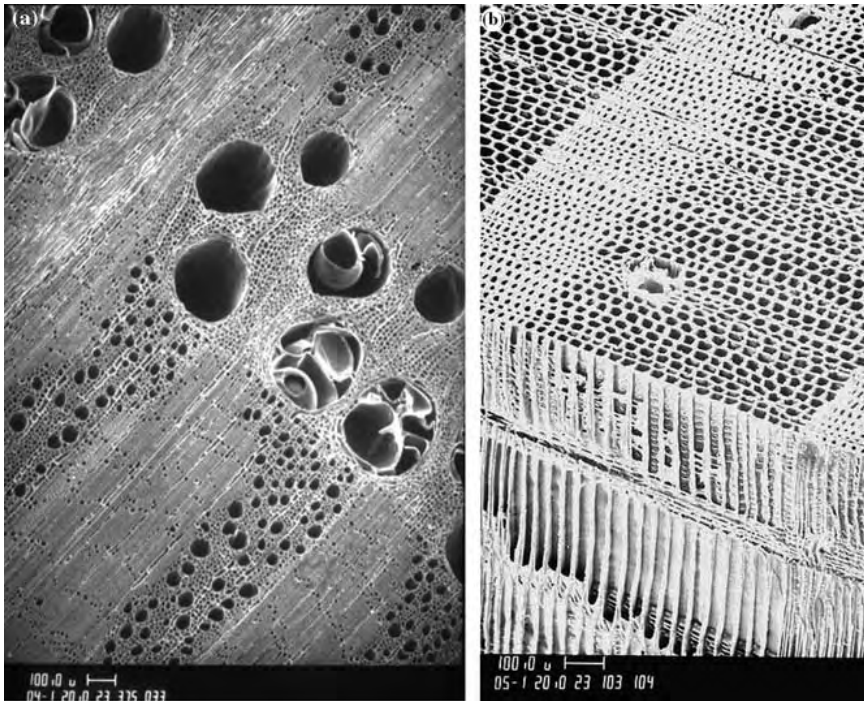


Fig. 3 Microscopic structure of ring-porous hardwood (*white oak*) (a), and softwood (*Douglas fir*) (b) (Structure of Wood 2003)

Whereas the applicability of the double porosity model seems very plausible for infiltration in the longitudinal direction, there seems to be less justification for using the approach to flow in the other two directions. However, in the radial direction, the presence of ray cells (Fig. 2) constitutes a possible rapid route for water transport, again with a simultaneous infiltration into the denser material surrounding the rays cells. In the tangential direction, the flow of water must necessarily be exclusively by way of the pits connecting the cells. In this direction no macropores are thus present. It seems, therefore, that for general three dimensional conditions, the double porosity model does not suffice. That is, the flow in the [no tag]matrix', especially in the tangential direction, is too significant to be ignored, and for this reason the double permeability model rather than the double porosity model should be considered in the general three dimensional case.

As for other porous materials the applicability of double porosity/permeability model could also be expected. In cement paste, for example, the problems with applying single continuum models for the infiltration of water is well documented (see e.g. Martys and Ferraris 1997; Krus et al. 1997). Similarly, in cellular concrete very poor agreement between theory and experiment has been reported (Nielsen 1974; Hansen 1993). Recently, a number of different porous materials, including fired-clay brick and sandstone, were all shown to exhibit a behaviour during infiltration which does not comply with the common theory (Kuntz and Lavallee 2001). The application of double porosity/permeability models to these materials could be justified on the basis of the pore size distribution, i.e. with water being transferred quite rapidly in the larger pores with a simultaneous infiltration into the smaller pores, similar to what is the case in

soils. Although there may well be other mechanisms involved, the double porosity/permeability models seem to be worth considering, at least because of their very clear physical interpretation.

In the following the conventional macroscopic single continuum model is briefly discussed after which several double porosity and permeability models are presented. Throughout, numerical examples demonstrating the differences between the single continuum and the double porosity/permeability model are given. Finally, the numerical solution of the various models by the finite element method is discussed.

Single continuum model

The single continuum model considers the conservation of the three water phases as well as dry atmospheric air and enthalpy. For reasons of simplicity we will assume isothermal and atmospheric conditions throughout. The relevant conservation equations are then

$$\begin{aligned}
 \text{Free water:} & \quad \frac{\partial}{\partial t} (\varepsilon_w \rho_w) + \nabla \cdot (\rho_w \mathbf{v}_w) = -\dot{m}_{wv} - \dot{m}_{wb} \\
 \text{Bound water:} & \quad \frac{\partial}{\partial t} (\varepsilon_s \rho_b) + \nabla \cdot (\rho_b \mathbf{v}_b) = -\dot{m}_{bv} - \dot{m}_{wb} \\
 \text{Water vapour:} & \quad \frac{\partial}{\partial t} (\varepsilon_g \rho_v) + \nabla \cdot (\rho_v \mathbf{v}_v) = \dot{m}_{wv} + \dot{m}_{bv}
 \end{aligned} \tag{1}$$

where ε_w , ε_s , ε_g are the volume fractions of free water, solid skeleton and gas (vapour and air) phases, and ρ_w , ρ_b and ρ_v are the corresponding concentrations of free water, bound water and water vapour. The mass average velocities of the different water phases are given by \mathbf{v}_w , \mathbf{v}_b and \mathbf{v}_v . These equations are quite general and also include the transition of one phase to another, i.e. \dot{m}_{wv} describes the rate of conversion of free water to bound water, \dot{m}_{bv} the conversion of bound water to water vapour, and \dot{m}_{wb} accounts for the conversion of bound water to free water and vice versa. Recently, it has been shown (Krabbenhoft and Damkilde 2003) that the non-equilibrium between water vapour and bound water is a key ingredient in accurately describing moisture transfer in the hygroscopic range. In this way the flow phenomena often referred to as [no tag]non-Fickian' (Wadsö 1994) can be accurately described. Nevertheless, in the interest of simplicity and because the primary focus is on the conditions above the fiber saturation point, we will assume equilibrium between all water phases as is usually done. The three conservation equations of Eqs. 1 can then be reduced to one describing the conservation of the total water

$$\text{Total water:} \quad \frac{\partial \theta}{\partial t} + \nabla \cdot (\rho_w \mathbf{v}_w + \rho_b \mathbf{v}_b + \rho_v \mathbf{v}_v) = 0 \tag{2}$$

where θ is the total water content (kg m^{-3}). Since wood is a highly hygroscopic material it is necessary to separate this total moisture content into bound water and free water

$$\theta = \theta_f + \theta_b \tag{3}$$

where the bound water content is defined as

$$\theta_b = \min(\theta, \rho_0 M_{\text{FSP}}) \tag{4}$$

with M_{FSP} being the dry base moisture content at the fiber saturation point and ρ_0 the dry density. Next, the conservation Eq. 2 must be supplemented with

appropriate constitutive relations. For the free water phase Darcy's law is applied

$$\rho_w \mathbf{v}_w = -\rho_w \frac{KK_r}{\mu_w} \nabla(p_w + \rho_w gz) \quad (5)$$

where K is the absolute permeability, K_r the relative permeability which depends on fluid saturation, μ_w the dynamic viscosity of water, and p_w the water pressure which under partially saturated and atmospheric conditions is equivalent to the capillary pressure p_c . Gravity is defined as acting opposite to the z -coordinate.

The bound water flux is described by a gradient law with the bound water moisture content as driving force (Siau 1984)

$$\rho_b \mathbf{v}_b = D_b \nabla \theta_b \quad (6)$$

For the vapour flux convective transfer is ignored and Fick's law used to describe the diffusive flux. Under isothermal conditions this can be written as

$$\rho_v \mathbf{v}_v = \frac{M_w}{RT} D_v \nabla p_v \quad (7)$$

where D_v is the effective water vapour diffusivity.

Thus, the full equation describing the transfer of water vapour, bound water and free water is given by

$$\frac{\partial \theta}{\partial t} = \nabla \cdot \left[\rho_w \frac{KK_r}{\mu_w} \nabla(p_w + \rho_w gz) + D_b \nabla \theta_b + \frac{M_w}{RT} D_v \nabla p_v \right] \quad (8)$$

The total water conservation Eq. 8 requires a significant number of material parameters which in principle can be determined in a number of independent experiments. In infiltration the far largest contribution to the total water flux is that of free water. To describe the transfer of this component the absolute and relative permeabilities as well as the capillary pressure-saturation curve must be determined. Such relations are available for green wood, although they are subject to a large degree of uncertainty and must generally be used with some caution (Couture et al. 1996; Goyeneche et al. 2002). For wood which has been dried, however, we do not know of any complete set of relations. Therefore, in the following, we will use a transport equation which does not explicitly involve these relations. If we assume partially saturated conditions and neglect gravity then Eq. 8 can be written in terms of θ only as

$$\frac{\partial \theta}{\partial t} = \nabla \cdot (D_\theta \nabla \theta) \quad (9)$$

where the effective total water diffusivity is given by

$$D_\theta = \rho_w \frac{KK_r}{\mu_w} \left(\frac{\partial p_c}{\partial \theta} \right) + D_b \left(\frac{\partial \theta_b}{\partial \theta} \right) + \frac{M_w}{RT} D_v \left(\frac{\partial p_v}{\partial \theta} \right) \quad (10)$$

Thus, instead of measuring each of the components in Eq. 10 in a number of independent experiments, there is also the possibility of measuring the effective diffusivity D_θ directly in a single experiment. This approach has been taken to wood in Tremblay et al. (2000) and Signe Kamp (2003), and in Pel (1995) to a number of other porous building materials. Thus, in the following we will make

reference to Eq. 9 rather than to Eq. 8 and assume the effective diffusivity given as function of the total water content.

It should be borne in mind that this approach is far from ideal. First of all, gravity is neglected, which in many applications may be quite erroneous. Furthermore, there is no real possibility of taking externally applied water pressures greater than the maximum capillary pressure into account. As a first approximation, however, the approach is acceptable although in the future the consistent Darcian model in Eq. 8 should be preferred.

Properties of the infiltration equation and reported anomalies

The governing equation (Eq. 9) belongs to the class of nonlinear diffusion problems which are treated extensively, e.g. in Crank (1967). Although usually very hard to solve analytically, quite a lot of information about the principal behaviour of these equations can be extracted. Since the effective diffusivity is usually a very strong function of the moisture content, often increasing over several decades from the dry to the fully saturated state, a shock-like behaviour is often seen when tracking the moisture content profiles in time. This is shown in Fig. 4a, where a one dimensional infiltration in the longitudinal direction of a 5-cm softwood sample has been simulated using standard material parameters (Perré and Turner 1999). For such experiments the fractional weight increase as a function of the square root of time is often plotted and a curve similar to the one shown in Fig. 4b should then result. That is, the curve should be linear up to the point where the front reaches the dry end of the sample. One of the most cited anomalies is deviations from this curve, and these are often of the form of a two-stage infiltration as reported by Martys and Ferraris (1997), Nielsen (1974), and Hansen (1993). That is, the fractional weight increase curve indicates a rapid initial sorption of a certain amount of water, followed by a much slower sorption which proceeds until full saturation.

In Fig. 5a the moisture content profiles resulting from infiltration into a sample of beech are shown. As can be seen the moisture content increases rapidly near the wet end, whereas the subsequent infiltration is very slow. This is clearly seen from the fractional weight increase curve in Fig. 5b which is not at all as should be expected. The explanation given in Perre (1998) for this behaviour is that a portion of the water is carried very rapidly in the vessels with

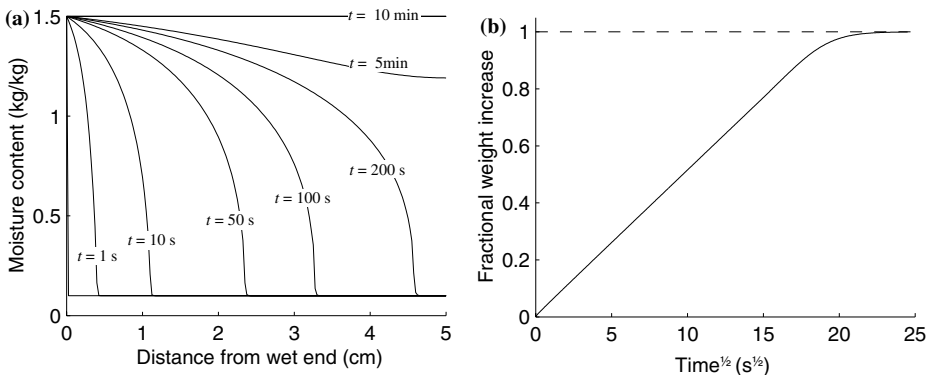


Fig. 4 One dimensional single continuum model infiltration

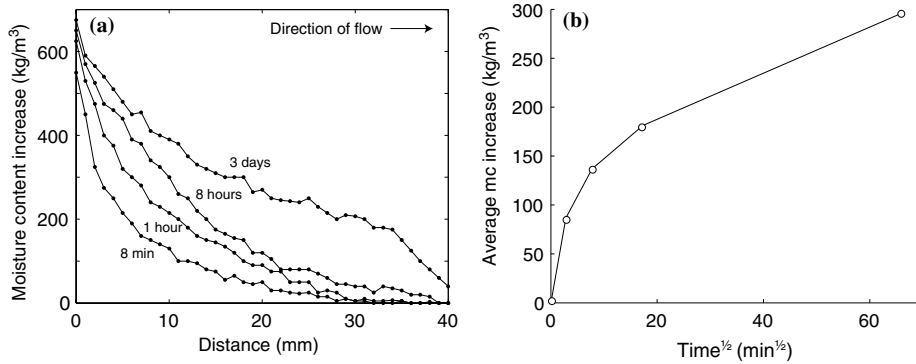


Fig. 5 Infiltration in beech (Perre 1998)

a simultaneous, but much slower, infiltration into the denser material surrounding the vessel. Another example of an anomalous infiltration in wood is shown in Fig. 6 where the material is fir sapwood. These moisture content profiles are particularly interesting in that they clearly reveal both the propagation of a front as well as a simultaneous slow absorption.

Clearly, the behaviour encountered in these two experiments cannot be simulated using the standard single continuum model. As previously mentioned, similar anomalies have been reported for a number of other porous materials. Recently, Kuntz and Lavalée (2001) proposed that instead of using the standard diffusion Eq. 9 the moisture flux should be taken as

$$j = -D(\theta) \left(\frac{\partial \theta}{\partial z} \right)^n \quad (11)$$

such that the governing equation would be

$$\frac{\partial \theta}{\partial t} = \frac{\partial}{\partial z} \left[D(\theta) \left(\frac{\partial \theta}{\partial z} \right)^n \right] \quad (12)$$

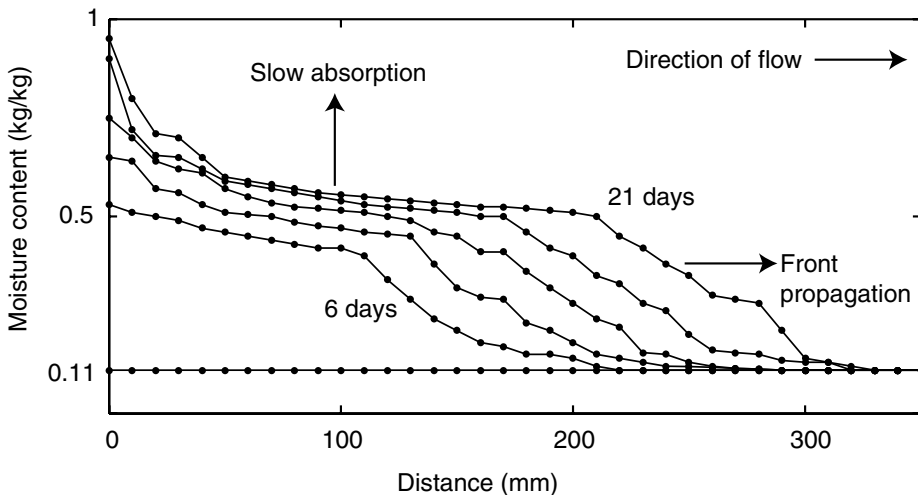


Fig. 6 Infiltration in fir sapwood (K.K. Hansen and J.B. Jensen, unpublished data)

where n is not necessarily equal to unity. This gives fractional weight increase curves which are linear when plotted as a function of $t^{1/(n+1)}$. Although such an expression for the flux cannot be ruled out, the underlying physics of the modified gradient law is somewhat unclear. Nevertheless, a number of infiltration experiments involving non-organic porous materials were fitted quite well.

Another recent proposition involves a time dependent diffusion coefficient. Thus, Lockington and Parlange (2003) argue that in cement based materials where there is the possibility of some chemo-mechanical interaction, a governing equation of the type

$$\frac{\partial \theta}{\partial t} = \frac{\partial}{\partial z} \left(\gamma(t) \delta(\theta) \frac{\partial \theta}{\partial z} \right) \quad (13)$$

should be considered. For wood, such a time dependent diffusion coefficient could be argued since in wood there is a swelling and a subsequent relaxation upon exposure to moisture. Moreover, the validity of using such a time dependent diffusion coefficient can easily be proved or disproved by initiating the experiment from conditions closer or further from the fiber saturation point, below which all moisture–mechanical interaction takes place.

In the following, an alternative explanation for the anomalies encountered is sought in terms of the double porosity/permeability models. We focus on the different principal behaviours which can be simulated using these models. Furthermore, an attempt to explain a set of experimental results in terms of the models is made.

Since no analytic solutions are available for the coupled nonlinear diffusion equations which define the models, all computations are done numerically by the finite element method as described in Appendix.

Double porosity and permeability models

In the following, the double porosity and permeability models are presented and some of their properties described.

The total moisture content is separated into two contributions α and β with the parameter η describing the volume fraction of the α -zone. Thus, the total moisture content is given by a weighted sum as

$$\theta = \eta \theta_\alpha + (1 - \eta) \theta_\beta = \eta_\alpha \theta_\alpha + \eta_\beta \theta_\beta \quad (14)$$

The double porosity model then describes the transport of moisture by two coupled equations which, in the one dimensional case, are given by

$$\begin{aligned} \eta_\alpha \frac{\partial \theta_\alpha}{\partial t} &= \frac{\partial}{\partial z} \left(\eta_\alpha D_\alpha \frac{\partial \theta_\alpha}{\partial z} \right) - \dot{m} \\ \eta_\beta \frac{\partial \theta_\beta}{\partial t} &= \frac{\partial}{\partial z} \left(\eta_\beta D_\beta \frac{\partial \theta_\beta}{\partial z} \right) + \dot{m} \end{aligned} \quad (15)$$

where \dot{m} describes the exchange of water between the two zones.

This leads to the double permeability model and follows as a natural extension of the double porosity model, namely, by also considering the flow water in the β -zone

$$\begin{aligned}\eta_\alpha \frac{\partial \theta_\alpha}{\partial t} &= \frac{\partial}{\partial z} \left(\eta_\alpha D_\alpha \frac{\partial \theta_\alpha}{\partial z} \right) - \dot{m} \\ \eta_\beta \frac{\partial \theta_\beta}{\partial t} &= \frac{\partial}{\partial z} \left(\eta_\beta D_\beta \frac{\partial \theta_\beta}{\partial z} \right) + \dot{m}\end{aligned}\quad (16)$$

Clearly, these models both reduce to the single continuum model when $\eta_\alpha=1$, i.e. when the volume fraction of the β -zone is equal to zero.

Besides determining the diffusivities in the two zones, the major problem consists of formulating appropriate mass exchange terms \dot{m} . Basically, this term must be determined experimentally. In the following, however, we assume it to be of the type

$$\dot{m} = \omega \left(\frac{\theta_\alpha}{\theta_\alpha^{\max}} - \frac{\theta_\beta}{\theta_\beta^{\max}} \right) \quad (17)$$

where θ_α^{\max} and θ_β^{\max} are the maximum attainable moisture contents in the two zones and ω is a parameter which governs the rate of mass transfer. This parameter should probably depend on the moisture content in the two zones in a way similar to what is the case with the effective diffusivity. However, for the time being we will assume it to be constant.

An alternative formulation of the mass exchange term uses the capillary pressures in the two zones, such that

$$\dot{m} = \omega_c [p_c^\alpha(S_\alpha) - p_c^\beta(S_\beta)] \quad (18)$$

where p_c^α and p_c^β are the capillary pressures, and S_α and S_β are the saturations, or effective saturations, in the two zones. Since fluid flow is driven by differences in pressure rather than saturation or moisture content, this form of the mass transfer term could be argued as being physically more correct. It does, however, require knowledge of the capillary pressure-saturation curves in the two zones, which naturally increases the complexity of the model. In fact, the departure from the consistent Darcian model of Eq. 8 was motivated by the difficulties involved with the determination of these values. In the following, therefore, we will only consider the moisture content driven mass exchange term (Eq. 17).

For moisture transfer below the fiber saturation point a similar mass exchange term is necessary in order to account for the exchange of water between the vapour found in the lumens and the bound water present in the cell walls. In Krabbenhoft and Damkilde (2003) and Krabbenhoft (2003) it is shown that this should depend on two quantities: the absolute bound water moisture content and some measure of the proximity to equilibrium, such that inter-phase mass exchange decreases dramatically as equilibrium is approached, i.e. much more than can be captured by a first-order expression with constant coefficients such as (Eq. 17). In the case of free water exchange between different zones a similar dependence thus seems worth considering.

Multiple porosity and permeability models

The double porosity and permeability models presented in the previous section are readily extended to include multiple zones. For example, in the case where three zones are present a relevant model could be

$$\begin{aligned}
 \eta_\alpha \frac{\partial \theta_\alpha}{\partial t} &= \frac{\partial}{\partial z} \left(\eta_1 D_\alpha \frac{\partial \theta_\alpha}{\partial z} \right) - \dot{m}_{\alpha\beta} \\
 \eta_\beta \frac{\partial \theta_\beta}{\partial t} &= \frac{\partial}{\partial z} \left(\eta_2 D_\beta \frac{\partial \theta_\beta}{\partial z} \right) + \dot{m}_{\alpha\beta} - \dot{m}_{\beta\gamma} \\
 \eta_\gamma \frac{\partial \theta_\gamma}{\partial t} &= \frac{\partial}{\partial z} \left(\eta_3 D_\gamma \frac{\partial \theta_\gamma}{\partial z} \right) + \dot{m}_{\beta\gamma}
 \end{aligned} \tag{19}$$

where

$$\eta_\alpha + \eta_\beta + \eta_\gamma = 1 \tag{20}$$

In this model exchange of water is assumed to take place between the α and β zones and between the β and γ zones, whereas no exchange takes place between the α and γ zones. Although the complexity of such models increases since more material parameters are required, they may be necessary. Thus, if the results shown in Fig. 5 are to be explained in terms of these models, more than two interacting zones may be required. Here the fractional weight increase curve indicates not only the presence of two, but several different zones.

Examples

In the following, some applications of the models described above are considered. First a set of experimental results is fitted by the double permeability model, after which several different properties of this model are described.

All examples are solved numerically by the finite element method described in the Appendix.

Example 1: Comparison with experimental results

The first example concerns the one dimensional infiltration experiment of fir sapwood (K.K. Hansen and J.B. Jensen, unpublished data) described in Sect. 2 and shown in Fig. 6.

Here the double permeability model was applied with the parameters shown in Table 1. The results in terms of predicted and measured moisture content profiles are shown in Fig. 7, where a dry wood density of 500 kg m^{-3} has been assumed. Even though the fits are not perfect, the results are quite encouraging. The general trend of a rapidly moving fraction with a simultaneous slow absorption is clearly picked up, and a more refined choice of diffusivities could surely lead to a better correspondence between computed and experimental results. The average moisture content as a function of the square root of time is shown in Fig. 8. Again the predicted moisture contents compare quite well to the experimental results.

Table 1 Parameters used in Example 1

Initial moisture content	$\theta_\alpha^0 = \theta_\beta^0 = 55.0 \text{ kg/m}^3$
Maximum moisture content	$\theta_\alpha^{\max} = \theta_\beta^{\max} = 500.0 \text{ kg/m}^3$
Zone fractions	$\eta_\alpha = 0.45, \eta_\beta = 0.55$
Diffusivities	$D_\alpha = 39.2 \times 10^{-9} \exp(0.011 \theta_\alpha) \text{ [m}^2/\text{s]}$
Mass exchange parameter	$D_\beta = 0.0005 D_\alpha$ $\omega = 55.0 \times 10^{-6} \text{ s}^{-1}$

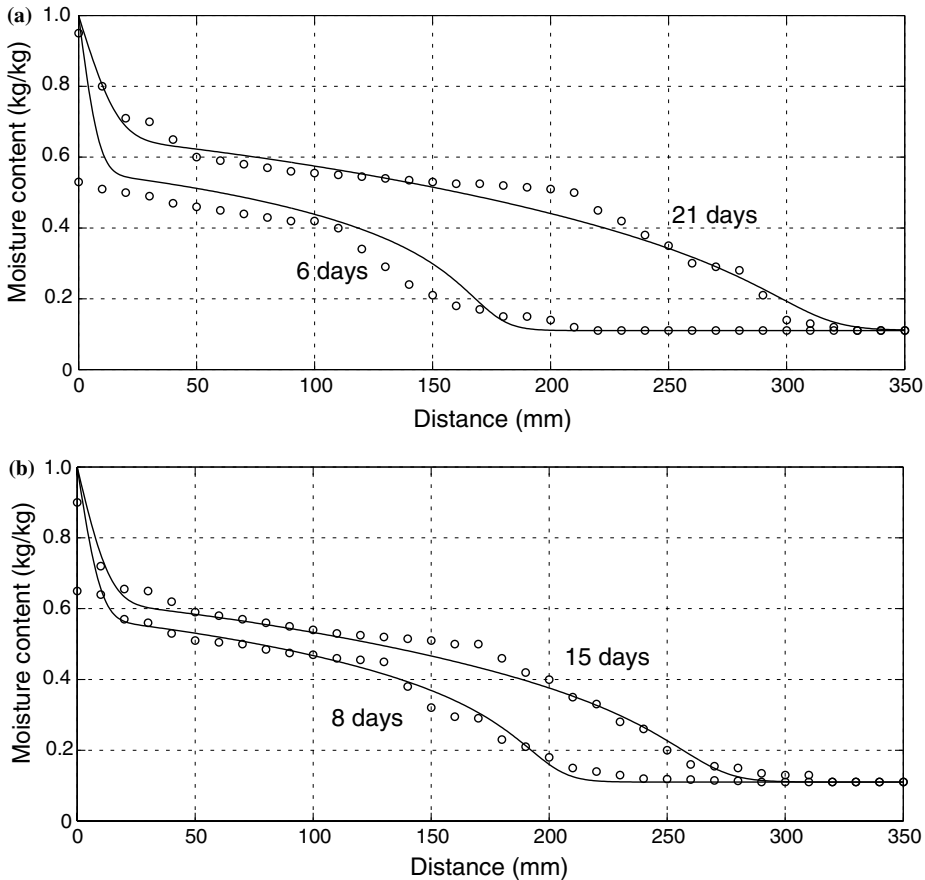


Fig. 7 Computed (-) and experimental (O) moisture profiles. Example 1

Example 2: Double permeability versus double porosity

Since the double porosity model is significantly simpler than the double permeability model in that only one diffusivity is required, it is of interest to compare the results produced by the two models. This is done in Fig. 9a-c. Except for the β -diffusivity all material parameters are identical to the ones used in the previous example.

In Fig. 9a the double permeability model used in the previous example is compared to the double porosity model and, as can be seen, there is a rather good agreement; only very close to the wet end do the models produce significantly different results. In Fig. 9b the β -diffusivity has been increased by a factor of ten and the results deviate slightly more. Finally in Fig. 9c, where yet another factor of ten increase is applied, the two models produce quite different results.

Example 3: Sample length dependence

An often reported anomaly is an apparent sample length dependence of the transfer parameters (see e.g. Dinwoodie 1981; Siau 1984; Banks 1981). This

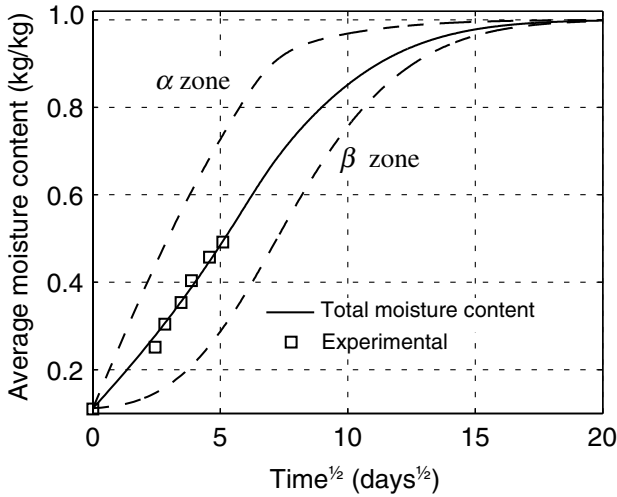


Fig. 8 Average moisture content as a function of square root of time. Example 1

phenomenon is usually attributed to the fact that between the cells, there is a probability of connectivity less than one. This may result in the measured permeabilities being significantly higher for smaller samples than for larger ones. However, the double permeability model results in a manifestation of the opposite phenomenon, namely, that the apparent diffusivity increases with increasing sample dimensions. This is due to non-equilibrium between the water in the two zones as expressed by the mass exchange term \dot{m} , and in this sense the situation is identical to what is experienced in moisture transfer below the fiber saturation point (Krabbenhoft and Damkilde 2003). Thus, it can be expected that there are two opposing mechanisms, which naturally complicates matters further.

From classical diffusion theory (see e.g. Crank 1967), it is well known that when the fractional weight increase is plotted as a square root of time divided by the sample length, then the resulting curves should be superimposed on one another. Furthermore, an apparent diffusivity may be computed as

$$D_{\text{app}} = \frac{\pi a^2}{4} \left(\frac{dE}{d\sqrt{t}} \right)^2 \quad (21)$$

where E is the fractional weight increase and a is the sample length (sample half-length if the experiment is conducted with infiltration from both ends), and the slope $dE/d\sqrt{t}$ refers to the initial slope of the $E-\sqrt{t}$ curve. However, as discussed previously, in true single continuum diffusion with diffusivity increasing with moisture content the $E-\sqrt{t}$ curve is linear up to around $E \approx 0.8$, and the slope may then be taken in any point between $E=0$ and $E \approx 0.8$.

In Fig. 10a, fractional weight increase curves as a function of \sqrt{t}/a are shown for samples of different length for the data set in Table 1. These curves are seen to be far from superimposed on one another. The greatest anomaly occurs for the shorter samples where the α -diffusion quickly comes to an end, and mass exchange between the two zones then takes over and accounts for the larger

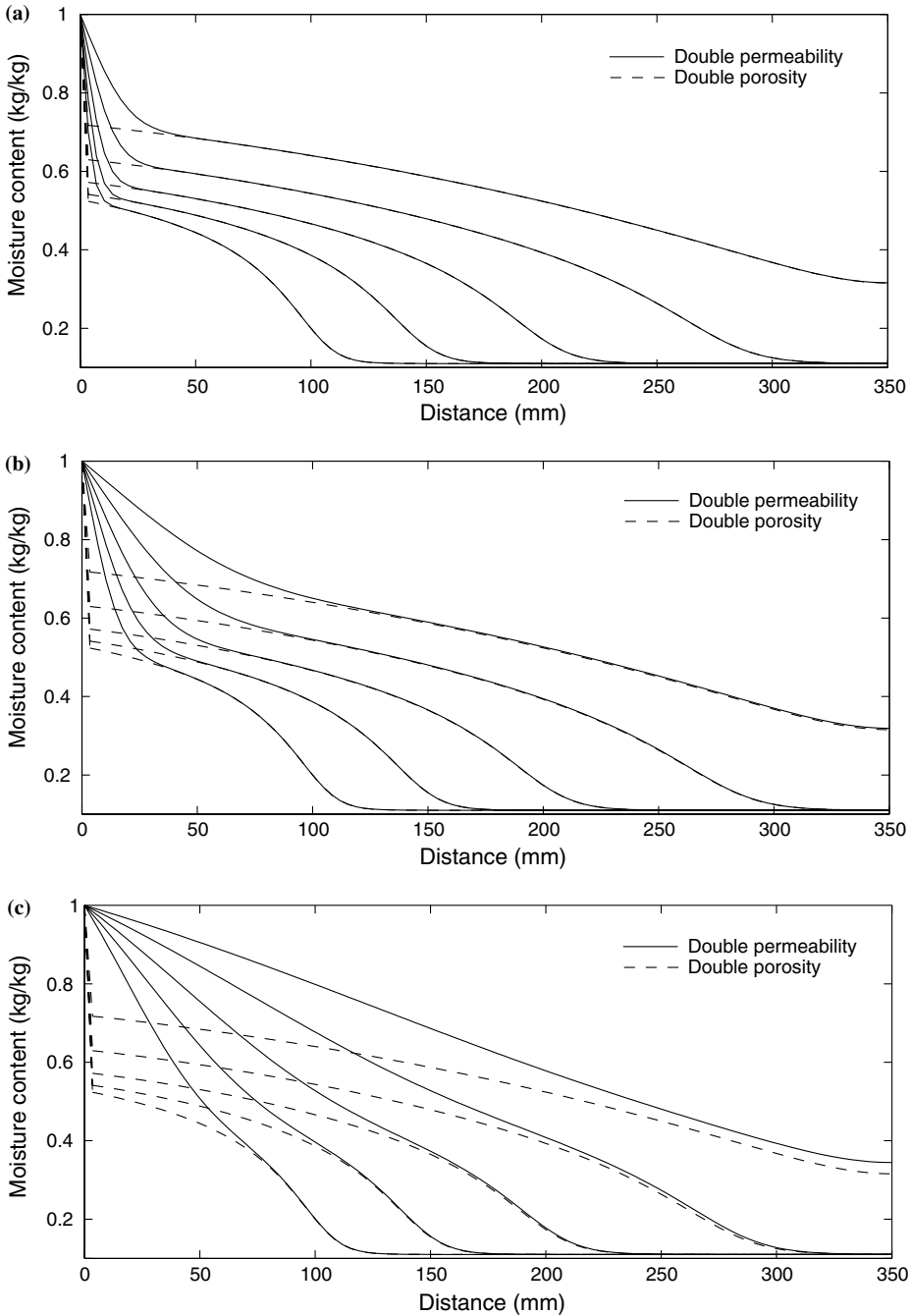


Fig. 9 Dual porosity and permeability models in one dimensional infiltration. Profiles shown after 2, 4, 8, 16, and 32 days. Example 2

part of the remaining uptake of water. The two-stage sorption which results from this becomes less apparent as the length is increased since diffusion then becomes the limiting mechanism.

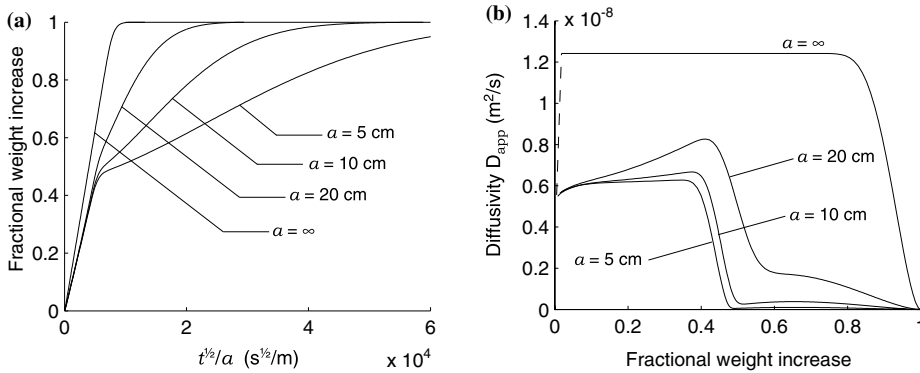


Fig. 10 Fractional weight increase curves (a) and apparent diffusivities (b). Example 3

In Fig. 10b the apparent diffusivities corresponding to the fractional weight increase curves are shown. These are shown as a function of the fractional weight increase, where at each point the slopes of the $E-\sqrt{t}$ curves have been used. As can be seen, it is only for very large sample lengths, in the order of several meters, that the $E-\sqrt{t}$ curve is perfectly linear and thus gives constant diffusivities up to a point around $E=0.8$ where Eq. 21 is no longer valid. This illustrates the fact that even though the fractional weight increase curve for a sample of $a=20$ cm appears to comply rather well with standard diffusion, the resulting computed diffusivity does not.

Conclusions

In this paper some of the possibilities of applying double porosity and permeability models to the problem of water infiltration into wood have been discussed. Whereas it seems that there is some justification of such models, the problem of determining the necessary material parameters still remains. For this purpose it would seem that determination of moisture profiles would be necessary, or in any case, a great help. Thus, the common total weight increase experiments have been shown to be somewhat problematic in that results which appear to comply rather well with the single continuum diffusion model may in fact be highly anomalous. However, the total weight increase experiment may be useful as a preliminary examination of the qualitative nature of the process, especially if conducted for several samples of different lengths. In this work the total diffusion model which is applicable only for partially saturated conditions and which neglects the effects of gravity has been used. Clearly, this model is not satisfactory, and the consistent Darcian model with water pressure as the driving force should generally be preferred.

Acknowledgements This work has been funded in part by the Danish Research Agency under Project No. 9901363: [no tag]Modeling the Effects of Moisture and Load History on the Mechanical Properties of Wood'. The financial support is gratefully acknowledged.

Appendix

Numerical solution procedure

The numerical solution procedure is described with reference to the double permeability model

$$\begin{aligned}\eta_\alpha \frac{\partial \theta_\alpha}{\partial t} &= \frac{\partial}{\partial z} \left(\eta_\alpha D_\alpha \frac{\partial \theta_\alpha}{\partial z} \right) - \omega \left(\theta_\alpha / \theta_\alpha^{\max} - \theta_\beta / \theta_\beta^{\max} \right) \\ \eta_\beta \frac{\partial \theta_\beta}{\partial t} &= \frac{\partial}{\partial z} \left(\eta_\beta D_\beta \frac{\partial \theta_\beta}{\partial z} \right) + \omega \left(\theta_\alpha / \theta_\alpha^{\max} - \theta_\beta / \theta_\beta^{\max} \right)\end{aligned}\quad (22)$$

The moisture content variables are approximated in terms of finite element functions as

$$\begin{aligned}\theta_\alpha(z, t) &\approx \mathbf{N}(z)\theta_\alpha(t) \\ \theta_\beta(z, t) &\approx \mathbf{N}(z)\theta_\beta(t)\end{aligned}\quad (23)$$

Similarly, the diffusivities are approximated in terms of their nodal values

$$\begin{aligned}D_\alpha &= \mathbf{A}D_\alpha \\ D_\beta &= \mathbf{A}D_\beta\end{aligned}\quad (24)$$

where the vectors $\mathbf{D}_\alpha = D_\alpha(\theta_\alpha)$ and $\mathbf{D}_\beta = D_\beta(\theta_\beta)$ contain the nodal diffusivities and \mathbf{A} is a vector which weights these in an appropriate way as being representative for the element. In all the examples presented $\mathbf{A} = \left[\frac{1}{2}, \frac{1}{2} \right]$. Alternative upstream weighting schemes are discussed in Forsyth and Kropinski (1997).

Applying the standard Galerkin scheme (see e.g. Zienkiewicz and Taylor 2000) to Eq. 22 yields two coupled nonlinear ordinary differential equations

$$\begin{aligned}r_\alpha &= \eta_\alpha \mathbf{M} \frac{d\theta_\alpha}{dt} + \mathbf{K}\theta_\alpha + \tilde{\omega}_\alpha \mathbf{M}\theta_\alpha - \tilde{\omega}_\beta \mathbf{M}\theta_\beta = \mathbf{0} \\ r_\beta &= \eta_\beta \mathbf{M} \frac{d\theta_\beta}{dt} + \mathbf{K}\theta_\beta + \tilde{\omega}_\alpha \mathbf{M}\theta_\alpha + \tilde{\omega}_\beta \mathbf{M}\theta_\beta = \mathbf{0}\end{aligned}\quad (25)$$

where $\tilde{\omega}_\alpha = \omega / \theta_\alpha^{\max}$ and $\tilde{\omega}_\beta = \omega / \theta_\beta^{\max}$. Assuming \mathbf{A} is constant, the matrices \mathbf{M} , \mathbf{K}_α and \mathbf{K}_β are given by

$$\mathbf{M} = \int_{\Omega} \mathbf{N}^T \mathbf{N} d\Omega \quad (26)$$

$$\mathbf{K}_\alpha = \tilde{\mathbf{K}}\mathbf{A}D_\alpha, \quad \mathbf{K}_\beta = \tilde{\mathbf{K}}\mathbf{A}D_\beta \quad (27)$$

where

$$\tilde{\mathbf{K}} = \int_{\Omega} \left(\frac{\partial \mathbf{N}}{\partial z} \right)^T \frac{\partial \mathbf{N}}{\partial z} d\Omega \quad (28)$$

It should be noted that in practice \mathbf{M} is replaced with a lumped equivalent in order to reduce the risk of non-physical oscillations (see e.g. Segerlind 1984).

The backward Euler scheme is now applied whereby the fully discretized equations can be written as

$$\begin{aligned} \mathbf{r}_\alpha &= [(\eta_\alpha + \tilde{\omega}_\alpha \Delta t)\mathbf{M} + \Delta t\mathbf{K}_{\alpha,n+1}] \theta_{\alpha,n+1} - \tilde{\omega}_\beta \Delta t \mathbf{M} \theta_{\beta,n+1} - \eta_\alpha \mathbf{M} \theta_{\alpha,n} = \mathbf{0} \\ \mathbf{r}_\beta &= [(\eta_\beta + \tilde{\omega}_\beta \Delta t)\mathbf{M} + \Delta t\mathbf{K}_{\beta,n+1}] \theta_{\beta,n+1} - \tilde{\omega}_\alpha \Delta t \mathbf{M} \theta_{\alpha,n+1} - \eta_\beta \mathbf{M} \theta_{\beta,n} = \mathbf{0} \end{aligned} \quad (29)$$

where subscript n refers to the current state and $n+1$ to the new unknown state. Due to the nonlinearity contained in \mathbf{K}_α and \mathbf{K}_β an iterative procedure is applied. If the standard Newton-Raphson scheme is applied, increments $\Delta\theta_\alpha$ and $\Delta\theta_\beta$ are computed by solution of the following linear system of equations

$$\begin{bmatrix} \mathbf{J}_{\alpha\alpha} & \mathbf{J}_{\alpha\beta} \\ \mathbf{J}_{\beta\alpha} & \mathbf{J}_{\beta\beta} \end{bmatrix}_{n+1}^j \begin{bmatrix} \Delta\theta_\alpha \\ \Delta\theta_\beta \end{bmatrix}_{n+1}^j = - \begin{bmatrix} \mathbf{r}_\alpha \\ \mathbf{r}_\beta \end{bmatrix}_{n+1}^j \quad (30)$$

after which the current state is updated as

$$\begin{bmatrix} \theta_\alpha \\ \theta_\beta \end{bmatrix}_{n+1}^{j+1} = \begin{bmatrix} \theta_\alpha \\ \theta_\beta \end{bmatrix}_{n+1}^j + \begin{bmatrix} \Delta\theta_\alpha \\ \Delta\theta_\beta \end{bmatrix}_{n+1}^j \quad (31)$$

where the initial point is taken as the last converged, i.e.

$$\begin{bmatrix} \theta_\alpha \\ \theta_\beta \end{bmatrix}_{n+1}^0 = \begin{bmatrix} \theta_\alpha \\ \theta_\beta \end{bmatrix}_n \quad (32)$$

The Jacobians in Eq. 30 are given by

$$\begin{aligned} \mathbf{J}_{\alpha\alpha} &= (\eta_\alpha + \tilde{\omega}_\alpha \Delta t)\mathbf{M} + \Delta t(\mathbf{K}_\alpha + \mathbf{K}_\alpha^g) \\ \mathbf{J}_{\beta\beta} &= (\eta_\beta + \tilde{\omega}_\beta \Delta t)\mathbf{M} + \Delta t(\mathbf{K}_\beta + \mathbf{K}_\beta^g) \\ \mathbf{J}_{\alpha\beta} &= -\tilde{\omega}_\beta \Delta t \mathbf{M} \\ \mathbf{J}_{\beta\alpha} &= -\tilde{\omega}_\alpha \Delta t \mathbf{M} \end{aligned} \quad (33)$$

where

$$\mathbf{K}_\alpha^g = \tilde{\mathbf{K}}\theta_\alpha \mathbf{A} \left[\frac{\partial \mathbf{D}_\alpha}{\partial \theta_\alpha} \right], \quad \mathbf{K}_\beta^g = \tilde{\mathbf{K}}\theta_\beta \mathbf{A} \left[\frac{\partial \mathbf{D}_\beta}{\partial \theta_\beta} \right] \quad (34)$$

These matrices are unsymmetric and are, for this reason, often left out. Although this does influence the convergence rate in a negative way, it may lead to smaller total cpu times as compared to the full Newton scheme (see Paniconi and Putti 1994).

References

- Banks WB (1981) Addressing the problem of non-steady state liquid flow in wood. *Wood Sci Technol* 15:171–177
- Couture F, Jomaa W, Puiggali JR (1996) Relative permeability relations: a key factor for a drying model. *Transport Porous Med* 23:303–335
- Crank J (1967) *The mathematics of diffusion*. Oxford University Press, Oxford
- Dinwoodie JM (1981) *Timber, its nature and behaviour*. Van Norstrand Reinhold, New York
- Forsyth PA, Kropinski MC (1997) Monotonicity considerations for saturated-unsaturated subsurface flow. *SIAM J Sci Comput* 18:1328–1354
- Goyeneche M, Lasseux D, Bruneau D (2002) A film-flow model to describe free water transport during drying of a hygroscopic capillary porous medium. *Transport Porous Med* 48:125–158
- Hansen MH (1993) *Estimation of transfer coefficients in models for coupled heat and moisture transfer in porous media*. PhD Thesis, Technical University of Denmark, Lyngby

- Haria HA, Hodnett MG, Johnson AC (2003) Mechanisms of groundwater recharge and pesticide penetration to a chalk aquifer in southern England. *J Hydrol* 275:122–137
- Krabbenhof K (2003) Transport phenomena in wood. PhD Thesis, Technical University of Denmark, Lyngby
- Krabbenhof K, Damkilde L (2003) A non-equilibrium model for non-Fickian moisture transfer in wood. *Mater Struct* (In press)
- Krabbenhof K, Bechgaard C, Damkilde L, Hoffmeyer P (2003) Finite element analysis of boron diffusion in wooden poles. In: Jarmer J (ed) Proceedings of the 34th annual conference of the international research group on wood preservation, Stockholm, pp 1–14
- Krus M, Hansen KK, Küntzel HM (1997) Porosity and liquid absorption of cement paste. *Mater Struct* 40:394–398
- Kuntz M, Lavallee P (2001) Experimental evidence and theoretical analysis of anomalous diffusion during water infiltration in porous building materials. *J Phys D Appl Phys* 34:2547–2554
- Lewis RW, Schrefler BA (2000) The finite element method in the static and dynamic deformation and consolidation of porous media, 2nd edn. Wiley, New York
- Lockington DA, Parlange JY (2003) Anomalous water absorption in porous materials. *J Phys D Appl Phys* 36:760–767
- Martys NS, Ferraris CF (1997) Capillary transport in mortars and concrete. *Cement Concrete Res* 27:747–760
- Mortensen AP (2001) Preferential flow phenomena in partially-saturated porous media. PhD Thesis, Environment and Resources, Technical University of Denmark, Lyngby
- Nielsen AF (1974) Moisture distributions in cellular concrete during heat and moisture transfer. PhD Thesis, Technical University of Denmark, Lyngby
- Ouelhazi N, Arnaud G, Fohr JP (1992) A two-dimensional study of wood plank drying. The effect of gaseous pressure below boiling point. *Transport Porous Med* 7(1):39–61
- Pang S (1998) Relative importance of vapour diffusion and convective flow in modelling of softwood drying. *Dry Technol* 16:271–281
- Paniconi C, Putti M (1994) A comparison of Picard and Newton iteration in the numerical solution of multidimensional variably saturated flow. *Water Resour Res* 30:3357–3374
- Pel L (1995) Moisture transport in porous building materials. PhD Thesis, Technical University Eindhoven, The Netherlands
- Perre P (1987) Measurements of softwoods' permeability to air: importance upon the drying model. *Int Commun Heat Mass* 14:519–529
- Perre P (1998) The use of homogenization to simulate heat and mass transfer in wood: towards a double porosity approach. In: *Drying '98—Proceedings of the international drying symposium*, vol A, Halkidiki, pp 57–72
- Perré P, Turner IW (1999) A 3-D version of TransPore: a comprehensive heat and mass transfer computational model for simulating the drying of porous media. *Int J Heat Mass Tran* 42:4501–4521
- Perre P, Turner IW (1999) Transpore: a generic heat and mass transfer computational model for understanding and visualising the drying of porous media. *Dry Technol* 17(7–8):1273–1289
- Segerlind LJ (1984) Applied finite element analysis, 2nd edn. Wiley, New York
- Siau JF (1984) Transport processes in wood. Springer, Berlin Heidelberg New York
- Signe Kamp J (2003) Drying of wood. PhD Thesis, Technical University of Denmark, Lyngby
- Structure of Wood (2003) Society of Wood Science and Technology, Teaching Unit No. 1, <http://www.swst.org/teach/set2/struct1.html>. Cited 16 June 2003
- Spolek GA, Plumb OA, Olmstead BA (1985) Heat and mass transfer in wood during drying. *Int J Heat Mass Tran* 28(9):1669–1678
- Tremblay C, Cloutier A, Fortin Y (2000) Determination of the effective water conductivity of red pine sapwood. *Wood Sci Technol* 34:109–124
- Wadsö L (1994) Describing non-Fickian water-vapour sorption in wood. *J Mater Sci* 29:2367–2372
- Whitaker S (1977) Simultaneous heat, mass, and momentum transfer in porous media: a theory of drying. *Adv Heat Transfer* 13:119–203
- Zienkiewicz OC, Taylor RL (2000) The finite element method. Butterworth-Heinemann, Oxford

FINITE ELEMENT ANALYSIS OF BORON DIFFUSION IN WOODEN POLES

Kristian Krabbenhoft

Research Academic
Department of Civil, Surveying, and Environmental Engineering
University of Newcastle
NSW 2308
Australia

Preben Hoffmeyer

Associate Professor
Department of Civil Engineering
Technical University of Denmark
Lyngby, Denmark

Carl G. Bechgaard

Director
Wood Slimp GmbH
Horsholm, Denmark

and

Lars Damkilde

Professor
Institute of Chemistry and Applied Engineering Science
Aalborg University Esbjerg
Esbjerg, Denmark

(Received July 2003)

ABSTRACT

The problem of describing the migration of dissolved boron in wood is treated with special reference to the commonly used remedial treatment of wooden poles. The governing equations are derived and discussed together with some of the material parameters required. The equations are solved by the finite element method and, finally, results showing the effect of different treatment strategies are presented.

Keywords: Wood, boron, remedial treatment, diffusion, finite elements, poles.

INTRODUCTION

Remedial treatment of wooden poles embedded in soil is frequently required. One such treatment consists of placing concentrated boron deposits in the pole near the ground level. In practice, two or more holes are drilled into the pole from a point above the ground level extending downwards and to the center of the pole,

(Fig. 1). These holes are filled with boric acid in solid form, which reacts with the water contained in the wood. The dissolved boric acid is then transported throughout the pole by diffusion with simultaneous leaching into the soil.

The transfer of boron is usually assumed to be a diffusive process (Ra 1999; Vianez 1993) with the diffusion coefficient depending on the wood moisture content and the temperature. The wood

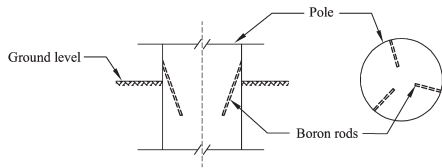


FIG. 1. Boron treatment of wooden poles.

moisture content and temperature are functions of the conditions in the surrounding environment, i.e., the moisture content and temperature in the soil and in the air. Also, the leaching of boron may be expected to depend on moisture content and temperature and, possibly, on the particular soil, e.g., sand or clay, in which the pole is embedded. Together with often rather complex geometries, (Fig. 1), this makes the description of the resulting transfer quite complicated. However, the constitutive relations governing each of the processes involved are well described, i.e., Fick's law for diffusive boron and bound water transfer, Darcy's law for the transfer of free water in the pole, Fourier's law for heat conduction, etc.

By considering heat and mass conservation and using the above-mentioned constitutive laws, a set of governing equations can be derived. These are all of the diffusive type as, e.g., the well-known unsteady-state heat conduction equation. However, only for very simple geometries can these equations be solved analytically, or otherwise, by hand calculation methods; and we therefore have to resort to numerical methods. Traditionally, the finite difference method has been popular for the type of transfer problems considered here. However, for complex three-dimensional geometries, the finite element method is much better suited.

In the following the problem of boron transfer in poles such as the one shown in Figure 1 is treated. First the governing equations are discussed together with some of the material parameters required, after which the actual finite element formulation is derived. Finally, numerical examples are given. In these examples we focus particularly on the geometry of the problem, i.e., the efficiency of the treatment as func-

tion of the number of boron rods and their placement in the pole.

MOISTURE DISTRIBUTION

Wooden poles partially embedded in soil interact with the moisture contained in the air and in the soil, where the moisture content in the soil is again a function of the climate, type of soil, vegetation, and a number of other factors. Thus, the accurate determination of the soil moisture content, which is by far the most important for the moisture content in the pole, is rather complicated. However, the field observations of Peylo and Bechgaard (1999) suggest that in practice there seems to be little difference between the wood moisture contents found in poles at different locations, i.e., embedded in different soils. Thus, at the surface of the poles inspected, moisture contents between 40 and 90% were found, irrespective of whether the surrounding soil was sand or clay. This is quite a surprising observation which can, however, be easily explained by considering the capillary pressure-saturation curves for sand, clay, and wood. At a soil-wood interface the relevant quantity to consider is the capillary pressure rather than the saturation or moisture content. In Fig. 2, typical capillary pressure-saturation curves for the three materials are shown. For a given de-

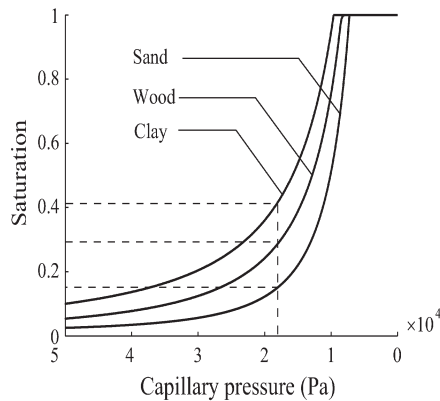


FIG. 2. Capillary pressure-saturation curves for wood, sand, and clay.

gree of saturation in the soil, the corresponding degree of saturation in the wood should be determined by considering continuity of the capillary pressure across the soil-wood interface. If we assume a degree of saturation in the wood of approximately $S = 0.3$ (MC = 60 %), the corresponding degrees of saturation in the clay and in the sand are approximately $S = 0.4$ and $S = 0.15$ respectively, which are in fact quite reasonable values for these two types of soils. In the following we assume a constant moisture content of MC 5 60% at the surface below the ground. Above the ground, the relative humidity can vary significantly over a day, especially during the summer period. However, the yearly variation, in Northern European countries are much smaller, and the relative humidity can with good approximation be assumed to be constant and equal to $RH = 80\%$. Furthermore, since moisture transfer below the fiber saturation point is a very slow process, the assumption of a constant relative humidity is quite reasonable. In other words, the dimensions of a typical pole taken into consideration, the daily variations in relative humidity do not cause any significant deviations from the year-average moisture content in the pole.

Governing equations

Water in wood appears in three different forms: water vapor, bound water, and free or capillary water. For each of these phases of water a conservation equation may be derived. These conservation equations can then be added, Perre and Turner 1999), to yield one equation for the total transfer of water. This equation can be written as

$$\rho_0 \frac{\partial X}{\partial t} = \nabla \cdot (\mathbf{K}\nabla(P + \gamma_w z) + \mathbf{D}_b \nabla X_b + \mathbf{D}_v \nabla P_v) \quad (1)$$

where X is the moisture content, P_c capillary pressure, X_b bound water content, and P_v the vapor pressure. Material parameters required are the effective conductivity for free water \mathbf{K} , the bound water diffusivity \mathbf{D}_b , the vapor diffusivity \mathbf{D}_v , the density of gross wood ρ_0 , and the effective weight of water $\gamma_w = 10 \text{ kN/m}^3$. Gravity, which is often neglected but in this application is

extremely important, is assumed to act opposite to the z -coordinate. Since we only consider the steady-state situation, the term $\partial X/\partial t$ in the above is equal to zero.

BORON DIFFUSION

In the following, the transfer of boron in the pole is treated. The governing equations are derived, and the variations of the boron diffusion coefficients with moisture content, temperature, flow direction and concentration are discussed.

Governing equations

The conservation equation for soluble boron takes the following form

$$\frac{\partial}{\partial t} (\varphi S C_i) + \nabla \cdot (C_i \mathbf{v}_w) = \nabla \cdot (\varphi S \mathbf{D}_B \nabla C_i) \quad (2)$$

where subscript “i” indicates that the concentration C_i is the intrinsic concentration, i.e., the mass of boron per unit volume of water within the wood. By multiplying by the porosity φ and the saturation S , we get the extrinsic concentration, i.e., the mass of boron per unit volume of wood. Apart from the left-hand side accumulation term, the above equation contains two contributions to the overall transfer of boron, namely a convective term, $\nabla \cdot (C_i \mathbf{v}_w)$ where is the mass average velocity of the water phase, accounting for boron carried in the water flow, and a diffusive term $\nabla \cdot (\varphi S \mathbf{D}_B \nabla C_i)$ accounting for transfer resulting from concentration gradients.

Under normal circumstances with a steady-state water phase, we can assume that diffusive boron transfer is dominant over the convective transfer, and thus we end up with the following equation

$$\frac{\partial C}{\partial t} = \nabla \cdot \left(\varphi S \mathbf{D}_B \left(\frac{\partial C_i}{\partial C} \right) \nabla C \right) \quad (3)$$

where C is the extrinsic concentration. The intrinsic concentration C_i is limited by the saturation concentration of boron in water, at 20°C approximately 50 kg/m³. Thus, we may relate

the intrinsic and extrinsic concentrations by

$$C_i = \min\left(\frac{1}{\phi S} C, C_i^{\text{sat}}\right) \quad (4)$$

where C_i^{sat} is the saturation concentration of boron in water. The governing Eq. (3) can then be written as

$$\frac{\partial C}{\partial t} = \nabla \cdot (\hat{\mathbf{D}}_B \nabla C) \quad (5)$$

where

$$\hat{\mathbf{D}}_B = \begin{cases} \mathbf{D}_B & \text{if } C \leq \phi S C_i^{\text{sat}} \\ 0 & \text{otherwise} \end{cases} \quad (6)$$

Thus, if at any point the maximum concentration is reached, no transport occurs before the intrinsic concentration is again within physically possible limits. With respect to the convective transfer, it should be borne in mind that this in certain cases could be significant, e.g., in connection with heavy rainfall or large abrupt temperature variations.

Boron diffusion coefficients

Although several authors, see e.g. (Wickens), have studied the migration of boron as influenced by moisture content, to our knowledge very few works have been concerned with determining boron diffusion coefficients in the framework of the theory outlined in the above. Recently, however, Ra (1999) attempted this in connection with dip-treatment. Although many discrepancies such as sample length and time dependent diffusion coefficients were reported, the results do give some important indications regarding the actual values and their variation with temperature and moisture content as well the variation with respect to the three principal directions of wood.

Moisture dependence

The influence of wood moisture content on the migration of boron is qualitatively well described. Morell et al. (1990) have shown that dif-

fusion of boron begins at moisture contents around 20%. However, when the fiber saturation point, i.e., MC \approx 30%, is approached, the diffusion increases significantly to reach a maximum at around 100% MC (Smith and Williams 1969). Thus, it can be expected that the free water contained within the wood provides the principal pathway of boron diffusion. At low moisture contents, this free water does not constitute a continuous phase, and thus the transfer of boron is hindered. However, as the moisture content increases and the free water phase becomes more and more continuous, the transfer speed of boron is also increased. Thus, it could be expected that the effect of raising the moisture content would gradually become less and less significant as full saturation is approached.

Directional dependence

Usually, transfer coefficients in wood, be they electrical resistance, heat conductivity, or bound water diffusivity, are given in terms of a single coefficient, which may depend on moisture content, temperature, etc. The transfer coefficients in the three principal directions are then given as fractions of this reference coefficient. An exception from this rule, however, appears in the transfer of free water and is related to the above-mentioned continuity of the water phase. Thus, at high degrees of saturation the 'conductivity' in the longitudinal direction is much higher than in the other directions. However, at low moisture contents this situation reverses. (Fig. 3) Since boron is carried in the free water, it could be expected that a similar rule would apply with respect to boron diffusion coefficients.

Temperature dependence

As is the case with most diffusive processes the diffusion coefficient can be expected to increase with increasing temperature. Thus, Ra (1999) found an increase in boron diffusion coefficients with increasing temperature. Measurements were performed at 30, 50, and 70°C and the temperature variation fitted by a straight line. This, however means that for low temperatures (\sim 5–10°C),

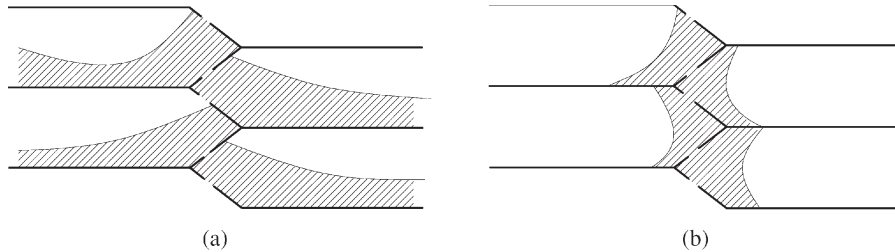


FIG. 3. Free water in wood at high (longitudinal transfer dominant) (a) and low (transverse transfer dominant) (b) degrees of saturation.

some of the coefficients become negative, which is clearly not satisfactory. A more commonly used relationship between diffusion coefficients and temperature is given by the Arrhenius relation which states that the diffusion coefficient D at a certain temperature is given by

$$D = D_0 e^{-E_a / RT} \tag{7}$$

where D_0 is a reference diffusion coefficient, R the universal gas constant, T the absolute temperature, and E_a the activation energy. On examining Ra's results, we found that the temperature variation could in fact be described very accurately by the Arrhenius relation using an activation energy of approximately $E_a = 20$ kJ.

Concentration dependence

In the experiments performed by Ra (1999) and Vianez (1993) time-dependent diffusion coefficients were reported. Although time-dependent diffusion coefficients do occur, it is usually as a result of some underlying process, e.g., swelling and subsequent relaxation in polymers. Since it is hard to find such explanations in connection with boron diffusion in wood, an obvious possibility is that the diffusion coefficient varies with the concentration of boron. To our knowledge, this possibility has not previously been considered. There is, of course, also the possibility that the apparent time-dependence is a result of a faulty experimental procedure, but under all circumstances this is an issue which needs further clarification.

Choice of diffusion coefficients

In the light of the foregoing discussion, it is clear, that estimating diffusion coefficients as input for the diffusion equation is a rather delicate issue. Based on previous attempts (Krabbenhoft et al. 2002) at simulating the experimental results of Wickens (1997) we have chosen a longitudinal diffusion coefficient of

$$D_L^0 = 3 \times 10^{-10} \text{ m}^2 / \text{s}, \quad D_L = 0.55 D_L^0 e^{2.15X} \tag{8}$$

where X is the moisture content (kg/kg). Below the fiber saturation point, in this work defined as $X_{\text{FSP}} = 0.28$, the diffusion coefficients are set equal to zero. The above relationship gives an approximate doubling when raising the moisture content from 30% to 60%, see Fig. 4. The radial

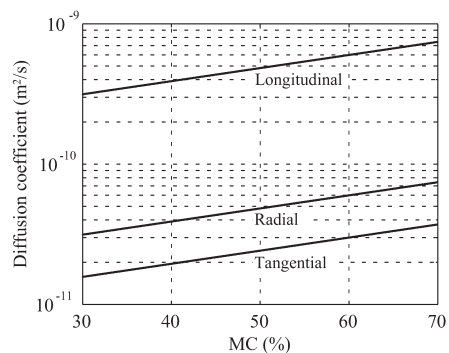


FIG. 4. Assumed diffusion coefficients.

and tangential diffusion coefficients are related to the longitudinal coefficient by

$$D_L : D_R : D_T = 20 : 2 : 1 \quad (9)$$

These values are, admittedly, somewhat arbitrarily chosen. However, apart from calibration with the above-mentioned experiments, the values are also within the limits of what has been reported by Ra (1999).

Leaching

When the boron reaches the surface of the pole, it will leach into the soil. The migration of boron in soil can, in analogy with the transfer in wood, be assumed to be a diffusive process. Thus, in principle we need not only diffusion coefficients for wood but also for soil. In addition, the domain of interest is increased significantly. To circumvent these difficulties, we propose a Robin boundary condition for the leaching of boron into the soil. If the concentration at the surface is denoted C_s and the concentration at an infinite distance from the pole C_∞ , the mass flux of boron into the soil is approximated as

$$j_s = \beta(C_s - C_\infty) \quad (10)$$

where C_∞ should be taken as being equal to zero. Thus, the rate of leaching is assumed to be directly proportional to the concentration at the surface. This type of boundary condition is commonly applied in connection with heat transfer from the air to a solid or vice versa. Here one would write

$$q = h(T - T_\infty) \quad (11)$$

where q is the heat flux and h is known as the convective heat transfer coefficient. This analogy provides a way of determining the convective mass transfer coefficient, or at least its magnitude. If the diffusion of boron in wood is assumed to be equivalent to heat conduction, the diffusion coefficient D and the convective mass transfer coefficient β should be related to the convective heat transfer coefficient h and the heat conductivity λ by

$$\frac{\beta}{D} = \frac{h}{\lambda} \quad (12)$$

For wood $h/\lambda \approx 30-60 \text{ m}^{-1}$, see e.g., (Perre and Turner 1999), and at 60% MC $D_R = 6 \times 10^{-11} \text{ m}^2/\text{s}$, $2D_T = D_R$. Thus, a value of $\beta = 12 \times 10^{-12} \text{ m/s}$, giving $\beta/D_R = 20 \text{ m}^{-1}$ and $\beta/D_T = 40 \text{ m}^{-1}$ is not unreasonable and will be used in the following.

FINITE ELEMENT FORMULATION

The basis of the numerical solution is the Galerkin finite element method. This procedure is now illustrated by the discretization of the diffusion Eq. (5)

$$\frac{\partial C}{\partial t} - \nabla \cdot (\mathbf{D}_B \nabla C) = 0 \quad (13)$$

Instead of trying to fulfill this equation exactly, the finite element method considers an average integral fulfillment of the equation. This is accomplished by multiplying the original equation by a suitable weight function $w = w(x, y, z)$ and integrating over the domain Ω

$$\int_{\Omega} w \left(\frac{\partial C}{\partial t} - \nabla \cdot (\mathbf{D}_B \nabla C) \right) d\Omega = 0 \quad (14)$$

By application of Green's theorem, this equation may be recast as

$$\int_{\Omega} w \frac{\partial C}{\partial t} + \nabla w \cdot \mathbf{D}_B \nabla C d\Omega = \int_{\Gamma} w j_n d\Gamma \quad (15)$$

where Γ denotes the boundary of the domain and j_n is the outward directed flux. The concentration and weight functions are now approximated by finite element functions as

$$\begin{aligned} C(x, y, z, t) &\approx \mathbf{N}(x, y, z) \mathbf{C}(t), \\ \nabla C(x, y, z, t) &\approx \nabla \mathbf{N}(x, y, z) \mathbf{C}(t) \\ w(x, y, z, t) &\approx \mathbf{N}(x, y, z) w(t), \\ \nabla w(x, y, z, t) &\approx \nabla \mathbf{N}(x, y, z) w(t) \end{aligned} \quad (16)$$

For a one-dimensional element, with $x \in [0; L]$, where L is the length, \mathbf{N} and \mathbf{C} may be chosen as

$$\mathbf{N}(x) = \left[1 - \frac{x}{L}, \frac{x}{L} \right], \mathbf{C} = \begin{bmatrix} C_1 \\ C_2 \end{bmatrix} \quad (17)$$

where $C_1 = C(x = 0)$ and $C_2 = C(x = L)$ are the concentrations at the beginning and end of the element. Thus, C is interpolated linearly between the nodal values. By inserting the functions defined in Eqs. (16) into (15), a set of equations are obtained and can be written in matrix form as

$$\mathbf{M} \frac{d\mathbf{C}}{dt} + \mathbf{K}\mathbf{C} + \mathbf{f} = 0 \quad (18)$$

The matrices \mathbf{M} and \mathbf{K} and the vector \mathbf{f} are given by

$$\mathbf{M} = \int_{\Omega} \mathbf{N}^T \mathbf{N} d\Omega, \quad \mathbf{K} = \int_{\Omega} (\nabla \mathbf{N})^T \mathbf{D}_B \nabla \mathbf{N} d\Omega, \quad \mathbf{f} = \int_{\Omega} \mathbf{N}^T j_n d\Omega \quad (19)$$

where the integration is to be performed for each entry in the matrices appearing under the integration sign.

In the above, it has been implicitly assumed that only one element is used. In practice, however, several elements are almost always used. The above procedure is then performed for a number of sub-domains of the entire domain and a set of global matrices comprising the contributions from the individual sub-domains follows.

Before solution, the finite element Eq. (18) must be discretized in time. This can be done by the unconditionally stable backward-Euler scheme

$$\mathbf{M}_{n+1} \frac{\mathbf{C}_{n+1} - \mathbf{C}_n}{\Delta t} + \mathbf{K}_{n+1} \mathbf{C}_{n+1} + \mathbf{f}_{n+1} = 0 \quad (20)$$

where $n+1$ denotes the unknown state and n the current state. Since \mathbf{M} , \mathbf{K} , \mathbf{f} may depend on the unknown state an iterative solution procedure should generally be considered. Further details on the numerical method with reference to the problem of boron diffusion can be found in Krabbenhoft et al. 2002.

NUMERICAL RESULTS

In the following, numerical results demonstrating some of the possibilities of the above outlined theory are presented. We focus particularly on the advantages and disadvantages of using several rods (two, three, and four) and on how these should be placed in the pole. In all the examples, the holes are filled with three 10×100 mm rods such that each hole contains approximately 50 g of boron. The rods are placed as shown in Fig. 5. With respect to the finite element discretization, the symmetry inherent in each of the problems is utilized such that only part of the pole is discretized as indicated by the shaded parts in Fig. 5. Also shown in the figure are the critical points, i.e. the points in the horizontal plane with the farthest distance from the rods.

Moisture distribution

As already discussed, a steady-state moisture field is considered. The moisture content in the soil is assumed to correspond to 60% MC in the

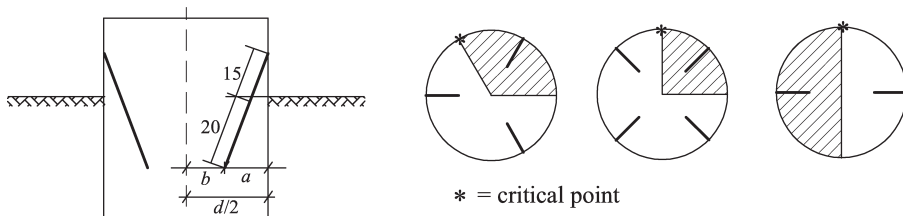


FIG. 5. Placement of rods.

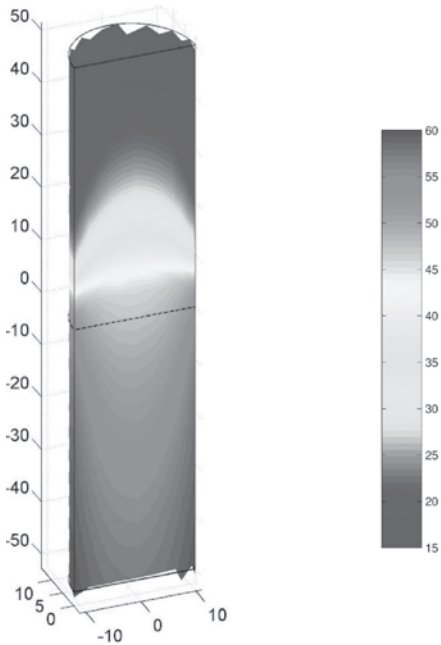


FIG. 6. Moisture distribution. Pole diameter of 22 cm.

pole, whereas above ground the relative humidity is 80% corresponding to a moisture content of $MC \approx 15\%$. The solution of (1) provides the moisture distribution shown in Fig. 6.

Influence of number of rods

A pole with a diameter of 22 cm is analyzed. Two, three, or four rods are inserted with the distances a and b being $a = 7$ cm and $b = 4$ cm. These distances correspond to those used in practice for poles with a diameter of 22 cm.

In Fig. 7(a), the cumulative release of boron from the rods as well as the cumulative leaching into the soil is shown for the cases of two, three, and four rods. Quite surprisingly, the results for two and three rods are very similar. We should mention that this is the case over a large range of the parameters, i.e., diffusion coefficients and convective mass transfer coefficients, used in the

simulations; and the fact that the results are so similar thus appears to be a geometric effect. In the case of four rods, the release and leaching (per rod) are somewhat smaller. Thus, it appears that the more rods are inserted, the longer time passes until the reservoirs are depleted. In other words, the release per rod is influenced by the number of rods present, although this influence is very small when comparing the cases of two and three rods.

In Fig. 7 the concentrations in the critical points at ground level are shown as function of time. As could be expected, the maximum concentration increases as the number of rods is increased, and this in a way which is almost proportional to the number of rods. Also, the more rods that are inserted, the faster a given concentration is reached; and since the maximum concentration increases the same is the case with respect to the time which passes after depletion and until the concentration has dropped to a certain level. This is illustrated in the figure with respect to a concentration of 1 kg/m^3 . Although the difference between the times to depletion in the case of three and four rods is only around 1.5 years, the difference between the periods of time where the concentration is above 1 kg/m^3 is more than twice this.

Thus, regarding the effect of increasing the number of rods in a pole it can be concluded that there is a pronounced effect and that this effect is more than proportional to the number of rods. In other words, if the number of rods is doubled, from two to four, the preservative effect is more than doubled.

In Figs. 8–10, the distributions of boron in horizontal sections are shown in the three cases considered. The sections are located 0, 15, and 30 cm below ground level. As has already been discussed, increasing the number of rods has a positive effect at the ground level, and from the figures it can be seen that this effect is not smaller below ground level.

Influence of rod placing

When the number of rods to be inserted has been determined, it must be decided how the

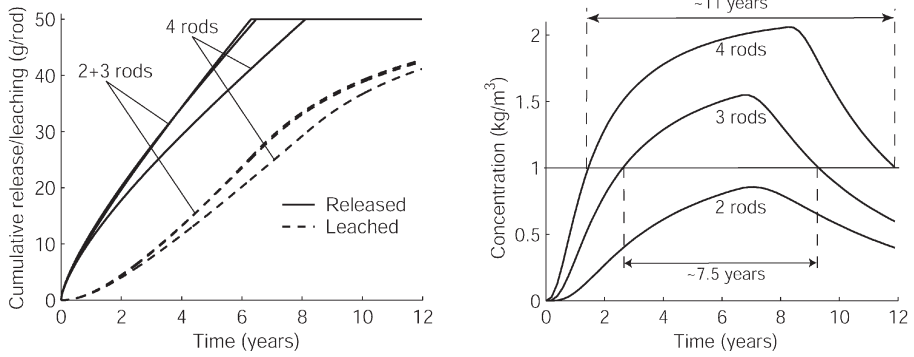


FIG. 7. Cumulative release and leaching (a) and concentration in critical points (ground level) (b) as function of number of rods. Pole diameter of 22 cm.

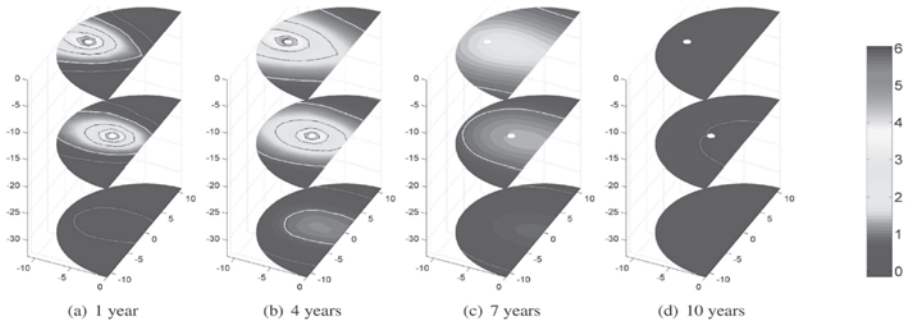


FIG. 8. Boron distributions (kg/m^3). Two rods, pole diameter of 22 cm. Red line indicates 0.5 kg/m^3 limit and green line 1.0 kg/m^3 limit.

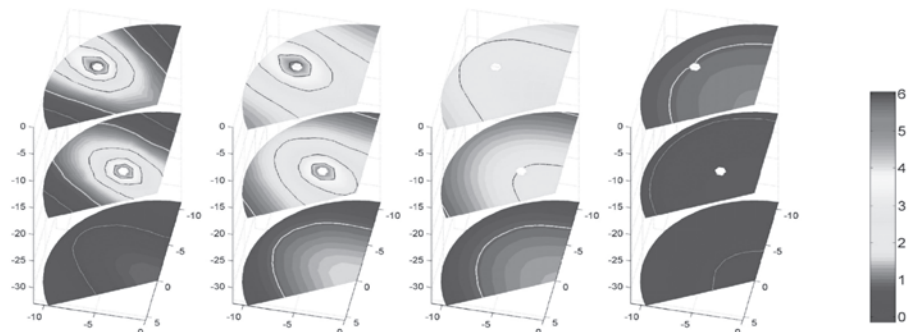


FIG. 9. Boron distributions (kg/m^3). Three rods, pole diameter of 22 cm. Red line indicates 0.5 kg/m^3 limit and green line 1.0 kg/m^3 limit.

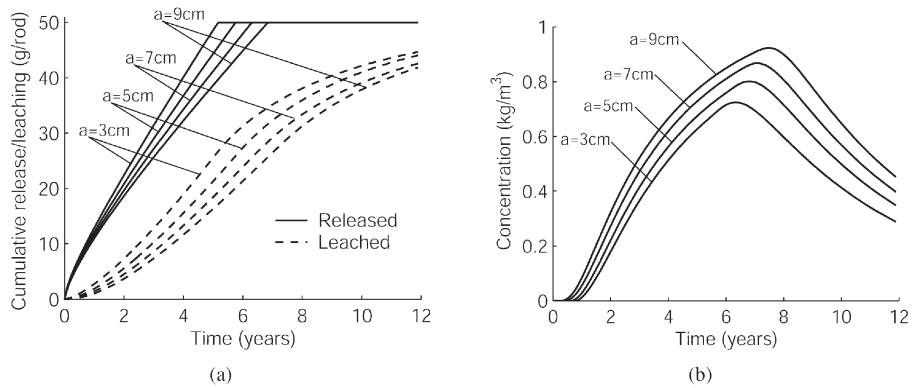


FIG. 10. Boron distributions (kg/m^3). Four rods, pole diameter of 22 cm. Red line indicates 0.5 kg/m^3 limit and green line 1.0 kg/m^3 limit.

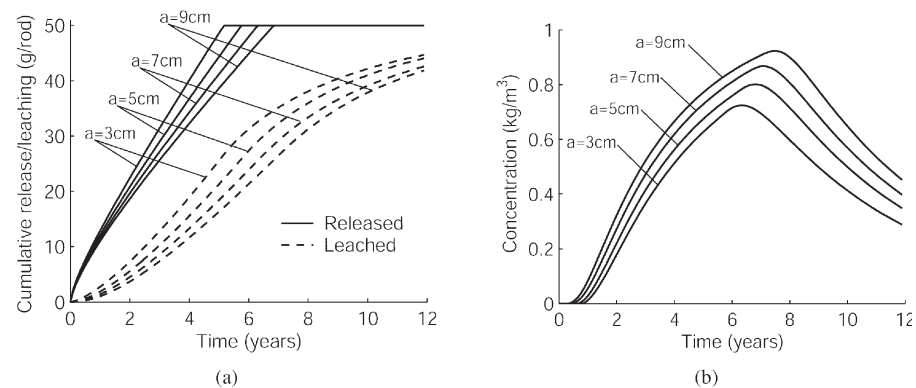


FIG. 11. Cumulative release and leaching (a) and concentration in critical points (b) as function of distance of rod to surface. Two rods, pole diameter of 22 cm.

rods should be placed in the pole. As shown in Fig. 5, this entails determining the distance a from the bottom of the rod to the pole surface. As a function of this distance, cumulative release and leaching rates have been computed, (Fig. 11 (a)). Also, the concentration in the critical point has been determined as a function of time for each of the distances to the surface, Fig. 11(b).

The results are intuitively reasonable: the smaller the distance from the rod to the surface, the shorter time to depletion; and since the dis-

tance from the critical point to the rod increases with decreasing distance from the rod to the surface, we see an increasing maximum concentration in the critical point as a increases. These two parameters, the time to depletion and the maximum concentration in the critical point, seem to be more or less proportional to the distance from the rod to the surface. However, the time interval over which a certain concentration is maintained increases more than proportionally with the rod-surface distance; and placing the rod as far away

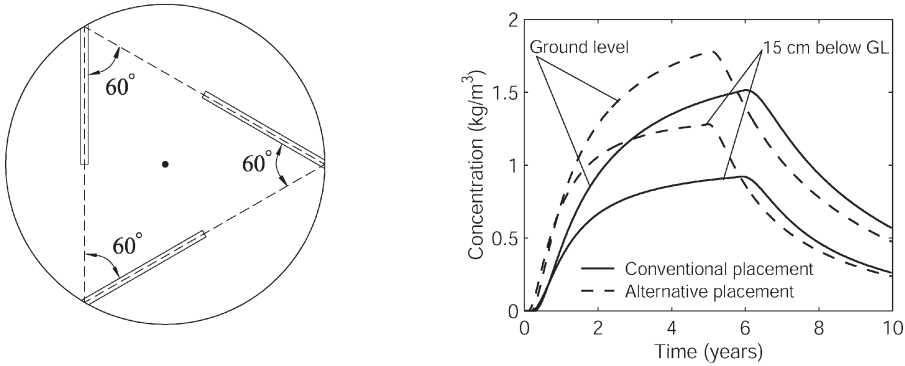


FIG. 12. Alternative placement of rods and some effects. Three rods, pole diameter of 22 cm.

from the surface is thus more beneficial than may appear from Fig. 11(b).

ALTERNATIVE PLACEMENT OF RODS

The next question which naturally arises is to whether the rod placement used in the foregoing is optimal. To answer this question partly, we have experimented with the alternative placement shown in Fig. 12(a). The rods still have a length of 35 cm and are placed such that 20 cm is below ground. Plotted in Fig. 12(b) are the concentrations in the critical points at ground level and 15 cm below. These are compared to the conventional case ($a = 7$ cm) and as can be seen the alternative placement produces higher maximum concentrations. However, leaching is greater since the rods are closer to the surface. This could be reduced by pointing the rods slightly more to the center of the pole, which then again would result in slightly lower concentrations in the critical points.

CONCLUSIONS

The conclusions of this paper are two-fold. First, concerning the obtained results the following can be concluded

- The boron rods should be placed as far away from the pole surface as possible. This increases the time to depletion as well as the

maximum concentration in the critical point and the time over which a certain concentration is maintained in these points.

- Increasing the number of rods increases the maximum concentration in the critical points and the time over which a certain concentration is maintained in these points. A smaller effect is observed with respect to the time to depletion. The trend, however, is towards longer times to depletion with increasing number of rods.
- Some improvement can be achieved by alternative rod placements as shown in Section 5.4. Whether these are significant enough to justify the additional practical difficulties involved is of course another question.

Secondly, concerning the nature of the physical problem considered. There is no doubt that the problem treated is extremely complicated regarding the different mechanisms involved and their mutual coupling. A further complication, however, is the fact that the most basic material parameters, e.g., boron diffusion coefficients, are non-existent. To our knowledge no rigorous experimental work has ever been undertaken to determine these as function of moisture content, temperature and possibly boron concentration, which in light of the numerous works concerned with observing and measuring the migration of boron in wood, is quite surprising. However, with the governing equations identified here we

feel that we have established a scientific basis for further study of the problem.

REFERENCES

- KRABbenhOFT, K., P. HoffMEYER, C. BECHGAARD, AND L. DAMKILDE. 2002. Finite element analysis of boron diffusion in wood. Pages 127–130. *In* E. Lund, N. Olhoff, and Stegmann, eds., Proc. 15th Nordic Seminar on Computational Mechanics. Aalborg University, Denmark.
- MORELL, J. J., C. M. M. SEXTON, AND A. F. PRESTON. 1990. Effect of moisture content of Douglas-fir heartwood on longitudinal diffusion from fused borate rods. *Forest Prod. J.* 40(4):37–40.
- PERRE, P., AND I. W. TURNER. 1999. TransPore: A generic heat and mass transfer computational model for under-standing and visualising the drying of porous media. *Drying Technol.* 17(7&8):1273–1289.
- PEYLO, A., AND C. G. BECHGAARD. 1999. Lifetime of impels in poles. *In* 32nd Annual Meeting of the IRG, Nara, Japan. Intl. Res. Group on Wood Preservation, Stockholm, Sweden.
- RA, J. B. 1999. Diffusion of Boron in Wood. Ph.D. thesis, Mississippi State University, MS.
- SMITH, W. C., AND A. I. WILLIAMS. 1969. Wood preservation by the boron diffusion process ñ the effect of moisture content on the diffusion time. *J. Int. of Wood Sci.* 22(4):37–40.
- VIANEZ, B. F. 1993. Aspects of boron diffusion through Hardwoods. Ph.D. thesis, University of North Wales.
- WICKENS, P. 1997. Treatment of Scots pine poles with boron rods. Imperial College/Wood Slimp GmbH.

K. Krabbenhoft · L. Damkilde · M. Nazem

An implicit mixed enthalpy–temperature method for phase-change problems

Received: 11 January 2005 / Accepted: 9 January 2006
© Springer-Verlag 2006

Abstract A finite element procedure for phase-change problems is presented. Enthalpy and temperature are interpolated separately and subsequently linked via the appropriate relation in the nodes of the mesh during the solution phase. A novel technique is here used where, depending on the characteristics of the problem, either temperature or enthalpy may be considered as primary variable. The resulting algorithm is both efficient and robust and is further easy to implement and generalize to arbitrary finite elements. The capabilities of the method are illustrated by the solution both isothermal and non-isothermal phase-change problems.

1 Introduction

In a large number of problems of engineering interest, the transition of the material from one phase to another is of vital importance in describing the overall physical behaviour. Common applications include metal casting, freezing and thawing of foodstuffs and other biological materials, ground freezing and solar energy storage.

The phase-change problem is characterized by an abrupt change in enthalpy per unit temperature in a narrow temperature range around the freezing point. Indeed, it is often assumed that the enthalpy increases by some, usually rather large, amount at one characteristic temperature as shown in Fig. 1a. This assumption gives rise to a moving boundary problem which in quite a few cases can be solved analytically or otherwise by approximate hand calculation methods, see [1, 2].

For many real problems such as the ones listed in the above, the change of phase does not take place at one characteristic temperature but over a temperature range as shown in Fig. 1b. One speaks of a mushy zone where at a given temperature both fluid and solid material may exist. This problem is no longer a moving boundary problem but rather a non-linear diffusion problem.

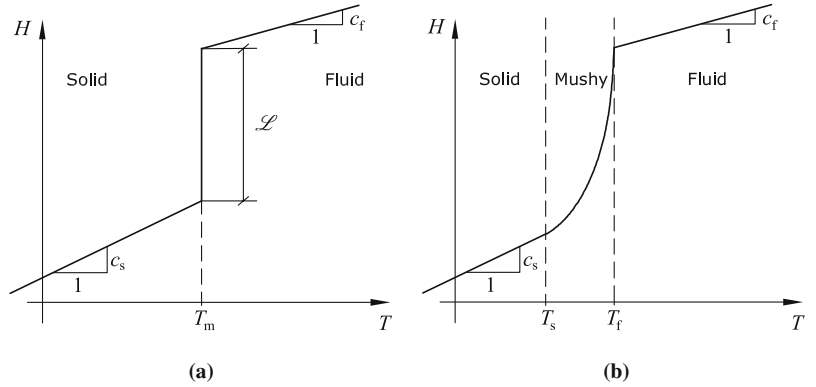
Usually, the mushy zone is sufficiently narrow for the assumption of isothermal phase-change to be a good approximation. However, whereas the isothermal phase-change assumption is convenient as a means at arriving at closed-form analytical solutions it can cause significant complications when it comes to numerical solution methods. To address the problem of a moving front explicitly so-called front-tracking methods have been devised. As the name suggests these methods track the solid–liquid interface and attempt at fulfilling the boundary conditions associated with the moving interface. The front-tracking methods usually involve a continuously deforming mesh which in itself is a considerable complication. Other complications include the treatment of multiple interfaces, appearing and disappearing fronts, and of course the inability to deal with non-isothermal phase-change problems. For these reasons the front-tracking methods have been applied mostly to simple one dimensional problems, although limited attempts at generalization to two spatial dimensions have also been carried out, see e.g. [3].

The alternative to the front-tracking methods are the fixed grid methods. These methods solve the weak form of the governing equations on a fixed grid without making any explicit reference to the conditions on the moving interface. For this reason they are also sometimes referred to as front-capturing methods. The fixed grid methods are more general than the front-tracking methods in that both isothermal and non-isothermal phase-change can be handled. Moreover, most fixed grid methods are not too difficult to extend from one to two and three spatial dimensions. The various fixed grid methods may again be subdivided into different categories depending on how the latent heat is accounted

K. Krabbenhoft (✉) · M. Nazem
Civil, Surveying and Environmental Engineering,
University of Newcastle, NSW, Newcastle, Australia
E-mail: kristian.krabbenhoft@newcastle.edu.au

L. Damkilde
Department of Engineering, Aalborg University,
Esbjerg, Denmark

Fig. 1 Enthalpy–temperature relations for isothermal (a) and non-isothermal phase change (b)



for. Two broad classes can here be identified: effective heat capacity methods and source methods.

The main challenge in the application of the effective heat capacity methods is that a heat capacity around the melting varies very rapidly and may be missed altogether if special procedures are not used. Therefore, some representative average quantity is usually used and large number of averaging schemes can be found in the literature, a review of which is given in Lewis et al. [4].

With the source methods the sensible and latent heats are separated and each quantity discretized in space using standard finite elements. This yields a set of non-linear equations which must be solved iteratively. If the standard Newton–Raphson procedure is used the Jacobian is needed. It turns out that the part of the Jacobian associated with the latent heat is crucial for the convergence of the iterations. In the case of isothermal phase-change the latent heat vector is evaluated exactly, i.e. by splitting up the domain into a solid and a liquid fraction and then integrating over each domain. If this is done, the exact Jacobian can be derived analytically as shown by Storti et al. [5]. Generally speaking, this is of course an attractive feature. However, only in the case of isothermal phase-change and for simple elements such as the linear triangle is the integration of latent heat contribution and its associated Jacobian straightforward (see e.g. [6] for the implementation in the plane isoparametric four-node element). In the case of non-isothermal phase-change the implementation becomes even more demanding with the elements being split up in solid, liquid and mushy regions, see [7, 8]. Moreover, because of the ‘consistent’ evaluation of the latent heat, temperature oscillations may occur as shown in [7]. As in linear heat conduction with a consistent capacitance matrix the only cure for this problem is for a given time step to refine the mesh or alternatively, for a given mesh to increase the time step. Thus, the full potential of a given spatial discretization cannot be realized because the time step must be adjusted accordingly.

In the following a new implicit method capable of dealing with generalized phase-change problems is presented. The procedure does not require a division of

the domain into liquid and solid part and is in this sense similar to the effective heat capacity methods. However, the resulting equations are solved iteratively (to within a specified tolerance) as with the source methods. Both the enthalpy and the temperature are discretized separately and then subsequently linked in the nodes of the finite element mesh during the iterative solution procedure. This iterative procedure differs from the standard Newton–Raphson scheme in that a modified update rule is used. This rule effectively avoids the drawbacks of temperature based formulations while at the same time formally retaining the temperature as the primary variable.

2 Governing equations

We consider the heat conduction equation [7]

$$\frac{\partial H}{\partial t} - \nabla \cdot (k \nabla T) = Q, \quad \mathbf{x} \in \Omega, \quad t \in \Upsilon = [0, \tau], \quad (1)$$

where H is the enthalpy, T the temperature, k the conductivity and Q an internal heat source/sink. The governing Eq. 1 is supplemented with the initial condition

$$T(\mathbf{x}, t = 0) = T_0(\mathbf{x}) \quad \text{in } \Omega \quad (2)$$

and the boundary conditions

$$\begin{aligned} T &= T_b && \text{on } \partial\Omega_T \times \Upsilon, \\ (k \nabla T) \cdot \mathbf{n} &= q && \text{on } \partial\Omega_q \times \Upsilon, \\ (k \nabla T) \cdot \mathbf{n} &= \beta(T_\infty - T) && \text{on } \partial\Omega_c \times \Upsilon, \end{aligned} \quad (3)$$

where $\partial\Omega_T$, $\partial\Omega_q$, and $\partial\Omega_c$ are non-overlapping portions of the boundary of Ω , T and q are the specified temperature and flux at $\partial\Omega_T$ and $\partial\Omega_q$, respectively, β is the heat convection coefficient and T_∞ the environment temperature.

In order to solve Eqs. 1, 2 and 3 a relation between temperature and enthalpy must be established. Instead of aiming at a closed-form expression for the enthalpy–temperature relation it is more convenient to consider the liquid fraction u_ℓ as a function of temperature. That is, when the temperature of a certain medium, e.g. a

metallic alloy, is lowered from some point above the freezing point T_f , Fig. 1b, the liquid fraction contained within the medium will gradually decrease until all liquid has undergone change of phase. The enthalpy can then be defined as

$$H = \int_{T_{\text{ref}}}^T \rho c(T) dT + \rho \mathcal{L} u_\ell = H^S + H^L, \quad (4)$$

where \mathcal{L} is the latent heat and $c(T)$ is the specific heat. Thus, the total enthalpy may be partitioned into two contributions, sensible heat H^S and latent heat H^L . In the important special case where the sensible heat is a linear function of the temperature, but with different specific heats c_f and c_s in the liquid and solid states, the total enthalpy can be written as

$$H = [\rho c_f u_\ell + \rho c_s (1 - u_\ell)](T - T_f) + \rho \mathcal{L} u_\ell, \quad (5)$$

which, if u_ℓ is smooth, yields a smooth total enthalpy–temperature relation.

3 Discretization

In the following the temporal and spatial discretizations of Eqs. 1, 2 and 3 are briefly described.

3.1 Spatial discretization

Both the temperature and the enthalpy variables are approximated by finite element functions, i.e.

$$T(\mathbf{x}, t) \approx \mathbf{N}(\mathbf{x})\mathbf{T}(t), \quad H(\mathbf{x}, t) \approx \mathbf{N}(\mathbf{x})\mathbf{H}(t). \quad (6)$$

This leads to a set of ordinary differential equations given by

$$\mathbf{r} = \mathbf{M} \frac{d\mathbf{H}}{dt} + \mathbf{K}\mathbf{T} - \mathbf{f} = \mathbf{0}, \quad (7)$$

where

$$\begin{aligned} \mathbf{M} &= \int_{\Omega} \mathbf{N}^T \mathbf{N} d\Omega, \\ \mathbf{K} &= \int_{\Omega} \mathbf{B}^T k \mathbf{B} d\Omega + \int_{\partial\Omega_c} \mathbf{N}^T h \mathbf{N} d\Gamma, \\ \mathbf{f} &= \int_{\Omega} \mathbf{N}^T Q d\Omega + \int_{\partial\Omega_q} \mathbf{N}^T q d\Gamma + \int_{\partial\Omega_c} \mathbf{N}^T h T_\infty d\Gamma. \end{aligned} \quad (8)$$

Note that in practice \mathbf{M} is often lumped. For the low-order elements used here this lumping is straightforward and will be implicitly assumed in the following. Thus, for an element defined by n_{dof} nodes we have

$$\mathbf{M} = \frac{V}{n_{\text{dof}}} \mathbf{I}, \quad (9)$$

where V is the element area and \mathbf{I} the unit matrix.

3.2 Temporal discretization

Two different methods of time discretization have been considered. The first is the basic backward Euler scheme by which Eq. 7 is approximated as

$$\mathbf{r}_{n+1} = \mathbf{M}\mathbf{T}_{n+1} - \mathbf{M}\mathbf{T}_n + \Delta t \mathbf{K}_{n+1} \mathbf{T}_{n+1} - \Delta t \mathbf{f}_{n+1} = \mathbf{0}. \quad (10)$$

Secondly, we consider the following approximation of the time derivative

$$\frac{d\mathbf{H}}{dt} \approx \frac{3\mathbf{H}_{n+1} - 4\mathbf{H}_n + \mathbf{H}_{n-1}}{2\Delta t}. \quad (11)$$

So that the final discrete system is given by

$$\begin{aligned} \mathbf{r}_{n+1} &= \mathbf{M}(3\mathbf{H}_{n+1} - 4\mathbf{H}_n + \mathbf{H}_{n-1}) + \Delta t \mathbf{K}_{n+1} \mathbf{T}_{n+1} - \Delta t \mathbf{f}_{n+1} \\ &= \mathbf{0}. \end{aligned} \quad (12)$$

The approximation (11), which has second order accuracy, has previously been applied to the Richards equation describing flow of water in unsaturated soils by Celia et al. [9]. Some gains were reported and since the problem studied here in many ways is similar to the unsaturated flow problem, similar gains may be expected. Examples demonstrating the effects of the above temporal discretization will be given in Section 5. It should be mentioned that we have also implemented the Adams–Moulton approximation

$$\frac{d\mathbf{H}}{dt} \approx \frac{\mathbf{H}_{n+1} - \mathbf{H}_{n-1}}{2\Delta t}, \quad (13)$$

which also possesses second order accuracy. However, in practice the results have been quite discouraging, i.e. regarding accuracy the approximation is not much better than the standard Euler scheme and often even worse. Furthermore, the non-physical oscillations are generally much more pronounced than with the use of (11). For these reasons the Adams–Moulton approximation will not be treated any further.

3.3 Tangent matrices

The iterative procedure presented in the next section requires the Jacobian (tangent matrix) of the residuals given in Eqs. 10 and 12. In the following the tangent matrix associated with the conductivity matrix is treated in some detail.

For the integration of matrix, two different approaches may be applied. In the first, the integration is performed as

$$\mathbf{K} = \int_{\Omega} \mathbf{B}^T k(\mathbf{A}\mathbf{T}) \mathbf{B} d\Omega, \quad (14)$$

where \mathbf{A} is an appropriately chosen set of shape functions determining the distribution of the conductivity over an element. Here it could be argued that $\mathbf{A} = \mathbf{N}$ is the natural choice. The tangent matrix associated with \mathbf{K} is given by

$$\mathbf{K}_t = \frac{\partial^T}{\partial \mathbf{T}}(\mathbf{K}\mathbf{T}) = \mathbf{K} + \int_{\Omega} \mathbf{B}^T k'(\mathbf{A}\mathbf{T}) \mathbf{B} \mathbf{T} \mathbf{A} \, d\Omega, \quad (15)$$

where $k' = dk/dT$. If numerical integration is used the same scheme should be used throughout. As can be seen, \mathbf{K}_t consists of the original symmetric conductivity matrix and a non-symmetric contribution.

In the second approach to the integration of \mathbf{K} the conductivity k is interpolated in a similar way as the enthalpy and temperature variables, i.e.

$$k(T) \approx \mathbf{A}\mathbf{k} \quad (16)$$

where $\mathbf{k} = [k(T_1), \dots, k(T_{n_{\text{dof}}})]^T$, contains the nodal conductivities. In this way \mathbf{K} is given by

$$\mathbf{K} = \int_{\Omega} \mathbf{B}^T \mathbf{A} \mathbf{k} \mathbf{B} \, d\Omega \quad (17)$$

and the associated tangent matrix is

$$\mathbf{K}_t = \frac{\partial^T}{\partial \mathbf{T}}(\mathbf{K}\mathbf{T}) = \mathbf{K} + \left[\int_{\Omega} \mathbf{B}^T \mathbf{A} \mathbf{k}' \mathbf{B} \mathbf{T} \mathbf{A} \, d\Omega \right] \text{diag}(\mathbf{k}'), \quad (18)$$

where $\mathbf{k}' = [k'(T_1), \dots, k'(T_{n_{\text{dof}}})]^T$.

An efficient special case consists of taking \mathbf{A} as being constant, for example with all entries equal to $1/n_{\text{dof}}$. We can then define

$$\tilde{\mathbf{K}} = \int_{\Omega} \mathbf{B}^T \mathbf{B} \, d\Omega \quad (19)$$

and subsequently compute \mathbf{K} as

$$\mathbf{K} = \tilde{\mathbf{K}} \mathbf{A} \mathbf{k} \quad (20)$$

and \mathbf{K}_t as

$$\mathbf{K}_t = \mathbf{K} + \tilde{\mathbf{K}} \mathbf{A} \mathbf{k}' \text{diag}(\mathbf{k}'). \quad (21)$$

The full Jacobian can now be written as

$$\mathbf{J} = \frac{\partial^T \mathbf{r}}{\partial \mathbf{T}} = \mathbf{M} \mathbf{G} + \Delta \mathbf{r} \mathbf{K}_t, \quad (22)$$

where \mathbf{G} is a diagonal matrix containing the derivative of the enthalpy–temperature relation evaluated at the nodes of the mesh:

$$\mathbf{G} = \begin{bmatrix} (dH/dT)_1 & & & \\ & \ddots & & \\ & & \ddots & \\ & & & (dH/dT)_{n_{\text{dof}}} \end{bmatrix}. \quad (23)$$

4 Solution algorithm

The discrete equations 10 now contain both the nodal enthalpies and the nodal temperatures and a choice must

be made as to which of these should be used as primary variable in the iterative solution procedure. Since enthalpy is usually given in terms of temperature and not vice versa it seems natural to use the temperature as primary variable. The Newton–Raphson scheme can then be written as

$$\begin{aligned} \Delta \mathbf{T}_{n+1}^j &= -(\mathbf{J}_{n+1}^j)^{-1} \mathbf{r}_{n+1}^j, \\ \mathbf{T}_{n+1}^{j+1} &= \mathbf{T}_{n+1}^j + \Delta \mathbf{T}_{n+1}^j, \\ \mathbf{H}_{n+1}^{j+1} &= H(\mathbf{T}_{n+1}^{j+1}). \end{aligned} \quad (24)$$

In each iteration, temperature increments \mathbf{T} are computed and the temperatures then updated. On the basis of these temperatures the corresponding enthalpies are computed by means of the relevant enthalpy–temperature relation.

This series of steps is in some sense consistent with the Newton–Raphson method, but is by no means the only way to proceed. The problem with the procedure is that if the enthalpy–temperature curve is very steep around the phase-change temperature, then the chances of producing pairs (T, H) lying in the narrow mushy zone is very slight, and the large gradients associated with such points will be missed in the tangent matrix. This may slow down convergence or, in most cases in fact, lead to situations where convergence is not achieved unless line search or other similar procedures are used.

One way of countering these problems is to, instead of computing the nodal enthalpies on the basis of the nodal temperatures, compute some enthalpy increment \mathbf{H} on the basis of the temperature increment, then update the nodal enthalpies and finally, compute the temperatures corresponding to these enthalpies. Thus, the iterative procedure can be written principally as

$$\begin{aligned} \Delta \mathbf{T}_{n+1}^j &= -(\mathbf{J}_{n+1}^j)^{-1} \mathbf{r}_{n+1}^j, \\ \Delta \mathbf{H}_{n+1}^j &= G(\Delta \mathbf{T}_{n+1}^j), \\ \mathbf{H}_{n+1}^{j+1} &= \mathbf{H}_{n+1}^j + \Delta \mathbf{H}_{n+1}^j, \\ \mathbf{T}_{n+1}^{j+1} &= T(\mathbf{H}_{n+1}^{j+1}). \end{aligned} \quad (25)$$

The question is now how the enthalpy increments should be computed. Here it seems natural to use the Taylor expansion

$$\mathbf{H} = \mathbf{H}_{n+1}^j + \left(\frac{d\mathbf{H}}{d\mathbf{T}} \right)_{n+1}^j \Delta \mathbf{T}_{n+1}^j \quad (26)$$

and thus,

$$\Delta \mathbf{H}_{n+1}^j = \mathbf{G}_{n+1}^j \Delta \mathbf{T}_{n+1}^j, \quad (27)$$

where

$$\mathbf{G}_{n+1}^j = \left(\frac{d\mathbf{H}}{d\mathbf{T}} \right)_{n+1}^j. \quad (28)$$

The difference between the two different types of temperature and enthalpy update is illustrated in Fig. 2

a. From an equilibrium point A a temperature increment is computed. If the conventional update is used an intermediate point A' is found after which the enthalpy-temperature relation is used to bring the solution to point A'' . In this case the mushy zone is missed which may result in the problems described in the above.

If the alternative method of update is used we are again initially at point A . On the basis of the temperature increment ΔT an enthalpy increment is computed to bring the solution to the intermediate point B from which the inverse enthalpy-temperature relation is used to finally arrive at point B' . In the next iteration the tangent matrix will now reflect the fact that the node is undergoing change of phase and chances of convergence should be much better.

However, the alternative method of update is not completely without any complications and generally, care should be taken when computing enthalpy increments. This is illustrated in Fig. 2 (b), where the initial point lies in the mushy zone. Since dH/dT is now large, the temperature increment will generally be quite small. However, since the gradient is large, even small increments will result in large changes. Again, the two different methods of update are considered. The conventional method produces points $A-A'-A''$ and thus, the overall change is moderate. The alternative update, however, results in a rather large change in enthalpy, $A-B$, which results in an even larger change in temperature, $B-B'$. Thus, the difference between the points produced by the two different methods is quite pronounced and which point is closer to the real solution of course depends on the particular circumstances. It can, however, be seen that the alternative update, just as the conventional one, may produce large increments under circumstances which may require more moderate changes.

Thus, it seems that the optimal method of update should embrace a combination of these two different methods of update. Alternatively, depending on the particular state, each node may be updated by either of the two methods. The critical issue is then the formulation of a proper test to decide as to which of the two methods of update should be applied for a given node. With these considerations in mind, a simple approach would be to choose the update which gives the smallest

temperature increment. Thus, the algorithm used in the following can be summarized by

$$\begin{aligned} \Delta \mathbf{T}_A &= -(\mathbf{J}_{n+1}^j)^{-1} \mathbf{r}_{n+1}^j, \\ \Delta \mathbf{T}_B &= T(\mathbf{H}_{n+1}^j + \mathbf{G}_{n+1}^j \Delta \mathbf{T}_A) - \mathbf{T}_{n+1}^j, \\ k &= 1, \dots, \text{No nodes} \\ &\text{if } |\Delta T_A^k| < |\Delta T_B^k| \\ &\quad \text{then } \Delta T^k = \Delta T_A^k \\ &\quad \text{else } \Delta T^k = \Delta T_B^k \\ \mathbf{T}_{n+1}^{j+1} &= \mathbf{T}_{n+1}^j + \Delta \mathbf{T}_{n+1}^j. \end{aligned} \quad (29)$$

Of course, other criteria for selecting the type of update may be used. The strategy used in the above may not be the most efficient in the sense that it is overly cautious. On the other hand, this makes the iterative procedure very robust and furthermore, no special parameters are needed to decide on the choice of update type.

The procedure presented above has some similarities with the method of Nedjar [10]. Here the enthalpy was used as the primary variable and the temperatures then updated based on the enthalpy. In the present procedure, however, temperature is retained as the primary variable in the 'global' heat balance equations 10. On the 'local' level, when updating the temperature at each

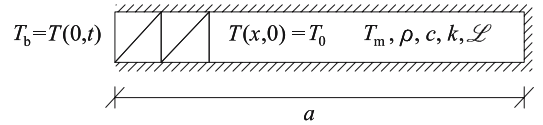
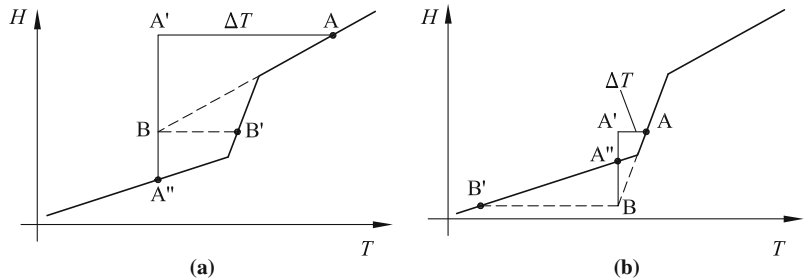


Fig. 3 Configuration of Example 1

Table 1 Parameters used in Example 1

$a = 4.0$ m	$\rho = 1.0$ kg/m ³
$T_0 = 0.0^\circ\text{C}$	$c = 1.0$ J/(Kkg)
$T_b = -45.0^\circ\text{C}$	$k = 1.08$ W/(K,m)
$T_m = -0.1^\circ\text{C}$	$\mathcal{L} = 70.26$ J/kg

Fig. 2 Iterative procedure



node, a procedure which is equivalent to a change of variable is performed if the circumstances for doing so are deemed favorable. Thus, the method combines the use of temperature and enthalpy as primary variables and should therefore in a certain sense, at least with the right criterion for choosing the type of update, be optimal.

For the examples presented in Section 5, the iterations are broken off when the following criteria are satisfied

$$\|\mathbf{r}_{n+1}^{j+1}\| < \varepsilon_1 \max\left(1, \|\mathbf{M}\mathbf{H}_{n+1}^{j+1}\|\right) \quad (30)$$

and

$$\|\Delta\mathbf{T}_{n+1}^j\| < \varepsilon_2 \max\left(1, \|\mathbf{T}_{n+1}^{j+1} - \mathbf{T}_n\|\right) \quad (31)$$

In the following we use $\varepsilon_1 = \varepsilon_2 = 10^{-9}$.

5 Examples

In the following three examples demonstrating the capabilities of the proposed method are given.

Fig. 4 Example 1, $h = 0.125$ m, $D t = 0.2$ s. Temperature at $x = 1.0$ m (a) and front position (b)

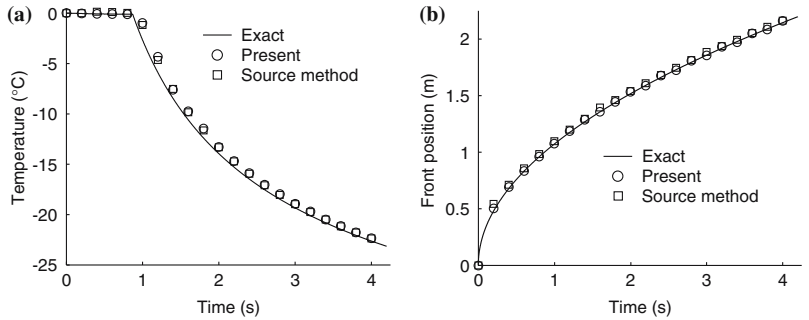


Fig. 5 Example 1. Temperature at $x = 1.0$ m for different Stefan numbers

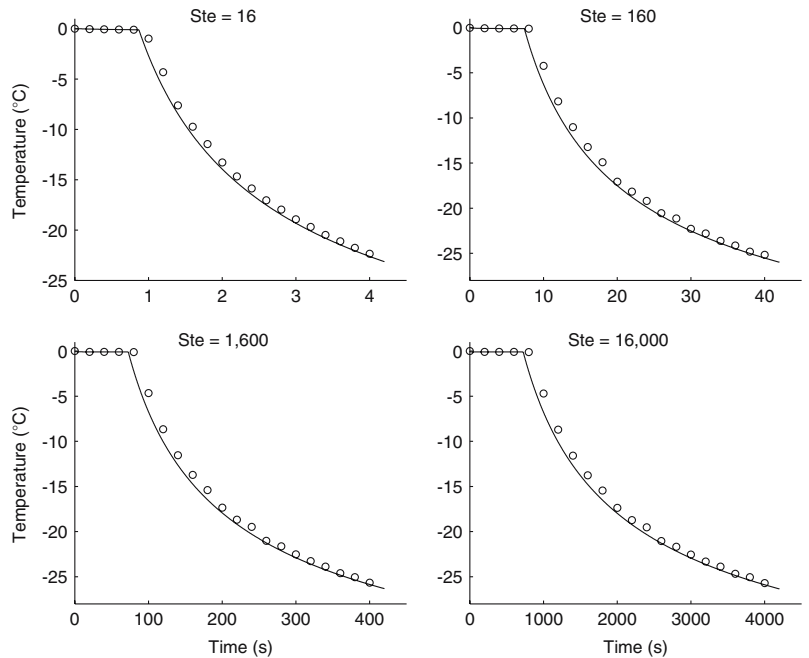
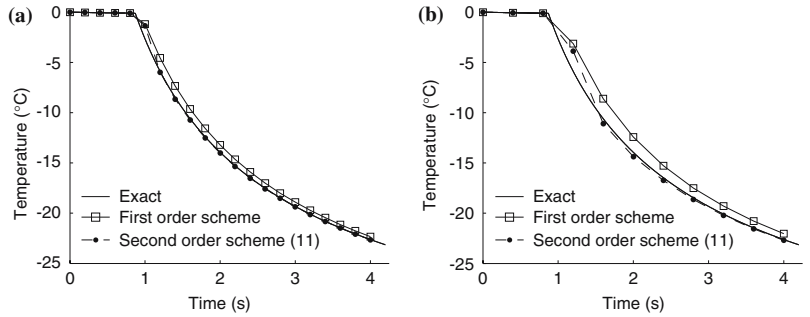


Fig. 6 Example 1. Effect of higher order temporal discretization $h = a/256$ m. Temperature at $x = 1.0$ m for $\Delta t = 0.2$ s (a) and for $\Delta t = 0.4$ s (b)



5.1 Example 1: one-dimensional solidification

A standard test example for isothermal phase-change, see e.g. [4–8], considers the solidification of a one-dimensional slab as shown in Fig. 3. The analytical solution for a semi-infinite slab can be found in [1, 2]. The problem is defined by the material parameters and initial and boundary conditions given in Table 1. As in [7] we use 2×32 triangular elements positioned as indicated in Fig. 3, i.e. the mesh size is $h = 0.125$ m. The time step is $\Delta t = 0.2$ s and the liquid fraction is approximated by a straight line from $T_f = T_m = -0.1^\circ\text{C}$ to $T_s = -0.1001^\circ\text{C}$ i.e. the mushy zone has an extent of 10^{-4}°C . The material parameters given in Table 1 define a Stefan number of

$$\text{St} = \frac{\rho \mathcal{L}}{\rho c (T_m - T_b)} = 1.6. \quad (32)$$

In Figure 4 the temperature evolution at 1.0 m is shown together with the front position. As can be seen the results produced by the two methods are hardly distinguishable. For the present method the problem poses no particular difficulties, the average number of iterations being only 2.9 on average. As for the source method we found, in accordance with [11], that a line search was necessary in order to achieve convergence in the first few time steps.

Next, four runs with Stefan numbers equal to $\text{St} = 16, 160, 1,600$ and $160,000$ are performed. These problems were generated by increasing the latent heat whereas all other material, boundary and mesh data remain unchanged. The time steps were chosen as $\Delta t = 2, 20, 200, 2,000$ s, respectively. The results of these analyses are shown in Fig. 5. As can be seen there is virtually no difference in the quality of the solutions.

Finally, to test the second order accurate temporal discretization 31 we run the same example with $h = a/256$ m and $\Delta t = 0.2$ and 0.4 s, respectively. The results are shown in Fig. 6 and suggest that the second order accurate discretization may be rather efficient. It should be borne in mind, however, that the higher order approximation does not possess the same good stability properties as the standard backward Euler scheme, and may result in non-physical temperature oscillations

although for a wide range of realistic examples these have generally been found to be very moderate.

5.2 Example 2: two-dimensional solidification

The next example concerns the solidification corner region as shown in Fig. 7. An analytical solution to this problem has been given by Rathjen and Jiji [11]. The

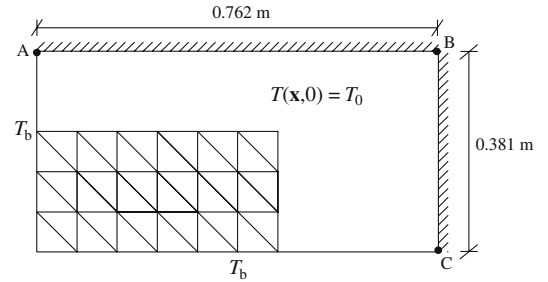


Fig. 7 Configuration of Example 2

Table 2 Parameters used in Example 2

$T_0 = 1,550^\circ\text{C}$	$\rho c = 5.4 \times 10^6 \text{ J}/(\text{K m}^3)$
$T_b = 1,150^\circ\text{C}$	$k = 30 \text{ W}/(\text{K m})$
$T_m = 1,500^\circ\text{C}$	$\rho \mathcal{L} = 1.89 \times 10^9 \text{ J}/\text{m}^3$

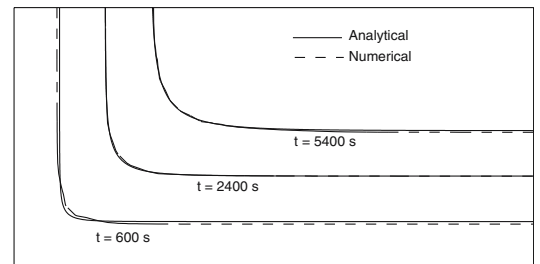


Fig. 8 Example 2. Front positions at different times

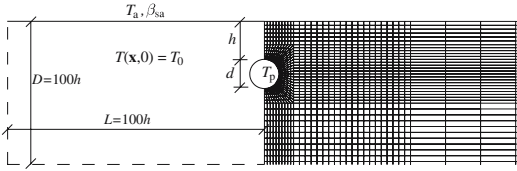


Fig. 9 Configuration of Example 3 (coarse mesh)

Table 3 Parameters used in Example 2

$\rho = 1,000 \text{ kg/m}^3$	$\rho_s = 2,200 \text{ kg/m}^3$
$c_w = 4,200 \text{ J/Kkg}$	$k_w = 0.56 \text{ W/mK}$
$c_i = 1,760 \text{ J/Kkg}$	$k_i = 2.2 \text{ W/mK}$
$c_s = 780 \text{ J/Kkg}$	$k_s = 1.4 \text{ W/mK}$
$\mathcal{L} = 338,000 \text{ J/kg}$	$n = 0.3$
$\beta_{sa} = 10.0$	$T_m = 0.0^\circ\text{C}$
$T_a = -^\circ\text{C}$	$T_0 = 2.0^\circ\text{C}$
$T_p = 1.0^\circ\text{C}$	$a = -1.19^\circ\text{C}$
$b = 1.6$	$h = 1.5 \text{ m}$
$a = 1.0 \text{ m}$	$W_0 = 0.04$

material parameters and initial and boundary conditions are given in Table 2. A regular 25×50 mesh constructed as indicated in Fig. 7 is used and the time step is $\Delta t = 600 \text{ s}$. The liquid fraction is taken to vary as

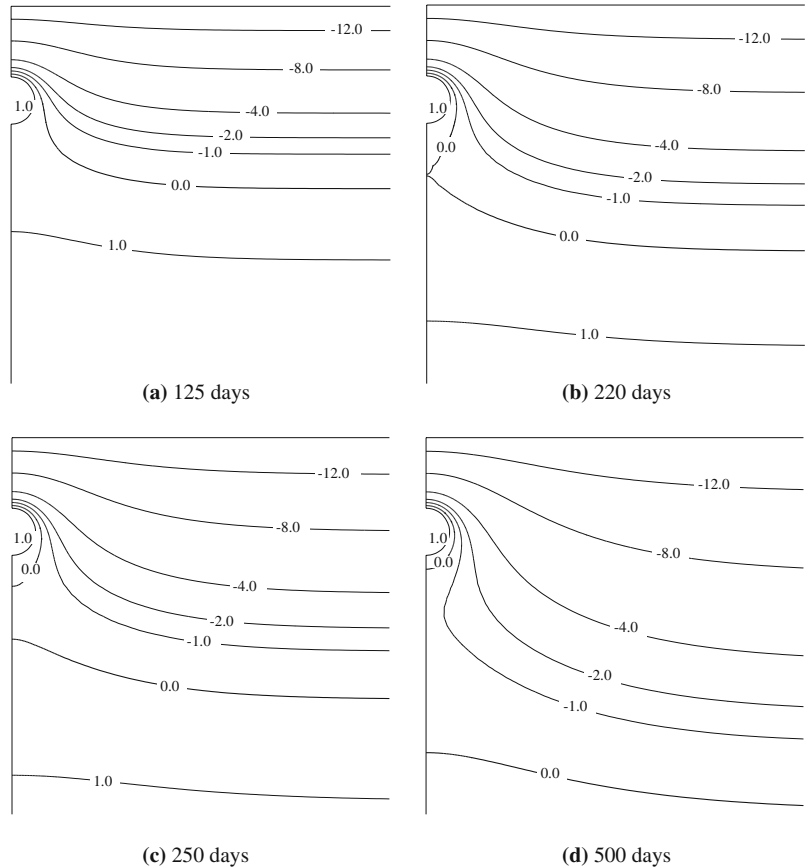
$$u_\ell = \min \left[1, \max \left(0, \frac{1}{2\delta} (T - T_m + \delta) \right) \right], \quad (33)$$

where a value of value of $2\delta = 2^\circ\text{C}$ has been used. This value should be compared to the characteristic temperature interval of the problem, i.e. $T_0 - T_b = 400^\circ\text{C}$. In Fig. 8 the front positions are shown at three different times and as can be seen the agreement between analytical and numerical solution is quite reasonable, even for the very coarse time discretization used. The number of iterations in each time step varies between 3 and 5, except in the very first step where 10 iterations are needed.

5.3 Example 3: freezing around a buried pipe

The last example deals with the problem of freezing around a pipe buried in wet soil as shown in Fig. 9. As

Fig. 10 Temperature distributions around buried pipe. a 125 days, b 220 days, c 250 days and d 500 days



already mentioned wet soil is a material whose enthalpy–temperature relation exhibits a mushy zone. The existence of a mushy zone is in part due to capillarity by which the chemical potential of the water is lowered and liquid water may exist at temperatures well below 0°C [12, 13]. For real soils also the naturally occurring salts will contribute to lowering the freezing temperature [13, 14].

Kujala [15] has experimentally examined some 68 soils and found that the volumetric unfrozen water content could be fitted by the expression

$$W = W_0 e^{-(T/a)^b}, \quad (34)$$

where W_0 is the moisture content at 0°C and a and b are empirical constants which depend on the particular type of soil.

Neglecting the heat capacity of the air found in an unsaturated soil the total enthalpy–temperature relation can be written as

$$H = [\rho c_w W + \rho c_i (W_0 - W) + (1 - n) \rho c_s] (T - T_m) + \rho \mathcal{L} W, \quad (35)$$

where n is the porosity and subscripts w , i and s refer to liquid water, ice and soil respectively. The conductivity is taken as the volumetric mean of the three components present (again neglecting the air), i.e.

$$k = k_w W + k_i (W_0 - W) + (1 - n) k_s. \quad (36)$$

For the transfer of heat from the surrounding air to the soil the convection boundary condition 3 with $q=0$ has been applied. The numerical values of the parameters used are listed in Table 3.

The results of the analysis are shown in Fig. 10 in terms of the temperature distributions at different times. It is interesting to observe how the ‘front’ as defined by $T = T_m$ separates around the pipe after approximately 220 days (c). As noted by Storti et al. [5] for the case of isothermal phase-change this may cause severe difficulties for front tracking methods.

As in the previous examples the number of iterations is quite moderate. For a mesh containing 13,600 nodes a time step of $\Delta t = 2.5$ days gives an average of 3.3 iterations per time step whereas using $\Delta t = 5$ days results in an average of 3.7 iterations per time step.

6 Conclusions

An implicit finite element procedure capable of handling phase-change problems with a mushy zone has been

described. The procedure used has proven to be quite efficient and very robust. Furthermore, the results produced by the method are generally accurate and the non-physical oscillations produced by other methods are completely avoided. In this paper only examples of two-dimensional phase-change problems have been presented. However, the extension to three-dimensional problems is straightforward, as is the extension to other two-dimensional elements than the ones used in the present paper.

References

1. Carslaw HS, Jaeger JC (1959) *Conduction of heat in solids*. Oxford University Press, New York
2. Crank J (1967) *The mathematics of diffusion*. Oxford University Press, New York
3. Voller VR, Peng S (1994) An enthalpy formulation based on an arbitrarily deforming mesh for solution of the Stefan problem. *Comput Mech* 14:492–502
4. Lewis RW, Morgan K, Thomas HR, Seetharamu KN (1996) *The finite element method in heat transfer analysis*. Wiley, New York
5. Storti M, Crivelli LA, Idelsohn SR (1988) An efficient tangent scheme for solving phase-change problems. *Int J Numer Meth Eng* 66:65–86
6. Storti M, Crivelli LA, Idelsohn SR (1987) Making curved interfaces straight in phase-change problems. *Int J Numer Meth Eng* 4:375–392
7. Fachinotti VD, Cardona A, Huespe AE (1999) A fast convergent and accurate temperature model for phase-change heat conduction. *Int J Numer Meth Eng* 44:1863–1884
8. Nigro N, Fachinotti VD, Huespe AE (2000) Phasewise numerical integration of finite element method applied to solidification processes. *Int J Heat Mass Transf* 43:1053–1066
9. Celia MA, Bouloutas ET, Zarba RL (1990) A general mass-conservative numerical solution for the unsaturated flow equation. *Water Resour Res* 26:1483–1496
10. Nedjar B (2002) An enthalpy-based finite element method for nonlinear heat problems involving phase change. *Comput Struct* 80:9–21
11. Rathjen KA, Jiji LM (1971) Heat conduction with melting or freezing in a corner. *J Heat Transf* 93:101–109
12. Grant S, Sletten RS (2002) Calculating capillary pressures in frozen and ice-free soils below the melting point. *Environ Geol* 42:130–136
13. Watanabe K, Mizoguchi M (2002) Amount of unfrozen water in frozen porous media saturated with solution. *Cold Regions Sci Technol* 34:103–110
14. Banin A, Anderson DM (1974) Effects of salt concentration changes during freezing of the unfrozen water content of porous materials. *Water Resour Res* 10(1):24–128
15. Kujala K (1989) Unfrozen water content of Finnish measured by NMR. In: Rathmayer H (ed) *International symposium on frost in geotechnical engineering*. Espoo, Finland, pp 301–310



Report no R-153
ISSN 1602-2917
ISBN 87-7877-225-7